ISSN 1816-8957

No. 28, December 2020

Scientific Drilling

Reports on Deep Earth Sampling and Monitoring

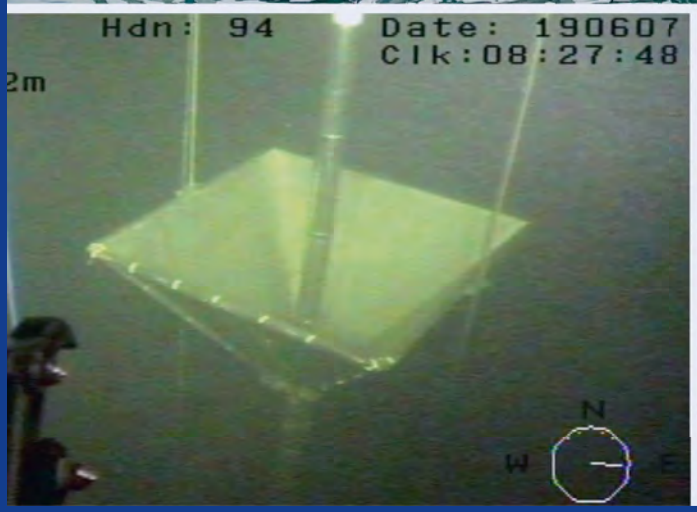

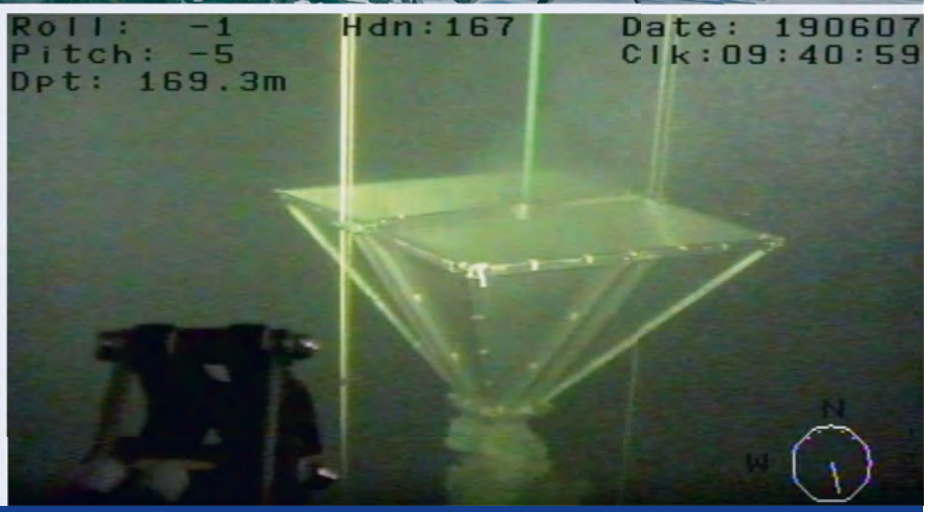

Editorial preface

Dear reader,

In challenging times with most scientists away from the field, this issue of your journal *Scientific Drilling* is providing a little scent of field operations. This includes new drilling and sampling technology developments as well as new ways of evaluating existing data and exciting prospects for future projects.

A new geohazard assessment workflow (SD-2020-12, p. 1) maximizes the use of 3D seismic reflection data to improve the safety and success of scientific drilling in the oceans. Advanced seismic interpretation techniques are used to identify, map, and spatially analyse features such as seabed structures, faults, fluids, and lithologies that may cause drilling hazards. This workflow can be utilized to guide site selection and to minimize risk of future IODP drilling.

SD-2020-15 (p. 29) reports about the first use of Hipercorig, an environmentally-friendly, hydraulic coring system designed to recover up to 100 m deep continuous high-quality cores in a cost-effective fashion. Two test projects on perialpine lakes resulted in 63 m deep coring in up to 204 m water depth and promise novel opportunities for future lacustrine drilling campaigns.

The Multi-Temperature Fluid Sampler (MTFS) is a newly designed, fabricated, and laboratory-tested titanium syringe-style fluid sampler that is composed of up to 12 sampling units of 1 L sample volume each and for borehole applications up to 190 °C (SD-2020-3, p. 43). Its unique triggering mechanism allows for utilization in deep oceanic and continental scientific boreholes with minimal training for operational success.

In addition, four workshop reports reflect the wealth of scientific topics addressed by international scientific drilling programmes. SD-2020-18 (p. 63) discusses the possibilities of drilling the Weihe Basin, enclosed by the Chinese Loess Plateau and the Qin Mountains, for obtaining high-resolution multi-proxy records reflecting environmental changes spanning most of the Cenozoic. Workshop report SD-2020-14 (p. 75) focuses on designing a research drill to investigate utilization and associated risks of low-enthalpy geothermal energy from Paleozoic strata and deep crystalline geologic systems in Ithaca (NY, USA). The northern boundary of the Caribbean plate around Haiti with two active strike-slip faults posing the area under high seismic risk was addressed by a workshop held for developing a land-to-sea drilling project, the new IODP-ICDP scheme for joint projects (SD-2020-4, p. 49). Finally, the DeepDust Workshop (SD-2020-6, p. 93) sheds light on the Permian period at two continental sites in the western United States and Europe to study environmental dynamics.

With this spectrum of themes, we wish the readers entertainment with education as well as good health.

Your editors,

Ulrich Harms, Thomas Wiersberg, Jan Behrmann,
Tomoaki Morishita, and Will Sager

Aims & scope

Scientific Drilling (SD) is a multidisciplinary journal focused on bringing the latest science and news from the scientific drilling and related programmes to the geosciences community. Scientific Drilling delivers peer-reviewed science reports from recently completed and ongoing international scientific drilling projects. The journal also includes reports on engineering developments, technical developments, workshops, progress reports, and news and updates from the community.

Editorial board

Additional information

ISSN 1816-8957 | eISSN 1816-3459

Copernicus Publications
The Innovative Open Access Publisher

Copernicus Publications
Bahnhofsallee 1e
37081 Göttingen
Germany
Phone: +49 551 90 03 39 0
Fax: +49 551 90 03 39 70

editorial@copernicus.org
production@copernicus.org

https://publications.copernicus.org

View the online library or learn more about Scientific Drilling on:
www.scientific-drilling.net

Cover figure: Hipercorig on Lake Constance during coring operations, including entry of coring assembly in the upper reentry cone (bottom left) and lowering the reentry cone with hydraulic hose (bottom right). Harms et al., 2020, this volume.
Insert 1: Multi-Temperature Fluid Sampler with 11 sampling modules assembled and ready for deployment. Wheat et al., 2020, this volume.
Insert 2: Lower Permian paleo-loess of the mid-continent US preserves high-resolution climate records. Soreghan et al., 2020, this volume.

Contents

Science Reports

Technical Developments

Workshop Reports

News & Views

Sci. Dril., 28, 1–27, 2020
https://doi.org/10.5194/sd-28-1-2020

Scientific Drilling
Open Access

Geohazard detection using 3D seismic data to enhance offshore scientific drilling site selection

David R. Cox[1], Paul C. Knutz[2], D. Calvin Campbell[3], John R. Hopper[2], Andrew M. W. Newton[1,4], Mads Huuse[1], and Karsten Gohl[5]

[1]Department of Earth and Environmental Sciences, University of Manchester, Williamson Building, Oxford Road, Manchester, M13 9PL, UK
[2]Geological Survey of Denmark and Greenland, Øster Voldgade 10, 1350 Copenhagen K, Denmark
[3]Geological Survey of Canada (Atlantic), Natural Resources Canada, Dartmouth, Nova Scotia B2Y 4A2, Canada
[4]School of Natural and Built Environment, Elmwood Building, Queen's University Belfast, University Road, UK, BT7 1NN, UK
[5]Alfred-Wegener-Institut Helmholtz-Zentrum für Polar- und Meeresforschung, Bremerhaven, Germany

Correspondence: David R. Cox (david.cox@manchester.ac.uk)

Received: 9 June 2020 – Revised: 24 August 2020 – Accepted: 6 October 2020 – Published: 1 December 2020

Abstract. A geohazard assessment workflow is presented that maximizes the use of 3D seismic reflection data to improve the safety and success of offshore scientific drilling. This workflow has been implemented for International Ocean Discovery Program (IODP) Proposal 909 that aims to core seven sites with targets between 300 and 1000 m below seabed across the north-western Greenland continental shelf. This glaciated margin is a frontier petroleum province containing potential drilling hazards that must be avoided during drilling. Modern seismic interpretation techniques are used to identify, map and spatially analyse seismic features that may represent subsurface drilling hazards, such as seabed structures, faults, fluids and challenging lithologies. These hazards are compared against the spatial distribution of stratigraphic targets to guide site selection and minimize risk. The 3D seismic geohazard assessment specifically advanced the proposal by providing a more detailed and spatially extensive understanding of hazard distribution that was used to confidently select eight new site locations, abandon four others and fine-tune sites originally selected using 2D seismic data. Had several of the more challenging areas targeted by this proposal only been covered by 2D seismic data, it is likely that they would have been abandoned, restricting access to stratigraphic targets. The results informed the targeted location of an ultra-high-resolution 2D seismic survey by minimizing acquisition in unnecessary areas, saving valuable resources. With future IODP missions targeting similarly challenging frontier environments where 3D seismic data are available, this workflow provides a template for geohazard assessments that will enhance the success of future scientific drilling.

1 Introduction

When planning an offshore drilling campaign, one of the primary technical concerns that governs site selection is safety (Jeanjean et al., 2005; Mearns and Flin, 1995). The subsurface can be hazardous and is full of unknowns; therefore, it requires the full interrogation of all available data to reduce risks during drilling. Common subsurface geohazards include phenomena related to excess pore pressure such as shallow hydrocarbons, shallow water flows, faulting to shallow depths, mud volcanoes, and pockmarks, all of which can lead to incompetent sediments and seabed instability (Aird, 2010; Jensen and Cauquil, 2013; Ruppelt and West, 2004; Wood and Hamilton, 2002). Identifying these hazards prior to drilling allows for decisions to be made during site selection to either avoid the hazard completely, mitigate it or se-

lect the lowest risk option (Aird, 2010; Jensen and Cauquil, 2013). This process, often termed a geohazard assessment, is integral to drilling success and safety, with its effectiveness often relying on the availability of high-quality data coverage such as seismic reflection, bathymetry and well data.

The importance of geohazard identification is amplified in environments such as deep water, high pressure/high temperature, glaciated margins and frontier petroleum provinces where there is little prior drilling experience (Galavazi et al., 2006; Moore et al., 2007; Weimer and Pettingill, 2007). Within these locations, the frequency and significance of geohazards are often increased, as well as the consequences of accidents (Eriksen et al., 2014; Li et al., 2016). Furthermore, it is often these locations where data coverage and quality are poorest, resulting in a limited subsurface understanding and higher risk to drilling. In the last few decades, exploration for subsurface resources has expanded into more challenging environments due to increased global demand for petroleum products (Mitchell et al., 2012; Poppel, 2018; Suicmez, 2016). This has led to the acquisition of extensive 2D and 3D seismic reflection datasets and industry drilling in frontier areas. The expansion, especially with regards to new 3D seismic reflection data coverage, provides an opportunity to use these data for reasons beyond their original commercial purpose. This includes regional geological mapping and geohazard assessments allowing site identification and de-risking for scientific boreholes (Dutta et al., 2010; Selvage et al., 2012; Hovland et al., 1998).

A geohazard assessment involves the geospatial quantification of drilling hazards, ideally through the use of densely sampled 2D or 3D reflection seismic data (Aird, 2010; Khan et al., 2018; Selvage et al., 2012; Heggland et al., 1996). In the past, the required resolution to detect small but potentially hazardous features could only be provided through dedicated high-resolution site surveys across potential drill sites using such tools as sub-bottom profilers, small-volume airguns, or sparker reflection systems (Jensen and Cauquil, 2013; Parkinson, 2000). Today, the acquisition of large-scale 3D seismic reflection datasets in frontier basins provides spatial coverage that far exceeds most conventional site surveys (Games and Self, 2017). The processing of these datasets has improved sufficiently to provide a vertical resolution that approaches that of a traditional site survey and often provides a horizontal resolution exceeding that of even closely spaced 2D seismic site surveys (Games and Self, 2017; Oukili et al., 2019). Three-dimensional seismic surveys thus minimize the need for additional data, except for particularly complicated areas (Hill, 1996; Selvage et al., 2012; Sharp and Badalini, 2013; Williams and Andresen, 1996; Roberts et al., 1996).

The increased availability of 3D seismic volumes in continental shelf areas often coincides with areas targeted by scientific drilling programmes. These include the International Ocean Discovery Program (IODP) that operates the drilling vessels *Joides Resolution* and *Chikyu* but also national facilities such as the Meeresboden-Bohrgerät (MeBO) of the Alfred Wegener Institute (AWI) and the British Geological Survey (BGS) Rock Drill. For this study, we present data from an Arctic frontier basin that support site selection for a proposed scientific drilling leg under the IODP. IODP has an excellent safety record, achieved through review of proposed sites by panels of international experts, and has drilled within frontier petroleum provinces in the past, with examples such as the early passive margin drilling along the western Atlantic margin (e.g. DSDP Legs 11 and 41; Ewing and Hollister, 1972; Lancelot and Seibold, 1977) and more recently in areas such as the Demerara Rise, offshore Suriname (Leg 207) and the Great Australian Bight (Leg 182) (National Research National Research Council, 2011). Several completed and proposed IODP expeditions report the availability of 3D seismic data within the study area, and it is possible that several others had undocumented access (Table 1). As commercial 3D seismic reflection datasets become more widely available for academic research, there is an opportunity to optimize both the scientific benefits and safety of proposed drilling sites by conducting more comprehensive geological and geohazard assessments. This study, whilst focussed on the hazards associated with IODP Proposal 909 within the north-western Greenland glaciated margin (Fig. 1), provides a geohazard assessment workflow that optimizes drill site selection through the use of 3D seismic data and serves as a template for the improved safety and success of future scientific drilling campaigns using 3D seismic data in frontier areas.

2 IODP Proposal 909

2.1 Setting

IODP Proposal 909 aims to drill a transect of seven sites across Melville Bay offshore north-western Greenland at water depths ranging from 0.5 to 1.9 km (Fig. 1). Here, a thick (>2 km) Cenozoic sedimentary succession overlies a rift basin topography that formed during several stages of Early Cretaceous to Early Paleogene rifting between Greenland and Canada (Altenbernd et al., 2015; Gregersen et al., 2013, 2017; Oakey and Chalmers, 2012). This includes the extensive, elongate inversion structures of the Melville Bay and Kivioq ridges. These ridges separate the deep sedimentary basins of the Melville Bay Graben and Kivioq Basin and contain up to 9 km thick successions of syn-rift (seismic megaunits (mu) mu-G, -F and the lowermost -E) and post-rift (mu-E, -D, -C, -B and -A) sediments (Figs. 1 and 2) (Altenbernd et al., 2015; Gregersen et al., 2013, 2017; Knutz et al., 2015; Whittaker et al., 1997). Mu-E is attributed to the continental drift phase as seafloor spreading commenced in Baffin Bay. The lower part of mu-D is considered to have formed during the final syn-drift stage influenced by compressional tectonics as a consequence of Greenland converging with the North American Plate (Knutz et al., 2020). Deposition of the upper part of mu-D, representing a hemipelagic succession, was

Table 1. IODP expeditions and proposals with 3D seismic data.

Leg/proposal number	Location	Ocean	Status
308	Ursa Basin, Gulf of Mexico	Atlantic	Completed
311	Cascadia Margin, OR, USA	Pacific	Completed
322	Nankai Trough, Japan	Pacific	Completed
372A	Hikurangi Margin, New Zealand	Pacific	Completed
P537A	Costa Rica	Pacific	Proposal
P603CDP	Nankai Trough, Japan	Pacific	Proposal
P857C	Balearic Promontory	Mediterranean	Proposal
P859	Amazon Fan, Brazil	Atlantic	Proposal
P908	Costa Rica	Pacific	Proposal
P909	Melville Bay, Greenland	Arctic	Proposal
P935	The Fram Strait	Arctic	Proposal
P943	West Iberian Margin	Atlantic	Proposal

presumably deposited during a phase of post-drift tectonic relaxation. The mega-units are separated by seismic horizons (hz) e1, d1, c1 and b1 that are generally expressed as regional unconformities.

On the inner shelf margin, thick late Miocene and Pliocene (mu-C and mu-B) marine sediments constitute the uppermost post-rift sequence (Knutz et al., 2015). This includes widespread, late Neogene contourites and their correlative mass transport deposits, down-slope from a major erosional scarp above the Melville Bay Ridge (Figs. 1 and 2). The Neogene sediments are exposed at the seabed on the inner shelf and are progressively buried towards the basin by thick glacigenic packages forming part of mu-A (Fig. 2) (Knutz et al., 2019). The exposure and burial of the Neogene marine successions occurred due to multiple phases of ice sheet expansion since the late Pliocene. Through these glaciations, material was eroded and redistributed, leading to over ~ 100 km of shelf edge progradation and accumulation of the Melville Bay Trough Mouth Fan (MB-TMF) (Figs. 1 and 2) (Knutz et al., 2019; Newton et al., 2017). These glacigenic progradational units likely consist of highly variable sediment lithologies and grain size compositions (Christ et al., 2020; Knutz et al., 2019). The prograding units are separated by unconformities that generate distinct unconformable seismic reflections that express detailed morphologies formed by sub-glacial erosion and deposition, similar to the features observed on the present seabed (Newton et al., 2020, 2017).

The glacigenic succession (mu-A) has been subdivided into progradational units that suggest a minimum of 11 major phases of ice advance and retreat across the shelf since ~ 2.7 Ma. These sub-units (1–11), proposed by Knutz et al. (2019), are used throughout this study (Fig. 2b). Furthermore, the regional stratigraphic framework consisting of seven seismic mega-unit subdivisions (mu-G to -A) (Fig. 2) was proposed after extensive regional mapping of the north-western Greenland continental margin by Gregersen et al. (2013, 2017) and Knutz et al. (2015).

2.2 Scientific drilling objectives

IODP Proposal 909 aims to illuminate the late Cenozoic history of the northern Greenland Ice Sheet (GrIS) and specifically to ascertain the paleo-ice sheet dynamics during past warm climates (Knutz et al., 2018). This will be achieved by recovering drill cores at seven sites along a transect crossing the north-western Greenland margin (Figs. 1 and 2), each recovering key stratigraphic targets (Targets I–VII) to obtain a composite stratigraphic succession from Oligocene/Early Miocene to Holocene (Fig. 2). The overall objective is to examine the range of feedback and forcing mechanisms (oceanic, atmospheric, orbital, tectonic) impacting the GrIS through time – addressing several current themes of the IODP Science Plan (Bickle et al., 2011).

2.3 Site-selection requirements

The seven stratigraphic targets (Targets I–VII) were selected along the south-west–north-east trending regional 2D seismic transect (Figs. 1 and 2) and represent high accumulation rate deposits within the hemipelagic sequence of mu-D, contourite drifts of mu-B and -C, as well as potential interglacial and proximal shelf deposits within the trough mouth fan system of mu-A (Fig. 2). Once stratigraphic targets were defined, specific drill sites were selected. The strategy for site selection was to maximize both the chance of reaching the stratigraphic target and the chance of good core recovery whilst avoiding all identified potential drilling hazards. Additionally, the selection of several alternate sites was required in preparation for unexpected drilling issues or iceberg mitigation management.

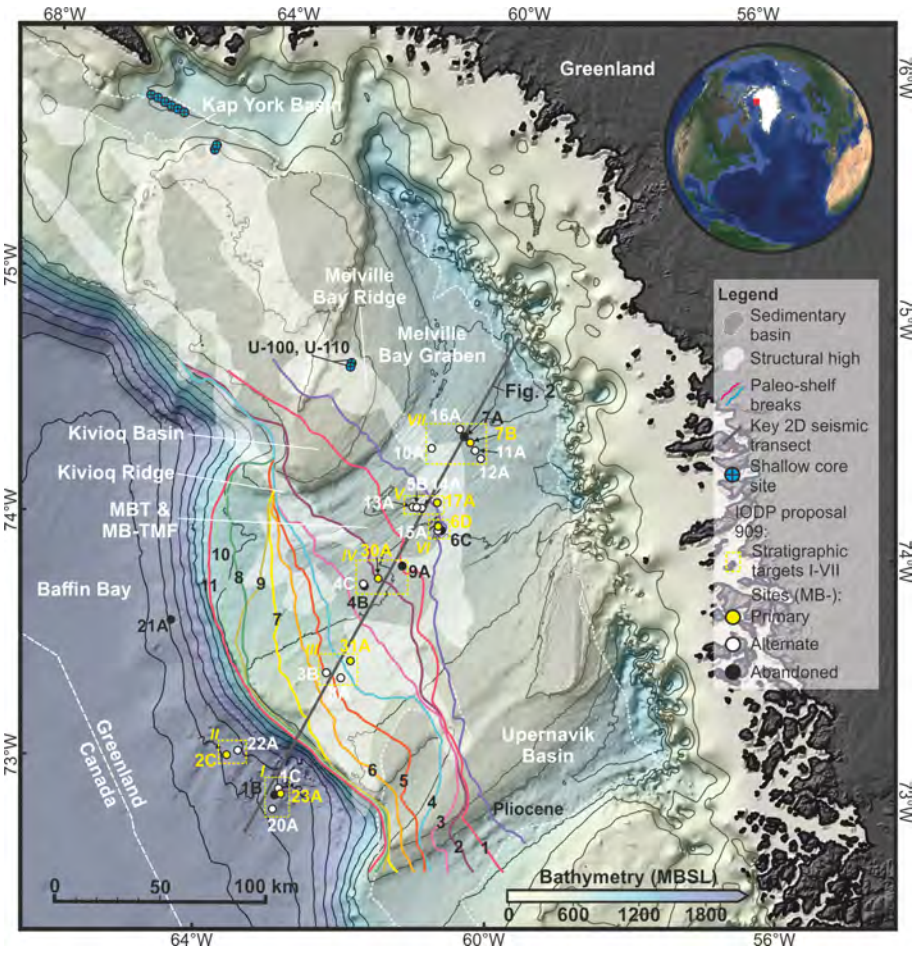

Figure 1. Location map. A bathymetric map of the Melville Bay area in north-western Greenland from Newton et al. (2017), showing the extensive influence of glaciation on the seabed including the Melville Bay Trough (MBT) and Melville Bay Trough Mouth Fan (MB-TMF). The red square on the inset map shows the global location of the bathymetry. Annotations on the map include the distribution of regional rift elements, including sedimentary basins and structural ridges, as well as the location of paleo-shelf break positions of glacigenic prograding units from Knutz et al. (2019). IODP Proposal 909 site locations are shown as well as the associated stratigraphic targets of each site (I–VII). Shallow cores that were drilled by a consortium led by Shell that provide stratigraphic information used within the proposal are also shown (Acton, 2012; Nøhr-Hansen et al., 2018). The location of the key regional 2D seismic transect used for original site selection is also shown and represents the location of Fig. 2.

2.4 Regional geohazard considerations

The north-western Greenland margin is a frontier petroleum province, with potential Cretaceous source rocks identified across the region in shallow cores and outcrop (Fig. 1) (Acton, 2012; Bojesen-Koefoed et al., 2004; Nøhr-Hansen et al., 2018; Núñez-Betelu, 1993) as well as deep unexplored sedimentary rift basins (Henriksen et al., 2009). The area experienced a surge in oil and gas exploration activity between 2007 and 2014, resulting in five exploration licenses being awarded within Melville Bay and the acquisition of extensive 2D and 3D seismic datasets. A shallow coring program was carried out in 2012, but no exploration wells have been drilled. Since then, the identification of a large potential gas reservoir (Cox et al., 2020a) and widespread evidence for shallow gas and gas hydrates (Cox et al., 2020b) further support an active petroleum system, thus underscoring the need for a geohazard assessment study prior to drilling.

Today, marine-terminating glacial outlets do not expand much beyond the coastline, and Melville Bay is generally free of sea ice cover during the summer, allowing access to industry and research vessels (Saini et al., 2020). However, Arctic weather conditions and the potential for icebergs carried northward by the West Greenland coastal current present a challenge to any logistical operations in the area. The environmental factors, considered alongside the possibility of shallow hydrocarbon occurrence and coarse-grained Quaternary sediments indurated by ice loading, makes drilling complicated and highly reliant on site survey data. To evaluate and select coring sites for Proposal 909, available 2D and

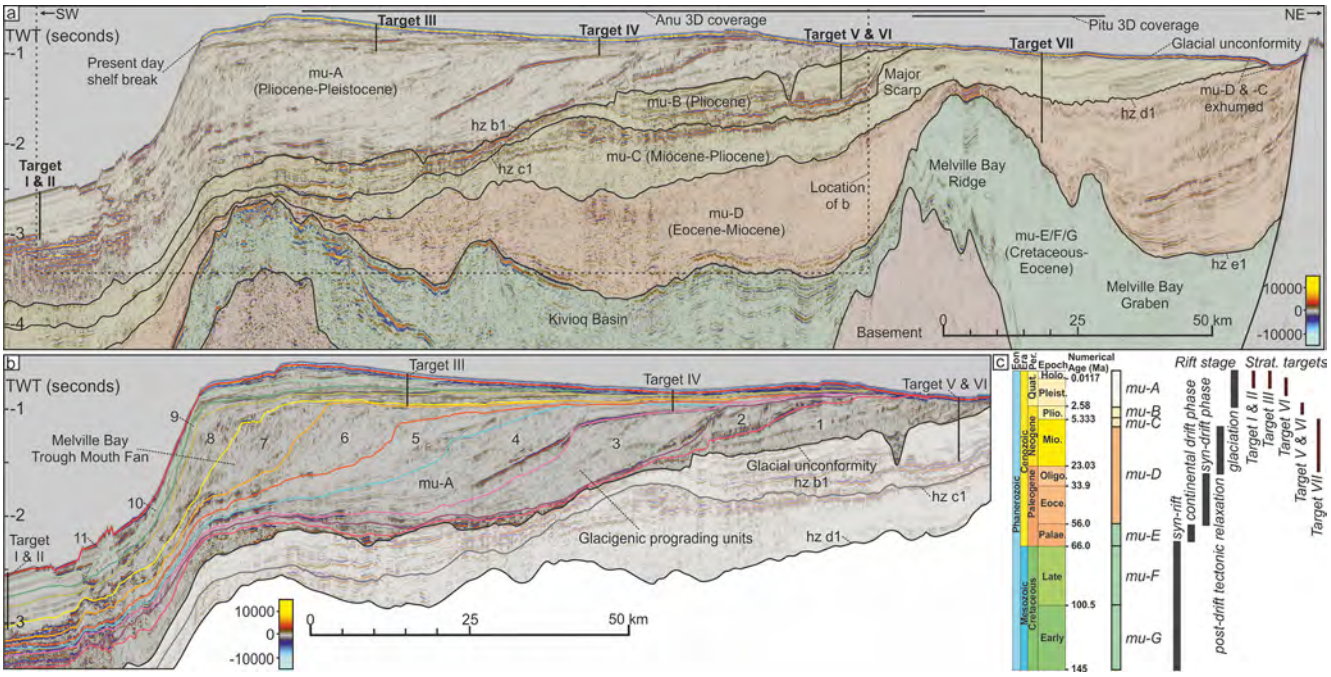

Figure 2. Regional geology. **(a)** A 2D regional seismic reflection line showing the stratigraphy and structure across the shelf. Regionally mapped seismic mega-unit interpretations from Gregersen et al. (2013, 2017) and Knutz et al. (2015) are shown as well as the projected locations of the seven IODP Proposal 909 stratigraphic targets and the comparative coverage of 3D seismic data. **(b)** An enlarged section of the seismic line from A that focusses on the glacigenic wedge that represents the Melville Bay Trough Mouth Fan system, showing the 11 interpreted sub-units of mega-unit (mu)-A from Knutz et al. (2019) as well as the projected location and depth of the IODP Proposal 909 sites. The location of the seismic line is shown in Fig. 1. **(c)** A stratigraphic column displaying seven seismic mega-units and their associated rift stages, as well as the expected age of the stratigraphy that comprises each of the stratigraphic targets (I–VII).

3D seismic reflection data were used to conduct a comprehensive geohazard assessment that maximized the chance of safe drilling and successful core recovery.

3 Data

The seismic data used within this study include four separate surveys that were acquired between 2007 and 2019 (Table 2). All data used were provided in SEG normal polarity with a downward increase in acoustic impedance represented by a red positive peak and a downward decrease in acoustic impedance represented by a blue negative trough (Fig. 2). The regional 2D data used in this study form part of four surveys that were acquired by the geophysical company TGS (2007–2010) as part of the Baffin Bay 2D regional dataset. The dataset was used to help understand the regional geology and map the spatial distribution of stratigraphic packages that represent drilling targets (full extent of the regional 2D survey shown by Gregersen et al., 2019 – Fig. 1). From the TGS 2D data, a subset of seven lines crossing the Melville Bay shelf was used directly within the site-selection process (Fig. 3, Table 2).

Two 3D seismic surveys represent the principle data used for geohazard detection within this study (Fig. 3). The first is the Pitu survey that was acquired by Cairn Energy PLC in 2011 (Table 2). This survey was also provided as a pre-stack depth migration (PSDM) volume. The survey was re-processed by CGG in 2013 to provide the Pitu HR (high-resolution) survey, which is a subset of the full volume with increased spatial and vertical resolution (Table 2). The second 3D survey, the Anu survey, provides extensive 3D coverage towards the shelf edge and was acquired by Shell in 2013 (Fig. 3). In 2019, a new ultra-high-resolution (UHR) survey, the LAKO UHR survey (LAKO is an acronym for the research vessel *HDMS Lauge Koch*), was acquired across several preliminary site locations through collaboration between the Geological Survey of Denmark and Greenland and Aarhus University (Pearce et al., 2019) (Table 2 and Fig. 3). The aim was to provide UHR imaging of the upper 500 ms below the seabed in order to supplement the existing industry seismic data within the pre-defined target areas. In addition, several longer transects were obtained that could provide additional seismic–stratigraphic information and add to the reconnaissance of additional sites. Eight lines from the UHR survey were used to characterize drill sites located within the areas of 3D seismic coverage (Fig. 3).

Table 2. Acquisition parameters and survey statistics for the four seismic surveys used within this study. A dash (–) represents a parameter that is not applicable for that survey. The Pitu HR parameters can be read from the Pitu survey. Abbreviations used within the table include two-dimensional (2D), three-dimensional (3D), ultra-high-resolution (UHR), reprocessed (repro.), number (No.), average (Avg) and two-way time (TWT). Units used include metres (m), kilometres (km), milliseconds (ms), seconds (s) and hertz (Hz).

Acquisition parameter		Seismic survey				
		Regional	Pitu	Pitu HR	Anu	LAKO UHR
Survey type		2D	3D	3D	3D	UHR 2D
Date acquired		2007–2010	2011	2013 repro.	2013	2019
Area/length used		2076 km	1672 km^2	1135.5 km^2	8700 km^2	306 km
No. of vessels		1	1	–	2	1
Pop interval		25 m	25 m (flip-flop)	–	25 m (flip-flop)	5–6 m
Source depth		8 m	8 m	–	8 m	3 m
Source separation		–	50 m	–	100 m	–
Streamer length		6000 m	10 × 7050 m	–	6 × 7050 m	150 m
Streamer separation		–	100 m	–	200 m	–
No. of channels		480	564	–	564	40
Receiver spacing		12.5 m	12.5 m	–	12.5 m	3.125 m
Sampling rate		2 ms	4 ms	2 ms	2 ms	1 ms
Sail line separation		–	1 km	–	600 m	–
No. of 3D sail lines		–	93	–	118	–
Bin spacing	Inline	–	25 m	12.5 m	6.25 m	–
	Crossline	–	12.5 m	6.25 m	50 m	–
Fold		120	70	–	70	12.5
Domain		TWT	TWT/depth	TWT	TWT	TWT
Provided depth (down to)		9 s	6.5 s/10 km	5 s	7.5 s	1.4 s
Depth of given resolution		1200 ms	1200 ms	1200 ms	1200 ms	900–1100 ms
Avg dominant frequency		40 Hz	55 Hz	90 Hz	45 Hz	120 Hz
Dominant wavelength*		50 m	36 m	22 m	44 m	16.5 m
Vertical resolution		12.5 m	9 m	6 m	11 m	4 m

* The dominant wavelength was calculated using an average velocity of 2000 m s^{-1}.

Depth conversion

Depth conversion was required to provide accurate estimates of seismically defined drill target depths in metres. Velocity information was provided from industry wells drilled by Cairn Energy PLC $\gtrsim$ 300 km south of the transect (location shown in Gregersen et al., 2019 – Fig. 1), from shallow core sites U0100/110 (Fig. 1) and from an interval velocity cube that was provided over the Pitu survey area (Figs. 3 and 4). The interval velocity cube was created from seismic velocities during seismic processing through the application of a Kirchhoff pre-stack TTI depth migration (PSDM) that used a bin size of 12.5 × 25 m and a migration half aperture of 4500 m (Fig. 4). This process produced a depth-converted version of the Pitu 3D survey. The interval velocities and the depth cube, however, have not been calibrated to measured depth data, due to large distances to the closest well ($\gtrsim$ 300 km), and likely contain some error.

Therefore, average velocities were determined using all of the velocity data available (mentioned above) and were then extrapolated across the study area using a comparison of the potential lithology and depositional setting of the sediments as well as their general depth. Linear time–depth equations were also generated for sites within the glacigenic wedge to consider elevated compaction and velocity due to ice loading. Velocities from this linear trend were then compared against the original estimated average velocities and interval velocities from the velocity cube to calculate the potential error (often $\sim$ 100 m). This error was used to adjust the final metric depth targets to minimize overestimation and avoid drilling into deeper, potentially hazardous intervals.

4 Geohazard assessment workflow

The following geohazard assessment workflow was used to select drill sites that represent the lowest possible risk whilst meeting the scientific objectives (Fig. 5). The workflow considers the increasing availability of data that are typical through a project's progression, starting with regional 2D seismic data to understand the regional geology and pick initial stratigraphic targets and sites. Three-dimensional seismic data are then used to conduct a more detailed interrogation of

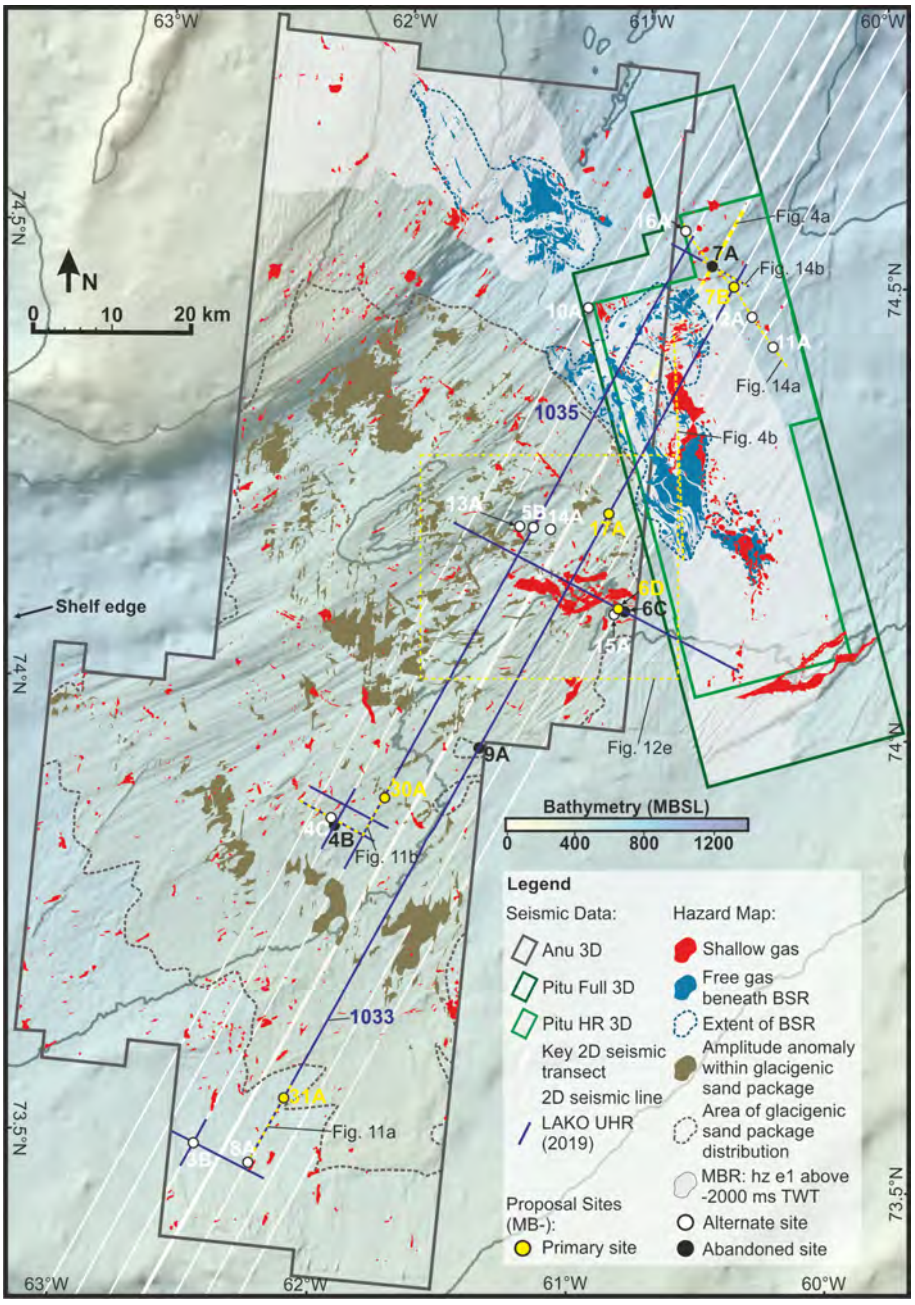

Figure 3. A fluid hazard and data map of the study area displaying the regional bathymetry from Newton et al. (2017) as well as the location of all seismic data used within the Proposal 909 study. The locations of potential fluid anomalies were identified and mapped via the shallow gas detection process within the geohazard assessment workflow. Active and abandoned IODP Proposal 909 sites that exist within the 3D seismic extent are shown as well as the location of the Melville Bay Ridge (MBR) and Figs. 4a, b, 11a, b, 12e, 14a and b.

the subsurface in order to delimit geohazards within the proposal area and guide site selection and minimize risk. Finally, additional data, in this case 2D UHR seismic data, are used in collaboration with the 3D seismic to fine-tune the selected sites to ensure they represent the most suitable and safest locations possible.

4.1 Seabed

The first step of the 3D seismic geohazard assessment is to map the strong, positive amplitude event that represents the seabed across the area of 3D coverage (Fig. 6). This provided the seabed depth, firstly in TWT and subsequently in metric depth, after a conversion using a typical seawater velocity of 1480 m s^{-1} (based on the Pitu interval veloc-

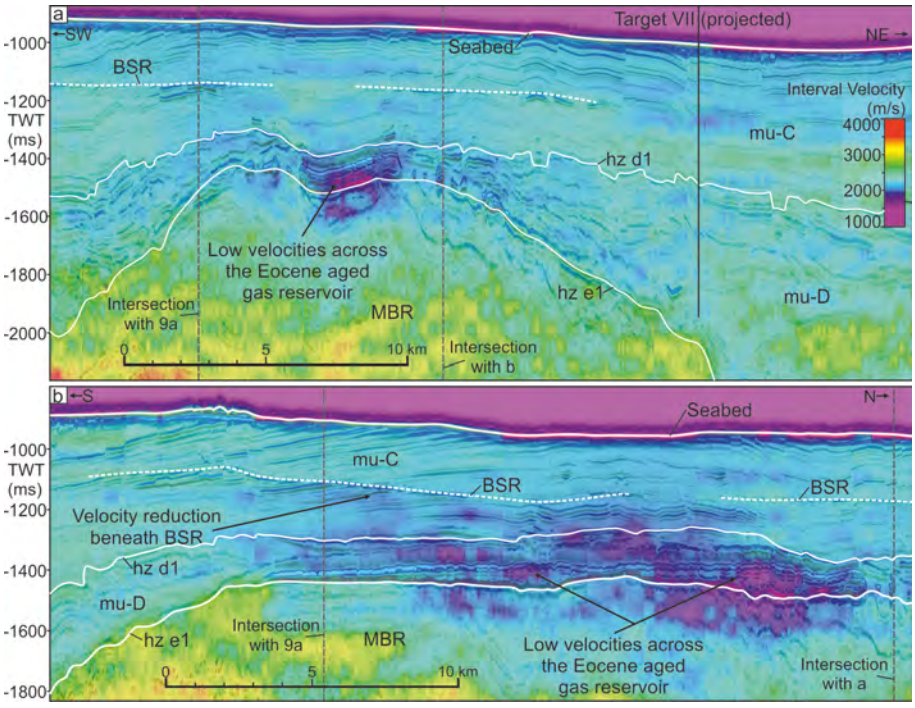

Figure 4. Interval velocities created through Kirchhoff pre-stack TTI depth migration (PSDM) for the Pitu survey overlaid on seismic reflection dip **(a)** and strike lines **(b)** in two-way time across the Melville Bay Ridge structure. Velocity reduction likely due to the presence of gas can be observed in the location of the Eocene-aged reservoir on top of the ridge as well as beneath a bottom-simulating reflector (BSR) within the free gas zone. The locations of panels **(a)** and **(b)** are shown in Figs. 3 and 9.

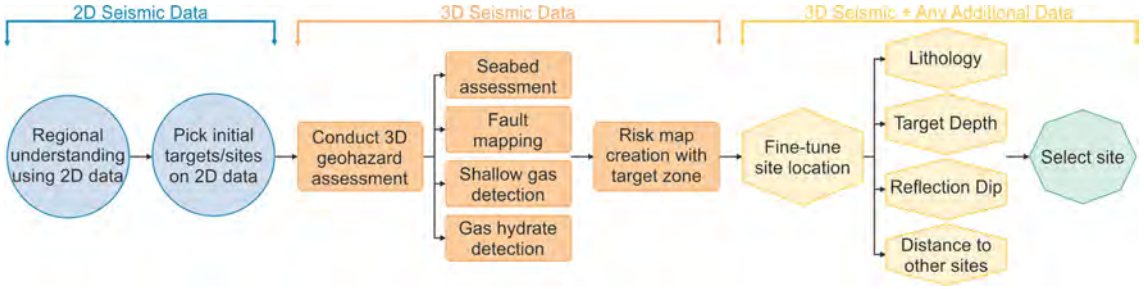

Figure 5. A workflow diagram that outlines both the steps conducted within the geohazard assessment leading to site selection and how the differing seismic data types were used throughout the process. This workflow should be used as a guide for future geohazard assessments using 3D seismic data but is not fully exhaustive and can be amended to fit different datasets and locations through the addition of extra steps that fulfil the requirements of future projects.

ity cube) (Fig. 6a). A bathymetric compilation from Newton et al. (2017) provided an additional high-resolution image of the seabed morphology. The mapping, supported by the bathymetry data, identified a wide range of seabed features that have been interpreted as being of glacial origin, created by recent shelf glaciations, including lineations, ridges, iceberg scours and near-circular depressions interpreted as iceberg pits (Fig. 6; Newton et al., 2017). These features can create localized areas of high-dip and highly compacted sediment and should be avoided to prevent instability of the coring equipment on the seabed (Bennett et al., 2014).

A structural dip attribute was extracted onto the mapped seabed surface to identify areas of high seabed dip (Fig. 6b). Filtering of the attribute allowed the severity of dip to be separated into areas of low (0–2°), medium (2–5°) and high (5°+) dip, which relates to areas of low, medium and high risk respectively. The seabed dip–risk cut-offs are used here primarily to help avoid glacial geomorphological features on the seabed, but this technique is applied in commercial geohazard assessments to consider the effect of the seabed structure on the critical failure of slope sediments as well as seafloor infrastructure tension and strength (Dan et al., 2014;

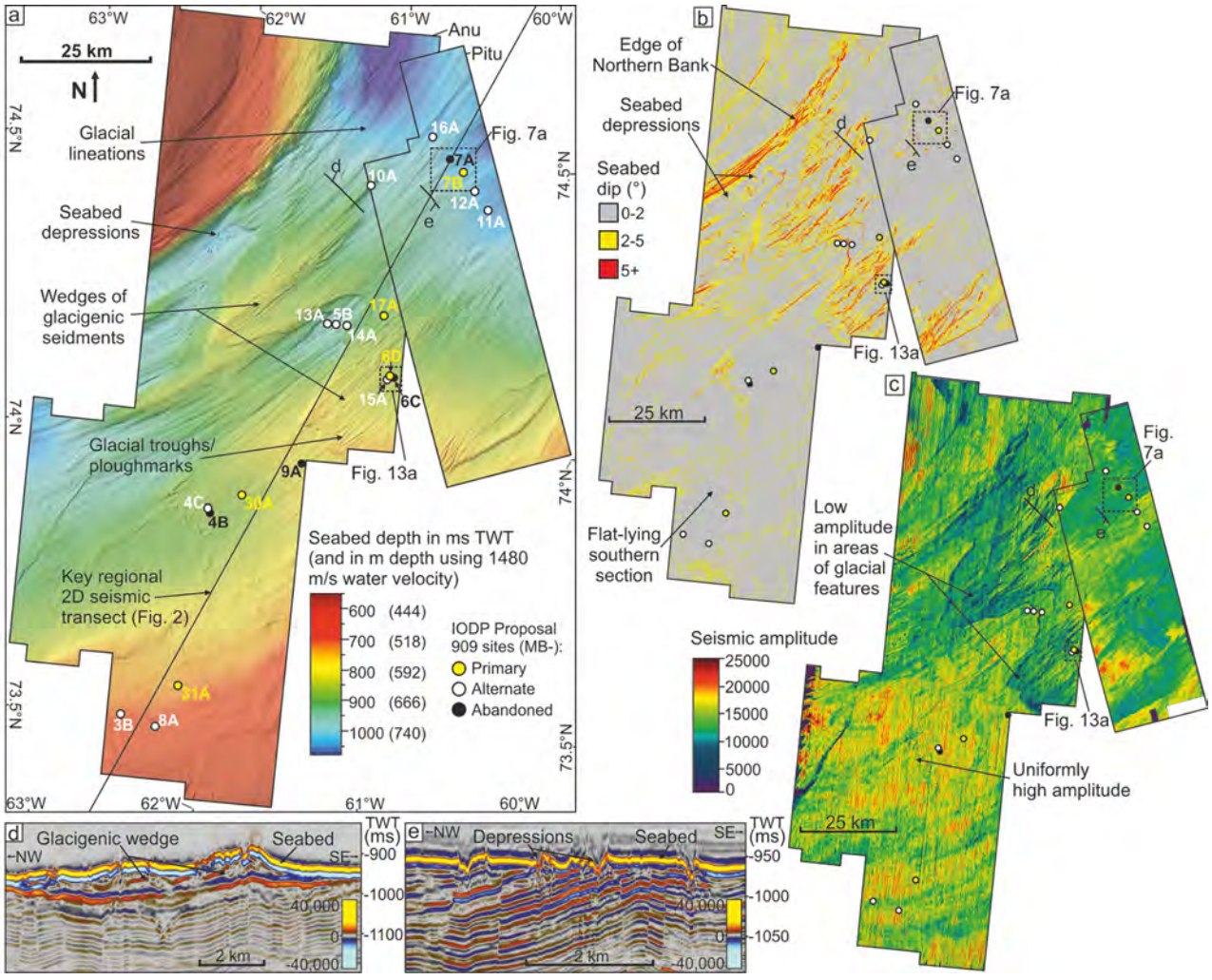

Figure 6. Seabed mapping. **(a)** A seabed structure map across the 3D seismic coverage shown in both two-way time and converted metric depth, with the bathymetry data from Newton et al. (2017) shown beneath. **(b)** A dip attribute map across the 3D seismic coverage that has been filtered to display features by dip severity, with colours amber and red relating to moderate (2–5°) and high (5+°) risk respectively. **(c)** An amplitude attribute extraction map at the seabed surface across the 3D seismic extent showing the variation in amplitude between areas dominated by or free from glacigenic features. The locations of both active and abandoned IODP Proposal 909 sites are shown in panels **(a)**–**(c)** along with the locations of panels **(d)** and **(e)**, Figs. 7a and 13a. **(d)** A seismic cross section from the Anu survey showing an example of a glacigenic wedge which is topped by glacial lineations. **(e)** A seismic cross section from the Pitu HR survey showing the unconformable nature of the seabed as well as seabed depressions that likely represent iceberg pit marks (cf. Brown et al., 2017).

Vanneste et al., 2014). The cut-offs selected are relatively low compared to other studies (e.g. Haneberg et al., 2015), but these were chosen to remain cautious and decrease potential risk, as much of the study area is relatively flat lying and therefore remains classified as low risk (Fig. 6b). Applying a cautious approach allows for steeper-dipping sections to be documented for further analysis should the underlying stratigraphy be potentially suitable for drilling – e.g. steep dip does not necessarily preclude drilling, but these bins allow for areas requiring greater consideration to be highlighted. Seismic amplitudes were also extracted onto the seabed surface (Fig. 6c). Extreme high or low amplitudes were shown to coincide with either glacial depositional features (such as Fig. 6d) (low amplitudes) or iceberg pit marks/depressions (high amplitudes) (Fig. 6e), supporting the inferred composition of elements represented by areas of high dip. Away from these features, the seabed amplitude is relatively uniform.

4.2 Faults

Fault mapping within the 3D survey area involved the use of the variance seismic volume attribute (coherency within other software packages) to image discontinuities, viewed mainly through time-slice intersections (z slice) (Fig. 7).

Faults in the immediate area of the drill sites were manually mapped, including small faults belonging to a dense polygonal fault system within the post-rift stratigraphy of mu-D and -C (mainly within the Pitu area) (Cox et al., 2020a). Several deep-seated faults are observed extending close to the seabed (Fig. 7b), potentially connecting deeper fluid pressures to the shallow stratigraphy, which would represent a significant drilling hazard. Therefore, in areas close to a proposed site, fault characteristics were assessed based on their vertical extents, offsets and possible connections to deeper seismic anomalies (as shown in Fig. 7). High risks were associated with faults displaying connections to deeper anomalies; however, it was recommended to avoid all fault penetrations where possible to maximize the chance of good and stratigraphically continuous core recovery.

4.3 Shallow gas detection

Gas-related seismic anomalies are expected to display "bright", anomalously high negative amplitudes due to gas fluids causing a reduction of the bulk modulus (due to the extremely low density of gas) causing a significantly negative acoustic impedance contrast across the boundary at the top of the gas-bearing reservoir (Cox et al., 2020c; Hilterman, 2001; Nanda, 2016). A positive seismic amplitude, often of comparable amplitude, is often associated with the gas–oil–water contact or the base of the reservoir if it contains anomalous fluids across its entire vertical extent. For thin reservoirs filled with gas, the response is often a highly asymmetric high negative to high positive doublet (Cox et al., 2020c; Raef et al., 2017). The presence of oil can cause a similar but often much reduced seismic anomaly. Due to these phenomena, the 3D seismic data were investigated to understand the seismic character of fluid-related anomalies within the study area. This included the physical character of anomalies, which were often isolated bright spots or brightening along single horizons (Fig. 8), as well as their spatial and stratigraphic distribution, which was widespread within all levels of the post-rift stratigraphy (mu-D to -A) and focussed around the Melville Bay Ridge (Cox et al., 2020b). The seismic amplitude range of the bright anomalies was also analysed to aid amplitude extractions. The analysis identified that an amplitude of negative (–) 10 000 or above likely represented a fluid anomaly, although some dim anomalies can occur beneath this limit, and this was considered during the filtering of results (Fig. 8c). Dimmer anomalies can be attributed to poorer reservoir quality or thin bed tuning effects, whereas amplitude is expected to be insensitive to gas saturation when this exceeds 10 % of the pore volume (e.g. Hilterman, 2001).

Once this initial analysis was complete, the information was used to automatically extract amplitude anomalies from the 3D seismic data above the defined threshold that likely represents hydrocarbon occurrences. This process used a series of minimum amplitude extraction windows that cut proportionally through the stratigraphy, extracting the most negative amplitude at every seismic trace (Fig. 8). The amplitude extraction result was then filtered to remove the majority of data and highlight just the most negative amplitudes (those that likely represent fluid anomalies) (Fig. 8c).

The stratigraphy was split into two units for the extractions, the first between the seabed and seismic horizon (hz) d1 with 10 proportional extraction windows (each ∼ 50 ms TWT thick) and the second between hz d1 and hz e1 with 5 windows (each ∼ 35 ms TWT thick) (Fig. 8). Using relatively narrow windows provided some depth control for each anomaly, which can be displayed through colour coding (Fig. 8a), instead of having a wide depth estimate that is as thick as the seismic mega-unit. This was important when selecting a shallow drill site where many of the deeper anomalies well below the target are less relevant. It also allowed the windows to be displayed separately, i.e. just for a particular depth zone. Furthermore, the resulting amplitudes for each window were often filtered differently (often using opacity rendering) in an attempt to highlight the anomalies at that level and also to try and remove unwanted amplitudes that may mask fluid events, such as naturally bright horizons, data acquisition footprints (near the seabed) and amplitudes interpreted as not representing fluid anomalies.

Once the data had been filtered, the individual scrutiny of each anomaly was conducted to determine whether that anomaly was in fact fluid-related or whether the anomalous amplitude may instead represent something else (such as the high amplitude causing features mentioned above). This evaluation is subjective to some degree, and this should be considered in the final result. Nonetheless, this evaluation was important as it stops potentially credible locations from being ruled out due to non-fluid-related anomalies and may also highlight other dimmer amplitude anomalies that were missed. This whole process was iterative and involved returning to the attribute extraction or filtering stage to adjust the parameters when required to ensure all potential anomalies were considered.

Once the result was finalized, the locations of the remaining amplitudes were used both within the interpretation software directly and within GIS software for spatial analysis. The remaining amplitudes were either converted into 2D automatic boundary polygons or extracted as 3D geobodies to allow efficient visualization and to aid the creation of multi-layer hazard maps used within the site-selection process (Fig. 3).

4.4 Gas hydrate detection

Bright fluid anomalies were identified hosted within inclined, likely sandy, strata that terminate abruptly at a certain depth beneath the seabed (Fig. 9) (Cox et al., 2020b). This level, characterized by a dim, negative amplitude reflection that cuts across the stratigraphic layering in a manner that mirrors the seabed topography, represents a bottom-simulating

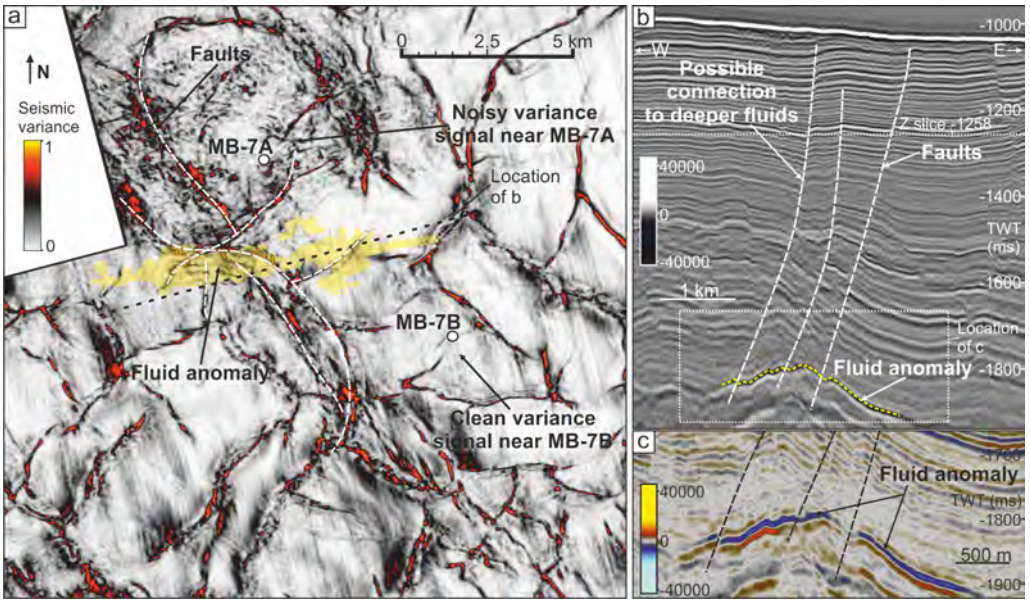

Figure 7. Fault mapping. **(a)** A time-slice intersection (z slice) through the Pitu HR survey displaying the variance structural attribute to highlight fault locations at a depth of −1258 ms two-way time. Interpreted fault planes (white dashed lines) are shown as well as the spatial distribution of a potential hydrocarbon fluid anomaly that may be in pressure communication to shallower depths due to the intersection with fault planes. IODP Proposal 909 sites MB-7A (abandoned) and MB-7B (primary) are also shown as well as the location of panel **(b)**. The location of panel **(a)** is shown in Fig. 6a. **(b)** A seismic cross section from the Pitu HR survey in black and white to emphasize faults, which displays interpreted fault planes and the location of a deeper fluid anomaly as well as the location of panel **(c)**. **(c)** An enlarged seismic cross section from the Pitu HR survey that shows the seismic character of the deeper fluid anomaly.

reflector (BSR). Such cross-cutting features have been interpreted as representing the base of a zone containing stable gas hydrates, below which free gas can become trapped, resulting in a bright negative cross-cutting reflection that may be discontinuous or continuous depending on the degree of porosity and permeability variations of the host strata (Fig. 9) (Berndt et al., 2004; Kvenvolden, 1993).

BSR features were mapped within the 3D seismic surveys to identify an area of 537 km^2 that likely contains gas hydrates (Figs. 3 and 9). Bright, negative amplitude free gas anomalies are observed trapped beneath the BSR boundary and suggest a free gas column of up to 50 m thick (Fig. 9c). However, away from the bright free gas anomalies, mapping of the BSR became difficult due to an intermittent and dim BSR reflection. Therefore, due to the relationship between the BSR and the seabed, a pseudo BSR surface was created to aid the identification of this boundary in other areas of the survey (Fig. 9). This pseudo surface was based on empirical evidence from obvious BSRs in the data (Fig. 9c) and was created by cross-plotting the thickness of the GHSZ in areas containing these BSRs against the seabed depth. The best fit line between these two data was then used to create a surface at the expected BSR depth across the entire 3D survey extent, a surface that tolerates variations in stability zone thickness in response to changes in seabed depth.

This guide surface was used to focus BSR reconnaissance throughout the 3D seismic data. It was also used to identify additional areas of free gas (a much higher risk) that may be trapped at the base of the gas hydrates (Figs. 3 and 9). This involved combining the extensive pseudo surface with the BSR map and producing a minimum amplitude extraction for a 20 ms window across this surface (Fig. 9b). This technique, along with the manual reconnaissance of the seismic character at the pseudo surface depth, resulted in the identification of a previously undiscovered BSR as well as trapped free gas in the north of the Anu survey (Fig. 9a and b).

South of the Pitu survey, a cross-cutting negative amplitude reflection has also been interpreted as potentially representing a BSR; however, this feature exists ∼ 100 ms TWT deeper than the guide surface (Fig. 9a, d and e). This potential BSR is not as obvious as in other areas, but multiple stacked bright anticlinal anomalies exist within the underlying stratigraphy that may represent the upward flow of hydrocarbon fluids that are subsequently trapped beneath the BSR boundary (Fig. 9d and e). Rapid changes in BSR depth over short distances can occur and have been observed in other areas, e.g. the Lower Congo Basin (Andresen et al., 2011). However, as the seabed depth and shallow sediments are relatively consistent with the main BSR area a short distance away (< 5 km) (Fig. 9a), a significant variation in the phase boundary depth is unlikely. Therefore, these deeper anomalies could instead represent more traditionally trapped gas unrelated to hydrates (Fig. 9d and e).

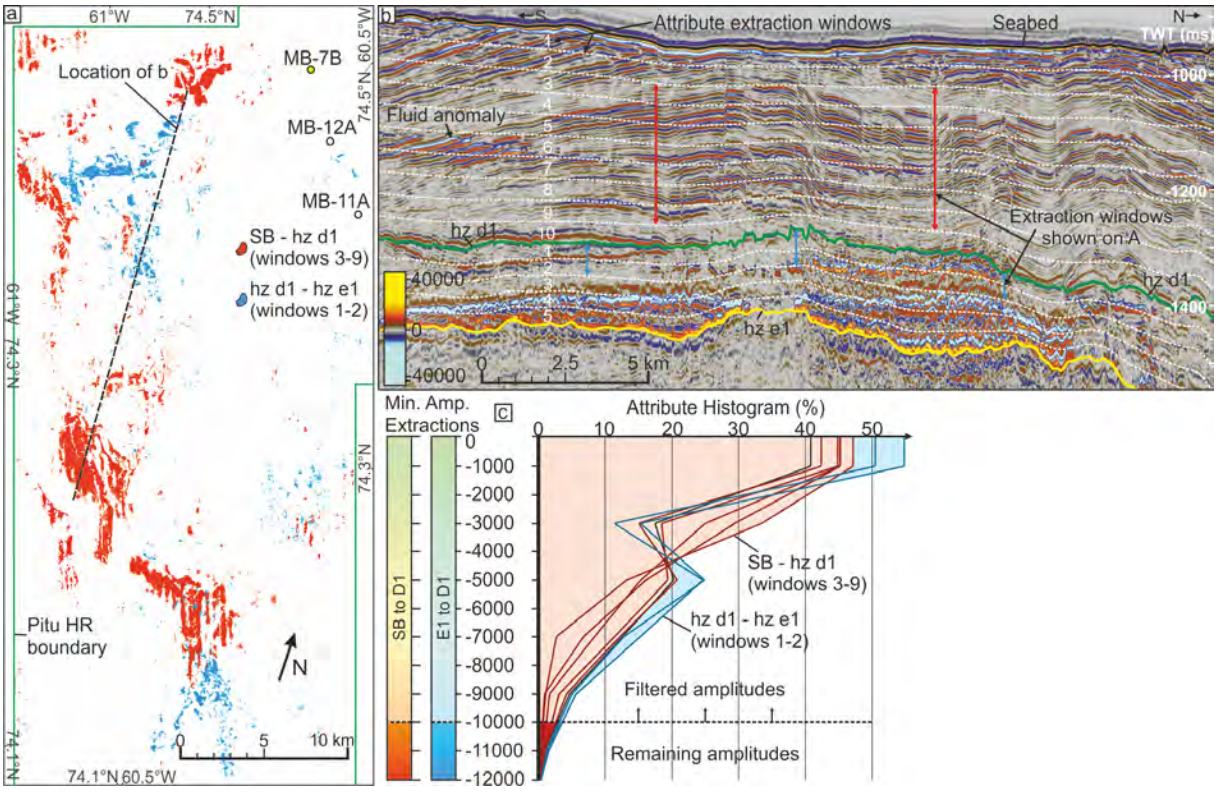

Figure 8. Shallow gas detection. **(a)** A 2D map view of several overlaid windowed minimum amplitude extractions from the Pitu HR survey that have been filtered to only display amplitudes that are greater than −10 000 and likely represent fluid anomalies. The extracted amplitudes have been colour coded to distinguish between windows from different mega-unit packages, giving a sense of anomaly depth, a technique which can also be applied to individual windows. The windows displayed are shown in both panels **(a)** and **(b)**. The IODP Proposal 909 sites in this area are also shown in locations that avoid the potential fluid anomalies as well as the location of the seismic line used in panel **(b)**. **(b)** A seismic cross section from the Pitu HR survey that highlights the main horizons used to create the proportionally distributed extraction windows. Several seismic anomalies that will be identified within the extractions are also shown along with the specific windows displayed in panel **(a)**. **(c)** A histogram that shows the distribution of amplitudes from the selected extraction windows shown in panels **(a)** and **(b)**. The histogram and the colour bars show how the amplitudes have been filtered to only show the extreme values which are more likely to represent fluid anomalies. These amplitude cut-offs can be altered for specific windows to either display or hide certain amplitude ranges.

4.5 Risking

Once the main geohazards described above were analysed, the individual results were combined to create a composite hazard map that was used directly for site selection (often known as a common risk segment – CRS – map) (Hill et al., 2015) (Fig. 10). The hazards considered within this process (seabed features, shallow gas and gas hydrates) were rated as either moderate risk, such as low dip glacial seabed features or areas containing gas hydrate (without free gas), or as high risk, such as seabed depressions or shallow gas occurrences. These features were then colour coded using a traffic light system, with red representing high risk, amber representing moderate risk, and green representing low risk. After initial site locations were proposed, significant faults were mapped in more detail around the site and subsequently added to the map to assess whether alterations were required.

All areas surrounding the moderate and high risk features could be considered minimum risk (green), but an attempt was made to maintain a minimum radius from each site location of 500 m to the nearest identified hazard. For each stratigraphic target (I–VII), a target seismic horizon and the maximum tolerable drilling depth to reach that horizon were defined, creating a more localized target zone where the site had to be located. These target zones were overlaid on the CRS maps to create the green, minimum risk zone, which highlighted the area that could be drilled safely and still reach the desired stratigraphic target within the tolerated depth (Fig. 10).

4.6 Site selection: geohazards and lithology

The geohazard assessment and CRS map creation provided a minimum risk target zone to guide safe site selection. However, several other logistical and geological factors had to

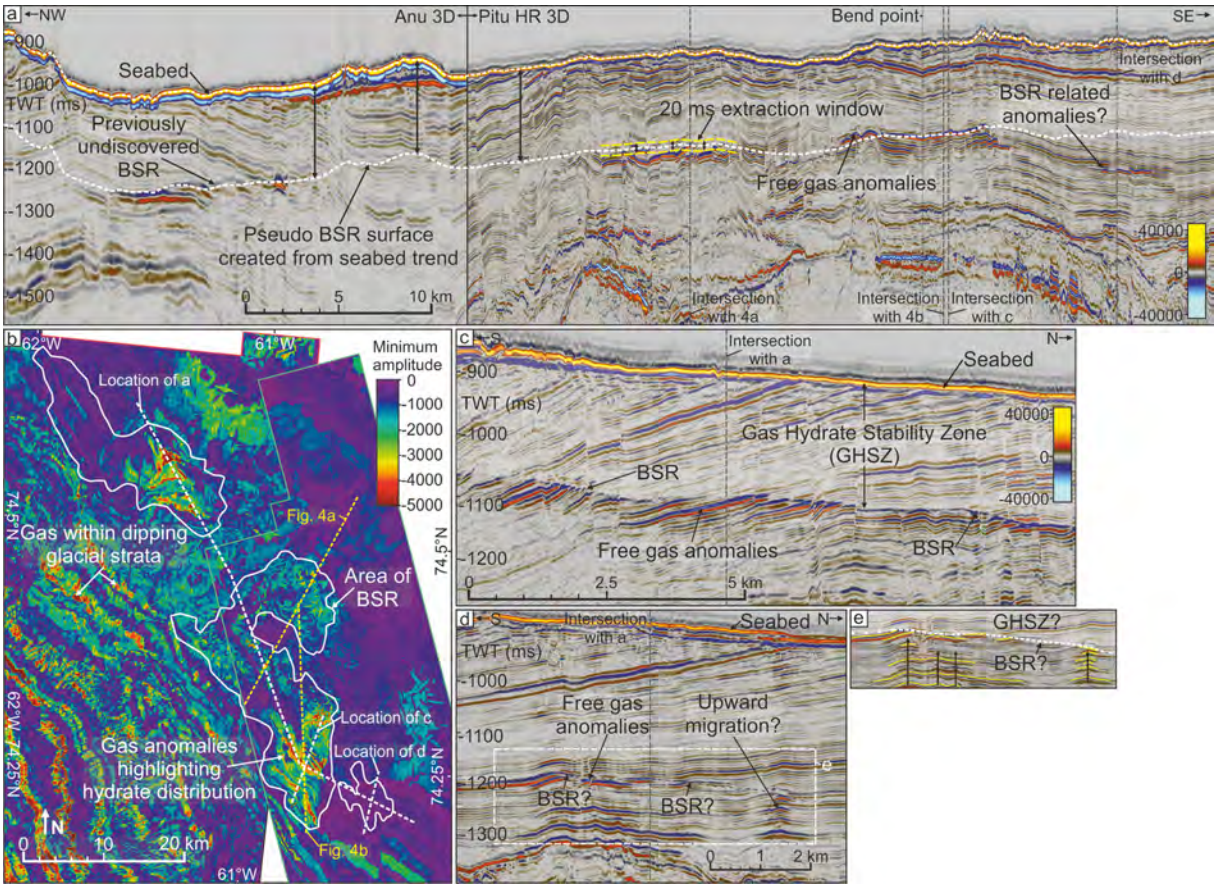

Figure 9. Gas hydrate detection. **(a)** A composite seismic cross section through the Anu and Pitu HR surveys showing the distribution and seismic character of the identified BSR in the study area. The white dashed line (ca. 200 ms below seabed) at the BSR represents the pseudo BSR surface. **(b)** A 2D map view of a minimum amplitude extraction across the pseudo BSR surface showing the distribution of bright negative amplitudes that likely represent trapped free gas. The mapped area of the BSR is shown as well as the locations of the seismic lines used in panels **(a)**, **(c)**, and **(d)**, Fig. 4a and b. **(c)** A seismic cross section from the Pitu HR survey confirming the presence of the BSR along with multiple free gas anomalies trapped beneath it. **(d)** A seismic cross section from the Pitu HR survey across the area containing a potential deeper BSR (ca. 300 ms below seabed). The location of panel **(e)** is also shown. **(e)** A zoom-in of a section of panel **(d)** showing the location of fluid anomalies (yellow lines) beneath the potential deeper BSR and much thicker gas hydrate stability zone (GHSZ).

then be considered whilst fine-tuning the final location of each site.

This included an assessment and interpretation of the seismic character to give an idea of the potential lithology of the sediments (following work by several authors on lithology interpretations from seismic data, e.g. Sangree and Widmier, 1979; Frey-Martínez, 2010; Hilterman, 2001; Badley, 1985; Stewart and Stoker, 1990). An attempt was made to avoid certain seismic features, such as (1) chaotic packages of reflections, often down-slope from erosional scarps, that likely represent mass transport deposits; (2) structureless to chaotic, near-surface packages that may represent boulder-prone glacigenic tills or debris flows; (3) high, positive amplitude reflections at the top of glacigenic progradational units that may represent paleo-seabeds that have been indurated due to ice loading during the following glacial period; and (4) relatively high, negative amplitude reflections that are often wavy (within mu-B or -C) or laterally continuous within mu-D that may represent the top of sand packages. These seismically inferred lithologies were considered risks and avoided due to the likelihood of poor core recovery and the possibility of the coring equipment becoming stuck in the hole.

The stratigraphic dip (on seismic) was also considered in an attempt to try and target flat horizons to maximize the chance of good core recovery. Finally, the site priority (either primary or alternate) had an influence on location, as alternate sites attempting to reach the same stratigraphic target as the primary one were required to be sited a minimum of 5–10 km away from the next nearest site (primary or alternate) if possible to manage the iceberg risk. After considering these additional factors within the low-risk zone provided by the CRS map, a suitable drilling location was selected.

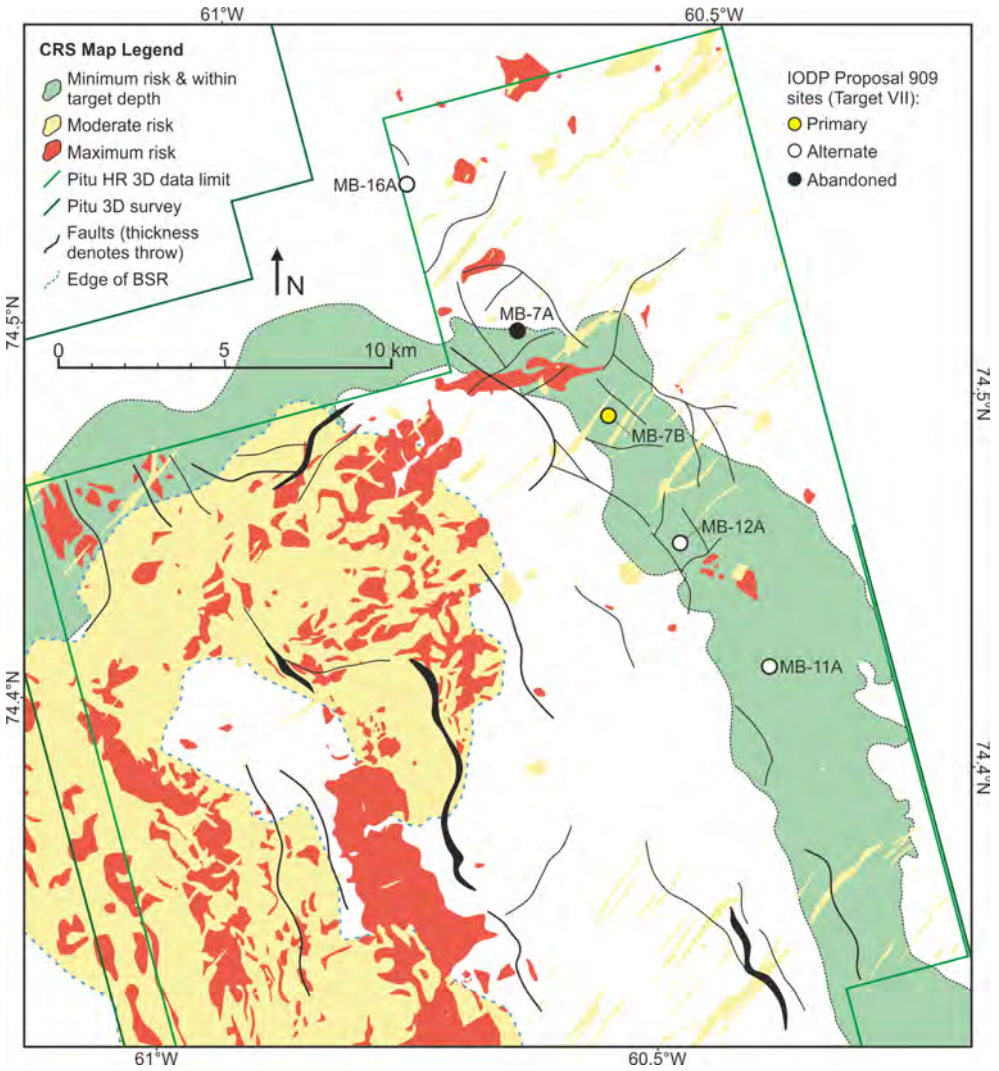

Figure 10. A common risk segment (CRS) map showing the green, minimum risk, depth target zone for Target VII where sites can be located safely whilst meeting the stratigraphic objectives. This CRS map was used to guide the site selection and abandonment of the shown Target VII sites. Similar CRS maps were also created to guide site selection and abandonment for the other stratigraphic targets within 3D seismic coverage (Targets III–VI).

5 Assessment results – Proposal 909 sites

Seven primary and 15 alternate sites have been identified for the 909-Full2 proposal (Figs. 1 and 3) (Knutz et al., 2018). These sites cover the seven stratigraphic targets (Targets I–VII) that have been identified in order to meet the scientific objectives of the drilling proposal (Figs. 1 and 2). The selection of these sites was based on multiple data that have become available as the proposal developed since its inception in 2016. Initially, the regional 2D seismic data represented the principle source of information for identifying drilling targets along the key seismic transect (Fig. 2). Since then, the majority of site selections have been refined based on industry 3D seismic volumes and the LAKO UHR seismic data that were collected in 2019 (Table 2). In the final iteration of the proposal, none of the proposed sites exists in an area only covered by regional 2D seismic reflection data (Table 3). The final review resulted in several site alterations and additions as part of Proposal 909-Full2 to accommodate alternate site requirements for iceberg-prone waters. This version was subsequently accepted by the Scientific Evaluation Panel and by the Environmental Protection and Survey Panel of IODP.

The coverage of the three seismic data types (2D, 3D and UHR) varies across the sites, and their availability restricts which data can be used within the site-selection process (e.g. Target I and II sites which are outside of 3D seismic coverage; Fig. 1 and Table 3). However, for all sites located within the 3D seismic extent, these data and the geohazard assessment were considered the principle data that either guided the selection of new sites or were used to amend and confirm

Table 3. A site information table for the active and abandoned sites of IODP Proposal 909. Seismo-stratigraphic units are from Gregersen et al. (2013, 2017) and Knutz et al. (2015) and are shown in Fig. 2. The ticks indicate the seismic data coverage at each site, while the red coloured ticks denote which data were used primarily for initial site selection. The result of the geohazard assessment column signifies the impact the assessment had on that site and includes confirm (site approved after being initially selected on a form of 2D seismic data), amended (site was moved to this location from an abandoned site), select (site was chosen as an initial location) and abandon (site was deemed an unfit location). Abbreviations used include stratigraphy (Strat), sub-unit (su), primary (Prim), alternate (Alt), abandoned (Ab), seabed (sb), metres below sea surface (mbss), metres below seafloor (mbsf), ultra-high-resolution (UHR), geohazard assessment (GHA), lithology (lith) and total depth (TD). All site locations are shown in Fig. 1.

Target	Strat. Targeted	Site (MB-)	Priority	Sb. Depth (mbss)	Target Depth (mbsf)	Seismic Data Coverage 2D	3D	UHR	Result of GHA	Notes
I	Mu-A	**23A**	**Prim.**	**1821**	**422**			✓	-	Primary due to reflection continuity
	(su. 9-11)	1C	Alt.	1809	473	✓		✓	-	
		20A	Alt.	1928	450	✓		✓	-	
		1B	Ab.	-	-	✓		✓	-	Ab. to avoid amplitude anomaly at TD
II	Mu-A	**2C**	**Prim.**	**1957**	**522**	✓		✓	-	
	(su. 8)	22A	Alt.	1850	611	✓		✓	-	Ab. considered due to lith. concerns
		21A	Ab.	-	-	✓			-	Ab. due to location on lower fan wedge
III	Mu-A	**31A**	**Prim.**	**531**	**282**	✓	✓	✓	**Confirm**	
	(su. 6-8)	8A	Alt.	503	370	✓	✓	✓	Confirm	
		3B	Alt.	497	375	✓	✓	✓	Confirm	
IV	Mu-A	**30A**	**Prim.**	**618**	**303**	✓	✓	✓	**Confirm**	
	(su. 4-6)	4C	Alt.	628	305		✓	✓	Confirm	
		4B	Ab.	-	-	✓	✓	✓	Abandon	Ab. due to amendment to MB-30A
		9A	Ab.	-	-	✓	✓	✓	Abandon	Ab. due to noisy seismic
V	Mu-A	**17A (1)**	**Prim.**	**655**	**224**	✓	✓	✓	**Select**	
	(su. 1)	5B	Alt.	704	520	✓	✓	✓	Confirm	
	and -B	13A	Alt.	707	540		✓		Select	
		14A	Alt.	663	510		✓		Select	
VI	Mu-B	**6D**	**Prim.**	**614**	**561**	✓	✓	✓	**Amend**	Plan to drill before Target V
	and -C	17A (2)	Alt.	655	411	✓	✓	✓	Select	Additional depth to Target V primary
		15A	Alt.	605	648		✓		Select	
		6C	Ab.	-	-		✓	✓	Abandon	Ab. due to potential gas anomalies
VII	Mu-C	**7B**	**Prim.**	**736**	**978**	✓	✓	✓	**Amend**	
	and -D	16A	Alt.	734	1089		✓		Select	
		11A	Alt.	747	1200		✓		Select	
		12A	Alt.	739	1186		✓		Select	
		10A	Alt.	698	1288	✓	✓		Confirm	
		7A	Ab.	-	-	✓	✓	✓	Abandon	Ab. due to reasons in main text

the suitability of locations that were previously selected on 2D data (Table 3). This led to several sites being abandoned (Figs. 1 and 3 and Table 3). In cases where the UHR seismic data were used to select a new site (such as MB-17A or MB-7B), the spatial analysis of drill targets and hazards from the 3D seismic reflection data were still the primary method used for final site approval.

5.1 Targets I and II

The deep water sites for Targets I and II (ca. 1950–1800 m water depth) are located beyond the present-day shelf break and aim to recover a paleoceanographic record of a Pleistocene drift system associated with the MB-TMF (Fig. 1 and Table 3). Target I represents mu-A subunits 9, 10 and 11, with Target II comprising an expanded section of the stratigraphically underlying subunit 8 (Fig. 2). These two sites were initially selected using regional 2D seismic data, with the majority having been subsequently refined by LAKO UHR data, apart from site MB-23A, which was selected directly on the LAKO UHR data. For the remaining sites, an assessment for potential drilling hazards was conducted using the 2D datasets (regional and UHR) which confirmed their suitability, but as these sites exist outside of the 3D seismic coverage, the full geohazard assessment could not be applied during the site-selection process.

5.2 Targets III and IV

Target III sites on the southern flank of the Melville Bay Trough (ca. 500 m water depth) aim to recover potential glacial and interglacial intervals expected to be of Early–Middle Pleistocene age within top-set strata of the MB-TMF that onlap onto glacial unconformities within mu-A subunits 6, 7 and 8 (Figs. 1, 2, and 11 and Table 3). Target IV sites in the southern central part of the Melville Bay Trough (MBT) (ca. 600 m water depth) focus on similar top-set strata covering a stratigraphic interval of likely Early Pleistocene age corresponding to mu-A subunits 3–6.

Three of the sites, including both primaries, have been selected predominantly using the LAKO UHR seismic, with the remaining two alternate sites using the regional 2D survey (Table 3). During this selection, potential hazards observed in the 2D surveys, including amplitude anomalies,

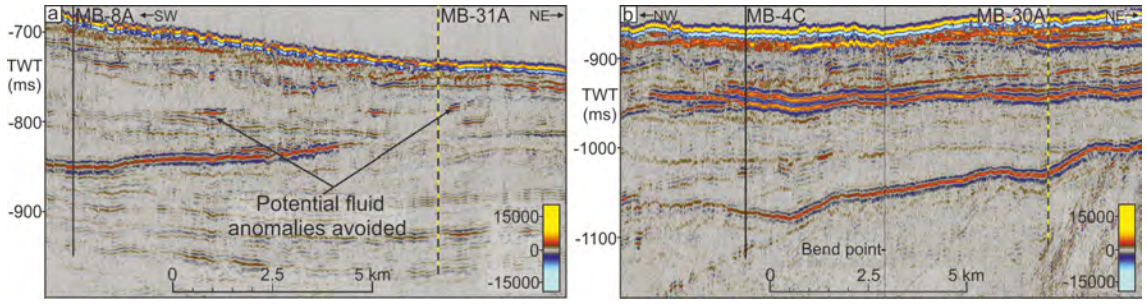

Figure 11. Targets III and IV. Seismic cross sections from the LAKO UHR survey that highlight the glacigenic stratigraphy of Targets III **(a)** and IV **(b)** as well as the locations of potential fluid anomalies and sites MB-31A (primary), MB-8A, MB-30A (primary) and MB-4C (alternate). The locations of both panels **(a)** and **(b)** are shown in Fig. 3, and uninterpreted versions are provided in Fig. S3.

were identified and avoided. All of the selected sites, however, exist within the 3D seismic coverage (Fig. 3) and therefore have been analysed as part of the geohazard assessment. Each site location and the depth of the target seismic horizon were assessed against each step of the geohazard assessment workflow through the process of CRS map creation. In this case, no site alterations were required, and all sites selected existed within the green, low-risk zone (Fig. 10), avoiding all identified hazards, for example the potential fluid anomalies shown in Fig. 11, by an acceptable radius (usually > 500 m).

5.3 Targets V and VI

Target V and VI sites, located in the central MBT (ca. 600–700 m water depth), aim to recover pre-glacial Neogene contourite drifts of presumed Early Pliocene age (Figs. 2, 3 and 12) and a limited portion of the overlying prograding sediments, which may reflect the earliest marine-based glaciations in north-western Greenland (mu-A subunit 1).

Analysis of both the new LAKO UHR data and the geohazard assessment from the 3D seismic reflection data led to the selection of a new primary site (MB-17A) that compared favourably to the originally proposed site (MB-5B). Site MB-17A fulfils the Target V criteria whilst avoiding several potential fluid anomalies and minimizes drilling through potentially boulder-prone glacial debris flow sediments (Fig. 12d). The new site also allows operational flexibility, providing an alternate site for Target VI by sampling both Target V and VI sediments (e.g. Option 1 and Option 2) (Fig. 12 and Table 3). The recovery of the youngest drift sediments has been optimized by targeting a sequence of evenly layered strata that are located less than ~ 60 m below the seabed (Fig. 12a).

Target VI sites aim to recover the oldest stratigraphic section of the Neogene contourite drift within mu-B. For Target VI, in combination with Target V, the overall strategy is to obtain a composite, high-resolution record containing the Early Pliocene warm phase to the Late Pliocene cooling (Table 3). The main drilling target is an expanded section of the wavy-mounded contourite drift that accumulated over an underlying erosional unconformity (hz c1) (Figs. 2, 12 and 13). Both the primary and alternate sites were picked directly on the 3D seismic data using the geohazard assessment as a guide. Primary site MB-6D is also covered by LAKO UHR data which were used to confirm the site (Table 3).

Initially, the primary for Target VI was selected using regional 2D data but was located in an area just beyond the limit of the 3D seismic coverage (between the Anu and Pitu surveys – Fig. 3). Therefore, it was decided to relocate the site to within the 3D seismic extent to allow a more detailed site analysis using the geohazard assessment (to MB-6C – Fig. 13). The shallow gas detection analysis (Fig. 8) identified two bright spots at the edges of the mounded contourite target package that may represent tuning effects between the negative amplitude reflection at the target top and a short-extent, possibly cross-cutting, positive amplitude event beneath it, but it could also (in a less likely worst case scenario) represent pockets of gas-charged sand at the target top (Fig. 13b and c). MB-6C, however, targeted the central part of the mound that looked evenly stratified and free of bright events (Fig. 13b), but after further considerations of the amplitude distributions and target dip, the site was moved to a new position (MB-6D), where it would penetrate the potential gas-hosting sandy horizon further down dip. This was a cautious effort to reduce the chance of encountering gases that have migrated up dip (Fig. 13).

The geohazard assessment also highlighted a potential fluid anomaly (bright spot) directly in the area where MB-6D is located (~ 180 m to the N/NE) but ~ 50 m beneath the base of the targeted drift package (Figs. 3 and 13). Due to this feature, a conservatively shallow target depth was selected that maintains a depth stand-off of ~ 80 m, minimizing the chance of drilling too deep and reaching the underlying anomaly (Figs. 12 and 13).

5.4 Target VII

Target VII sites are located in the inner central part of the MBT (ca. 750 m water depth) within the area covered by the Pitu 3D (and Pitu HR) seismic survey and comprise the deepest planned sites within the proposal (Fig. 1 and Table 3).

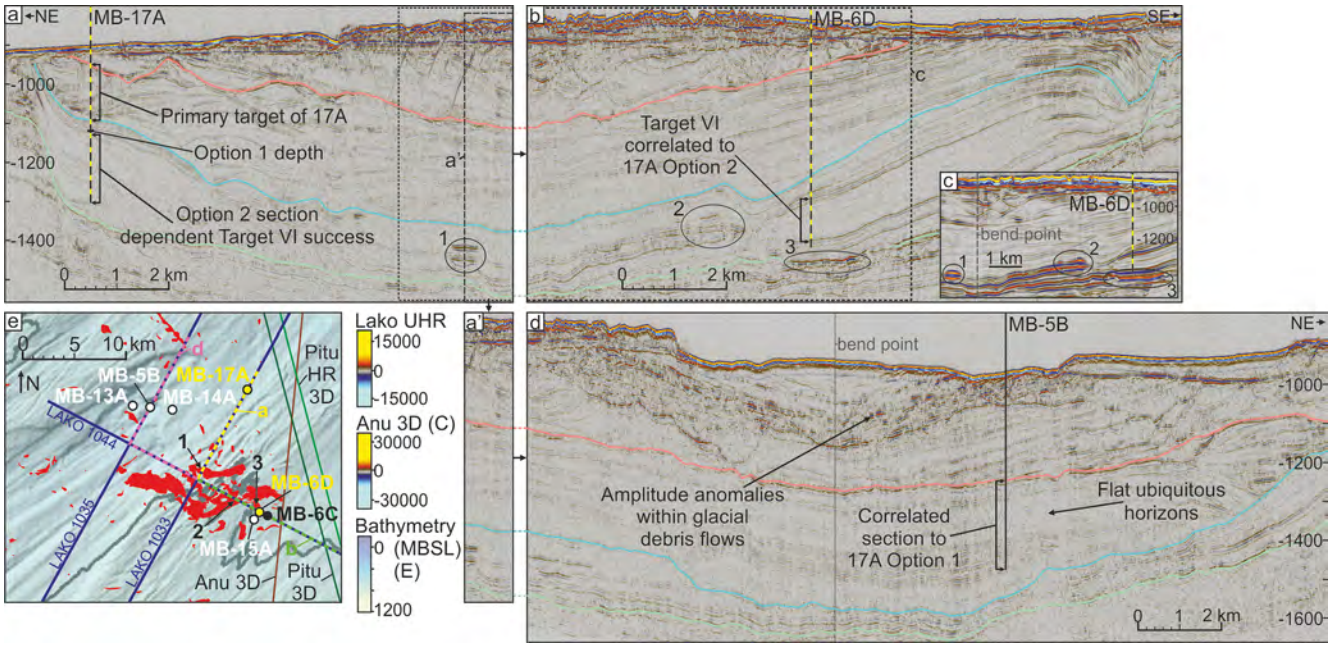

Figure 12. Target V. **(a)** A seismic cross section from the LAKO UHR survey showing the location of primary site MB-17A. Both depth options for this site are shown along with horizon interpretations (coloured) that were mapped throughout the area to allow the correlation of target stratigraphy with the other sites. The section of seismic that represents panel **(a')** is also shown, with panel **(a')** displayed beneath, next to panel **(d)**, to show how both the seismic lines in panels **(b)** and **(d)** are connected to the seismic line of panel **(a)**. **(b)** A LAKO UHR seismic cross section displaying the stratigraphic correlation between sites MB-17A and MB-6D. **(c)** A seismic cross section from the Anu survey shown for comparison between the two surveys. Fluid anomalies are shown and numbered and their appearance can be compared with the associated anomalies displayed in the LAKO UHR survey in both panels **(a)** and **(b)**. The location of panel **(c)** is also shown in both panels **(a)** and **(b)**. **(d)** A LAKO UHR seismic cross section displaying the stratigraphic correlation between sites MB-17A and MB-5B. **(e)** A location map for the seismic lines used in panels **(a)**, **(b)** and **(d)** that represents an enlarged section of Fig. 3 displaying the regional bathymetry from Newton et al. (2017) as well as the location of seismic data and mapped seismic fluid anomalies (red). The locations of the seismic anomalies that are highlighted and numbered in panel **(c)** are also shown. The location of panel **(e)** is shown in Fig. 3. Uninterpreted versions of panels **(a)**, **(b)** and **(d)** are provided in Fig. S2.

Target VII represents an apparently continuous Miocene succession (including a middle Miocene unconformity – hz d1) that has been exhumed on the inner shelf (Figs. 3 and 14), down to the top of a sedimentary wedge of likely Oligocene age (the target horizon) (Figs. 10 and 14a) (Gregersen et al., 2019, 2013). All of the Target VII sites have been selected using the geohazard assessment (Fig. 10 and Table 3).

The previous primary site, MB-7A, had been selected on the key transect of regional 2D seismic (Figs. 2 and 14). However, the geohazard assessment, in combination with the LAKO UHR seismic, identified a number of issues with the original site location that were not identified using the regional 2D seismic.

1. Narrow, vertical sections of acoustic blanking were identified in both the 3D and LAKO UHR seismics that have been interpreted as possibly representing fluid-flow pipes (cf. Cartwright et al., 2007) or gas streaking (Fig. 14). Although site MB-7A did not intersect these features, they were within close proximity (< 500 m).

2. The MB-7A location was within close proximity to a deep-seated fault that potentially could create pressure communication between the shallow subsurface and a deeper, anticlinal anomaly that may represent trapped hydrocarbon fluids (Fig. 7).

3. The seismic signal is locally disturbed around the MB-7A site in both the 3D and LAKO UHR seismics (Figs. 5a and 7). This is likely caused by an overlying chaotic package of sediments directly beneath the seabed, affecting the signal beneath and possibly containing heterogeneities that would affect drilling, but this may also suggest a higher sand content at the target interval.

4. Potential thick mass transport deposit (MTD) sand packages were identified in the lowermost section of the MB-7A site, both beneath the highlighted target horizon and onlapping onto it (Fig. 14). These sediments would likely cause poor core recovery and could contain high fluid pressures due to their structural dip and proximity to the ridge flanks (Figs. 1 and 14). The top

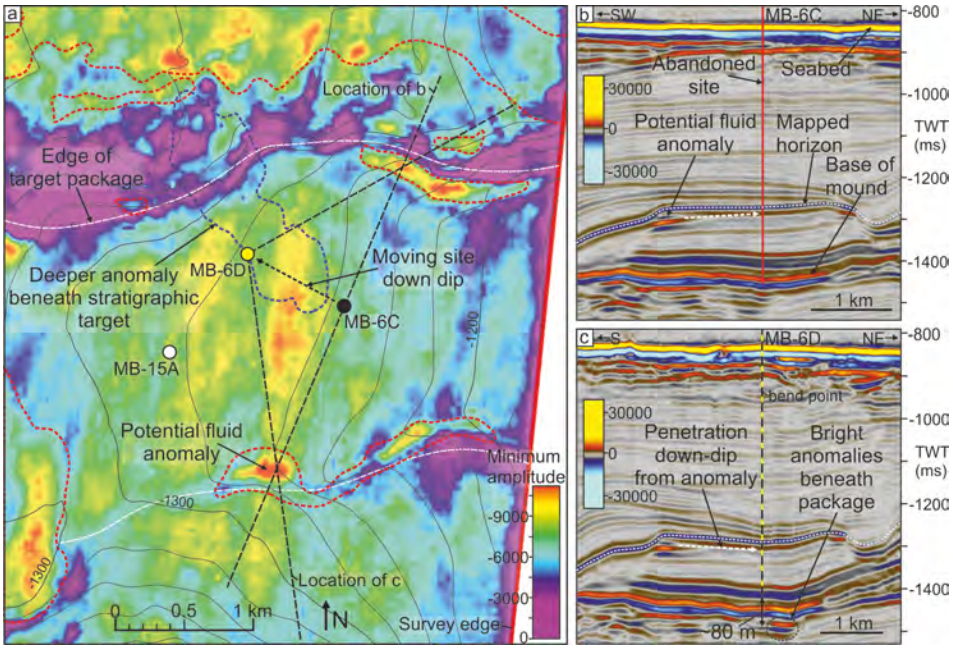

Figure 13. Target VI. **(a)** A minimum amplitude attribute extraction along a mapped horizon representing the top of the contourite mound package that constitutes Target VI (horizon shown in panels **b** and **c**). The attribute extraction highlights bright amplitudes that may represent either tuning or fluid anomalies. The spatial relationship between these bright anomalies and fluid anomalies extracted through the shallow gas detection process (red dashed polygons) (displayed in Fig. 3) is highlighted. The Target VI site locations are shown as well as the locations of panels **(b)** and **(c)**. The location of panel **(a)** is shown in Fig. 6. **(b)** A seismic cross section from the Anu survey showing the contourite mound that comprises Target VI. The occurrences of the potential fluid anomalies are also displayed along with the location of abandoned site MB-6C. **(c)** A seismic cross section from the Anu survey showing the location of the Target VI primary site MB-6D. The site location is shown to penetrate the top mound horizon down dip from the potential fluid anomalies on the packages' flanks.

of the MTD sand package was used as the target seismic horizon within the geohazard assessment and the site-selection strategy was to avoid drilling into these sands, maintaining realistic maximum drill depths and including as much of the overlying Miocene section as possible (Figs. 10 and 14).

These issues led to site MB-7A being abandoned and relocated to the new primary site MB-7B, which targets an area of flat-lying strata within a 1–1.5 km wide fault block (with no fault intersections) that is bounded by a combination of north-west–south-east trending deep-seated faults and the polygonal fault system (Figs. 7, 10 and 14).

6 Discussion

A geohazard assessment is conducted prior to drilling in an attempt to restrict unnecessary delays, reduce costs, avoid poor data collection and, most importantly, reduce the likelihood of dangerous drilling events (Aird, 2010; Nadim and Kvalstad, 2007). The assessment allows the selection of sites that represent the lowest possible risk whilst also achieving the scientific objectives. This requires a detailed spatial analysis of all potential risks and the consideration of additional viable target areas, both regionally and stratigraphically (Selvage et al., 2012). For IODP Proposal 909, the sensitive environment associated with high-latitude continental shelves, as well as the likelihood of hydrocarbon occurrences, made a robust risk analysis increasingly important (Hasle et al., 2009; Nadim and Kvalstad, 2007; Li et al., 2016). The geohazard assessment was conducted in line with commercial site safety analyses (Jensen and Cauquil, 2013) whilst focussing on hazards that commonly create risks to drilling operations within both deep water continental margin settings (hydrocarbon occurrences, gas hydrates, near-surface faults, etc.; Aird, 2010; Jensen and Cauquil, 2013; Minshull et al., 2020; Ruppelt and West, 2004) and glaciated margins (glacial seabed features, problematic lithologies, indurated horizons, etc.; Bennett et al., 2014; Newton et al., 2017).

The assessment identified a pervasive distribution of hydrocarbon-related anomalies across the 3D seismic coverage which exist within all levels of the post-rift stratigraphy (mu-D to -A) (Figs. 3 and 8–10). The majority of these anomalies exist within the shallow subsurface (top 1 km of sediment) and most likely represent pockets of trapped gas or gas hydrates (Hilterman, 2001; Nanda, 2016). It was imperative to identify and avoid the shallow fluid anomalies prior to drilling as unexpected pressure kicks caused by low-density hydrocarbons can often lead to shut-ins and site abandon-

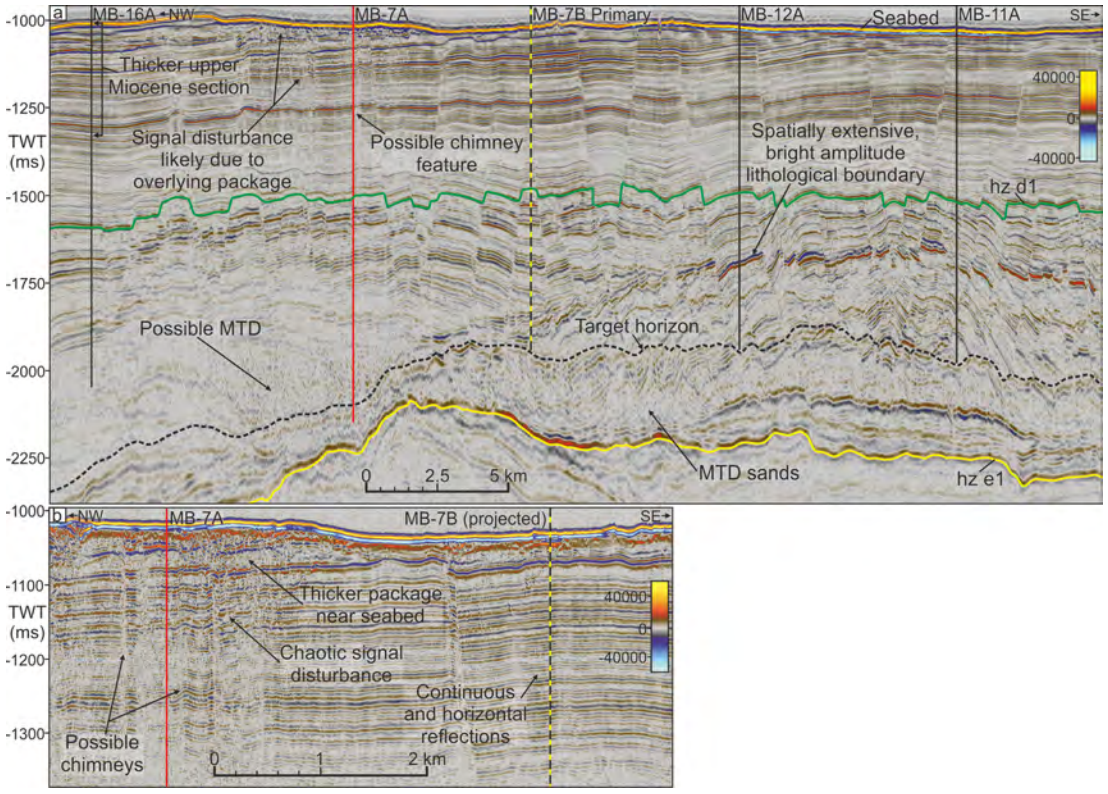

Figure 14. Target VII. **(a)** A seismic cross section from the Pitu HR survey that displays the location of primary site MB-7B, the alternate sites MB-16A, MB-12A and MB-11A and the abandoned site MB-7A. Regional seismic mega-unit interpretations are shown as well as the target seismic horizon used to define the depth target used within the CRS map in Fig. 10 that represents the top of a potentially sandy MTD package. **(b)** A seismic cross section from the LAKO UHR seismic that shows potentially hazardous seismic features near site MB-7A that are also observed in the Pitu HR survey (shown in panel **a**) and ultimately led to the abandonment of that site. A projection of primary site MB-7B is also shown penetrating a section containing continuous and horizontal seismic reflections. The locations of panels **(a)** and **(b)** are shown in Fig. 3, and uninterpreted versions are provided in Fig. S3.

ment and, in a worst case scenario, can cause blow-outs to occur (Holland, 1997; Prince, 1990). Gas hydrates, however, can be drilled through successfully and have even been the focus of several recent coring campaigns (Khabibullin et al., 2011; Ruppel et al., 2008; Ruppel, 2018; Wei et al., 2019). Though the hydrate deposits in this area are underlain by a free gas column that is up to 50 m thick (Fig. 9) (Cox et al., 2020b) and although overpressure beneath the hydrates is unlikely (thought to be at hydrostatic pressure; Dickens and Quinby-Hunt, 1994), the free gas content may create significant buoyancy pressure which could be catastrophic if drilled (Holland, 1997; Minshull et al., 2020). Therefore, all potential hydrocarbon fluid anomalies were classified as "maximum risk" and avoided as a priority (Fig. 10).

A dense network of both tectonic and polygonal faults was also identified within the study area (Figs. 2, 7 and 10). Avoiding fault intersections while drilling is important as deep-seated near-surface tectonic faults can pass high fluid pressures and hydrocarbons along the fault plane and, if not controlled, can lead to a loss of borehole control (Fig. 7) (Frydman et al., 2017; Jensen and Cauquil, 2013). Fault zones also have a much lower fracture gradient than non-faulted zones, which may lead to sediments breaking up during drilling and poor core recovery. Polygonal faults, however, are thought to be sealing under non-extreme pressure conditions (caused by factors such as glacial loading) and exist within many effective petroleum system seals worldwide, thereby negating the risk of fluid flow along the fault plane (Cartwright, 2019). Still, densely polygonally faulted successions close to the seabed can hold significant fluid pressures, although it is likely that the shallow fluid system here would have been depressurized during repeated glacial loading and unloading cycles (Fjeldskaar and Amantov, 2018; Goulty, 2008; Ostanin et al., 2017) that occurred from 2.7 Ma (Knutz et al., 2019). Polygonally faulted clays with high smectite content can be problematic, however, as they can cause drill pipes to become stuck due to the clays swelling when in contact with borehole fluids (Anderson et al., 2010).

Lithology variations were identified during the fine-tuning of site locations in an attempt to avoid problematic lithologies such as glacial debris flow deposits which may contain boulders (potentially damaging coring equipment), hard

indurated horizons or mass transport deposits which affect the continuous chronostratigraphic nature of successions due to sediment re-deposition (Bennett et al., 2014; Jensen and Cauquil, 2013). An attempt was also made to avoid sandy horizons that were identified through certain acoustic impedance contrasts (often semi-bright, negative amplitude events denote a top sand horizon) or through a chaotic seismic facies (e.g. Fig. 14). These uncompacted horizons would likely cause poor core recovery, possibly exacerbated by high fluid pressures within the sands which would further promote sediment collapse (shallow water flow) (Ruppelt and West, 2004). Uncompacted coarse sand could even lead to the coring equipment getting stuck, such as was experienced on ODP Leg 174A (Austin et al., 1998).

Once a potential hazard was identified, the primary concern was to eliminate any drilling through or near to the potential hazard, more so than to unravel the detailed nature of the feature observed. However, the detailed results provided by the geohazard assessment coupled with a desire to understand the complex geological and fluid migration history of the area allowed a closer assessment of the identified hazards, with the most notable conclusions being discussed below.

Firstly, the varying seismic character of the identified fluid anomalies (Figs. 3 and 8) along with their relationship with stratigraphic and structural elements (Fig. 15) suggests various styles of trapping mechanisms along with a complex fluid migration history (Figs. 2, 8, 9 and 15) (Cox et al., 2020b). The distribution of fluid anomalies shows a concentration above the Melville Bay Ridge, suggesting that this positive relief feature focussed the upward migration of hydrocarbons in this area (Figs. 2, 3 and 15). This conclusion is further evidenced by the discovery of an extensive, likely gas-charged, Eocene-aged reservoir on the crest of the ridge (Figs. 8 and 15) (Cox et al., 2020a). Cretaceous source rocks are expected to exist within the buried syn-rift stratigraphy of the Melville Bay Graben and Kivioq Basin (Bojesen-Koefoed, 2011; Gregersen et al., 2019; Planke et al., 2009), which onlap onto the ridge high, thus providing the potential for hydrocarbon migration along sandy carrier beds or fault planes either up towards the ridge crest (charging the Eocene reservoir) or into the shallower post-rift stratigraphy (Figs. 2 and 15). Furthermore, the stratigraphy directly above the Eocene reservoir displays evidence for gas leakage, which is likely linked to the onset of multiple cycles of glacial loading and unloading of the crust and the mass redistribution of sediment associated with the development of the MB-TMF (Cox et al., 2020a, b; Knutz et al., 2019; Newton et al., 2017). These processes likely caused episodic variations in subsurface conditions and structural tilt that may have promoted pulses of fluid leakage (Figs. 1, 2 and 15) (Fjeldskaar and Amantov, 2018).

These processes also contributed to the concentration of hydrocarbons within the stratigraphy directly overlying the Melville Bay Ridge, causing the majority of this zone to be unsuitable for scientific drilling (Fig. 3). Moreover, expected fluid migration pathways from the deep basins and leakage from the Eocene reservoir are likely connected to the presence of gas hydrates, again within areas directly overlying the Melville Bay Ridge (Figs. 2, 3, 9 and 15). It is likely that the hydrate-forming fluids followed similar migration pathways to that of the identified gas anomalies, with free gas anomalies observed trapped at the base of the GHSZ at the present day, suggesting continued hydrocarbon migration and post-hydrate formation (Figs. 9 and 15) (Cox et al., 2020b). A portion of these fluids is possibly sourced from the leaking Eocene reservoir, but the presence of free gas anomalies within regional sandy horizons suggests that upward migration of these fluids may have occurred away from the ridge before entering these horizons and migrating laterally up dip into areas uplifted above the ridge structure (Figs. 9 and 15). Numerous fluid anomalies also exist in areas away from the ridge (Fig. 3), suggesting a more complex regional migration history which is likely characterized by the trapping and subsequent remigration of fluids in areas above the deeper basins (Cox et al., 2020b; Grecula et al., 2018). In addition, biogenic gas production, possibly from organic horizons within the contourite succession (mu-B and -C), may represent the source of gas observed within glacigenic progradational sands (mu-A) (Figs. 3 and 9b) (Muller et al., 2018; Rebesco et al., 2014). Anomalies away from the ridge, however, are more sporadic, and there are no identified gas hydrates or deeper gas reservoirs within the section investigated (Fig. 15).

Although not part of the principle task of identifying geohazards to minimize risk, the conclusions drawn from the more detailed assessment of the nature of the geohazard features identified provided a greater understanding of fluid distribution and an enhanced prediction of what identified seismic features may represent. This knowledge ultimately informed the assessment of risk and actively affected site-selection decisions and stratigraphic target amendments by avoiding areas characterized as representing focussed pathways for historical fluid migration (Fig. 15).

6.1 Influence on IODP Proposal 909

On the north-western Greenland continental margin, the geohazard assessment workflow was used to identify and document a wide range of potential drilling risks (Figs. 3, 5–10, and 15), which were considered on par with the scientific objectives and expedition logistics (number of drilling days available) when defining the final site localities. This process led to an efficient and informed selection of the primary and alternate sites, and the added detail and understanding provided through the assessment positively influenced the progression of the proposal through several stages of review and was integral to its success when considering its location within such a challenging region.

The influence of the assessment on minimizing risk is highlighted through a re-assessment of several original sites

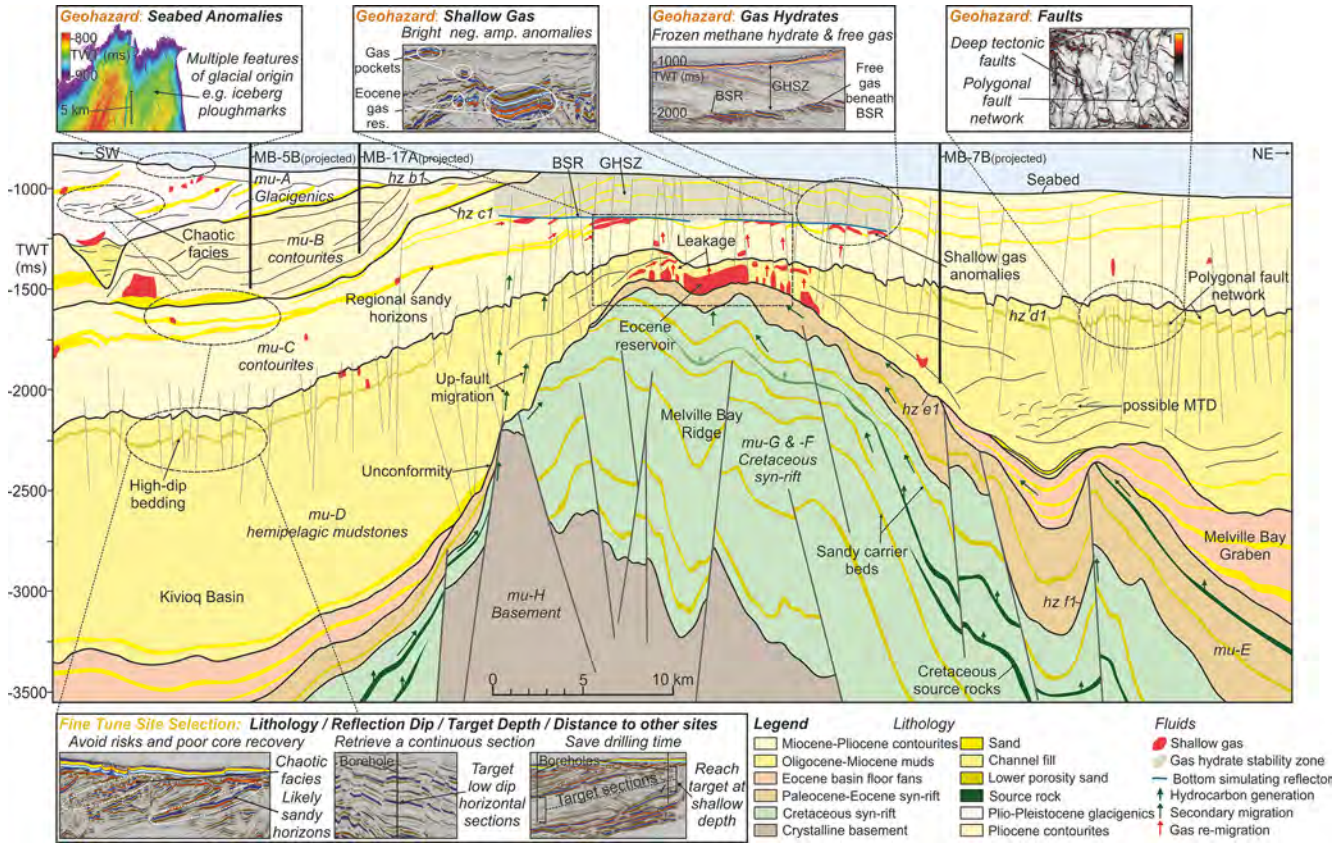

Figure 15. A schematic summary of the structure, stratigraphy, geohazards, and fluid flow history that has been analysed and used within the process of site selection for IODP Proposal 909. Key features related to the elements of the geohazard assessment workflow are shown, including the location of hydrocarbon fluids, sandy lithologies, faults, and the potential source rock horizons and possible fluid migration pathways. The surrounding thumbnails show how these features were analysed and considered within the geohazard assessment workflow. Highlighting the distribution of these features across the schematic aims to provide context on how these features fit together and interact within the subsurface. The understanding of this system, along with the distribution of potential geohazards, was crucial in the identification of viable stratigraphic targets and safe drill sites.

that were selected using regional 2D seismic data against the spatial distribution of geohazards identified through the 3D seismic assessment (Figs. 3, 7, 10, and 13–15 and Table 3). An attempt was already made to avoid potential drilling risks when selecting sites on the 2D data, but the restricted spatial coverage and lower seismic resolution led to a number of features remaining unseen in the 2D assessment, such as close-proximity out-of-plane fluid anomalies and faults (Figs. 3 and 7) or variations in seismic character suggesting sandy lithologies (Figs. 12 and 14). These types of geohazards were identified through the 3D assessment (and augmented by the LAKO UHR survey), leading to the alteration of these original sites to new and likely safer locations (Figs. 12–14 and Table 3). These alterations highlight the benefit of using 3D seismic analysis to identify safer areas outside of the 2D seismic lines whilst achieving the same or more optimal target parameters. Most importantly, the geohazard analysis enabled refined site selection within the Target VII area, which would have likely been abandoned if only covered by 2D seismic due to the deep drilling target, shallow gas distribution and a dense polygonal fault network, coupled with deeper faults and deeper gas sands (Figs. 2, 7, 10, 14 and 15).

The results of the 3D geohazard assessment workflow (along with the location of the regional 2D seismic) also significantly influenced the acquisition plan for the 2D UHR seismic survey. This survey was acquired in 2019 to complement the 3D assessment by providing a higher-resolution image of the top ~500 ms below the seabed (Figs. 3, 11, 12, 14 and Table 2). These additional data both confirmed features observed on 3D seismic data and highlighted additional, more subtle features (such as potential lithology changes) which prompted several site amendments. Importantly, tailoring the acquisition using the 3D assessment results allowed the UHR survey to be focussed over areas that contained either the selected sites (to confirm location), more complex geology or a concentration of geohazards and also for target areas outside of the existing 3D seismic coverage

(Targets I and II – Fig. 1). This allowed a more efficient integration of the two data types whilst minimizing acquisition within unnecessary areas, saving valuable expedition time.

6.2 Benefits to future projects

The geohazard assessment workflow provides a blueprint that maintains the high level of safety assessment associated with IODP drilling by incorporating modern 3D seismic data manipulation and interpretation techniques to take full advantage of the available data (e.g. Heggland et al., 1996; Sharp and Samuel, 2004; Sharp and Badalini, 2013) (Fig. 5 and Table 1). This helps improve both safety and the chance of success of future scientific drilling. Improved 3D seismic acquisition and processing workflows have led to significant improvements in 3D resolution and a reduced reliance on dedicated site surveys (Games and Self, 2017; Oukili et al., 2019). Comparison of the 3D seismic volumes as pseudo site surveys within Proposal 909, against the recently acquired 2D UHR site survey lines, shows that the quality and resolution of imaging are mostly consistent across the two data types, confirming its suitability (comparison in Figs. 12 and 14 and Table 2). The main differences observed included subtle seismic variations, possibly due to lithology differences noted on the UHR seismic, as well as some additional brightening observed in the Anu 3D survey, possibly caused by tuning effects from thin beds that are thicker than the resolution threshold on the UHR seismic and therefore do not display as brightly (seismic survey vertical resolution shown in Table 2 and Fig. 12b and c; Francis, 2015; Marzec and Pietsch, 2012). The 3D seismic volumes also meet the minimum acceptability criteria set out by the International Association of Oil & Gas Producers (IOGP) for using exploration 3D seismic data for site survey studies (Jensen and Cauquil, 2013).

Still, many projects never gain access to 3D seismic data, but the techniques defined within the workflow are still applicable in the 2D sense, especially when using high-resolution and closely spaced 2D site survey data instead. Therefore, the seismic interpretation techniques presented could help maximize the use of available data whilst increasing interpretation quality and efficiency for a wide range of future projects (Selvage et al., 2012; Smith et al., 2019). These methods include using amplitude extraction windows to quickly identify potential fluid anomalies (Fig. 8), using pseudo BSR surfaces created using the BSR–seabed relationship to expand and guide BSR interpretations (Fig. 9) or using stratigraphic depth target zones within CRS maps to collate all identified hazards while focussing site selection within an appropriate, low-risk area (Figs. 10 and 14).

The workflow also outlines how the increasing availability of seismic data through a project's progression can be combined to further assess potential geohazards and provide increased confidence in the chosen sites (Fig. 5). Importantly, the workflow addresses the key hazards that are likely considered within all site-selection safety assessments (Figs. 5 and 15), though the list is not fully exhaustive and several other geohazards or geophysical techniques could be included dependent on context and whether additional data are available. Additional datasets could include acoustic or elastic impedance volumes and derivative rock property estimations (e.g. Dutta, 2002; Huuse and Feary, 2005), "fluid" volumes, electromagnetic-derived resistivity volumes (e.g. Weitemeyer et al., 2006), angle stacks for use in amplitude versus offset/angle (AVO/AVA) studies (Castagna and Swan, 1997), etc.

Examples of additional or modified techniques include using stratigraphical (instead of proportional) attribute extraction windows to follow reflection dip and remove interference from bright amplitude regional reflections and also predicting the BSR depth from the water depth in areas conducive to gas hydrate formation but where no obvious BSR is observed (Field and Kvenvolden, 1985; Kvenvolden et al., 1993; Gehrmann et al., 2009). Alterations to selected cut-offs (such as seabed dip and amplitude filters; Figs. 6 and 8) and other parameters used to define the site location (such as the minimum radius to the nearest hazard) within the geohazard assessment workflow can also be made. If required, this may even include expanding the area where a specific site can be drilled, as seen used in regions even more prone to sea ice and icebergs, such as for IODP Exp. 379 (Amundsen Sea) (Gohl et al., 2019), where the safety radius (in this case along the 2D seismic line) defined around each site locality as being free of hazards was used as a zone of which last minute borehole adjustments could be made in response to the predicted ice trajectory.

The Gohl et al. (2019) study provides an example in which the subsurface- or geohazard-related requirements of a particular location would have influenced the techniques and processes considered within the workflow presented here. Other location-specific requirements include areas containing deep and active fault zones (e.g. the Nankai Trough, Japan) or hydrocarbon fluid venting and extensive gas hydrate deposits (e.g. the Cascadia Margin, offshore Oregon, USA). Drilling safely within such locations with specific geohazard requirements may only be possible when 3D seismic data are available for the assessment of geohazards and drill site selection. This is why IODP legs targeting such areas (Legs 322 and 311; Table 1) have been supported by dedicated, research council funded, 3D seismic acquisition and processing (Bangs et al., 2009; Scherwath et al., 2006). This again demonstrates the importance of 3D seismic data analysis for the future of scientific drilling.

7 Conclusions

IODP Proposal 909 aims to drill a transect of seven sites across the north-western Greenland continental margin that represents an area that is both a frontier petroleum province and a glaciated margin. A geohazard assessment was con-

ducted that was optimized by the use of high-resolution 3D seismic data to accurately extract, document, and spatially analyse potential geohazard evidence and select drill sites that represent the lowest risk possible whilst meeting the scientific objectives in terms of realistic drill depths, section age, completeness, and thickness. The workflow undertaken for this assessment used 3D seismic analytical techniques to identify geohazards such as seabed features, fluid anomalies, faults, and certain lithologies. The mapped geohazards were combined to create common risk segment maps for each of the primary site groups, using a restricted (green) zone defined by the depth to the stratigraphic target to focus site selection. This process led to the alteration or abandonment of several sites that were originally sited on regional 2D seismic data to more optimal locations within the 3D seismic coverage. The workflow and results were also used to tailor the acquisition of an ultra-high-resolution site survey which optimized acquisition and overall expedition planning. This survey was then used in combination with 3D seismic to verify site locations and identify more subtle shallow features such as potential lithology changes. Ultimately, the full geohazard assessment workflow was used to support 7 primary and 15 alternate sites for the scientific drilling proposal.

The detailed, accurate and comprehensive results provided by the 3D geohazard assessment, as well as its influence on the success of IODP Proposal 909, highlight the importance and benefit of maximizing the use of all available data during the planning of a drilling campaign within a challenging environment. With both past and future IODP campaigns targeting areas such as frontier petroleum provinces or glaciated margins whilst having access to 3D seismic data, the detailed consideration of geohazards outlined by this workflow provides a template for future projects. Incorporation of 3D seismic data analysis into site selection and hazard evaluation will help allow a more comprehensive safety assessment that could enable scientific drilling in areas otherwise considered too risky whilst maintaining the high safety standards required by the IODP.

Data availability. All seismic data that support the findings of this study are publicly available by request from the Greenland Ministry of Foreign Affairs and Energy or GEUS data department (http://greenpetrodata.gl, last access: 27 October 2020). The authors received the data used in this paper in 2016, before being made public, from the companies who acquired them: TGS (survey BB2007-2010 – BBRE11), Shell (survey SHELL-ANU-3D-2013), Cairn Energy (survey CAPRI-PITU-3D-2011), and GEUS (survey LAKO-UHR-2019). There is thus currently no direct link to these data.

Uninterpreted versions of the 2D seismic cross sections used in Figs. 11, 12 and 14 are provided in the Supplement.

Supplement. The supplement related to this article is available online at: https://doi.org/10.5194/sd-28-1-2020-supplement.

Author contributions. DRC conducted the 3D seismic geohazard assessment and was lead author of the manuscript and figures. PCK and DCC are lead proponent and data lead on IODP Proposal 909 respectively and assisted this work by leading the selection of stratigraphic targets (Targets I–VII), conducting depth conversions and, in collaboration with DRC, selecting drill site locations. JRH was the lead on LAKO UHR data acquisition and processing. AMWN assisted DRC with the geohazard assessment and figure creation. All the authors were part of the Proposal 909 seismic team and assisted with initial stratigraphic target and site selections, along with conducting co-author reviews on the manuscript and figures.

Competing interests. The authors declare that they have no conflict of interest.

Acknowledgements. The authors would like to thank the IODP and the members of the Science Evaluation Panel as well as all of the proponents who contributed to Proposal 909. We would also like to thank Cairn Energy PLC (Pitu survey), Shell (Anu survey), TGS (2D Regional Survey), and both the Geological Survey of Denmark and Greenland and Aarhus University (LAKO UHR) for the provision of seismic data and the permission to publish the images and results. Acquisition of the LAKO UHR data was possible through grants to Paul C. Knutz and John R. Hopper from the Danish Center for Marine Research and the Carlsberg Foundation and we would like to thank the scientific party involved with the acquisition during the LAKO 2019 expedition. The results and opinions expressed within this work are solely of the authors and not a representation of the companies or institutions. Finally we would like to thank both Schlumberger (Petrel) and Esri (ArcGIS) for providing the software packages used to complete the analysis within this work.

David R. Cox also thanks his PhD sponsors, the University of Manchester (50 %) and the British Geological Survey (BGS) via the British University Funding Initiative (BUFI) (50 %). His PhD forms part of the Natural Environment Research Council (NERC) Centre for Doctoral Training (CDT) in Oil & Gas. Andrew M. W. Newton thanks the Natural Environment Research Council and Cairn Energy for doctoral and postdoctoral funding.

Financial support. This research has been supported by the BGS British University Funding Initiative (grant no. S356), the NERC Centre for Doctoral Training in Oil and Gas (grant no. NE/M00578X/1), and NERC (grant nos. NE/K500859/1 and NE/R013675/1).

Review statement. This paper was edited by Will Sager and reviewed by Martin Hovland and Katrine Juul Andresen.

References

Acton, G.: Proceedings of the Baffin Bay Scientific Coring Program – Expedition 344S, Reporting by company consortium with

eight companies led by Shell, The Hague, the Netherlands, 1–842, 2012.

Aird, P.: Assessing geo-hazards, BP Norge AS, Stavanger, Norway, 1–36, 2010.

Altenbernd, T., Jokat, W., Heyde, I., and Damm, V.: Geophysical evidence for the extent of crustal types and the type of margin along a profile in the northeastern Baffin Bay, J. Geophys. Res.-Sol. Ea., 120, 7337–7360, https://doi.org/10.1002/2015JB012307, 2015.

Anderson, R., Ratcliffe, I., Greenwell, H., Williams, P., Cliffe, S., and Coveney, P.: Clay swelling – a challenge in the oilfield, Earth-Sci. Rev., 98, 201–216, https://doi.org/10.1016/j.earscirev.2009.11.003, 2010.

Andresen, K. J., Huuse, M., Schødt, N. H., Clausen, L. F., and Seidler, L.: Hydrocarbon plumbing systems of salt minibasins offshore Angola revealed by three-dimensional seismic analysis, AAPG bulletin, 95, 1039–1065, https://doi.org/10.1306/12131010046, 2011.

Austin Jr., J. A., Christie-Blick, N., and Malone, M. J.: Leg 174A Preliminary Report - Continuing the New Jersey Mid-Atlantic sea-level transect, Ocean Drilling Program, College Station, Texas, USA, 97 pp., 1998.

Badley, M. E.: Practical seismic interpretation, Prentice Hall, Englewood Cliffs, N.J., USA, 1107 pp., 1985.

Bangs, N., Moore, G., Gulick, S., Pangborn, E., Tobin, H., Kuramoto, S., and Taira, A.: Broad, weak regions of the Nankai Megathrust and implications for shallow coseismic slip, Earth Planet. Sc. Lett., 284, 44–49, https://doi.org/10.1016/j.epsl.2009.04.026, 2009.

Bennett, R., Campbell, D. C., Furze, M. F., and Haggart, J. W.: The shallow stratigraphy and geohazards of the Northeast Baffin Shelf and Lancaster Sound, B. Can. Petrol. Geol., 62, 217–231, https://doi.org/10.2113/gscpgbull.62.4.217, 2014.

Berndt, C., Bunz, S., Clayton, T., Mienert, J., and Saunders, M.: Seismic character of bottom simulating reflectors: examples from the mid-Norwegian margin, Mar. Petrol. Geol., 21, 723–733, https://doi.org/10.1016/j.marpetgeo.2004.02.003, 2004.

Bickle, M., Arculus, R., Barrett, P., DeConto, R., Camoin, G., Edwards, K., Fisher, F., Inagaki, F., Kodaira, S., and Ohkouchi, N.: Illuminating Earth's Past, Present and Future The Science Plan for the International Ocean Discovery Program 2013–2023, International Ocean Discovery Program, Washington, USA, 1–92, 2011.

Bojesen-Koefoed, J. A.: West Greenland Petroleum Systems – an Overview of Source Rocks and Oil Seepages and Their Implications for Offshore Petroleum Exploration, The Geological Survey of Denmark and Greenland, Copenhagen, Denmark, vol. 42, 49 pp., 2011.

Bojesen-Koefoed, J. A., Nytoft, H. P., and Christiansen, F. G.: Age of oils in West Greenland: Was there a Mesozoic seaway between Greenland and Canada, Geol. Surv. Den. Greenl., 4, 49–52, https://doi.org/10.34194/geusb.v4.4783, 2004.

Brown, C. S., Newton, A. M., Huuse, M., and Buckley, F.: Iceberg scours, pits, and pockmarks in the North Falkland Basin, Mar. Geol., 386, 140–152, https://doi.org/10.1016/j.margeo.2017.03.001, 2017.

Cartwright, J.: Polygonal Faults and Seal Integrity, Sixth EAGE Shale Workshop, 28 April 2019, Bordeaux, France, 2019, 1–4, 2019.

Cartwright, J. A., Huuse, M., and Aplin, A.: Seal Bypass Systems, AAPG Bulletin, 91, 1141–1166, https://doi.org/10.1306/04090705181, 2007.

Castagna, J. P. and Swan, H. W.: Principles of AVO crossplotting, The Leading Edge, 16, 337–344, 1997.

Christ, A. J., Bierman, P. R., Knutz, P. C., Corbett, L. B., Fosdick, J. C., Thomas, E. K., Cowling, O. C., Hidy, A. J., and Caffee, M. W.: The northwestern Greenland Ice Sheet during the Early Pleistocene was similar to today, Geophys. Res. Lett., 47, 1–9, https://doi.org/10.1029/2019GL085176, 2020.

Cox, D. R., Huuse, M., Newton, A. M. W., Gannon, P., and Clayburn, J.: Slip Sliding Away: Enigma of Large Sandy Blocks within a Gas Bearing Mass Transport Deposit, Offshore NW Greenland, AAPG Bulletin, 104, 1011–1043, https://doi.org/10.1306/10031919011, 2020a.

Cox, D. R., Huuse, M., Newton, A. M. W., Sarkar, A. D., and Knutz, P. C.: Shallow gas and gas hydrate occurrences on the northwest Greenland shelf margin, Mar. Geol., accepted, 2020b.

Cox, D. R., Newton, A. M. W., and Huuse, M.: An introduction to seismic reflection data: acquisition, processing and interpretation, in: Regional Geology and Tectonics – Principles of Geologic Analysis, edited by: Scarselli, N., Adam, J., and Chiarella, D., Elsevier, Amsterdam, the Netherlands, 571–603, 2020c.

Dan, G., Cauquil, E., and Bouroullec, J.-L.: 3D seismic and AUV data integration for deepwater geohazard assessment: Application to offshore northwest Borneo, Brunei, Offshore Technology Conference-Asia, 25–28 March 2014, Kuala Lumpur, Malaysia, 1–9, 2014.

Dickens, G. R. and Quinby-Hunt, M. S.: Methane hydrate stability in seawater, Geophys. Res. Lett., 21, 2115–2118, https://doi.org/10.1029/94GL01858, 1994.

Dutta, N. C.: Deepwater geohazard prediction using prestack inversion of large offset P-wave data and rock model, The Leading Edge, 21, 193–198, https://doi.org/10.1190/1.1452612, 2002.

Dutta, N. C., Utech, R. W., and Shelander, D.: Role of 3D seismic for quantitative shallow hazard assessment in deepwater sediments, The Leading Edge, 29, 930–942, https://doi.org/10.1190/1.3480006, 2010.

Eriksen, F. N., Assad, M., Eriksen, O. K., Stokke, H. H., and Planke, S.: HiRes P-Cable 3D data for shallow reservoir mapping and geohazard predictions – case examples from the Barents Sea, Near Surface Geoscience 2014 – 20th European Meeting of Environmental and Engineering Geophysics, 14–18 September 2014, Athens, Greece, 2014, 1–5, 2014.

Ewing, J. I. and Hollister, C. H.: Regional aspects of deep sea drilling in the western North Atlantic, Deep sea drilling project intial reports, 11, 951–973, https://doi.org/10.2973/dsdp.proc.11.132.1972, 1972.

Field, M. E. and Kvenvolden, K. A.: Gas hydrates on the northern California continental margin, Geology, 13, 517–520, https://doi.org/10.1130/0091-7613(1985)13<517:GHOTNC>2.0.CO;2, 1985.

Fjeldskaar, W. and Amantov, A.: Effects of glaciations on sedimentary basins, J. Geodyn., 118, 66–81, 2018.

Francis, A.: A simple guide to seismic amplitudes and detuning, GEO ExPro, 12, 68–72, 2015.

Frey-Martínez, J.: 3D seismic interpretation of mass transport deposits: Implications for basin analysis and geohazard evaluation, in: Submarine mass movements and their consequences, edited

by: Mosher, D. C., Moscardelli, L., Shipp, R. C., Chaytor, J. D., Baxter, C. D. P., Lee, H. J., and Urgeles, R., Springer, Dordrecht, the Netherlands, 553–568, 2010.

Frydman, M., Holzberg, B., Pastor, J., Salies, J., and Pedroso, C.: Reducing Fault Reactivation Risk on Deepwater Drilling, SPE Latin America and Caribbean Petroleum Engineering Conference, 17–19 May 2017, Buenos Aires, Argentina, 1–15, 2017.

Galavazi, M., Moore, R., Lee, M., Brunsden, D., and Austin, B.: Quantifying the impact of deepwater geohazards, Offshore Technology Conference, 1–4 May 2006, Houston, Texas, USA, 1–5, 2006.

Games, K. P. and Self, E.: HRS 3D data – a fundamental change in site survey geohazard interpretation, First Break, 35, 39–47, https://doi.org/10.3997/1365-2397.2017008, 2017.

Gehrmann, R., Müller, C., Schikowsky, P., Henke, T., Schnabel, M., and Bönnemann, C.: Model-based identification of the base of the Gas hydrate stability zone in multichannel reflection seismic data, Offshore Costa Rica, Int. J. Geophys., 2009, 1–9, https://doi.org/10.1155/2009/812713, 2009.

Gohl, K., Wellner, J. S., and Klaus, A.: Expedition 379 Preliminary Report: Amundsen Sea West Antarctic Ice Sheet History, International Ocean Discovery Program, https://doi.org/10.14379/iodp.pr.379.2019, 2019.

Goulty, N.: Geomechanics of polygonal fault systems: a review, Petrol. Geosci., 14, 389–397, https://doi.org/10.1144/1354-079308-781, 2008.

Grecula, M., Wadsworth, S., Maloney, D., Lauferts, H., Cooke, G., Jones, A., and Stevanovic, S.: Baffin Bay Elusive Plays: Geological Surprises of an Arctic Exploration Campaign, American Association of Petroleum Geology International Conference and Exhibition (ICE), 15–18 October 2017, London, UK, 1–20, 2018.

Gregersen, U., Hopper, J. R., and Knutz, P. C.: Basin seismic stratigraphy and aspects of prospectivity in the NE Baffin Bay, Northwest Greenland, Mar. Petrol. Geol., 46, 1–18, 2013.

Gregersen, U., Knutz, P. C., and Hopper, J. R.: New geophysical and geological mapping of the eastern Baffin Bay region, offshore West Greenland, Geol. Surv. Den. Greenl., 35, 83–86, https://doi.org/10.34194/geusb.v35.4945, 2017.

Gregersen, G., Knutz, P. C., Nøhr-Hansen, H., Sheldon, E., and Hopper, J. R.: Tectonostratigraphy and evolution of the West Greenland continental margin, B. Geol. Soc. Denmark, 67, 1–21, https://doi.org/10.37570/bgsd-2019-67-01, 2019.

Haneberg, W. C., Kelly, J. T., Graves, H. L., and Dan, G.: A GIS-based decision-support approach to deepwater drilling-hazard maps, The Leading Edge, 34, 398–404, https://doi.org/10.1190/tle34040398.1, 2015.

Hasle, J. R., Kjellén, U., and Haugerud, O.: Decision on oil and gas exploration in an Arctic area: case study from the Norwegian Barents Sea, Safety Sci., 47, 832–842, https://doi.org/10.1016/j.ssci.2008.10.019, 2009.

Heggland, R., Nygaard, E. T., and Gallagher, J.: Techniques and experiences using exploration 3D seismic data to map drilling hazards, Offshore Technology Conference, 6–9 May 1996, Houston, Texas, USA, 1–9, 1996.

Henriksen, N., Higgins, A. K., Kalsbeek, F., Christopher, T., and Pulvertaft, R.: Greenland from Archaean to Quaternary: Descriptive text to the 1995 Geological map of Greenland, 1 : 2 500 000, Geol. Surv. Den. Greenl., 18, 1–126, https://doi.org/10.34194/ggub.v185.5197, 2009.

Hill, A. W.: The use of exploration 3D data in geohazard assessment: where does the future lie?, Offshore Technology Conference, Houston, Texas, USA, 1996, 1-5, 1996.

Hill, A. W., Hampson, K. M., Hill, A. J., Golightly, C., Wood, G. A., Sweeney, M., and Smith, M. M.: ACG field geohazards management: unwinding the past, securing the future, Offshore Technology Conference, 4–7 May 2015, Houston, Texas, USA, 1–22, 2015.

Hilterman, F. J.: Seismic Amplitude Interpretation, Distinguished Instructor Series No. 4, Society of Exploration Geophysicists, Tulsa, OK, USA, 1–244, 2001.

Holland, P.: Offshore blowouts: causes and control, Gulf Publishing Company, Houston, Texas, USA, 1–176, 1997.

Hovland, M., Francis, T. J. G., Claypool, G. E., and Ball, M. M.: Strategy for scientific drilling of marine gas hydrates, JOIDES Journal, 25, 20–24, 1998.

Huuse, M. and Feary, D. A.: Seismic inversion for acoustic impedance and porosity of Cenozoic cool-water carbonates on the upper continental slope of the Great Australian Bight, Mar. Geol., 215, 123–134, https://doi.org/10.1016/j.margeo.2004.12.005, 2005.

Jeanjean, P., Liedtke, E., Clukey, E. C., Hampson, K., and Evans, T.: An operator's perspective on offshore risk assessment and geotechnical design in geohazard-prone areas, Frontiers in Offshore Geotechnics: Proceedings of the International Symposium on Frontiers in Offshore Geotechnics (IS-FOG 2005), 19–21 September 2005, Perth, WA, Australia, 115–143, 2005.

Jensen, P. J. and Cauquil, E.: Guidelines for the conduct of offshore drilling hazard site surveys, International Association of Oil & Gas Producers, London, UK, 1–46, 2013.

Khabibullin, T., Falcone, G., and Teodoriu, C.: Drilling through gas-hydrate sediments: Managing wellbore-stability risks, SPE Drill. Completion, 26, 287–294, https://doi.org/10.2118/131332-PA, 2011.

Khan, F. A., Zohdi, S. B. M., Beng, Q. K., Mohamed, H. B., and Yahya, M. A. M.: High-resolution pseudo 3D seismic data for shallow marine exploration and geohazard assessment in Offshore Malaysia, 80th EAGE Conference and Exhibition 2018, 11–14 June 2018, Copenhagen, Denmark, 1–5, 2018.

Knutz, P. C., Hopper, J. R., Gregersen, U., Nielsen, T., and Japsen, P.: A contourite drift system on the Baffin Bay–West Greenland margin linking Pliocene Arctic warming to poleward ocean circulation, Geology, 43, 907–910, https://doi.org/10.1130/G36927.1, 2015.

Knutz, P. C., Campbell, D. C., Bierman, P. R., de Vernal, A., Huuse, M., Jennings, A., Cox, D. R., DeConto, R., Gohl, K., Hogan, K., Hopper, J. R., Keisling, B., Newton, A. M. W., Perez, L., Rebschläger, J., Sliwinska, K. K., Thomas, E., Willerslev, E., Xuan, C., and Stoner, J.: Cenozoic evolution of the northern Greenland Ice Sheet exposed by transect drilling in northeast Baffin Bay (CENICE), International Ocean Discovery Program, Online, 5, available at: https://docs.iodp.org/Proposal_Cover_Sheets/909-Full2_Knutz_cover.pdf (last access: 27 October 2020), 2018.

Knutz, P. C., Newton, A. M. W., Hopper, J. R., Huuse, M., Gregersen, U., Sheldon, E., and Dybkjær, K.: Eleven phases of Greenland Ice Sheet shelf-edge advance over

the past 2.7 million years, Nat. Geosci., 12, 361–368, https://doi.org/10.1038/s41561-019-0340-8, 2019.

Knutz, P. C., Harrison, C., Brent, T. A., Gregersen, G., and Hopper, J. R.: Baffin Bay Tectono-Sedimentary Element, in: Arctic Sedimentary Basins, edited by: Drachev, S., and Moore, T. E., Geological Society London, London, submitted, 2020.

Kvenvolden, K. A.: A primer on gas hydrates, in: The Future of Energy Gases, edited by: Howell, D. G., Wiese, K., Fanelli, M., Zink, L. L., and Cole, F., USGS, Washington DC, USA, 279–291, 1993.

Kvenvolden, K. A., Ginsburg, G. D., and Soloviev, V. A.: Worldwide distirbution of subaquatic gas hydrates, Geo-Mar. Lett., 13, 32–40, https://doi.org/10.1007/BF01204390, 1993.

Lancelot, Y. and Seibold, E.: The evolution of the central Northeastern Atlantic – Summary of results of DSDP Leg 41, in: Initial reports of the DSDP, edited by: Lancelot, Y., Seibold, E., and Gardner, J. V., U.S. Government Printing Office, Washington, USA, 1215–1245, 1977.

Li, P., Cai, Q., Lin, W., Chen, B., and Zhang, B.: Offshore oil spill response practices and emerging challenges, Mar. Pollut. Bull., 110, 6–27, https://doi.org/10.1016/j.marpolbul.2016.06.020, 2016.

Marzec, P. and Pietsch, K. M.: Thin-bedded strata and tuning effect as causes of seismic data anomalies in the top part of the Cenomanian sandstone in the Grobla–Rajsko–Rylowa area (Carpathian foreland, Poland), Geol. Q., 56, 690–710, https://doi.org/10.7306/gq.1050, 2012.

Mearns, K. and Flin, R.: Risk perception and attitudes to safety by personnel in the offshore oil and gas industry: a review, J. Loss Prevent. Proc., 8, 299–305, https://doi.org/10.1016/0950-4230(95)00032-V, 1995.

Minshull, T. A., Marín-Moreno, H., Betlem, P., Bialas, J., Bünz, S., Burwicz, E., Cameselle, L., Cifci, G., Giustinaini, M., Hillman, J. I. T., Hölz, S., Hopper, J. R., Ion, G., León, R., Magalhaes, V., Makovsky, Y., Mata, M., Max, M. D., Nielsen, T., Okay, S., Ostrovsky, I., O'Neil, N., Pinheiro, L. M., Plaza-Faverola, A., Rey, D., Roy, S., Schwalenberg, K., Senger, K., Vadakkepuliyambatta, S., Vasilev, A., and Vázquez, J. T.: Hydrate occurrence in Europe: A review of available evidence, Mar. Petrol. Geol., 111, 735–764, https://doi.org/10.1016/j.marpetgeo.2019.08.014, 2020.

Mitchell, J., Marcel, V., and Mitchell, B.: What next for the oil and gas industry?, Chatham House, London, UK, 128 pp., 2012.

Moore, R., Ushet, N., and Evans, T.: Integrated multidisciplinary assessment and mitigation of West Nile Delta geohazards, Offshore Site Investigation and Geotechnics, Confronting New Challenges and Sharing Knowledge, London, UK, 1–10, 2007.

Muller, S., Reinhardt, L., Franke, D., Gaedicke, C., and Winsemann, J.: Shallow gas accumulations in the German North Sea, Mar. Petrol. Geol., 91, 139–151, https://doi.org/10.1016/j.marpetgeo.2017.12.016, 2018.

Nadim, F. and Kvalstad, T. J.: Risk assessment and management for offshore geohazards, Proceedings of the ISGSR, 18–19 October 2007, Shanghai, China, 159–173, 2007.

Nanda, N. C.: Direct Hydrocarbon Indicators (DHI), in: Seismic Data Interpretation and Evaluation for Hydrocarbon Exploration and Production, Springer, Cham, Switzerland, 103–113, 2016.

National Research Council: Scientific ocean drilling: accomplishments and challenges, The National Academies Press, Washington, DC, USA, 1–158, 2011.

Newton, A. M. W., Knutz, P. C., Huuse, M., Gannon, P., Brocklehurst, S. H., Clausen, O. R., and Gong, Y.: Ice stream reorganization and glacial retreat on the northwest Greenland shelf, Geophys. Res. Lett., 44, 7826–7835, https://doi.org/10.1002/2017GL073690, 2017.

Newton, A. M. W., Huuse, M., Knutz, P. C., and Cox, D. R.: Repeated ice streaming on the northwest Greenland continental shelf since the onset of the Middle Pleistocene Transition, The Cryosphere, 14, 2303–2312, https://doi.org/10.5194/tc-14-2303-2020, 2020.

Nøhr-Hansen, H., Pedersen, G. K., Knutz, P. C., Bojesen-Koefoed, J. A., Sliwinska, K. K., and Hovikoski, J.: Potential Cretaceous source-rocks from the north-east Baffin Bay, West Greenland, AAPG Europe Regional Conference – Global Analogues of the Atlantic Margin, 2–3 May 2018, Lisbon, Portugal, 2018.

Núñez-Betelu, L. K.: Rock-Eval/TOC pyrolysis data from the Kanguk Formation (Upper Cretaceous), Axel Heiberg and Ellesmere Islands, Canadian Arctic, Geological Survey of Canada, Calgary, Alberta, Canada, 29 pp., 1993.

Oakey, G. N. and Chalmers, J. A.: A new model for the Paleogene motion of Greenland relative to North America: Plate reconstructions of the Davis Strait and Nares Strait regions between Canada and Greenland, J. Geophys. Res., 117, 1–28, https://doi.org/10.1029/2011JB008942, 2012.

Ostanin, I., Anka, Z., and Di Primio, R.: Role of faults in Hydrocarbon Leakage in the Hammerfest Basin, SW Barents Sea: Insights from seismic data and numerical modelling, Geosciences, 7, 28, https://doi.org/10.3390/geosciences7020028, 2017.

Oukili, J., Gruffeille, J.-P., Otterbein, C., and Loidl, B.: Can high-resolution reprocessed data replace the traditional 2D high-resolution seismic data acquired for site surveys?, First Break, 37, 49–54, https://doi.org/10.3997/1365-2397.n0052, 2019.

Parkinson, R.: High-resolution site surveys, CRC Press, London, UK, 2000.

Pearce, C., Knutz, P. C., and Party, S. S.: Baffin Bay Ice-Ocean-Sediment Interactions (BIOS) cruise report, available at: https://geo.au.dk/fileadmin/ingen_mappe_valgt/Paleoceanography_group/LAKO_BIOS19_cruise_report.pdf (last access: 27 October 2020), 2019.

Planke, S., Symonds, P. A., Alvestad, E., and Skogseis, J.: Mid-Cretaceous source rock subcropping in the Baffin Bay, GEO ExPro, 6, 1–8, 2009.

Poppel, B.: Arctic Oil & Gas Development: The Case of Greenland, Arctic Yearbook 2018, 32 pp., available at: https://arcticyearbook.com/images/yearbook/2018/Scholarly_Papers/19_AY2018_Poppel.pdf (last access: 27 October 2020), 2018.

Prince, P. K.: Current drilling practices and the occurrence of shallow gas, in: Safety in offshore drilling, edited by: Ardus, D. A., and Green, C. D., Springer, Dordrecht, the Netherlands, 3–25, 1990.

Raef, A., Totten, M., Vohs, A., and Linares, A.: 3D Seismic Reflection Amplitude and Instantaneous Frequency Attributes in Mapping Thin Hydrocarbon Reservoir Lithofacies: Morrison NE Field and Morrison Field, Clark County, KS, Pure Appl. Geophys., 174, 4379–4394, https://doi.org/10.1007/s00024-017-1664-1, 2017.

Rebesco, M., Hernández-Molina, F. J., Van Rooij, D., and Wåhlin, A.: Contourites and associated sediments con-

trolled by deep-water circulation processes: state-of-the-art and future considerations, Mar. Geol., 352, 111–154, https://doi.org/10.1016/j.margeo.2014.03.011, 2014.

Roberts, H. H., Doyle, E. H., Booth, J. R., Clark, B. J., Kaluza, M. J., and Hartsook, A.: 3D-Seismic Amplitude Analysis of the Sea Flooc An Important Interpretive Method for Improved Geohazards Evaluations, Offshore Technology Conference, Houston, Texas, USA, 1996,

Ruppel, C. D.: The US Geological Survey's Gas Hydrates Project, US Geological Survey, Reston, VA, USA, 1–4, 2018.

Ruppel, C., Boswell, R., and Jones, E.: Scientific results from Gulf of Mexico gas hydrates Joint Industry Project Leg 1 drilling: introduction and overview, Mar. Petrol. Geol., 25, 819–829, https://doi.org/10.1016/j.marpetgeo.2008.02.007, 2008.

Ruppelt, A. U. and West, C. L.: Shallow Water Flow Geopressures Arising From Confined Subsurface Slumps, SPE Annual Technical Conference and Exhibition, 26–29 September 2004, Houston, Texas, USA, 1–8, https://doi.org/10.2118/90980-MS, 2004.

Saini, J., Stein, R., Fahl, K., Weiser, J., Hebbeln, D., Hillaire-Marcel, C., and de Vernal, A.: Holocene variability in sea ice and primary productivity in the northeastern Baffin Bay, Arktos, 1–19, https://doi.org/10.1007/s41063-020-00075-y, 2020.

Sangree, J. B. and Widmier, J. M.: Interpretation of depositional facies from seismic data, Geophysics, 44, 131–160, https://doi.org/10.1190/1.1440957, 1979.

Scherwath, M., Riedel, M., Spence, G., and Hyndman, R.: Data report: seismic structure beneath the north Cascadia drilling transect of IODP Expedition 311, Proceedings of the Integrated Ocean Drilling Program: Scientific Results, 311, 1–25, 2006.

Selvage, J., Jones, C., and Edgar, J.: Maximizing the value of 3D seismic data for shallow geohazard identification, First Break, EAGE, Houten, the Netherlands, 30, 73–83, ISSN 0263-5046, 2012.

Sharp, A. and Badalini, G.: Using 3D seismic data to map shallow-marine geohazards: a case study from the Santos Basin, Brazil, Petrol. Geosci., 19, 157–167, https://doi.org/10.1144/petgeo2011-063, 2013.

Sharp, A. and Samuel, A.: An example study using conventional 3D seismic data to delineate shallow gas drilling hazards from the West Delta Deep Marine Concession, offshore Nile Delta, Egypt, Petrol. Geosci., 10, 121–129, https://doi.org/10.1144/1354-079303-588, 2004.

Smith, P., Milne, R., Vey, G., Apeland, G., and Way, S.: Can Shallow Hazard 3D Seismic Cubes Enable Leaner Exploration Workflows?, 81st EAGE Conference and Exhibition, 3–6 June 2019, London, UK, 1–5, 2019.

Stewart, F. S. and Stoker, M. S.: Problems associated with seismic facies analysis of diamicton-dominated, shelf glacigenic sequences, Geo-Mar. Lett., 10, 151–156, https://doi.org/10.1007/BF02085930, 1990.

Suicmez, V. S.: Future Direction in Oil and Gas Exploration and Production, in: Exploration and Production of Petroleum and Natural Gas, edited by: Riazi, M., ASTM International, West Conshohocken, PA, USA, 693–710, 2016.

Vanneste, M., Sultan, N., Garziglia, S., Forsberg, C. F., and L'Heureux, J.-S.: Seafloor instabilities and sediment deformation processes: The need for integrated, multi-disciplinary investigations, Mar. Geol., 352, 183–214, https://doi.org/10.1016/j.margeo.2014.01.005, 2014.

Wei, J., Liang, J., Lu, J., Zhang, W., and He, Y.: Characteristics and dynamics of gas hydrate systems in the northwestern South China Sea-Results of the fifth gas hydrate drilling expedition, Mar. Petrol. Geol., 110, 287–298, https://doi.org/10.1016/j.marpetgeo.2019.07.028, 2019.

Weimer, P. and Pettingill, H. S.: Deep-water exploration and production: A global overview, in: Atlas of deep-water outcrops: AAPG Studies in Geology, edited by: Nilsen, T. H., Shew, R. D., Steffens, G. S., and Studlick, J. R. J., AAPG and Shell Exploration & Production, Tulsa, OK, USA, CD-ROM, 1–29, 2007.

Weitemeyer, K., Constable, S., and Key, K.: Marine EM techniques for gas-hydrate detection and hazard mitigation, The Leading Edge, 25, 629–632, https://doi.org/10.1190/1.2202668, 2006.

Whittaker, R. C., Hamann, R. E., and Pulvertaft, T. C. R.: A New Frontier Province Offshore Northwest Greenland: Structure, Basin Development, and Petroleum Potential of the Melville Bay Area, AAPG Bull., 81, 978–998, 1997.

Williams, J. P. and Andresen, P. C.: Application of conventional 3D data to geohazard assessment, Offshore Technology Conference, 6–9 May 1996, Houston, Texas, USA, 1–7, 1996.

Wood, G. A. and Hamilton, I. W.: Current geohazard problems and their geophysical interpretation-An international overview, Offshore Technology Conference, 6–9 May 2002, Houston, Texas, USA, 1–9, 2002.

Sci. Dril., 28, 29–41, 2020
https://doi.org/10.5194/sd-28-29-2020

Scientific Drilling
Open Access

Hipercorig – an innovative hydraulic coring system recovering over 60 m long sediment cores from deep perialpine lakes

Ulrich Harms[1], Ulli Raschke[2], Flavio S. Anselmetti[3,4], Michael Strasser[5], Volker Wittig[6], Martin Wessels[7], Sebastian Schaller[3], Stefano C. Fabbri[3,4], Richard Niederreiter[8], and Antje Schwalb[2]

[1]Helmholtz Centre Potsdam, GFZ German Research Centre for Geosciences, Telegrafenberg, 14473 Potsdam, Germany
[2]Institute of Geosystems and Bioindication, Technische Universität Braunschweig, Langer Kamp 19c, 38106 Braunschweig, Germany
[3]Institute of Geological Sciences, University of Bern, Baltzerstrasse 1–3, 3012 Bern, Switzerland
[4]Oeschger Centre for Climate Change Research, University of Bern, Baltzerstrasse 1–3, 3012 Bern, Switzerland
[5]Department of Geology, University of Innsbruck, Innrain 52f, 6020 Innsbruck, Austria
[6]Fraunhofer IEG, Lennershofstraße 140, 44801 Bochum, Germany
[7]Institut für Seenforschung (ISF) der Landesanstalt für Umwelt Baden-Württemberg (LUBW), Argenweg 50, 88085 Langenargen, Germany
[8]Uwitec GmbH, Umwelt und Wissenschaftstechnik, Weißensteinstraße 30, A-5310 Mondsee, Austria

Correspondence: Ulrich Harms (ulrich.harms@gfz-potsdam.de)

Received: 5 August 2020 – Revised: 17 October 2020 – Accepted: 29 October 2020 – Published: 1 December 2020

Abstract. The record of past environmental conditions and changes archived in lacustrine sediments serves as an important element in paleoenvironmental and climate research. A main barrier in accessing these archives is the undisturbed recovery of long cores from deep lakes. In this study, we have developed and tested a new, environmentally friendly coring tool and modular barge, centered around a down-the-hole hydraulic hammering of an advanced piston coring system, called the Hipercorig. Test beds for the evaluation of the performance of the system were two periglacial lakes, Mondsee and Constance, located on the northern edge of the Alpine chain. These lakes are notoriously difficult to sample beyond ∼ 10 m sediment depths due to dense glacial deposits obstructing deeper coring. Both lakes resemble many global lake systems with hard and coarse layers at depth, so the gained experience using this novel technology can be applied to other lacustrine or even marine basins.

These two experimental drilling projects resulted in up to 63 m coring depth and successful coring operations in up to 204 m water depth, providing high-quality, continuous cores with 87 % recovery. Initial core description and scanning of the 63 m long core from Mondsee and two 20 and 24 m long cores from Lake Constance provided novel insights beyond the onset of deglaciation of the northern Alpine foreland dating back to ∼ 18 400 cal BP.

1 Introduction

Many lakes have been identified as outstanding recorders of local, regional, and sometimes even global climate and environment in high resolution and with long-lasting continuity over several glacial–interglacial cycles. These archives cover major parts of the Quaternary (Litt and Anselmetti, 2014; Johnson et., 2016; Wagner et al., 2019; Melles et al., 2012) and beyond (Brigham-Grette et al., 2013). However, the identification of lacustrine strata bearing highly resolved time series requires studies that show high-quality proxy data and, at the same time, radiometric dating possibilities. Such investigations are usually performed on cores (∼ 10–15 m long) that can be recovered using inexpensive gravity or piston coring devices. In order to access sediment archives with a long geological history, as a first step, hydro-acoustic data

(bathymetric and seismic data) need to be acquired to elucidate if such promising strata continue to greater depth. The second step is to plan and conduct coring to depths of at least several decameters. This requires, in most cases, drilling operations conducted with the help of commercial contractors to ensure the achievement of sediment depths beyond 20 m. Because costs for coring deep, continuous, and undisturbed strata from large lakes require budgets in the range of USD 1 million, well-developed project proposals often involve complex, lengthy international funding efforts before they can be realized.

Our approach to addressing the lack of easily available coring techniques to recover up to 100 m long sediment cores was twofold, as follows:

- Design, construct and field-test a novel, high-quality soft sediment coring system that allows penetration beyond today's hand-driven piston corers, while remaining, economically, well below industry coring operations.
- Test the new coring system on two lakes in which sediments are known to resist standard coring attempts that are hitherto unexplored but bear high scientific potential.

We have chosen Mondsee in Austria and the transboundary Lake Constance in Austria, Germany, and Switzerland (Fig. 1) as test beds because previous attempts to core deeper than 14 m in both basins failed. At the same time, the previously recovered Holocene clay-rich lake deposits include a wealth of data on the environmental, climate, and hydrologic evolution of these perialpine basins (see e.g., Wessels et al., 1999; Schwalb et al., 2013; Daxer et al., 2018 and references therein; Blattmann et al., 2020).

This study provides insights into the technique of the new coring system named Hipercorig (derived from "high percussion coring rig") and its deployment on the test lakes. The core material recovered from 63 m depth in Mondsee and at 204 m water depth in Lake Constance is described, and the first analytical results are discussed.

2 Key components and functions of Hipercorig

Hipercorig consists of a highly mobile modular barge system, a coring rig, a hydraulic piston coring device, steel casings, lake bottom ground plate and winches, ropes, and other auxiliary equipment (Fig. 2) that can all be packed and shipped in four 20 ft (6 m) standard shipping containers. The platform is 6.3 × 8 m in size, comprising 14 floating tanks of aluminum of 2, 3, or 4 m × 1 × 1 m dimension. A moon pool (2 × 2 m) in the center ensures centralized lowering of all underwater equipment via the drill rig. The barge is self-propelled by two outboard engines up to a speed of 9 km h^{-1} and accompanied by two outboard-engine-driven rubber boats, also stored in the containers. The barge has a draft of 30 to 40 cm, and its freeboard can be adjusted using four blow ballast tanks, depending on needs for speedier taxi or wave action dampening on-site.

At coring position, the four Bruce-type anchors are each set on 700 m of Kevlar rope and placed outwards from the barge to keep station. Precise stationing and readjustment perpendicular to the drill site are achieved with four hydraulic anchor winches. Coring operations are prepared by lowering a 4 m high ground plate through the moon pool with four winged basal plates to the bottom of the lake (Fig. 3). It is applied to ensure a vertical angle of the coring equipment to the lake bottom. Entry for the casing pipe is provided through a 1.3 × 1.3 m reentry cone mounted on top of the base plate.

Hoisting and mounting of the ground plate and all underwater equipment is done using a 7 m high coring rig. A 46 kW gasoline engine drives, through a hydraulic aggregate, all winches and motors, including the four anchor winches and winches for the ground plate, casing, coring unit, hydraulic hose, and data cable, with biodegradable oil. In the following step, 2 m long pipe sections, together forming an up to 100 m long casing, are connected with a pipe spinner rotary unit and are finally topped by an upper reentry cone. This casing pipe setup is lowered to the ground plate through the reentry cone in the right position.

Coring preparation starts on the drilling platform by assembling the core barrel unit, hammer unit, and heavyweight pipes, i.e., the innovative centerpiece of Hipercorig. It is a combination of a hydraulic down-the-hole (DTH) hammer with a proven piston coring system. The principles of the piston corer are described, e.g., in Gallmetzer et al. (2016) and references therein. The water-driven DTH hammer (e.g., Wassara W 50 hammer, with up to 170 bar and about 100 L water min^{-1} consumption), developed originally for deep drilling or mining, is connected to the piston corer with a special adaptor. The key advantage of such a DTH hammer is that the force is transferred to the corer directly, without dampening the effects of the drill pipe connectors when using uphole percussion. Furthermore, by using the lake water instead of oil as hydraulic fluid to drive the hammer, oil spills are excluded, and hazard-free operations in fragile lake ecosystems are possible.

The 2 m long coring barrel is tipped by a stainless-steel piston at the lower end (Fig. 4a) and harbors a 90 mm diameter and 2 m long plastic core liner to ensure high-quality coring success. The DTH hammer (Fig. 4b) and heavy-weight rods (2 m, 300 kg) on top ensure that the required weight for percussion momentum is sufficient and directed downwards (Fig. 4c). A high-pressure water pump controls the latter, with flow rates of maximum 120 L min^{-1} and up to 200 bar operating pressure through a reeled hydraulic hose. This hydraulic hose transfers water and hydraulic energy down the hole and is led in parallel to the Kevlar ropes holding the coring unit and allowing additional axial pull forces.

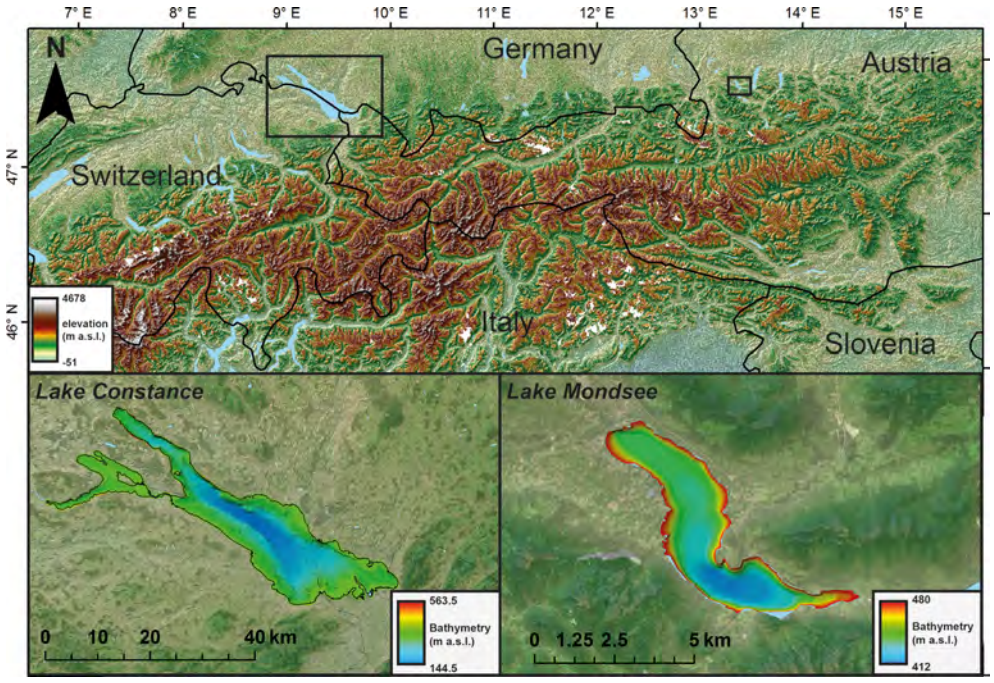

Figure 1. Digital elevation model of the Alpine chain in central Europe based on Shuttle Radar Topography Mission (SRTM) 1 arcsec imagery (30 m; USGS Explorer) with borders as solid black lines and all major lakes in blue. Insets show lakes Constance (Wessels et al., 2015; bathymetry and offshore lidar) and Mondsee, with bathymetric information (data from Mondsee bathymetry courtesy of Immo Trinks, Ludwig Boltzmann Institute for Archaeological Prospection and Virtual Archaeology, Vienna) superimposed using Universal Transverse Mercator (UTM) coordinates. The inset maps combine elevation data with topographic maps (orthographic aerial and satellite imagery from Bing Maps, © Microsoft Corporation).

Once the piston coring unit, DTH hammer, and heavyweights are assembled, they are lowered through the moon pool down into the upper reentry cone (1×1 m) on top of the casing pipe that sits on the ground plate. This rigging is controlled online, using two underwater cameras mounted to the ground plate. Coring starts when the piston at the end of the core barrel hits the sediment surface. Within the uppermost few meters, the power of its own weight presses the core barrel into the sediment, while further down the hammer produces impulses up to 70 Hz. This drives the corer and spills pumped water out of the core cutter crown to reduce friction between the sediment and core barrel. After 1.85 m, the piston reaches the top of the core barrel where the plastic liner sits. At this position, the piston is locked, and the hydraulic pressure in the system activates the core catcher and closes the liner at the end of the core barrel. The sediment-infilled coring unit is then winched up to the platform, the core is retrieved and the unit is cleaned for the next run (Fig. 5). After each core trip, the outer casing pipe sinks down deeper, either due to its own weight or by being pushed or hammered to the depth of the previous core run once compacted sediment is reached. If borehole instabilities occur and sediment narrows the borehole to cause stuck casing pipes, water jetting through the holes in the lowered piston can be activated to flush the casing pipe of blocking sediment. In addition, a closed piston system was fabricated and tested at Mondsee to be used once the borehole walls remain steady, and stabilizing casing is not needed anymore.

An operating staff for coring and initial core handling of at least four persons are required to run Hipercorig in coring mode. The assembly or dismantling onshore requires 5 d of work, also for a crew of four to five.

3 Test sites, operations, and methodology

3.1 Mondsee

Mondsee is a glaciogenic perialpine lake. Its uppermost sedimentary infill has previously been studied for paleoclimate, paleolimnology, and paleoecology since the Bølling–Allerød interstadial ~ 14 ka, as covered by several, up to 14 m long, sediment cores retrieved from the deepest part of the lake at ~ 60 m water depth (Schultze and Niederreiter, 1990; Lauterbach et al., 2011; Swierczynski et al., 2013; Namiotko et al., 2015; Andersen et al., 2017; Daxer et al., 2018). Reflection seismic data, however, imaged a well-stratified, undisturbed postglacial sedimentary sequence of at least 60 m thickness (Fig. 6; Daxer et al., 2018) deposited within a rather short time period of ~ 4–5000 years after the Traun glacier had retreated from the Mondsee area at about 19 ka (Ivy-Ochs et

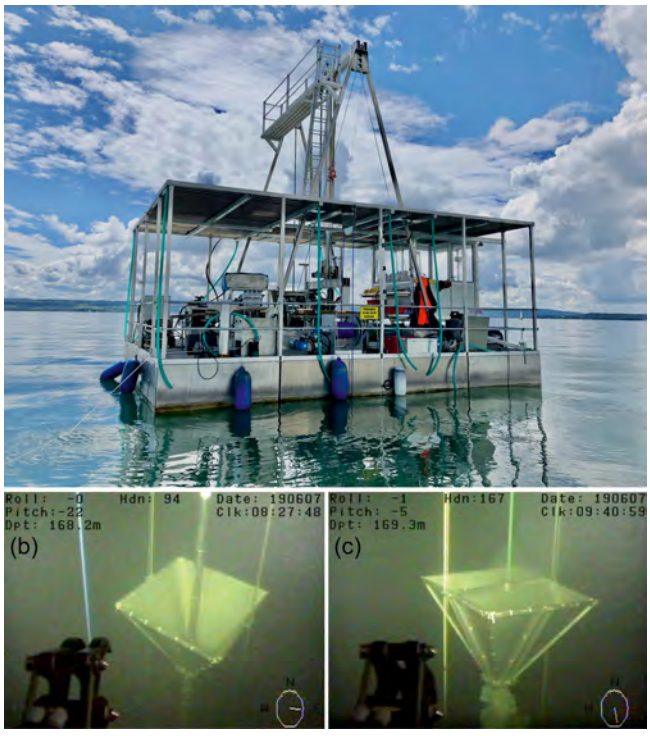

Figure 2. Hipercorig on Lake Constance during coring operations in 2019 **(a)**. Video stills from research vessel (R/V) *Kormoran* remotely operated vehicle (ROV) showing the entry of coring assembly in the upper reentry cone **(b)**. The reentry cone with hydraulic hose (green) after the coring assembly was lowered into the hole **(c)**.

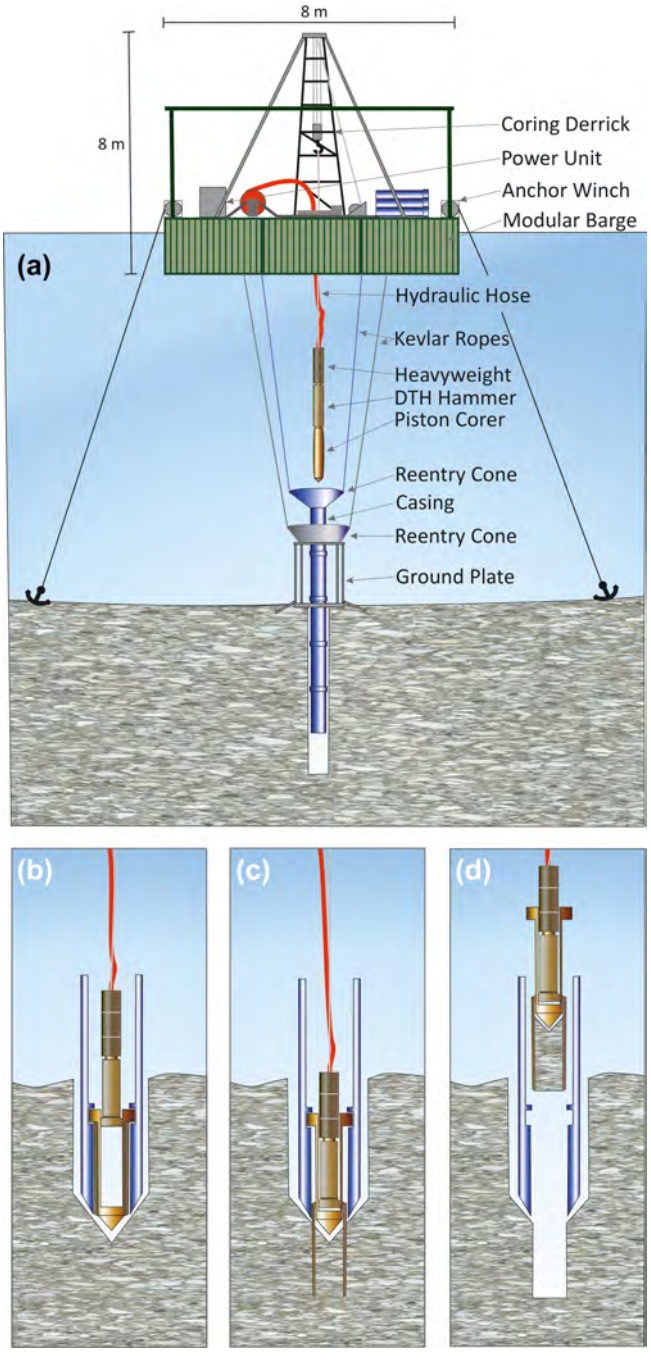

Figure 3. Scheme of Hipercorig key elements, with the ground plate set and coring assembly lowered half-way **(a)**. Illustration of coring operations with the coring assembly placed in the hole **(b**, the corer hammered into sediment **(c)**, and the extraction of coring assembly, including the new core, to the platform while the casing remains in place **(d)**.

al., 2008; Reitner, 2011). This scientific setting thus provided an ideal local test site; moreover, the nearby location of the manufacturer's workshops (Uwitec GmbH) in Mondsee village, Austria, eased logistics.

Design, building, assembly, and acquisition of parts of the Hipercorig system were conducted in 2016 and 2017, while component assembly was performed during fall of 2017. A first test of the complete system was conducted from 16 April to 1 October 2018 near the previous long coring site, by Daxer et al. (2018) at 60 m water depth (47°40′565″ N, 9°17′12682″ E), where reflection seismic data show clear coring targets up to 60 m below the lake floor (b.l.f.; Fig. 6a). The assembly of all parts, including the barge with all equipment, was performed within 6 d. On 27 April, the test drive for the nautical certificate (known as the "Schifffahrtstechnisches Gutachten") was achieved successfully.

After anchoring and site set up, a first adaptation of the coring process and platform layout was necessary. While it was originally planned to use the casing pipes with a reentry cone for the coring device on top, it turned out that it was possible to connect the casing pipes directly from the lake bottom to the platform without a reentry funnel in water depths below 60 m. With this adaptation, the ground plate was assembled, lowered to the lake floor, and connected with the casing and core barrel unit by Kevlar ropes to the platform. As the cameras, tilt sensors, and remote control of the casing brackets worked perfectly, sediment coring began on 9 May 2018. Because of its own weight, the casing pipe sank to the

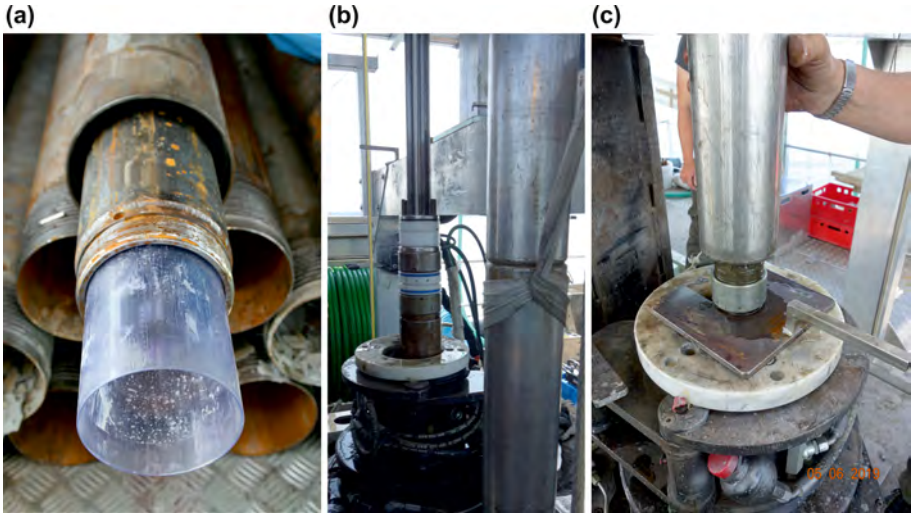

Figure 4. Casing, core barrel, and inner liner before setup **(a)**. Coring assembly lowered into the lake with the connection of the core barrel with the DTH hammer atop the rotary unit **(b)**. Heavyweight rods above the hammer unit hold the rotary unit in place through a makeup plate **(c)**.

Figure 5. Opening of the coring barrel showing a 1.85 m long, sediment-filled plastic liner (gray) and core catcher (white) **(a)**. The piston in the core-filled upper end of the liner **(b)**. The piston after core retrieval, with sandy sediment from Lake Constance **(c)**.

depth reached after each core retrieval up to 10 m b.l.f. Consequently, hole reaming after every 2 m core section was not necessary. At a depth of 26 m b.l.f., operations were halted to solve constructional issues including wear-free seals and a new twist-proof construction of the entire DTH. In addition, dismantling of the entire 86 m (26 m sediment depth plus 60 m water depth) casing pipe was needed to control the crown seal.

During the operational pause, the platform moved slightly away from the ground plate due to wave action, so it was not possible to reenter into the ground plate. In order to avoid such shifts during future operations, a best practice was developed to correct the position with the anchor winches, using the inclination sensors. From late June 2018 on, coring commenced from a minimally offset position (Hole B) from 20 to 30 m depth after displacing the upper 20 m in noncoring mode. Coring in Hole B was continued from 28 m b.l.f., using a manual 70 kg in-hole hammer. However, it took 2 h and 4000 strokes to reach 30 m b.l.f., and 4 t traction was needed to pull out the coring assembly while the casing could neither be progressed nor retrieved. Consequently, it was necessary to invent a new method to continue coring without a casing pipe. For this purpose, the end piece of the coring chamber was modified so that the piston was hydraulically locked, using a valve, until the core filled the chamber and locking could be released. This modification allowed us to reach 52 m b.l.f. coring depth in Hole B (termed section C in Fig. 7). Further tests with different diameter coring (63 and 90 mm) below 52 m b.l.f. coring depth (termed section D) in Hole B were conducted in September 2018 to finally reach a 63 m b.l.f. total coring depth.

The cores retrieved were sealed with end caps in 2 m long clear plastic liners and marked onboard before being stored at an ambient temperature at Uwitec Mondsee and then transported to the Austrian Core Facility (ACF) at the University of Innsbruck for curation and further analysis. Overall core recovery, as calculated from the effective length of sediment-

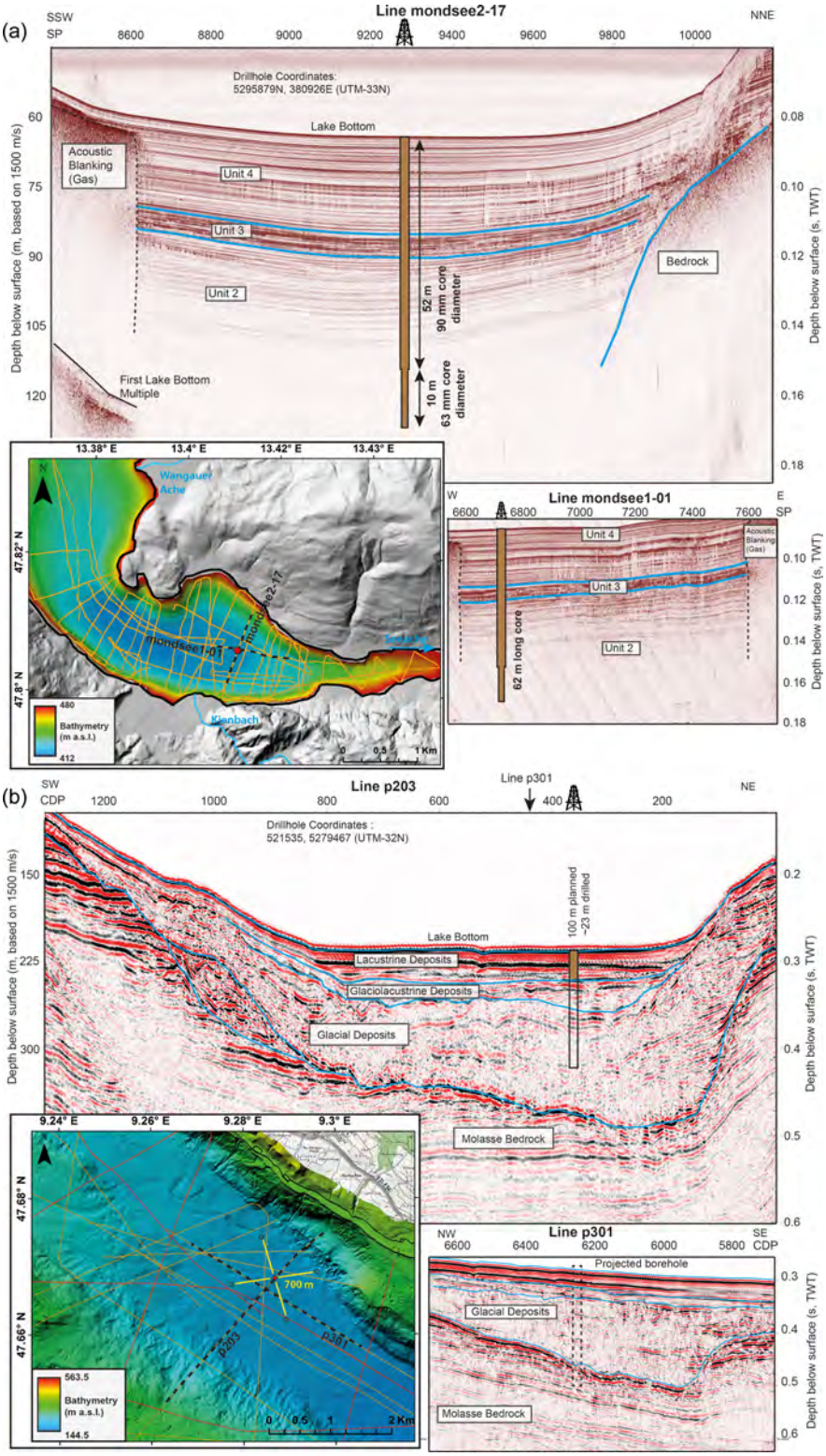

Figure 6. Lakes Mondsee and Constance site survey data and coring sites. **(a)** Bathymetric overview of Mondsee (Austria; data courtesy of Immo Trinks), with the digital elevation model superimposed. Largest (dis-)tributaries are outlined. Orange lines indicate the 3.5 kHz high-resolution single channel seismic tracks. The extent of the seismic profiles is shown as dotted black lines. Seismic interpretation follows Daxer et al. (2018), where all details can be found. **(b)** Bathymetric overview of Lake Constance, east of Hagnau, with multichannel reflection seismic lines superimposed, recorded in 2016 (red) and in 2017 (orange), using two chamber Mini GI and GI 210 air guns, respectively (unpublished data). Drilling location is given as a red dot, anchor locations are in green, and the seismic stratigraphic horizons are blue lines in Lines p201 and p301, respectively (including borehole locations). The extent of the seismic profiles is shown as a dotted black lines.

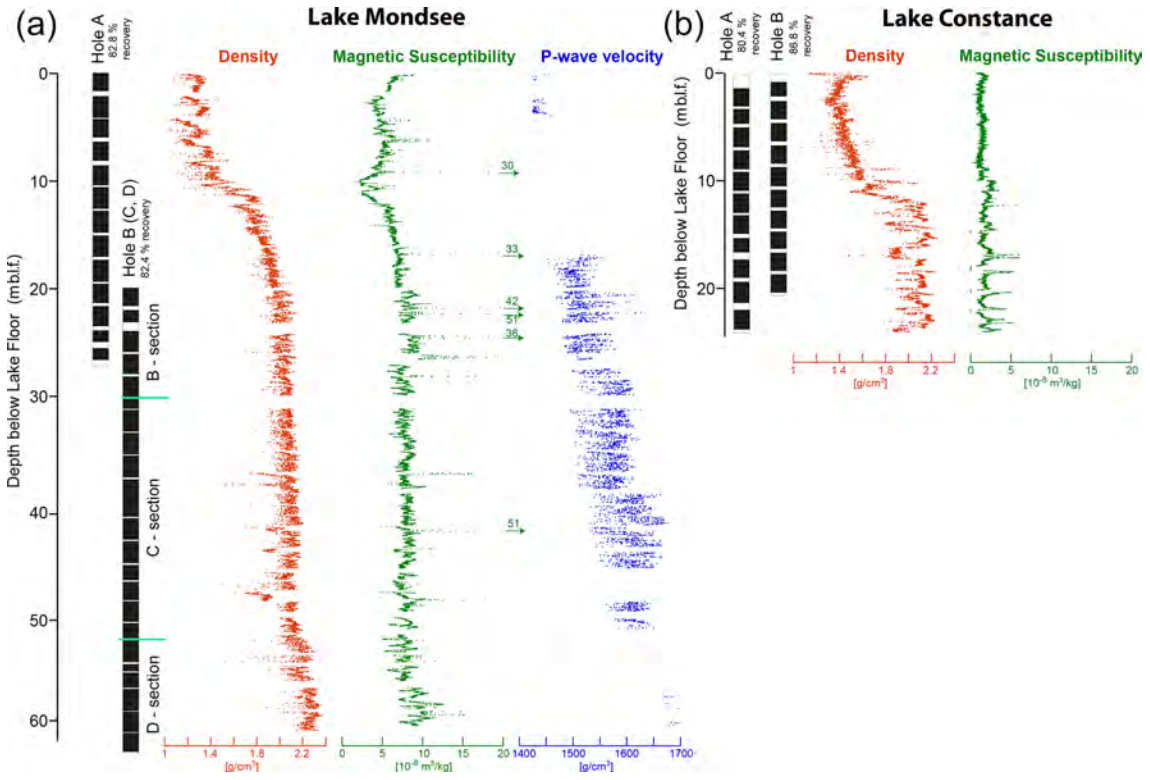

Figure 7. Core recovery **(a)** and physical property data by multisensor core logger (MSCL) **(b)** data for the composite cores from lakes Mondsee (above) and Constance (below).

filled core liners compared to the actual penetration advance of the bit (Fig. 7), ranged between 82 % and 78 % for Hole A and B, respectively. Apart from the coring intervals with technical challenges as described above, where core recovery dropped to 50 %, most coring advances achieved nearly 90 % of core recovery. This slightly reduced recovery is due to a systematic loss of core of about 15 cm in the core catcher at the bottom of each run.

At the ACF, cores were further cut into 1 m sections and measured for physical properties (bulk density, P-wave velocity, and magnetic susceptibility) at 0.5 cm resolution, using a Geotek Ltd. multisensor core logger (MSCL). Selected core sections representing different lithofacies, as interpreted from MSCL data (see Sect. 4.1), were split, line-scan photographed and described, and sediment from the lowermost core section, between 62.0 and 62.8 m b.l.f., was sieved to sample terrestrial leaf fragments and cuticles of macroremains for accelerator mass spectrometry (AMS) ^{14}C analysis at the Ion Beam Physics Laboratory of ETH Zürich (ages presented here were calibrated using the IntCal20 calibration curve; Reimer et al., 2020). Furthermore, and for assessing core quality and lithology in 3D, selected core segments were also scanned for X-ray computed tomography (CT), using a Siemens SOMATOM Definition AS at the Medical University of Innsbruck, with a voxel size of $0.2 \times 0.2 \times 0.3\,\mathrm{mm}^3$. Unopened core sections remain stored at 4 °C at the ACF and are awaiting further scientific analyses.

3.2 Lake Constance

The lacustrine infill of Lake Constance carries distinctive paleoenvironmental signals (Wessels, 1998; Schwalb et al., 2013) which, so far, could only be recovered from the upper ∼ 11 m thick sediments, although more than ∼ 100 m infill has been interpreted from seismic data (Müller and Gees, 1968). New surveys indicate up to 250 m of Quaternary sediments (Fabbri et al., 2018). The well-defined and horizontally bedded lacustrine sediments of the upper tenth of the meters drilled were thought to be most likely Holocene deposits that overlay the deeper undisturbed Late Glacial sediments. In order to shed new light on the lake as a paleoenvironmental archive and to test Hipercorig in deep lake waters, a second Hipercorig test drilling campaign took place from May to July 2019 at Lake Constance. Site selection was based on a new reflection seismic profiling campaign from 2017, with a focus on the up to 250 m deep central part of the lake (Fabbri et al., 2018, Fig. 6b). A site located ∼ 2 km southwest of Hagnau, Germany (Fig. 6b), was selected based on seismically undisturbed and at least 100 m deep strata in 204 m water depth that is away from the ferry routes and underwater cables but close to a harbor.

The coring campaign began on 13 May 2019 with the setup of Hipercorig in Langenargen harbor, 20 km east of Hagnau. The platform was taxied on 22 May, after a weather delay, to the preselected position for the dropping of the four anchors (Fig. 6). The platform was winched precisely on-site, and the ground plate was lowered to the lake floor in 204 m water depth. The casing was connected on the next day but sank without control due to a failure of the casing winch; it hit the ground plate and damaged the reentry cone. Using an ROV deployment with research vessel (R/V) *Kormoran* of the Institut für Seenforschung on 28 May 2019, the damage was inspected via video and the ground plate recovered. On 5 June 2019, the ground plate was replaced with a repaired reentry cone before new casings were assembled and set so that coring Hole A could begin. The first five core runs to 10 m depth were piloted smoothly through clay-rich sediments. Below a depth of $\sim$ 10 m b.l.f., sandy intercalations prevailed, requiring disassembling of the coring system for cleaning after each coring run. Additionally, sand intrusions in the lowermost part of the hole choked the casing pipe. After each core recovery, a cleaning run was necessary to reach the depth of the previous core. On 13 June, a depth of 24 m b.l.f. was reached, with a total recovery of 80 % (Fig. 7), when the coring unit became stuck within the casing pipe due to sand accumulations in the annulus. In order to avoid future wedged coring devices in the casing, a reverse-circulation mode for the water outflowing from the hammer was built during an operational break. It flushes sediment out of the annulus between the casing and coring assembly. During the break, a thunderstorm with $> 100\,\mathrm{km\,h^{-1}}$ gusts slackened one of the anchors, displaced the platform 12 m away from the ground plate, and bent some casing pipes. The hole was not accessible anymore, so the casing pipe and the ground plate had to be dismantled.

The second hole, Hole B, $\sim$ 10 m away from the original location, was started on 3 July 2019 at 0.5 m b.l.f. depth to create core overlap with the first hole. Coring to 10.5 m b.l.f. proceeded without any problems, until sediments became sandy again and cleaning the coring device and the well from the mobilized sand became necessary, as in Hole A. Coring continued with slightly slower progress, and a total 87 % core recovery to a depth of 20.5 m b.l.f. was reached. Then, on 8 July, a shackle failure in the rig caused a loss in the coring assembly. On 9 July, the situation underwater was inspected, again using the R/V *Kormoran* ROV. On 10 July, the ground plate unit and casing pipe were pulled onboard and dismantled and Hole B was abandoned. Finally, three 2 m long surface cores were taken to have a undisturbed sediment–water interface and, 1 d later, all the remaining parts and the anchors were retrieved, and the barge was driven back to Langenargen harbor. Within 5 d, the entire system was dismantled and packed into the four containers for shipping. A total of 21 core runs produced 42 m of core and demonstrated Hipercorig's capability to access deep, coarse, and severely compacted lake sediments.

The cores retrieved were sealed with end caps in the 2 m long clear plastic liners, marked, and curated onboard. After being packed into thermoboxes and cooled with ice, they were brought directly by boat to the microbiology labs of the University of Constance to minimize degradation or loss of volatiles. In the labs, the liners were cut into 1 m long sections. First, small samples were taken for methane and DNA measurements before the liners were sealed again and stored at 4 °C. After the end of the field campaign, all cores were transported to the Institute of Geological Sciences at the University of Bern. MSCL core logging, core opening, initial core description, and the sampling party were held in Bern in October 2019. From the marking on the barge, all data were entered into the new drilling information software called mDIS, of the International Continental Scientific Drilling Program (ICDP; Behrends et al., 2020), following the guidelines of international lake-drilling projects in ICDP. This was the first application of mDIS in a field campaign, and it serves as blueprint for future ICDP projects.

4 Initial core description, measurements, and results

4.1 Mondsee

The upper 10 m of the cored lacustrine stratigraphic succession of Mondsee is composed of faintly laminated sediment (the dominant lithology is authigenic micritic carbonate and diatoms with little to no detrital grains), with abundant organic material (revealing rather low-density values $< 1.4\,\mathrm{g\,cm^{-3}}$) and intercalated layers of high detrital input (characterized by elevated magnetic susceptibility (MS) values). Distinctly lower MS values, around 10 m b.l.f., and the rather sharp downcore increase in bulk density, from 1.4 to $1.9\,\mathrm{g\,cm^{-3}}$ between 10 and 15 m b.l.f. (Fig. 7), match well with the previously reported physical properties across the Late Glacial to Holocene transition from denser mixed detrital to lower density authigenic carbonate with intercalated calcitic detrital layers lithofacies (Daxer et al., 2018; Lauterbach et al., 2011). X-ray computed tomography (XCT) data of cores from these upper 15 m reveal abundant gas cracks (Fig. 8) and core disturbances (the latter due to core handling and noncooled storage of the gas- and organic-rich postglacial sediment cores), which also explains the lack of reliable P-wave velocity data in the upper coring interval (Fig. 7).

Below 15–20 m b.l.f., XCT data reveal excellent core quality with only minimal deformation drag along the liner wall and no evidence for any coring-induced flow structures in sand layers. The cored succession is composed of laminated detrital carbonates with centimeter-scale fine-grained calcitic turbidites with siliciclastic components, intercalated yellowish detrital layers (poorly sorted medium-sized silt), occasional dropstones, and soft sediment deformation structures (Fig. 8). Density values remain rather constant at $\sim 2\,\mathrm{g\,cm^{-3}}$,

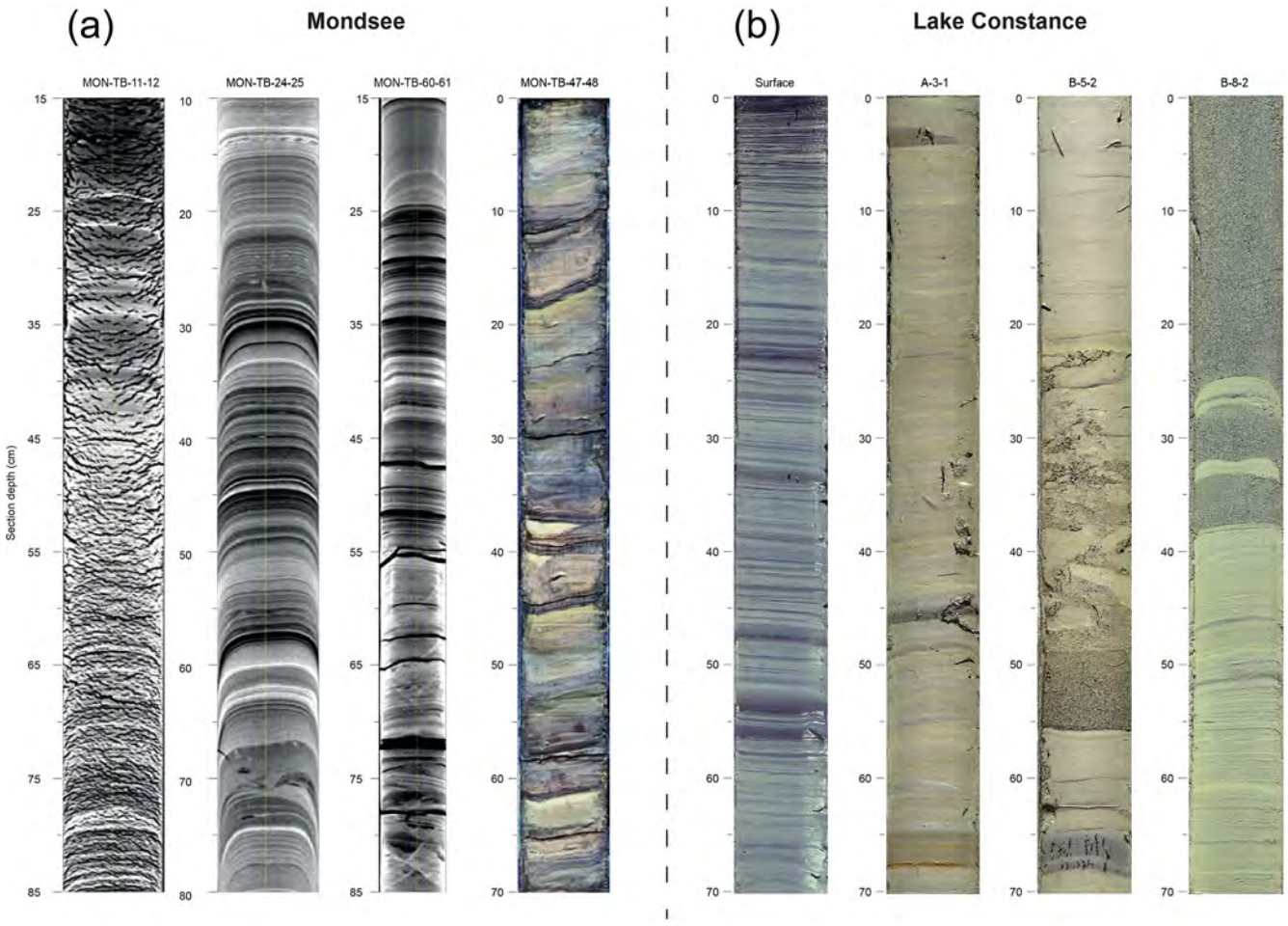

Figure 8. **(a)** Examples from the X-ray computed tomography (XCT) scan (the first three sections from the left; labeled numbers on top of sections indicate subsurface depth range of 1 m core segments) and core photos from Mondsee (histogram-equilibrated images at depth intervals of 47.0–47.7 m b.l.f.) and Lake Constance (four segments to the right). Note the frequent gas expansion cracks in the XCT segment of Mondsee (11.15–11.85 m b.l.f.) and dense (high XCT value in white) conjugated faults at Mondsee (60.80–60.85 m b.l.f), which are further discussed in the text. **(b)** Four examples of line-scan images from core sections of Lake Constance's composite sections. Depth in centimeters indicates section depths. From left to right: surface core (0–70 cm in meters composite depth – mcd); finely layered brown-gray laminated muds with upcore increasingly darker colors (eutrophication signal); core A-3-1 (5.75–6.45 mcd) – carbonate-rich tan and laminated marls; core B-5-2 (9.75–10.45 mcd) – stiff detrital mud with intercalated sand layers. The middle part of this section shows some core disturbance. Core B-8-2 (15.90–16.60 mcd) – massive sand layers with intercalated thin, graded gray and yellowish silt layers, which indicate an annually laminated loess and/or meltwater record deposited during the Oldest Dryas (Wessels, 1998).

while P-wave velocities increase constantly with depth, from about 1500 to 1650 m s^{-1}. Distinct layers, showing peaks 2 to 5 times higher than the general background values of 8×10^{-8} m^3 kg^{-1}-corrected, mass-specific MS, occasionally occur throughout but are more abundant between 20 and 26 m b.l.f. This coring interval correlates to seismic unit 3 by Daxer et al. (2018), interpreted as a phase of increased erosion in the hinterland that is possibly linked to the Gschnitz stadial (Heinrich event 1).

Below 52 m b.l.f., MSCL data are reported with caution because the smaller diameter and partially opened and dried-out core conditions are likely to have influenced the higher density values of up to 2.3 cm^3 and P-wave values up to 1700 m s^{-1} (Fig. 7). The sediment, however, also differs in this lowermost cored succession and is composed of mixed laminated detrital carbonates and up to 1 dm thick fine-grained turbidites. There are distinct, localized, high-density conjugated deformation features (Fig. 8), which cannot be explained by coring artifacts. Instead, they show that the sediment was compressed, possibly by glaciotectonic processes, which would explain the higher density and P-wave values as measured by MSCL.

The radiocarbon age from small leaf fragments and cuticles of macroremains obtained from sieving the sediment of the lowermost 50 cm of the cored interval (sample ETH-105425; 62.3–62.8 m b.l.f.; C14 age – 15 142 ± 41 years

BP) reveals a calibrated (95.5 % probability) age of 18 262–18 650 cal BP. This age is well within the range of the dated deglaciation of the region (19 ± 1 ka; Ivy-Ochs et al., 2008; Reitner, 2011) and supports the lithology-based core interpretation that Hipercorig reached glacial sediments and, thus, recovered a complete lacustrine sedimentary succession since the deglaciation of the Mondsee region. The new Mondsee record, unraveled by Hipercorig, represents one of only few that have actually sampled and dated an undisturbed sedimentary sequence since deglaciation in the Alpine foreland (Zübo core; Lister et al., 1988). The record comprises a ~ 50 m thick, high-resolution glaciolacustrine sedimentary succession that was deposited within the first ~ 3800 years after deglaciation (between $\sim 18\,450$ and $\sim 14\,670$ cal BP; average sedimentation rate ~ 1.32 cm yr^{-1})

4.2 Lake Constance

The average core recovery of 80 % and 87 % in Holes A and B, respectively, allows us to construct a gapless composite record from the lake bottom downcore to 14.5 m composite depth (mcd). Below, down to 24.01 m final composite depth, four intervals ranging in thickness between 13 and 40 cm were not recovered, representing minor gaps. This longest ever recovered sedimentary succession from Lake Constance allows a novel look into the paleoenvironmental evolution of the lake well back into the Last Glacial Period. Core quality is high, with minor disturbances usually in the uppermost 20–30 cm of each 2 m run, in particular in the softer upper part of the section. The coring system was able to fully recover lithologies that are usually challenging for any coring technique. These include intercalations of centimeter-scale coarse sand layers with laminated silty intervals or meter-thick sand units (Fig. 8) that are recovered without evident disturbances.

A previously studied core collected at a site nearby reached a depth of 8.7 m (BO97/14; Wessels 1998; Hanisch et al., 2009; Schwalb et al., 2013). Comparing the MSCL-density curve of the new core with the porosity curve of the former core suggests that the sedimentation rate is a bit higher at the new site. The bottom of the 8.7 m long former core, with a basal age of $\sim 17\,000$ cal BP, may correlate to the new core at ~ 12 mcd (Fig. 7; Schwalb et al., 2013). The lithologies from the surface to that depth can be correlated to various lithologic units described in previous studies, ranging from brown-gray laminated muds in the uppermost meters (surface core; Fig. 8) to underlying carbonate-rich tan and laminated marls (Core A-3-1; Fig. 8), both representing the Holocene section (Wessels, 1998). Densities in this upper part of the core range between 1.3 and 1.5 g cm^{-3}, with a few coarse-grained and graded layers reaching up to ~ 1.8 g cm^{-3} (Fig. 7). Noteworthy is the recent upcore increase in organic matter towards the surface, with dark blackish colors reflecting anthropogenic eutrophication (surface core; Fig. 8; Wessels, 1998; Wessels et al., 1999; Blattmann et al., 2020).

These Holocene units are underlain by massive (density up to ~ 2.1 g cm^{-3}) detrital mud with occasional sand layers (Core B-5-2; Fig. 8) deposited during the Younger Dryas and by finely laminated yellow-brown to gray clayey silt, dating further back into the Late Glacial, containing alternating layers of yellow loess and gray meltwater deposits (Niessen et al., 1992; Wessels, 1998). From there, downcore (i.e., from ~ 12–24 mcd), the recovered lithologies represent a previously unstudied succession that is currently not dated. Sediments consist of layers of structureless coarse sand that may reach bed thicknesses of over 1 m, with density values partly over 2.2 g cm^{-3} (Fig. 7). These sands are intercalated by fine-grained and laminated silty sections, up to few decimeters thick, consisting of numerous graded millimeter- to centimeter-scale layers (Core B-8-2; Fig. 8). These lithologies represent typical depositional processes in periglacial or proglacial lake–near delta environments that occasionally provide high-energy underflows delivering sand, even to water depths of over 200 m. The laminated finer grained graded layers, in contrast, likely reflect deposition away from active channels and presumably have lower sedimentation rates. The site most probably represents an initial stage of the evolving lake, as described elsewhere (Wessels, 1998; Schwalb et al., 2013), but with a high proportion of river-borne sand, reflecting the interplay of the lake with its catchment during the Last Glacial Period.

5 Discussion

Motivated by the lack of cost-effective, deep, continuous, and high-quality coring capabilities in unconsolidated sediments, our primary technological goal of this study was to develop and test a new system that meets these requirements. Although various coring devices have been deployed (Leroy and Colman, 2001) in the past, recent experiences in the framework of ICDP have shown (e.g., Russell et al., 2016) that, for lake sediment thicknesses in the 100 m range, no viable alternative to commercial wire line drilling operations exists so far. Therefore, our goal was to provide a system with a number of key objectives discussed below.

The primary ambition to overcome the usual 20 to 30 m coring depth limit (although exceptional soft sediments in special cases allow coring deeper; e.g., Mingram et al., 2007) was very well achieved, and previous attempts to core deeper in lakes Mondsee and Constance were convincingly outnumbered. In addition, the penetration of hard layers was successfully performed in the stiff glacial sediments of Mondsee and the massive sand intercalations of Lake Constance. This is highly promising for future drilling campaigns in, for example, turbiditic or volcanic ash layers as well. However, these achievements need additional technical modifications, such as a sand cleaning tool and reverse circulation water flow for

jetting the annulus free from sand, that added complexity to Hipercorig's operations. Observations using an ROV showed that hydraulic hammering and pumping of large volumes of water had only negligible effects on the lake floor and did not lead to large plumes of turbid water which might affect sensitive organisms.

The target depth of 100 m coring penetration has not been achieved. However, the 63 m maximum depth reached provided an excellent prospect for matching the initial goal in a variety of sedimentary basins. Nevertheless, future Hipercorig projects still need to tackle this challenge. On the other hand, operations at 204 m water depths were performed despite major challenges. The strong water currents in Lake Constance caused deviations in the coring system from the ground plate that call for control of reentry via either ROV or an additional upward-looking underwater camera at the reentry cone. A concept for using the reentry cone and ground plate system for geophysical wire line logging has been developed but could, so far, not be tested and awaits deployment in future missions. The mooring works well for calm conditions but enhanced anchoring will be needed in storms.

Core quality and continuity are as convincing as with other well-proven modern coring systems, while the perseverance to hitherto inaccessible depths is convincing. However, it must be noted that there is a limit of core recovery due to the inevitable loss of core catcher material at the lower end of the corer. Therefore, approximately 90 % core recovery is a realistic upper limit. The way to achieve full coverage is by double coring with a second hole at the same drill site. This remains an immense cost and time factor, as it is for all other systems at this point. However, the effective costs of operating Hipercorig at Lake Constance were a factor of 10 times lower than comparable wire line coring operations in similar environments and consequently provided an outstanding opportunity for the cost-effective coring of unconsolidated deposits. The limitations of Hipercorig's operational range, as experienced with the experiments in the two perialpine lakes, are (i) strongly compacted sediment layers over several tens of meters and (ii) strong wave actions over 1 m and winds over 8 Bt that require a halt in operations with temporary evacuation.

6 Conclusions

Hipercorig is a novel, high-quality soft sediment coring system. Its performance has been demonstrated on perialpine lakes in over 200 m water depths and more than 60 m coring depth of lacustrine and glacial sediments. It offers promising prospects for similar environments, including targets in shallow marine environments. The new Mondsee core, obtained by Hipercorig, represents the first core that sampled, without extensive commercial drilling efforts, a complete and undisturbed sedimentary sequence since the deglaciation of the Alpine foreland. It also allowed recovery of material for ^{14}C dating and framing the age of deglaciation of the Mondsee region to 18.456 ± 194 cal BP. The new Lake Constance core comprises Holocene laminated muds and marls underlain by massive detrital muds and intercalated sand layers of the Younger Dryas and alternating finely laminated silt, loess, and meltwater deposits from the Oldest Dryas. This is underlain by previously unsampled thick coarse sand beds and intercalated fine silts, showing a dynamic distal delta development adjacent to an Alpine glacier.

Data availability. Data sets used in this article are available upon request. The data sets will be published independently in an open access data publication as soon as they are complemented by further laboratory data.

Author contributions. UH, AS, and VW designed the study. RN and VW designed Hipercorig. RN performed coring on Mondsee. RN, with UR, AS, and MW, led the expedition on Lake Constance. MS directed the seismic campaign on Mondsee and investigated the Mondsee cores. FSA, SCF, and SeS conducted and interpreted the seismic profiling and investigated the cores from Lake Constance. UH, UR, MS, and FSA were the primary authors of the paper, with input from all other coauthors.

Competing interests. The first author is an editor of *Scientific Drilling*; all other authors declare that they have no conflict of interest.

Acknowledgements. We are grateful for the financial support from the Deutsche Forschungsgemeinschaft and the German Scientific Earth Probing (GESEP) consortium for the building and testing of Hipercorig. We deeply appreciate the dedicated work of the Uwitec staff who built Hipercorig and conducted operations. Administrative and logistical support for the Lake Constance operations was provided by Landratsamt Bodenseekreis, Schifffahrtsamt, in Friedrichshafen and the Hagnau local authorities. We would also like to thank the many participants from Universität Konstanz, Anja Grießer for the MSCL measurements of Mondsee cores at the Austrian Core Facility, University of Innsbruck, and Christoph Daxer for the sampling material for radiocarbon dating and discussion of Mondsee data, results, and interpretations.

Financial support. This research has been supported by the Deutsche Forschungsgemeinschaft (grant nos. SCHW 671/19-1, BR 3573/3-1, and 290492639).

Review statement. This paper was edited by Jan Behrmann and reviewed by Laurent Augustin and Bernd Zolitschka.

References

Andersen. N., Lauterbach, S., Erlenkeuser, H., Danielopol, D. L., Namiotko, T., Hüls, M., Belmecheri, S., Dulski, P. Nantke, C., Meyer, H., Chapligin, B., von Grafenstein, U., and Brauer, A.: Evidence for higher-than-average air temperatures after the 8.2 ka event provided by a Central European $\delta^{18}O$ record, Quaternary Sci. Rev., 172, 96–108, https://doi.org/10.1016/j.quascirev.2017.08.001, 2017.

Behrends, K., Heeschen, K., Kunkel, C., and Conze, R.: The mobile Drilling Information System (mDIS) for core repositories, EGU General Assembly 2020, Online, 4–8 May 2020, EGU2020-13663, https://doi.org/10.5194/egusphere-egu2020-13663, 2020.

Blattmann, T., Lesniak, B., García-Rubio, I., Charilaou, M., Wessels, M., Eglinton, T. I., and Gehring, A. U.: Ferromagnetic resonance of magnetite biominerals traces redox changes, Earth Planet. Sc. Lett., 545, 11640, https://doi.org/10.1016/j.epsl.2020.116400, 2020.

Brigham-Grette J., Melles M., Minyuk P., Andreev A., Tarasov P., DeConto R., Koenig S., Nowaczyk N., Wennrich V., Rosén P., Haltia E., Cook T., Gebhardt C., Meyer-Jacob C., Snyder J., and Herzschuh U.: Pliocene warmth, polar amplification, and stepped Pleistocene cooling recorded in NE Arctic Russia, Science, 340, 1421–1427, https://doi.org/10.1126/science.1233137, 2013.

Daxer, C., Moernaut, J., Haas, J., Strasser, M., and Taylor, T.: Late Glacial and Holocene sedimentary infill of Lake Mondsee (Eastern Alps, Austria) and historical rockfall activity revealed by reflection seismics and sediment core analysis, Austrian J. Earth Sc., 111, 111–134, https://doi.org/10.17738/ajes.2018.0008, 2018.

Fabbri S. C., Allenbach, R., Herwegh, M., Krastel, S., Lebas, E., Lindhorst, K., Madritsch, H., Wessels, M., Wielandt-Schuster, U., and Anselmetti F. S.: Bedrock structure, postglacial infill and neotectonic fault structures in Lake Constance, 16th Swiss Geoscience Meeting, 30 November–1 December 2018, Bern, Switzerland, 2018.

Gallmetzer I., Haselmair A., Stachowitsch M., and Zuschin M.: An innovative piston corer for large-volume sediment samples, Limnol. Oceanogr.-Meth., 14, 698–717, https://doi.org/10.1002/lom3.10124, 2016.

Hanisch, S., Wessels, M., Niessen, F., and Schwalb, A.: Late Quaternary lake response to climate change and anthropogenic impact: biomarker evidence from Lake Constance sediments, J. Paleolim., 41, 393–406, https://doi.org/10.1007/s10933-008-9232-4, 2009.

Ivy-Ochs, S., Kerschner, H., Reuther, A., Preusser, F., Heine, K., Maisch, M., Kubik, P. W., and Schlüchter, C.: Chronology of the last glacial cycle in the European Alps, J. Quaternary Sci., 23, 559–573, https://doi.org/10.1002/jqs.1202, 2008.

Johnson, T. C., Werne, J. P., Brown, E. T., Abbott, A., Berke, M., Steinman, B. A., Halbur, J., Contreras, S., Grosshuesch, S., Deino, A., Scholz, C. A., Lyons, R. P., Schouten, S., and Sinninghe Damste, J. S.: A progressively wetter climate in southern East Africa over the past 1.3 million years, Nature, 537, 220–224, https://doi.org/10.1038/nature19065, 2016.

Lauterbach, S., Brauer, A., Andersen, N., Danielopol, D. L., Dulski, P., Hüls, M., Milecka, K., Namiotko, T., Obremska, M., and Von Grafenstein, U.: Environmental responses to Lateglacial climatic fluctuations recorded in the sediments of pre-Alpine Lake Mondsee (northeastern Alps), J. Quaternary Sci., 26, 253–267, https://doi.org/10.1002/jqs.1448, 2011.

Leroy, S. A. G. and Colman, S. M.: Coring and drilling equipment and procedures for recovery of long lacustrine sequences, in: Tracking Environmental Change Using Lake Sediments, Volume 1: Basin Analysis, Coring, and Chronological Techniques, edited by: Last, W. M. and Smol, J. P., Kluwer, Dordrecht, the Netherlands, 2001.

Lister, G. S.: A 15,000-year isotopic record from Lake Zurich of deglaciation and climatic change in Switzerland, Quaternary Res., 29, 129–141, https://doi.org/10.1016/0033-5894(88)90056-7, 1988.

Litt, T. and Anselmetti, F.S.: Lake Van Deep Drilling Project PALEOVAN, Quaternary Sci. Rev., 104, 1–7, https://doi.org/10.1016/j.quascirev.2014.09.026, 2014.

Melles, M., Brigham-Grette, J., Minyuk, P., Nowaczyk, N. R., Wennrich, V., DeConto, R. M., Anderson, P. M, Andreev, A. A., Coletti, A., Cook, T. M., Haltia-Hovi, E., Kukkonen, M., Lozhkin, A. V., Rosen, P., Tarasov, P., Vogel, H., and Wagner, B.: 2.8 Million Years of Arctic Climate Change from Lake El'gygytgyn, NE Russia, Science, 337, 315–320, https://doi.org/10.1126/science.1222135, 2012.

Mingram, J., Negendank, J. F., Brauer, A., Berger, D., Hendrich, A., Köhler, M., and Usinger, H.: Long cores from small lakes – recovering up to 100 m-long lake sediment sequences with a high-precision rod-operated piston corer (Usinger-corer), J. Paleolimnol., 37, 517–528, 2007.

Müller, G. and Gees, R. A.: Origin of the Lake Constance Basin, Nature, 217, 836–837, 1968.

Namiotko, T., Danielopol, D. L., von Grafenstein, U., Lauterbach, S., Brauer, A., Andersen, N., Hüls, M., Milecka, K., Baltanás, A., Geiger, W., Belmecheri, S., Desmet, M., Erlenkeuser, H., and Nomade, J.: Palaeoecology of late glacial and Holocene profundal Ostracoda of pre-Alpine lake Mondsee (Austria) – A base for further (palaeo-) biological research, Palaeogeogr. Palaeocl., 419, 23–36, https://doi.org/10.1016/j.palaeo.2014.09.009, 2015.

Niessen, F., Lister, G., and Giovanoli, F.: Dust transport and palaeoclimate during the oldest Dryas in Central Europe – implications from varves (Lake Constance), Clim. Dynam., 8, 71–81, https://doi.org/10.1007/BF00209164, 1992.

Reimer, P., Austin, W., Bard, E., Bayliss, A., Blackwell, P., Bronk Ramsey, C., Butzin, M., Cheng, H., Lawrence Edwards, R., Friedrich, M., Grootes, P. M., Guilderson, T. P., Hajdas, I., Heaton, T. J., Hogg, A. G., Hughen, K. A., Kromer, B., Manning, S. W., Muscheler, R., Palmer, J. G., Pearson, C., van der Plicht, J., Reimer, R., Richards, D. A., Scott, E. M., Southon, J. R., Turney, C. S. M., Wacker, L., Adolphi, F., Büntgen, U., Capano, M., Fahrni, S., Fogtmann-Schulz, A., Friedrich, R., Miyake, F., Olsen, J., Reinig, F., Sakamoto, M., Sookdeo, A., and Talamo, S.: The IntCal20 Northern Hemisphere Radiocarbon Age Calibration Curve (0–55 cal kBP), Radiocarbon, 62, 725–757, https://doi.org/10.1017/RDC.2020.41, 2020.

Reitner, J. M.: Das Inngletschersystem während des Würm-Glazials, in: Arbeitstagung der Geologischen Bundesanstalt, 19–23 September 2011, Achenkirch, Austria, 79–88, https://doi.org/10.13140/RG.2.1.3754.1520, 2011.

Russell, J. M., Bijaksana, S., Vogel, H., Melles, M., Kallmeyer, J., Ariztegui, D., Crowe, S., Fajar, S., Hafidz, A., Haffner, D., Hasberg, A., Ivory, S., Kelly, C., King, J., Kirana, K., Morlock,

M., Noren, A., O'Grady, R., Ordonez, L., Stevenson, J., von Rintelen, T., Vuillemin, A., Watkinson, I., Wattrus, N., Wicaksono, S., Wonik, T., Bauer, K., Deino, A., Friese, A., Henny, C., Imran, Marwoto, R., Ngkoimani, L. O., Nomosatryo, S., Safiuddin, L. O., Simister, R., and Tamuntuan, G.: The Towuti Drilling Project: paleoenvironments, biological evolution, and geomicrobiology of a tropical Pacific lake, Sci. Dril., 21, 29–40, https://doi.org/10.5194/sd-21-29-2016, 2016.

Schultze, E. and Niederreiter, R.: Paläolimnologische Untersuchungen an einem Bohrkern aus dem Profundal des Mondsees (Oberösterreich), Linzer Biologische Beiträge, 22, 213–235, 1990.

Schwalb, A., Dean, W.E., Güde, H., Hanisch, S., Sobek, S., and Wessels, M.: Benthic ostracode $\partial^{13}C$ as sensor for early Holocene establishment of modern circulation patterns in Central Europe, Quaternary Sci. Rev., 66, 112–122, https://doi.org/10.1016/j.quascirev.2012.10.032, 2013.

Swierczynski, T., Lauterbach, S., Dulski, P., Delgado, J., Merz, B., and Brauer, A.: Mid- to late Holocene flood frequency changes in the northeastern Alps as recorded in varved sediments of Lake Mondsee (Upper Austria), Quaternary Sci. Rev., 80, 78–90, https://doi.org/10.1016/j.quascirev.2013.08.018, 2013.

Wagner, B., Vogel, H., Francke, A., Friedrich, T., Donders, T., Lacey, J. H., Leng, M. J., Regattieri, E., Sadori, L., Wilke, T., Zanchetta, G. Albrecht, C., Bertini, A., Combourieu-Nebout, N., Cvetkoska, A., Giaccio, B., Grazhdani, A. Hauffe, T., Holtvoeth, J., Joannin, S., Jovanovska, E., Just, J., Kouli, K., Kousis, I., Koutsodendris, A., Krastel, S., Lagos, M., Leicher, N., Levkov, Z., Lindhorst, K., Masi, A., Melles, M., Mercuri, A. M., Nomade, S., Nowaczyk, N., Panagiotopoulos, K., Peyron, O., Reed, J. M., Sagnotti, L., Sinopoli, G., Stelbrink, B., Sulpizio, R., Timmermann, A., Tofilovska, S., Torri, P., Wagner-Cremer, F., Wonik, T., and Zhang, X.: Mediterranean winter rainfall in phase with African monsoons during the past 1.36 million years, Nature, 573, 256–260, https://doi.org/10.1038/s41586-019-1529-0, 2019.

Wessels, M.: Natural environmental changes indicated by Late Glacial and Holocene sediments from Lake Constance, Germany, Palaeogeogr. Palaeocl., 140, 421–432, https://doi.org/10.1016/S0031-0182(98)00026-1, 1998.

Wessels, M., Mohaupt, K., Kümmerlin, R., and Lenhard, A.: Reconstructing Past Eutrophication Trends from Diatoms and Biogenic Silica in the Sediment and the Pelagic Zone of Lake Constance, Germany, J. Paleolimnol., 21, 171–192, https://doi.org/10.1023/A:1008080922586, 1999.

Wessels, M., Anselmetti, F., Artuso, R., Baran, R., Daut, G., Geiger, A., Gessler, S., Hilbe, M., Möst, K., Klauser, B., Niemann, S., Roschlaub, R., Steinbacher, F., Wintersteller, P., and Zahn, E.: Bathymetry of Lake Constance – State of the Art in Surveying a Large Lake, Hydrographische Nachrichten, 100, 6–11, 2015.

Sci. Dril., 28, 43–48, 2020
https://doi.org/10.5194/sd-28-43-2020

Scientific Drilling
Open Access

A new high-temperature borehole fluid sampler: the Multi-Temperature Fluid Sampler

C. Geoffrey Wheat[1], Christopher Kitts[2], Camden Webb[3], Rachel Stolzman[2], Ann McGuire[2], Trevor Fournier[1], Thomas Pettigrew[4], and Hans Jannasch[5]

[1]College of Ocean and Fisheries Sciences, University of Alaska Fairbanks, P.O. Box 475, Moss Landing, CA 95039, USA
[2]Robotic Systems Laboratory, Santa Clara University, Santa Clara, CA 95053, USA
[3]Materials Engineering, California Polytechnic State University, San Luis Obispo, CA 93407, USA
[4]Pettigrew Engineering, Milam, TX 75959, USA
[5]Monterey Bay Aquarium Research Institute, Moss Landing, CA 95039, USA

Correspondence: C. Geoffrey Wheat (wheat@mbari.org)

Received: 5 February 2020 – Revised: 5 May 2020 – Accepted: 18 May 2020 – Published: 1 December 2020

Abstract. Deep (> 1 km depth) scientific boreholes are unique assets that can be used to address a variety of microbiological, hydrologic, and biogeochemical hypotheses. Few of these deep boreholes exist in oceanic crust. One of them, Deep Sea Drilling Project Hole 504B, reaches ∼ 190 °C at its base. We designed, fabricated, and laboratory-tested the Multi-Temperature Fluid Sampler (MTFS), a non-gas-tight, titanium syringe-style fluid sampler for borehole applications that is tolerant of such high temperatures. Each of the 12 MTFS units collects a single 1 L sample at a predetermined temperature, which is defined by the trigger design and a shape memory alloy (SMA). SMAs have the innate ability to be deformed and only return to their initial shapes when their activation temperatures are reached, thereby triggering a sampler at a predetermined temperature. Three SMA-based trigger mechanisms, which do not rely on electronics, were tested. Triggers were released at temperatures spanning from 80 to 181 °C. The MTFS was set for deployment on International Ocean Discovery Program Expedition 385T, but hole conditions precluded its use. The sampler is ready for use in deep oceanic or continental scientific boreholes with minimal training for operational success.

1 Introduction

The current and future direction of scientific ocean drilling depends on technological advances to achieve a wide range of scientific objectives. Objectives related to microbial life in the subseafloor and a dynamic Earth represent two of the four current themes that guide scientific ocean drilling within the International Ocean Discovery Program (IODP; IODP Science Plan for 2013–2023). While advances in these areas have been achieved using traditional coring and sample analyses, nontraditional means of instrumenting boreholes and direct sampling of legacy boreholes continue to transform our knowledge of these themes (D'Hondt et al., 2019; Orcutt et al., 2011; Smith et al, 2011; Neria et al., 2016; Wheat et al., 2020). To meet new challenges afforded by future and legacy boreholes, including the potential for in situ manipulative experiments, a new arsenal of samplers and sensors needs to be developed.

Scientific ocean drilling during the past 5 decades has resulted in more than 100 cased boreholes, many of which are suitable for reentry and further discovery (Edwards et al., 2012). Such boreholes tap a range of thermal, hydrologic, physical, and crustal conditions, providing the underpinnings for a range of potential experiments to elucidate crustal and microbial evolution and function as well as the impact of both on ocean processes. Of special interest are the few deep boreholes that penetrate more than a kilometer below the seafloor, each taking many months to years to establish. As a result of natural geothermal heating from below, temperatures within such boreholes exceed 100 °C; Deep Sea Drilling Project (DSDP) Hole 504B reaches temperatures of

more than 190 °C at its base, which is ∼ 2000 m below the seafloor (Guerin et al., 1996). Additional warm, deep boreholes exist in continental settings (e.g., KTB; Emmermann and Lauterjung, 1997) and in active high-temperature hydrothermal systems (e.g., Brothers Arc Flux; de Ronde et al., 2019). To study in situ conditions within these challenging environments, a new array of sensors and samplers need to be developed. Standard electronics do not tolerate such temperatures and, in general, do not function above 150 °C without costly vacuum jackets (dewars) or cooling mechanisms. Because of (a) the uniqueness of these warm, deep boreholes; (b) the aspiration to characterize the thermal limits of life within the crust; (c) the desire to elucidate water–rock reactions and crustal alteration in a natural setting; and (d) the lack of a fluid sampler that is inexpensive, easy to operate, and affords a versatile array of experimental possibilities, we developed the Multi-Temperature Fluid Sampler (MTFS). The MTFS is a non-gas-tight, syringe-style fluid sampler that employs no electronics. Instead, it incorporates a mechanical trigger that utilizes the thermal-response properties of a shape memory alloy (SMA), which is a precise mixture of metals that allows the alloy to be physically modified at room temperature and to return to its original shape at an activation temperature that depends on the composition of the alloy, the geometry of the SMA material, and the design of the trigger mechanism.

2 Existing samplers

Prior to the MTFS, borehole fluid samplers in the IODP inventory included the water-sampling temperature probe (WSTP), the Kuster sampler, and the single-phase fluid sample collection system from Schlumberger. The WSTP has been used for decades (Mottl and Gieskes, 1990) and is lowered on a wire to the desired depth with a preset timer that opens the intake valve. The pressure differential between in situ and surface (∼ 100 kPa) pressure drives fluids into the sampler, possibly lysing microbial cells. Only ∼ 40 mL is collected in the sample tubing with ∼ 1 L spilling into a chamber that cannot be aseptically cleaned for trace metal and microbial determinations. The Kuster fluid sampler was most recently used on IODP Expedition 376 (Brothers Arc Flux; de Ronde et al., 2019). This sampler collects ∼ 500 mL of borehole fluid during a single lowering and is closed by a mechanical clock. However, the sample container is open during deployment, potentially exposing the sample container to contamination (e.g., accumulation of grease, microbial mats, and other particulates). Neither sampler can be preloaded with acid, microbial preservatives, or metabolic tracers, and only one sample can be collected during a single lowering.

More complex samplers require dedicated technicians, such as the single-phase fluid sample collection system from Schlumberger that was used in conjunction with the Quicksilver in situ fluid analyzer on IODP Expedition 337 (Inagaki et al., 2013). Multiple sample modules may be used. For example, six samples were collected on IODP Expedition 337 (Inagaki et al., 2013). Other complex samplers include the high-temperature two-phase downhole sampler from Thermochem Inc., which is a vacuum jacket-type, memory tool, and the positive displacement sampler and One Phase sampler from Leutert. The latter is a gas-tight system with an internal clock that opens and closes a valve. This system can collect a 0.6 L sample at temperatures to 180 °C (Kampman et al., 2013).

3 Design criteria

The MTFS design was primarily based on the Walden–Weiss titanium sampler, which is a non-gas-tight fluid sampler that has been used for more than 4 decades to collect hydrothermal fluids at the seafloor (Von Damm et al., 1985), and the borehole fluid samplers mentioned above. To meet the physical requirements of IODP boreholes and ensure sample integrity, the design criteria included the capability of the sampler to be (a) cleaned for trace element analysis, (b) aseptic prior to deployment, (c) tolerant of temperatures greater than 250 °C, and (d) chemically inert. Additional criteria for flexibility in sample recovery and experimental design included the capability to be primed with a reagent, such as acid in order to keep metals mobilized; a stable isotope for in situ microbial rate studies; or a biocide. The sampler design also needed to consider the possibility of storing the sampler at in situ temperatures, either in the hole or on the ship, to conduct incubation and other time-dependent experiments. A large volume of sample (1 L) and an easy to access sampling port were desired to aliquot fluids into a range of sample containers for a myriad of chemical and microbial analytical assays. Additional design criteria included (a) a diameter that would allow the sampler to fit within the confines of the drill pipe used by IODP; (b) a modular framework so that multiple samplers with different treatments could be deployed during a single lowering; (c) compatibility with other borehole instruments; and (d) deployment with a wireline system, using either a drilling vessel, submersible, or remotely operated underwater vehicle. Most importantly, the sampler design had to include a temperature-sensitive trigger that was independent of electronics, could operate at temperatures from ∼ 80 to 180 °C, and could withstand higher temperatures.

4 Fabrication and testing

To meet these design criteria we designed and fabricated a modular, 1 L, syringe-style, non-gas-tight, titanium fluid sampler in which the sample is only in contact with titanium, two high-temperature silicone o-ring seals and a Viton fluoroelastomer gasket (Fig. 1). The syringe design affords sterile sample collection at in situ pressures, and the

Figure 1. Cross section of a single module of the MTFS highlighting its primary components before the sampler is triggered and after.

sample is contained by a custom spring-loaded titanium and Viton gasket check valve. Because the sampler is not gas-tight, pressure within the sampler is the same as that outside the sampler, similar to the Walden–Weiss titanium fluid sampler. Thus, if dissolved gases in recovered fluids remain undersaturated at shipboard temperatures and pressures, either sampler (Walden–Weiss or MTFS systems) will provide reliable dissolved gas data. In contrast, if dissolved gases are supersaturated in either the Walden–Weiss or MTFS samplers, fluid and or gas will leak out of the sampler during recovery. In the case of the MTFS, fluids or gas would leak out of the Viton gasket check valve, again providing a sample at shipboard pressure.

A fluid sample is drawn slowly into the sample reservoir to prevent degassing, filling the reservoir within ~ 10 s. Upon recovery, a sample is withdrawn after detaching the constant-force spring from the piston (Fig. 1). Next, a titanium plug, which is adjacent to the intake and has a pipe thread, is removed. A titanium tube is then threaded into this opening with the other end of the tube attached to a sample container or collection device (e.g., syringe, filter, or bottles). Fluids are expelled by manually applying pressure to the piston, forcing fluid out of the sample chamber through the titanium tube and into the attached sampling apparatus.

Each sample unit is made of 35.5-inch-long (90.2 cm), 3-inch (7.62 cm) inner diameter (i.d.; schedule 40) grade 2 titanium seamless tubing (Fig. 1) with ACME threads to connect units. Connectors were made from 3.75-inch (9.525 cm) titanium rod with ACME threads. The lower section of the unit

Table 1. Average temperature and standard deviation at which an SMA trigger was activated. Data from three trigger mechanisms and multiple discrete SMAs are listed for combinations that were tested more than three times.

Type of trigger	Temperature and standard deviation (°C)
Spring	80 ± 1; 93 ± 2
Bolt	102 ± 2; 107 ± 1; 126 ± 3; 128 ± 5; 136 ± 3; 161 ± 4; 174 ± 3; 181 ± 7
Precision tube	134 ± 9; 152 ± 5; 152 ± 8; 155 ± 7; 157 ± 2; 159 ± 4

provides a cavity for fluid mixing as the sampler descends within the borehole. Fluids from this cavity enter the sampler through a check valve and into the 1 L sample chamber as the piston extends to the base of the trigger platform. This platform acts as a guide for the piston and houses the trigger, which, when activated, releases a 28-pound (12.7 kg) constant force spring to draw in the sample.

Two types of SMAs were used to trigger the samplers. The first was a commercially available Nitinol material (nickel–titanium SMA), available in spring form and suitable for triggers in the 80 to 90 °C range. These springs are relatively weak; thus, they were used in a configuration that mechanically leverages the change in the SMA spring's form to release the constant force spring. Two springs were selected for use and tested at least five times by heating the MTFS module in a water-filled bath. The empirically determined activation temperatures were 80 and 93 °C, respectively, with a relative standard deviation of < 2 % ("Spring" in Table 1).

A second type of SMA (CuAlNi) was produced in the shape of a 5 mm diameter rod by TiNi Aerospace. Portions of the rod were cut into 0.6-inch-long long (1.52 cm) pieces and machined to allow a notched titanium bolt to pass. TiNi Aerospace has a proprietary method in which an SMA is heated such that as it reverts back to its original shape, it breaks a notched titanium bolt. We tested this trigger process within the MTFS using a heated oil-filled (canola) bath to affect the SMA and release the tension on the constant force spring once the bolt broke (Fig. 2). Eight SMA pieces were tested, each at least three times, resulting in a range of release temperatures ($\sim$ 100–180 °C) with a relative standard deviation of < 4 % for each of the eight pieces ("Bolt" in Table 1).

Other SMAs pieces from this rod material were compressed within a new piece of precision stainless-steel tubing. A trigger was designed in which the SMA was ejected by a spring once the SMA was warmed to the prescribed temperature. Six SMA pieces from two alloys were tested, each at least three times, resulting in a range of release temperatures ($\sim$ 134 to 159 °C) with a relative standard deviation of < 7 % for each of the six pieces ("Precision tube" in Table 1). Un-

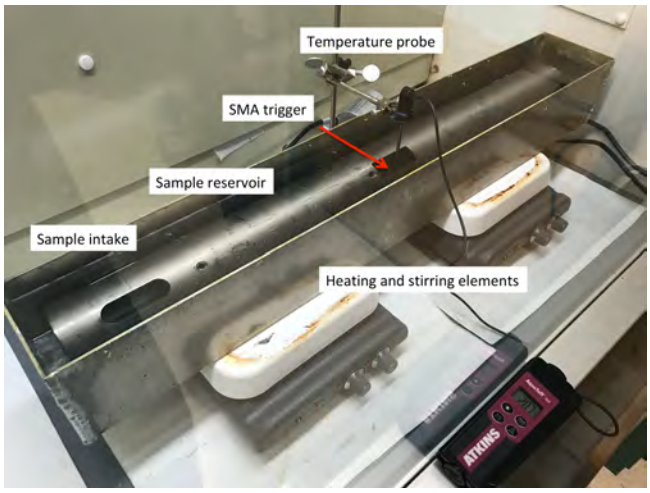

Figure 2. Tests of trigger mechanisms were conducted in a custom bath of canola oil within a chemical hood. The bath holds one 35.5-inch-long (0.90 m) MTFS module, two magnetic stir bars, and a temperature sensor. The temperature sensor is placed within millimeters of the shape metal alloy (SMA) to document the temperature at which the trigger is activated. Two heaters with magnetic stirrers keep the oil bath well mixed, heating the bath to 190 °C in 1 h.

like the other two triggers, this trigger was tested alone and not within the MTFS.

Similar to the Walden–Weiss samplers, the MTFS has no implodable volumes, and the bulk modulus of titanium requires pressures to deform the material that are well in excess of the deepest boreholes under hydrostatic pressure. The pressure effect on the activation temperature of these SMAs is about 5 K GPa^{-1} (Kakeshita et al., 1988, 1999); thus, no pressure tests were conducted on the MTFS triggers. Except for a prototype, which was tested at the seafloor (31 MPa) to assess the piston-syringe and spring-style mechanism, all systems tests were conducted in water- or oil-filled baths, depending on the temperature of activation. We continue to improve the MTFS system. For example, in 2020 the "bolt" trigger option will be recalibrated using precision torque wrenches that will hopefully improve the repeatability and lower the standard deviation of the temperature that activates the trigger.

5 Applications

The first use of the MTFS was planned during the reentry of DSDP Hole 504B on IODP Expedition 385T "Panama Basin Crustal Architecture and Deep Biosphere: Revisiting Hole 504B and 896A" (Tominaga et al., 2019). The goal was to clear scientific equipment in both holes, sample borehole fluids, and log the boreholes. Neither hole was cleared; thus, the MTFS was not deployed (Fig. 3). DSDP Hole 504B is ∼ 190 °C at the base of the open borehole (Guerin et al., 1996), making it an ideal hole to assess the thermal limits of life in basaltic crust. The current verified thermal limit for life is 122 °C (Takai et al., 2008; Clarke, 2014); however, the thermal limit for life may reach or exceed 150 °C (Wharton, 2007; Hoehler, 2007), based on (1) protein and lipid structures that compensate for high temperatures, (2) the increased stability of ribosomal and transfer RNA at high temperatures, and (3) the increased thermal stability of proteins at higher pressures, among other arguments (Galtier and Lobry, 1997; Holland and Baross, 2003). The current MTFS design and availability of triggers allows for up to 12 samples to be collected during a single lowering in the interval from 80 to 181 °C.

Figure 3. A total of 11 modules were combined in three section on the catwalk in anticipation for deployment within DSDP Hole 504B on IODP Expedition 385T in August 2019 (Tominaga et al., 2019). Final assembly and connection to other sensing instruments would occur on the rig floor, which is up the four steps at the end of the catwalk. Aseptic aluminum foil covers the fluid intake to minimize microbial contamination prior to deployment.

A second deployment was proposed to collect flocculent material from Ocean Drilling Program (ODP) Hole 896A, which was based on a biofilm-forming microorganisms and images from a downhole camera (Becker et al., 2004; Nigro et al., 2012). This biofilm is distinctly different from those

observed within the eastern flank of the Juan de Fuca Ridge, even though the thermal and chemical compositions of formation fluids are nearly identical. Differences may suggest site-specific characteristics or biogeographic influences. The MTFS triggers would allow for the collection of samples in the interval from 80 to 90 °C, which is the temperature at the base of the borehole.

For both deployments, we planned on attaching the elevated temperature borehole sensor (ETBS) tool, which measures borehole temperature and records measurements with electronics that are housed within a vacuum jacket (de Ronde et al., 2019). If a vacuum-jacketed system is not available, self-contained temperature recorders (i.e., Onset Hobo) can withstand temperatures to ∼ 150 °C before likely battery failure, but the data may be recoverable according to suppliers. We have not tested this possibility. Such data coupled with measurements of time and the amount of wire deployed would provide a measure of the depth within the borehole at which the samplers were triggered.

Although we were unable to deploy the MTFS during IODP Expedition 385T, the MTFS is suitable for use in a range of oceanic or continental boreholes where fluid collection is desired in the temperature range from 80 to 181 °C. As noted above, the syringe-style design of the MTFS allows for a broad range of priming fluids (e.g., acid, biocide, and metabolic tracers) to conduct a range of potential experiments. In addition, once recovered, the samplers can be placed in oil-filled baths for incubation experiments at in situ temperatures. Although not a current capability, the intake could be modified to filter a sample in situ. The simplicity of the sampler design affords other potential modifications to accommodate a range of community interests. The MTFS is available for community use. Readers interested in using the MTFS should contact the first author (wheat@mbari.org).

Data availability. Data are available in the text. Data from additional testing, specifications, and the operational manual will reside with IODP.

Author contributions. CGW and CK led this project. CW tested the bolt and tube triggers. RS and AM designed and tested the spring trigger. TF machined, modified, and troubleshot the MTFS. TP designed the system for use with IODP. HJ designed triggers and provided machine drawings. All authors contributed to the paper.

Competing interests. The authors declare that they have no conflict of interest.

Acknowledgements. We acknowledge the inspiration from David Johnson, an expert in SMA materials and properties. We thank John Van Hyfte, Bill Rhinehart, and Kevin Grigar for inspecting design elements for compatibility with the *JOIDES Resolution*. We also thank Beth Orcutt and IODP technical staff for help with preparing and assembling the MTFS on IODP Expedition 385T. This is C-DEBI contribution 530.

Financial support. This research has been supported by the U.S. National Science Foundation (grant no. OCE-1830087; Ocean Technology and Interdisciplinary Coordination).

Review statement. This paper was edited by Thomas Wiersberg and reviewed by Jochem Kück and one anonymous referee.

References

Becker, K., Davis, E. E., Spiess, F. N., and Demoustier, C. P.: Temperature and video logs from the upper oceanic crust, Holes 504B and 896A, Costa Rica Rift flank: implications for the permeability of upper oceanic crust, Earth Planet. Sci. Lett., 222, 881–896, https://doi.org/10.1016/j.epsl.2004.03.033, 2004.

Clarke, A.: The thermal limits to life on Earth, Int. J. Astrobiol., 13, 141–154, https://doi.org/10.1017/S1473550413000438, 2014.

de Ronde, C. E. J., Humphris, S. E., Höfig, T. W., and the Expedition 376 Scientists: Brothers Arc Flux, Proc. IODP, 376, International Ocean Discovery Program, College Station, TX, USA, https://doi.org/10.14379/iodp.proc.376.2019, 2019.

D'Hondt, S., Inagaki, F., Orcutt, B. N., and Hinrichs, K. U.: IODP Advances in the understanding of subsurface seafloor life, Oceanography, 32, 198–207, https://doi.org/10.5670/oceanog.2019.146, 2019.

Edwards, K. J., Becker, K., and Colwell, F.: The deep, dark energy biosphere: intraterrestrial life on earth, Annu. Rev. Earth Planet. Sc., 40, 551–568, https://doi.org/10.1146/annurev-earth-042711-105500, 2012.

Emmermann, R. and Lauterjung, J.: The German continental deep drilling program KTB: overview and major results, J. Geophys. Res.-Sol. Ea., 102, 18179–18201, https://doi.org/10.1029/96JB03945, 1997.

Galtier, N. and Lobry, J. R.: Relationships between genomic G+C content, RNA secondary structures, and optimal growth temperature in prokaryotes, J. Mol. Evol., 44, 632–636, https://doi.org/10.1007/PL00006186, 1997.

Guerin, G., Becker, K., Gable, R., and Pezard, P. A.: Temperature mea-surements and heat-flow analysis in Hole 504B, in: Proc. IODP, Sci. Results, edited by: Alt, J. C., Kinoshita, H., Stokking, L. B., and Michael, P. J., 148, Ocean Drilling Program, College Station, TX, USA, 291–296, https://doi.org/10.2973/odp.proc.sr.148.141.1996, 1996.

Hoehler, T. M.: An energy balance concept for habitability, Astrobiology, 7, 824–838, https://doi.org/10.1089/ast.2006.0095, 2007.

Holland, M. E. and Baross, J. A.: Limits to Life in Hydrothermal Systems, in: Energy and mass transfer in marine hydrothermal systems, edited by: Halbach, P., Tunnicliffe, V., and Hein, J. R., Dahlem University Press, Berlin, Germany, 235–248, 2003.

Inagaki, F., Hinrichs, K.-U., Kubo, Y., and the Expedition 337 Scientists: Proc. IODP, Integrated Ocean Drilling Program Management International, 337, Tokyo, Japan, Inc., https://doi.org/10.2204/iodp.proc.337.2013, 2013.

Kakeshita, T., Yoshimura, Y., Shimizu, K. I., Endo, S., Akahama, Y., and Fujita, F. E.: Effect of hydrostatic pressure on martensitic transformations in Cu–Al–Ni shape memory alloys, Trans. JPN I Met., 29, 781–789, https://doi.org/10.2320/matertrans1960.29.781, 1988.

Kakeshita, T., Saburi, T., Kind, K., and Endo, S.: Martensitic transformations in some ferrous and non-ferrous alloys under magnetic field and hydrostatic pressure, Phase Transit., 70, 65–113, https://doi.org/10.1080/01411599908240678, 1999.

Kampman, N., Maskell, A., Bickle, M. J., Evans, J. P., Schaller, M., Purser, G., Zhou, Z., Gattacceca, J., Peitre, E. S., Rochelle, C. A., Ballentine, C. J., Busch, A., and Scientists of the GRDP: Scientific drilling and downhole fluid sampling of a natural CO_2 reservoir, Green River, Utah, Sci. Dril., 16, 33–43, https://doi.org/10.5194/sd-16-33-2013, 2013.

Mottl, M. J. and Gieskes, J. M.: Chemistry of waters sampled from oceanic basement boreholes, 1979–1988, J. Geophys. Res.-Sol. Ea., 95, 9327–9342, https://doi.org/10.1029/JB095iB06p09327, 1990.

Neira, N. M., Clark, J. F., Fisher, A. T., Wheat, C. G., Haymon, R. M., and Becker, K.: Cross-hole tracer experiment reveals rapid fluid flow and low effective porosity in the upper oceanic crust, Earth Planet. Sc. Lett., 450, 355–365, https://doi.org/10.1016/j.epsl.2016.06.048, 2016.

Nigro, L. M., Harris, K., Orcutt, B. N., Hyde, A., Clayton-Luce, S., Becker, K., and Teske, A.: Microbial communities at the borehole observatories on the Costa Rica Rift flank (Ocean Drilling Program Hole 896A), Front. Microbiol., 3, article 232, https://doi.org/10.3389/fmicb.2012.00232, 2012.

Orcutt, B. N., Bach, W., Becker, K., Fisher, A. T., Hentscher, M., Toner, B. M., Wheat, C. G., and Edwards, K. J.: Colonization of subsurface microbial observatories deployed in young ocean crust, ISME J., 5, p. 692, https://doi.org/10.1038/ismej.2010.157, 2011.

Smith, A., Popa, R., Fisk, M., Nielsen, M., Wheat, C. G., Jannasch, H. W., Fisher, A. T., Becker, K., Sievert, S. M., and Flores, G.: In situ enrichment of ocean crust microbes on igneous minerals and glasses using an osmotic flow-through device, Geochem., Geophy., Geosy., 12, Q06007, https://doi.org/10.1029/2010GC003424, 2011.

Takai, K., Nakamura, K., Toki, T., Tsunogai, U., Miyazaki, M., Miyazaki, J., Hirayama, H., Nakagawa, S., Nunoura, T., and Horikoshi, K.: Cell proliferation at 122 C and isotopically heavy CH_4 production by a hyperthermophilic methanogen under high-pressure cultivation, P. Natl. Acad. Sci. USA, 105, 10949–10954, https://doi.org/10.1073/pnas.0712334105, 2008.

Tominaga, M., Orcutt, B. N., Blum, P., and the Expedition 385T Scientists: Expedition 385T Preliminary Report: Panama Basin Crustal Architecture and Deep Biosphere, International Ocean Discovery Program, https://doi.org/10.14379/iodp.pr.385T.2019, 2019.

Von Damm, K. L., Edmond, J. M., Grant, B., Measures, C. I., Walden, B., and Weiss, R. F.: Chemistry of submarine hydrothermal solutions at 21° N, East Pacific Rise, Geochim. Cosmochim. Ac., 49, 2197–2220, https://doi.org/10.1016/0016-7037(85)90222-4, 1985.

Wharton, D. A.: Life at the limits: organisms in extreme environments, Cambridge University Press, Cambridge, UK, 2007.

Wheat, C. G., Becker, K., Villinger, H., Orcutt, B. N., Fournier, T., Hartwell, A., and Paul, C.: Subseafloor cross-hole tracer experiment reveals hydrologic properties, heterogeneities, and reactions in slow spreading oceanic crust, Geochem., Geophy., Geosy., 21, e2019GC008804, https://doi.org/10.1029/2019GC008804, 2020.

Sci. Dril., 28, 49–62, 2020
https://doi.org/10.5194/sd-28-49-2020

Scientific Drilling
Open Access

Haiti-Drill: an amphibious drilling project workshop

Chastity Aiken[1], Richard Wessels[2], Marie-Hélène Cormier[3], Frauke Klingelhoefer[1], Anne Battani[4], Frédérique Rolandone[5], Walter Roest[1], Dominique Boisson[6], Kelly Guerrier[6], Roberte Momplaisir[6], and Nadine Ellouz-Zimmerman[7]

[1]Institut Français de Recherche pour l'Exploitation de la Mer (IFREMER), Géosciences Marines, Laboratoire Aléas géologiques et Dynamique sédimentaire (LAD), 29280 Plouzané, France
[2]Faculty of Geosciences, Utrecht University, 3512 Utrecht, the Netherlands
[3]Graduate School of Oceanography, University of Rhode Island, Narragansett, 02882 Rhode Island, USA
[4]Isotope Geoscience Unit, SUERC, G75 0QF East Kilbride, UK
[5]CNRS-INSU, ISTeP UMR 7193, Sorbonne Université, 75005 Paris, France
[6]Unité de Recherche en Géosciences, Faculté des Sciences, Université d'Etat d'Haïti, HT 6110 Port-au-Prince, Haiti
[7]French Institute of Petroleum, Energies Nouvelles (IFPEN) – Direction Géosciences, 92500 Rueil-Malmaison, France

Correspondence: Chastity Aiken (seismo.chas@gmail.com)

Received: 13 February 2020 – Revised: 24 June 2020 – Accepted: 20 July 2020 – Published: 1 December 2020

Abstract. The Haiti region – bounded by two strike-slip faults expressed both onshore and offshore – offers a unique opportunity for an amphibious drilling project. The east–west (EW)-striking, left lateral strike-slip Oriente–Septentrional fault zone and Enriquillo–Plantain Garden fault zone bounding Haiti have similar slip rates and also define the northern and southern boundaries of the Gonâve Microplate. However, it remains unclear how these fault systems terminate at the eastern boundary of that microplate. From a plate tectonic perspective, the Enriquillo–Plantain Garden fault zone can be expected to act as an inactive fracture zone bounding the Cayman spreading system, but, surprisingly, this fault has been quite active during the last 500 years. Overall, little is understood in terms of past and present seismic and tsunami hazards along the Oriente–Septentrional fault zone and Enriquillo–Plantain Garden fault zone, their relative ages, maturity, lithology, and evolution – not even the origin of fluids escaping through the crust is known. Given these unknowns, the Haiti-Drill workshop was held in May 2019 to further develop an amphibious drilling project in the Haiti region on the basis of preproposals submitted in 2015 and their reviews. The workshop aimed to complete the following four tasks: (1) identify significant research questions; (2) discuss potential drilling scenarios and sites; (3) identify data, analyses, additional experts, and surveys needed; and (4) produce timelines for developing a full proposal. Two key scientific goals have been set, namely to understand the nature of young fault zones and the evolution of transpressional boundaries. Given these goals, drilling targets were then rationalized, creating a focus point for research and/or survey needs prior to drilling. Our most recent efforts are to find collaborators, analyze existing data, and to obtain sources of funding for the survey work that is needed.

1 Introduction

Haiti-Drill, an amphibious drilling project workshop, was held in Plouzané, France, from 20 to 22 May 2019. The workshop was funded by several agencies, namely the MagellanPlus Scientific Steering Committee (SSC), the Interdisciplinary School for the Blue Planet (ISblue) program of the Université de Bretagne Occidentale, the Finistère prefecture, the Institute Français de Recherche pour l'Exploitation de la Mer (IFREMER), and the city of Brest, France. It is the second workshop held for developing an amphibious drilling project along the two strike-slip faults existing at the northern boundary of the Caribbean Plate in the Haiti region. The first MagellanPlus workshop was held in France from 26 to 28 October 2015 after preproposals were submitted earlier that same year to the International Continental Drilling Progam (ICDP) and International Ocean Drilling Program (IODP). A full amphibious drilling proposal has not yet been submitted following the 2015 workshop. Moreover, the leadership of the project, which was initially the French Institute of Petroleum Energies Nouvelles (IFPEN) and Centre Nationale de la Recherche Scientifique (CNRS), has changed to the IFREMER. Since the 2015 workshop, additional work has been done, which includes a marine deep-coring experiment (Haiti-BGF, 2015) and onshore experiments (2017, 2019); further analyses on data from marine field campaigns (Haiti-OBS, 2010; Haiti-SIS, 2012 and 2013) and onshore field campaigns (2014, 2015); and multichannel seismic acquisition in Lake Azuei (2017, http://projectlakeazuei.org, last access: 10 February 2020). These studies have fostered new partnerships for understanding both of the active strike-slip faults that surround Haiti and have provided new insights for prospective drilling.

Reviews of the 2015 preproposal recommended developing a stronger alignment between the objectives and drilling sites and also recommended developing a clear scientific and globally important link between the onshore and offshore targets. Thus, the primary purpose of the 2019 Haiti-Drill workshop was to identify scientific questions that link the onshore and offshore targets, based on recent results, and to enlarge the scientific participant pool. During the 2.5 d workshop, 34 participants from nine countries discussed recent scientific results from land and sea surveys and their implications for the development of an amphibious drilling proposal. Many of the participants in the workshop had never participated in a deep-drilling project before. Thus, one session focused on learning from past drilling experiences onshore and offshore, namely drilling strategies (e.g., management, technicalities, and policies), how to develop a successful drilling proposal, funding a drilling project, etc. In this article, we present the tectonics of the Haiti region and our research interests for an amphibious drilling project in the northern Caribbean, as well as research opportunities and our long-term plans for developing the project. The full agenda of the Haiti-Drill workshop is available at https://wwz.ifremer.fr/gm/Activites/Colloques/Haiti-DRILL-Magellan-Plus-Workshop-May-20-22-2019 (last access: 11 July 2019).

2 Seismotectonics of western Hispaniola

The Gonâve Microplate is one of several blocks that make up the diffuse northern Caribbean Plate boundary, separating the Caribbean Plate in the south from the North American Plate in the north (Mann and Burke, 1984; Mann et al., 1995, 2002; Symithe et al., 2015; Calais et al., 2016). In the western part of this region the geological setting is strongly controlled by two strike-slip fault systems (Burke et al., 1978). These crustal-scale seismogenic fault systems bound a spreading center and oceanic lithosphere (Rosencrantz and Mann, 1991) and also transect and displace lithosphere affected by arc volcanism and flood basalts (Mann and Burke, 1984).

The existence of the Gonâve Microplate has been supported by seismicity along the two left lateral strike-slip faults of the northern Caribbean Plate boundary (e.g., Calais et al., 1998, 2010). The Gonâve Microplate is bounded to the south by the Enriquillo–Plantain Garden fault zone (EPGFZ), to the north by the Oriente–Septentrional fault zone (OSFZ), and to the west by the mid-Cayman spreading center (MCSC; Fig. 1). Geodetic slip rates are similar for both the EPGFZ and OSFZ; however, the velocity vector is parallel to the along strike of the OSFZ, while for the EPGFZ the velocity vector becomes more oblique onshore Hispaniola and to the east (e.g., Symithe et al., 2015; Saint Fleur et al., 2015; Calais et al., 2016). Oblique convergence along the EPGFZ is also expressed geologically as en echelon folds and thrusts adjacent to its main trace (Wang et al., 2018). The eastern boundary between the Gonâve Microplate and Hispaniola consists of a diffuse zone of deformation trending northwest–southeast (NW–SE) through western Hispaniola (Benford et al., 2012; Symithe et al., 2015, 2016; Calais et al., 2016; see Fig. 1). Shortening between the eastern Cayman margin and Hispaniola is thought to be accommodated through a fold-and-thrust belt known as the Trans-Haitian fold-and-thrust belt, which is sandwiched between the eastern segments of the EPGFZ and OSFZ (Pubellier et al., 2000). However, Wang et al. (2018) suggest there is no active folding in the Trans-Haitian Belt – only active faulting and folding along the trend of the EPGFZ. Near the Trans-Haitian Belt, the trace of the EPGFZ disappears, bringing into question whether this wedge zone is where the EPGFZ terminus is located, or if, instead, the EPGFZ is more deeply rooted without a surface expression that might connect with the Muertos Trench (Pubellier et al., 2000 and references therein). Furthermore, the EPGFZ and OSFZ strike-slip faults are characterized by alternating seismic activity on each of the fault strands (Ali et al., 2008), with historical and paleoseismic records dating back some 500 years (e.g., Bakun et al., 2012;

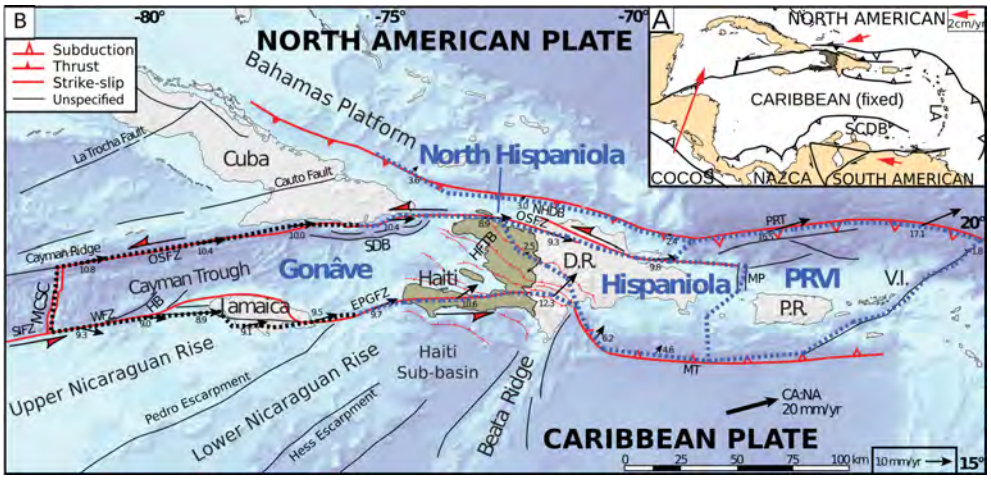

Figure 1. Map view of the Caribbean Plate northern boundary. **(a)** Geodynamic setting. GPS velocities (red arrows) with reference to a fixed Caribbean Plate are from DeMets et al. (2010). **(b)** Geodynamic setting of the northern Caribbean. Dashed lines delineate the Gonâve Microplate and Hispaniola, Puerto Rico–Virgin Islands and North Hispaniola blocks. Blue dashed lines and corresponding GPS velocity vectors are from Calais et al. (2016), while black dashed lines and corresponding GPS velocity vectors are from Symithe et al. (2015). Velocity vectors indicate the motion of the southern (western) boundary with reference to northern (eastern) boundary. Faults are modified after Leroy (1995). Caribbean–North American plate motion is from DeMets et al. (2010). Abbreviations are as follows: LA – Lesser Antilles; SCDB – South Caribbean deformed belt; SIFZ – Swan Island fault zone; MCSC – mid-Cayman spreading center; OSFZ – Oriente–Septentrional fault zone; SDB – Santiago deformed belt; NHDB – North Hispaniola deformed belt; MP – Mona Passage; PRT – Puerto Rico Trench; MT – Muertos Trough; HFTB – Haitian fold-and-thrust belt; EPGFZ – Enriquillo–Plantain Garden fault zone; HB – Hendrix pull-apart basin; WFZ – Walton fault zone; D. R. – Dominican Republic; P. R. – Puerto Rico; V. I. – Virgin Islands; and PRVI – Puerto Rico–Virgin Islands block. Modified from Wessels (2018).

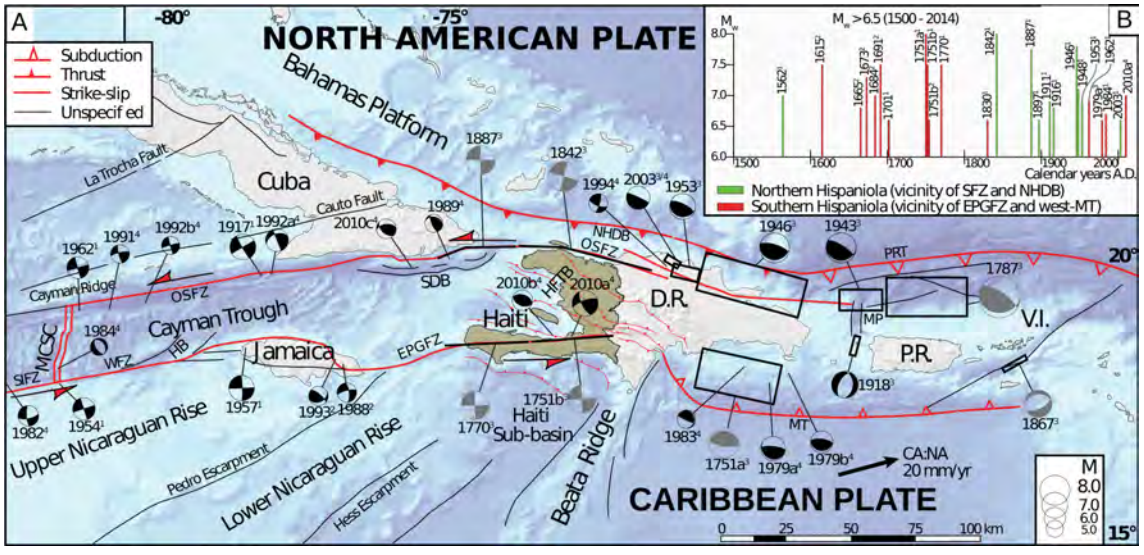

Figure 2. Historical earthquakes along the Caribbean Plate northern boundary. **(a)** Selection of historical and recent earthquakes. Focal mechanisms in gray are historical ($M_w > 7.0$; pre-1900) earthquakes, and focal mechanisms in black are recorded earthquakes ($M_w > 5$; post-1900). Sources: Van Dusen and Doser (2000), Wiggins-Grandison and Atakan (2005), Ali et al. (2008), and the International Seismological Centre (2014; $M_w > 5$; 1976–2014). **(b)** Earthquakes of $M_w > 6.5$ in northern Hispaniola between 1500 and 2016. Earthquakes, in green, from northern Hispaniola and possibly linked to the offshore OSFZ and subduction at the NHDB. Earthquakes, in red, from southern Hispaniola and possibly linked to the EPGFZ or underthrusting at the MT. Sources: McCann (2006), ten Brink et al. (2011), with magnitude on intensity scale (Mi), International Seismological Centre (2014; National Earthquake Information Service – NEIS), and International Seismological Centre (2014; global centroid-moment-tensor – GCMT). Note the magnitude difference for event 1751b between McCann (2006) and ten Brink et al. (2011). Modified from Wessels (2019); same notation as Fig. 1.

Prentice et al., 2010; ten Brink et al. 2013). It remains unclear, however, whether pure strike-slip earthquakes larger than M 6.0 have occurred along the onshore trace of the EPGFZ (Wessels, 2019), although small stream offsets are inferred to be a result of historically reported 18th century earthquakes with an estimated magnitude of 7–7.6 (Prentice et al., 2010; Fig. 2). In addition, recent trenching efforts have also suggested that the EPGFZ is capable of producing magnitude > 7 events, at least to the west of Port-au-Prince (Saint Fleur et al., 2020). Comparatively, trenching efforts along the Septentrional Fault in eastern Hispaniola suggest that events of magnitude ~ 7 occur at least every 800 years (e.g., Prentice et al., 2003), while others suggest recurrence intervals of just 300 years along northern Hispaniola (ten Brink et al., 2011).

Recent onshore and offshore surveys indicate that the EPGFZ and OSFZ are complex fault zones; they are highly segmented by pull-apart basins and have multiple splay faults, as evidenced by flower structures observed in seismic reflection profiles (e.g., Calais and Mercier de Lépinay, 1995; Leroy et al., 2015; Corbeau et al., 2016a; Ellouz et al., 2013; Ellouz-Zimmermann et al., 2016; Wessels et al., 2019; Wessels, 2019; and Saint Fleur et al., 2020 and references therein). Mechanically, the EPGFZ and OSFZ display various behaviors, with some segments having the potential to produce large uplift from big earthquakes (e.g., Hayes et al., 2010; Hashimoto et al., 2011; Symithe et al., 2013) and others producing deep, slow creep near the Mohorovičić (Moho) discontinuity (e.g., Peng et al., 2013; Aiken et al., 2016; see Fig. 3). However, no observable shallow creep has been expressed either geologically or in the infrastructure at the surface. In 1842, a major earthquake also occurred along the OSFZ offshore, which destroyed the cities of Cap-Haïtien and Port-de-Paix due to shaking and an induced tsunami (Scherer, 1913; Fig. 2). In 2010, Haiti was struck by a moment magnitude 7.0 earthquake near Port-au-Prince that led to one of the highest earthquake death tolls ever recorded ($> 235\,000$; Gailler et al., 2015). The tragic 2010 earthquake produced a tsunami due to coastal landslides (Hornbach et al., 2010; McHugh et al., 2011) but did not rupture the main EPGFZ fault segment in this area. The earthquake initiated on the blind north-northwest (NNW)-dipping Léogâne thrust fault, which lies just north of the EPGFZ and merges with the EPGFZ at depth (Calais et al., 2010). It is one of the en echelon structures that accommodates transpression along the EPGFZ (Saint Fleur et al., 2015; Wang et al., 2018). The 2010 earthquake highlights that stress along the EPGFZ zone is distributed among a network of faults and not a single fault plane. More recently, two earthquakes – with a magnitude 5.9 and 5.5 – occurred on 7 October 2018 along the OSFZ, just northwest of Port-de-Paix in the northern Haiti peninsula (Fig. 3). These moderate-sized earthquakes, occurring near the 1842 ruptured area, also produced thrust components based on results published in the Harvard CMT catalog. However, their relationship to the OSFZ remains unclear.

3 Workshop discussions

3.1 Recent surveys and results

Since the 2010 earthquake, a series of scientific surveys have been carried out. These include a marine deep-coring experiment (Haiti-BGF, 2015), marine field campaigns (Haiti-OBS, 2010; Haiti-SIS, 2012, 2013), onshore field campaigns (2014, 2015, 2017, and 2019), and short cores and multichannel seismic acquisition in Lake Azuei (2017). Marine campaigns passively recorded the aftershocks of the 2010 M_w 7.0 earthquake, made high-resolution bathymetry maps, sampled sediments and fluids, and measured heat flow over the offshore western Hispaniola region. Seismic profiles from the Haiti-SIS and Haiti-SIS2 cruises in the vicinity of the EPGFZ and OSFZ conducted after the 2010 earthquake demonstrate that the EPGFZ is separated into ~ 100 km long segments bordered by steep walls (Leroy et al., 2015; Corbeau et al., 2016a, b).

Actively expelled fluids (including gas) with a partial mantle origin have been documented along the onshore prolongation of the OSFZ and EPGFZ (Ellouz-Zimmermann et al., 2016). This seepage activity may significantly modify the thermal regime of the onshore fault segments. Offshore Haiti, heat flow measurements collected during the Haiti-SIS cruise provided constraints on the regional conductive heat flow (Rolandone et al., 2020). In that study, heat flow estimates from in situ measurements and bottom-simulating reflector depth suggest a regionally low heat flow in the western Hispaniola region, respectively 46 ± 7 and 44 ± 12 mW m^{-2}, with locally high values exceeding 80 mW m^{-2}. High values were only found near the large strike-slip faults system (OSFZ and EPGFZ) or near smaller reverse faults. Because conductive mechanisms (shear heating and heat refraction) cannot explain heat flow values as high as 100–180 mW m^{-2}, Rolandone et al. (2020) propose that fluid circulation might be the source of the fault-related high heat flow values.

Onshore, the Trans-Haiti project (2013–2014), a 27 station temporary passive seismic experiment, was conducted to determine the crustal thickness and bulk composition along a north–south coast-to-coast transect in eastern Haiti (Corbeau et al., 2017). Other onshore field campaigns include stratigraphic analysis and geological mapping, kinematic measurements, and sampling of along-fault fluids to investigate tectonic evolution, fault architecture, and paleo-fluid circulation patterns (IFPEN field campaigns, 2014, 2015, 2017). The Lake Azuei project (2017) collected a tightly spaced grid of multichannel seismic and Chirp subbottom profiles over the entire lake to image tectonic structures and also recovered three short cores for age constraints on stratigraphy. These data are intended to characterize how plate motion is partitioned between the strike-slip EPGFZ and compressional structures of the Trans-Haitian Belt, and some results from these surveys were presented at the 2019 American Geophysical Union (AGU) Fall Meeting (Charles et al., 2019; James

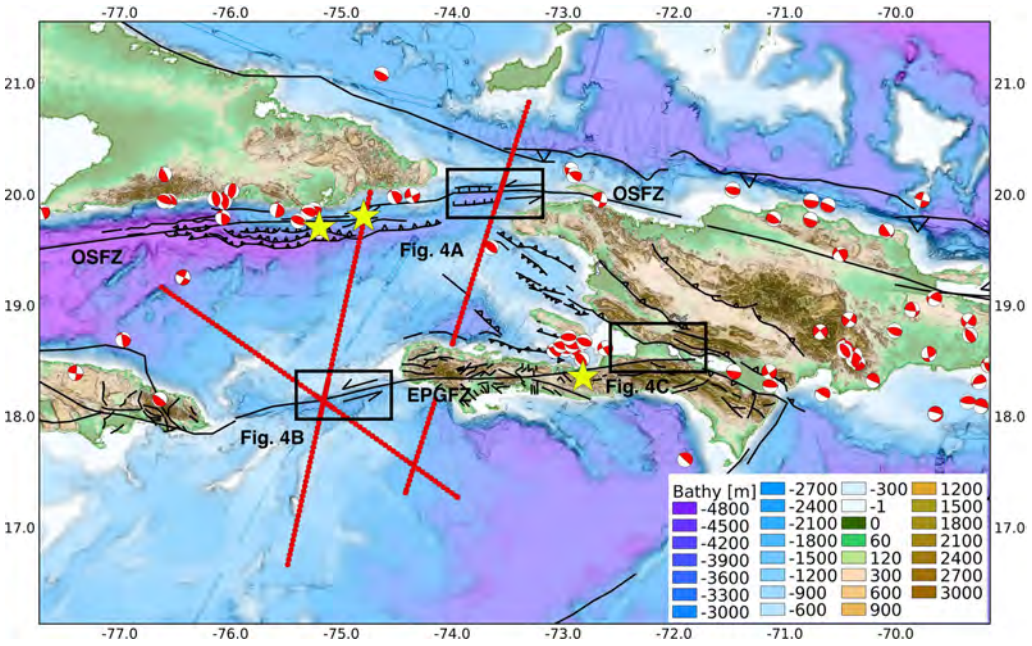

Figure 3. Recent seismotectonics of the northern Caribbean region and offshore survey plan. Red beach balls – earthquake focal mechanisms from the Harvard centroid-moment-tensor (CMT) catalog from 1976 to 2019; yellow stars – slow slip and/or tremor observations (Peng et al., 2013; Aiken et al., 2016); red profiles – proposed transects for the Haiti–TWiST cruise (see Sect. 4). The trace of the EPGFZ terminus east of Port-au-Prince, while illustrated, is actually unknown. Boxes show the locations of panels in Fig. 4.

et al., 2019). The seismic data revealed that a shallow gas front obscures much of the flat-lying turbiditic infill of the lake floor, but structures are well resolved closer to the shore. Profiles imaged a set of subtle EW-trending en echelon folds at the southeastern (SE) corner of the lake; although these folds may be associated with the presence of the EPGFZ, the seismic profiles did not image any fault scarp or stratigraphic offset. A NW-striking monoclinal fold, as wide as 3–5 km, extends along the western shore of the lake, possibly the expression of a southwestern (SW)-dipping blind thrust fold. In addition, Aiken et al. (2016) discovered slow slip in the form of tectonic tremor on the deeper extension of the EPGFZ onshore using passive seismic data collected during both onshore and offshore campaigns (Haiti-OBS 2010) that recorded the aftershocks of the 2010 Haiti earthquake.

3.2 Scientific perspectives

Our overarching research interest is to provide evidence that benefits seismic hazard assessments for the Hispaniola region.

Important input parameters for seismic risk assessment include, amongst others: (a) fault characteristics, to determine the potential energy that can be released by a seismic event and the possible location and depth; (b) the geology and geomorphology of the area, to assess ground motion amplification, liquefaction, tsunami, and landslide potential; and (c) demographics and construction quality, to determine how many people are at risk and what structural loads buildings in the region can withstand. Key aspects for understanding the seismogenic behavior of faults are the fault architecture and fracture network, rheological and mechanical fault parameters, and fault fluid and gas plumbing system. These parameters can then be combined with recurrence events from paleoseismic and historical earthquake records, and geodetic slip rates, to determine the seismogenic behavior and structural maturity (e.g., Perrin et al., 2016). These types of fault characteristics have already been investigated in at least three strike-slip fault drilling expeditions, funded by the ICDP, namely the Nojima Fault in Japan, the San Andreas Fault in the USA, and the Deep Fault Drilling Project (DFDP) along the Alpine Fault in New Zealand (https://www.icdp-online.org/projects/world/australia-and-new-zealand/alpine-fault-new-zealand/details/, last access: 29 December 2019).

The Nojima Fault ruptured in the 1995 $M_{JMA} = 7.2$ Hyogo-ken (Kobe) earthquake, resulting in 6400 casualties (Famin et al., 2014). Activity on this reverse dextral strike-slip fault (Boullier et al., 2004) dates back to $\sim$ 56 Ma (Murakami and Tagami, 2004). The Nojima Fault was the target of the 1995 Nojima Fault Zone Probe project, which sought to examine the physical and chemical processes immediately following the 1995 Kobe earthquake (Ando, 2001) along the Nojima Fault of Japan, which is thought to have already initiated at least $\sim$ 56 Ma (Murakami and Tagami, 2004). This expedition successfully drilled three boreholes at depths

of 500 m (pilot hole), 800 m (passive monitoring hole), and 1800 m (fault penetration hole). A seismometer and thermometer were placed into the deepest borehole, which penetrated the active Kobe Fault, and water was injected into it to trigger seismicity. The drilling expedition resulted in a geological and geophysical reconstruction of the structure and evolution of the Nojima Fault, the identification of the maximum regional compressional stress axis, induced microearthquakes, and measurement of fault width from cores (e.g., Famin et al., 2014, and references therein).

The San Andreas Fault (SAF) is a dextral strike-slip system with a displacement of around 200 km that initiated ~ 5 Ma (Darin and Dorsey, 2013). Geological slip rates are estimated at 50 mm yr^{-1} (DeMets and Dixon, 1999), while geodetic slip rates indicate a 48 ± 5 mm yr^{-1} (Bennett et al., 1996) right lateral offset. The San Andreas Fault Observatory at Depth (SAFOD) project targeted the SAF in the early 2000s. The SAFOD drilling project penetrated three active strands of the San Andreas Fault near Parkfield, California, a segment of the San Andreas Fault that has produced at least seven large-sized repeating earthquakes since the late 19th century. The SAFOD project had two objectives, namely to (1) investigate the physical and chemical processes that control deformation and earthquake generation within an active fault zone; and (2) make near-field observations of earthquake nucleation, propagation, and arrest to test laboratory-derived concepts about the physics of faulting (Zoback et al., 2011). A pilot borehole was drilled to ~ 2.2 km depth near the terminus of the creeping section of the Parkfield segment to obtain geological and geophysical knowledge for the main SAFOD borehole (e.g., Hickman et al., 2004). A total of 27 experimental deployments were also placed in the pilot hole in preparation for a long-term observatory in the main borehole, which was drilled to a depth of ~ 2.7 km (Zoback et al., 2011). The results of the SAFOD experiment are numerous, but in general, the drilling project yielded a deeper understanding of the structure and physical properties of the San Andreas Fault; the composition of fault zone rocks; the stress, temperature, and fluid-pressure conditions that nucleate earthquakes; and the absence of deep-seated fluids in fault zone processes (Zoback et al., 2011).

Based on results from previous successful ICDP strike-slip fault campaigns, drilling the OSFZ and EPGFZ can provide insight into, amongst others, the physical properties, geological evolution, and fluid-flow characteristics that are responsible for the seismogenic hazard along comparatively young, transpressive strike-slip fault zones. Although different in kinematics, complexity, age, and lithology, portions of the OSFZ and EPGFZ can both produce earthquake swarms as a form of slow slip (e.g., Possee et al., 2019) and deep creep in the lower crust (tectonic tremor; e.g., Peng et al., 2013; Aiken et al., 2016). Yet, in the Windward Passage segment of the OSFZ, deep tectonic tremor has not yet been observed, and it is still not known if escaping fluids may exist that may drive shallow earthquake swarms. In terms of physical properties, the onshore part of the EPGFZ is characterized by high angles between maximum principal paleostress directions and the trace of the fault (Wessels et al., 2019), signaling a weak fault zone. However, it remains to be shown if fault weakness is observable when comparing earthquake focal mechanisms from present-day passive seismic recordings to fault orientation. Fault weakness, as is typical for the Nojima Fault and SAF (e.g., Famin et al., 2014), is either related to a very low friction coefficient or to elevated fluid pressures in the fault zone. The dominant lithology controlling the friction coefficient of the EPGFZ fault zone predominantly consists of mafic rocks (e.g., Wessels et al., 2019), which are unfortunately only exposed in a very weathered state at the surface. Samples of spring waters found proximal to the trace of the EPGFZ indicate a mantle component (Ellouz-Zimmermann et al., 2016), but these diffuse sample locations provide little insight into the fault plumbing system and fault zone fluid pressures. A receiver function study has shown that the mantle is elevated near the presumed EPGFZ (Corbeau et al., 2017), but tomographic studies did not yield any strong evidence for the presence of fluids (Possee et al., 2019). Drilling, coring, and monitoring the OSFZ and EPGFZ would result in fresh rock samples, in situ fluid chemistry and pressure measurements, and stress measurements and seismic observations in the long term. Together, these measurements provide important insights into the similarities and differences in the OSFZ and EPGFZ failure properties and, in turn, the seismogenic potential of these fault zones. In terms of recurrence intervals for the pair of strike-slip faults, we certainly lack paleorecords dating more than 500 years for which deep drilling can provide insight into their long-term seismic history. Pull-apart basins along the offshore segments of the EPGFZ and OSFZ may record activity on these faults. In addition, seismogenic lake turbidites (seismites) in lakes proximal to the onshore trace of the EPGFZ can also give estimates of earthquake recurrences. Structurally, there is the question of whether the eastern Cul-de-Sac–Enriquillo Valley portion of the EPGFZ terminates or continues to propagate into eastern Hispaniola. At the very least, geologic markers west of Port-au-Prince seem to indicate that the EPGFZ is eastward propagating (Saint Fleur et al., 2020). In general, propagation of strike-slip faults in heterogeneous basement terrains remains poorly understood. Drilling the EPGFZ onshore at different segments may provide insights into the propagation and maturity of this fault system.

Beyond the physical and chemical fault properties of strike-slip faults and fault propagation, we also entertained the idea that with drilling we could potentially identify whether or not a seaway closure occurred at onshore Haiti during the formation of the Cayman Trough. A paleo-reef has been identified surrounding Lake Enriquillo in the Dominican Republic (Taylor et al., 1985; Mann et al., 1995). However, there is no evidence for an equivalent reef around Lake Azuei, for which the level is 50–60 m higher than Lake

Enriquillo. It has also been suggested that there are marine stages in both Lake Azuei and Lake Enriquillo at roughly 20 m below the lake bottoms (Wang et al., 2018), but this has not yet been supported by coring data. There may be evidence of ancient shells, corals, and other marine organisms in cores or samples recovered from deep drilling. These could also extend the historical record of sea surface temperature. Specifically, if a seaway closure has occurred, we might see differences in benthic foraminiferal Mg/Ca records in Lake Azuei, compared to those observed along offshore segments of the OSFZ and the EPGFZ, as have been observed in a previous seaway closure study (Lear et al., 2003). Lake Azuei, which lies between two high mountain ranges (> 1500 m), also provides an opportunity to address the question of how surface geology changes with climate (e.g., Whipple and Meade, 2006). Lake Azuei may even hold archaeological evidence of the time when humans first arrived on Hispaniola.

Clearly, there are many interesting questions to be asked and explored in the western Hispaniola region, both onshore and offshore. However, we determined two primary research goals for drilling as follows:

1. *The nature of young fault zones* – does fault weakness exist equally at different segments of the fault zones? What mechanisms control the occurrence of destructive earthquakes that can generate landslides and tsunamis? How are fluids linked to tectonic, thermal, and biogeochemical processes?

2. *The evolution of transpressional boundaries* – how do landscapes, hydrology, thermal regimes, and climate interact? How are atmospheric processes and lithospheric processes linked to orogeny? How do stress, strain, and fluid pressure conditions change along and across strike of juvenile, advancing transpressional fault systems?

3.3 Drilling perspectives

During the 2015 workshop, six drilling targets – three offshore and three onshore sites – were selected. These sites are the Windward Passage basin along the OSFZ offshore (Fig. 4a), the Navassa Basin along the EPGFZ in the Jamaica Passage (Fig. 4b), the Jérémie Basin just north of the southern peninsula, Lake Azuei (which may overlay the terminus of the EPGFZ), the EPGFZ near the southern shore of Lake Azuei, and the frontal thrust plane of the Matheux Range. Participants at the 2019 workshop agreed that basins along the OSFZ and the EPGFZ offshore remain ideal targets because they have been extensively surveyed (Haiti-SiS 2012, 2013) and require very little additional survey work. These offshore target sites are located in the releasing bends of the OSFZ and EPGFZ, where compression along the fault is expected to be lowest. Submarine pull-apart basins along strike-slip faults are capable of holding a wealth of paleoseismic records, as has been evidenced along the North Anatolian Fault system in the Sea of Marmara (McHugh et al., 2006). On the other hand, the onshore targets identified during the 2015 workshop may not be suitable because the EPGFZ terminus fault architecture in the Lake Azuei region is still unknown, requiring additional survey work that may prove difficult. Thus, we discussed and rationalized three potential sites for onshore drilling during the workshop. We elaborate on these sites further below.

Along the EPGFZ, one potential target is near the Momance River, which follows the trace of the EPGFZ as it enters the Léogâne delta plain (Fig. 4c). This locality is ∼ 20 km west of Port-au-Prince and proximal to the site of the M_w 7.0 2010 earthquake. In this area, the EPGFZ can easily be identified in the topography and is presumed to be vertical or to have a slight southern dip. At this locality, the EPGFZ juxtaposes the Caribbean large igneous province (CLIP) basement in the south against Miocene carbonate sediments in the north. Further west of the Momance River, where the EPGFZ exits the fan complex, Hornbach et al. (2010) collected Chirp high-resolution seismic profiles offshore, and Kocel et al. (2016) collected near-surface seismic reflection profiles onshore. In that region, the fan is known to be relatively thick and coarse grained with boulder-sized limestones. However, we do not know the stratigraphy near the Momance River site or if it may be more conducive for drilling. Alternatively, we could consider a site just a few hundred meters offshore where high-resolution seismic data highlight the fault trace and where sediments have ponded between patch reefs (Hornbach et al., 2010). The Momance River site does provide a unique opportunity to drill through a relatively mature part of the EPGFZ to take fresh samples of the dominant crustal lithology (basalt) that this fault is penetrating and to take in situ pressure, temperature, and chemical measurements. In situ stress measurements will provide insights into the loading of the EPGFZ as a result of the 2010 earthquake, and continued monitoring would provide insights into the earthquake hazard that this fault poses. Samples from the EPGFZ onshore would be an ideal comparison to samples taken from the EPGFZ offshore, as the EPGFZ is thought to be an eastward-propagating fault (Saint Fleur et al., 2020). Differences in fault weakness may be apparent between samples, as the fault may be more mature in the west compared to the east. They could also be compared to the OSFZ, which may or may not have developed simultaneously with the EPGFZ. The benefit of this site is that the location and occurrence of the EPGFZ are certain, and the drill rig can be placed directly on (weathered) mafic basement. This site also allows a direct comparison with the outcropping core of the EPGFZ in calcareous rocks in quarries some 25 km eastwards along strike. It would require only a limited site survey consisting of detailed geological mapping and stratigraphic observations and perhaps even passive seismic monitoring. The difficulty with this site would be to bring the material inside this river valley and to find a large enough flat surface to install the drill rig. An alternative to this site could be the southern border of Lake Miragoâne.

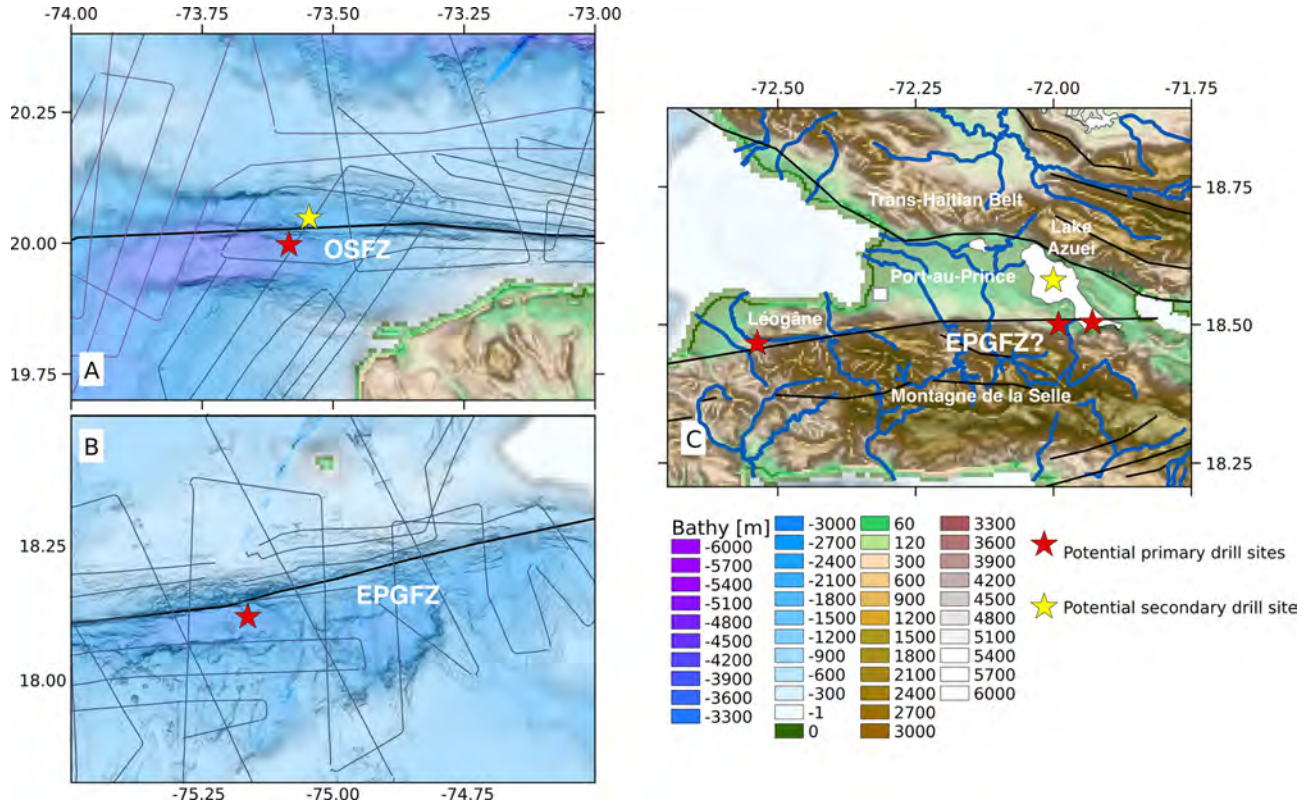

Figure 4. Potential drilling sites (red stars) and alternates (yellow stars). **(a)** In a basin of the Windward Passage along the OSFZ offshore the northern Haitian peninsula, **(b)** in the Navassa Basin of the Jamaica Passage along the EPGFZ offshore the southern Haiti peninsula and **(c)** onshore near the EPGFZ terminus – one site on land and one site in Lake Azuei. At the potential Momance River site, west of Port-au-Prince near the Léogâne delta plain, the fault trace is better defined and the fault is also more vertical. To the east, less is known. The trace of the EPGFZ terminus east of Port-au-Prince, while illustrated in panel **(c)**, is actually unknown, and the fault possibly dips south-southwest. The site near the Léogâne delta plain requires less additional survey work and is preferred but difficult to link scientifically to the Lake Azuei site. Multichannel seismic (MCS) data were acquired during Haiti-SIS and Haiti-SIS2 along the ship tracks, as shown in panels **(a)** and **(b)**.

There are a few benefits to this site. Chirp high-resolution seismic profiles (< 10 m) are available for Lake Miragoâne (Wang et al., 2018) and a 17 m core that has been thoroughly analyzed, reconstructing Caribbean climate change over the past 10 500 years (Hodell et al., 1991). In addition, it would be comparatively easy to bring the drill equipment in place. The downsides are a thick alluvial sedimentary cover, less knowledge about the stratigraphy and thicknesses, a less defined fault trace, and potential fisheries in the lake.

A second potential site is the EPGFZ on the southern shore of Lake Azuei (Fig. 4c). Recent studies support a model where a large fault is likely dipping south under the Montagne de la Selle (Saint Fleur et al., 2015; Symithe and Calais, 2016; Possee et al., 2019), with diffuse deformation accommodated by various sets of oblique-slip and strike-slip faults (Wessels et al., 2019). Wang et al. (2018) suggest that the EPGFZ in this area transitions closer to vertical and is deeply buried. However, where this transition occurs is not exactly known as seismicity in the region is sparse (e.g., Possee et al., 2019), and seismic reflection surveys detailing the fault architecture are nonexistent. While there is no observable trace of the EPGFZ, this area of diffuse deformation likely represents the tip of the advancing EPGFZ. Drilling through the sequence of faults can provide insights into the distribution of stress, strain, and pressure conditions of juvenile, advancing fault systems but would provide less information about the rheological parameters controlling the fault characteristics. These characteristics could also be easily compared to characteristics observed offshore – along the OSFZ and EPGFZ – to understand the differences between young fault zones and their evolution. Located directly adjacent to Port-au-Prince, investigating this segment of the EPGFZ would also benefit earthquake risk assessments in the region. However, without proper control of the location, dimensions, and thickness of splay faults, it would require a much more extensive site survey, including detailed geological mapping over a wider area, stratigraphic investigations, and possibly a seismic survey over topographically challenging terrain. Passive seismic recordings could also elucidate the fault slip mode in this region – whether creeping or locked. A benefit of this site is

that it can be relatively easily reached when approached from the north, and it can be more easily combined with drilling in Lake Azuei compared to a project further west of Port-au-Prince.

A third potential site is located within Lake Azuei (Fig. 4c). Lake Azuei, a brackish and perhaps anoxic lake (Eisen-Cuadra et al., 2013), with depths down to 30 m (Moknatian et al., 2017; James et al., 2019), is an ideal drilling target for a multidisciplinary drilling project. Based on recent short coring (namely, Project Lake Azuei), the sediment deposition is mostly continuous and undisturbed, and the fact that the lake is wedged between two high, active mountain ranges guarantees that it collects the by-product of mountain erosion. Therefore, the lake likely contains an exquisite sedimentary record that can be used to study paleoseismicity, paleoclimate, paleogeography, and possible even determine when humans first arrived on Hispaniola. In terms of paleoclimate, drilling Lake Azuei can extend the Holocene climate record in the northern Caribbean. Drilling here could also confirm if erosional rates are linked to drought and humid climate intervals and the influence of recent deforestation on sediment flux. The area was an open seaway during the Pliocene (e.g., Mann et al., 1984), but the timing of the closure of that seaway remains to be documented. Because Lake Azuei is probably anoxic at its depocenter (Fig. 4c, yellow star), it should preserve a pristine stratigraphy (not bioturbated). Its sediments may thus host a detailed climate record and earthquake record and may also allow one to precisely date the arrival of humans on Hispaniola based on detailed pollen and charcoal analysis. Finally, Lake Azuei lies near the presumed terminus of the EPGFZ, which may hold information about paleoseismic records. With influx from distinctly different sources (basements) in the north and south, it is potentially possible to distinguish between earthquakes triggering seismites in central versus southern Hispaniola. Paleoseismic records from Lake Azuei would also make a desirable scientific link between drilling onshore and offshore – giving historical records of earthquake activity along the OSFZ and EPGFZ that can provide clues to the evolution of the dual strike-slip system. Lastly, multichannel seismic profiles faintly imaged a deformation zone present beneath the shallow gas front and that extends across a 2–3 km wide corridor paralleling the southern shore of the lake. However, it remains unclear whether this deformed layer reflects faulting and/or folding. Drilling into those deformed rocks may provide a useful test with respect to the competing models for the nature of the EPGFZ in that area.

4 Future plans

The future of the Haiti-Drill project was discussed on the last day of the workshop. It was agreed that there are three imperative tasks for producing a successful amphibious drilling project in the western Hispaniola region. First, more preliminary work should be done, especially for the onshore sites. Second, we need additional expertise to analyze existing data and diversify the science related to drilling. Third, local Haitian researchers and students must be included in small-scale projects leading up to the drilling proposal to build training, understanding, and community support. We identified additional data, research, surveys, and scientists needed in order to develop a future proposal. Finally, we created realistic timelines for both onshore and offshore projects.

Despite several oceanographic surveys conducted within the last decade, some questions still remain about the architecture of the OSFZ and EPGFZ offshore. In particular, the dipping angles of the OSFZ and EPGFZ target areas are not well constrained, which is required for selecting the ICDP and IODP sites. A marine deep seismic cruise proposal (namely, Haiti–TWiST) was submitted in September 2019 to investigate the structural and mechanical behaviors of the OSFZ and EPGFZ offshore and target the offshore drilling sites (Fig. 3) and was successfully classed as being a top priority for scheduling from 2021. During this campaign, we will conduct a wide-angle seismic reflection survey offshore Haiti, take heat flow measurements, sediment cores, and sample interstitial fluids across the fault zones near the drilling target sites to characterize the possible hydrothermal system and make passive seismic recordings near the fault zones to observe the different types of seismicity. The wide-angle seismic survey will constrain the fault structure, sediment coring across and along the faults will help constrain paleoseismic records, and fluid sampling will help to understand their origins and relationship with present-day seismicity on passive seismic recordings. Onshore, the 2017 marine seismic survey of Lake Azuei revealed the presence of a diffuse gas front in the shallow sediments, except for its deepest basin floor. A deformation zone is visible below the gas front along the presumed extension of the EPGFZ in the southern part of the lake (Charles et al., 2019). Although, at this stage of data processing, it remains unclear whether that deformation zone reflects folding or faulting. If deeper pockets of pressurized gas exist, this would prevent drilling for safety reasons.

The other potential onshore targets, south of Lake Azuei and along the Momance River or the alternative site on the southern border of Lake Miragoâne require additional site surveys. While the Momance River requires only limited additional geological mapping and refining of the local stratigraphy, Lake Miragoâne and the onshore site near Lake Azuei's southern shore require extensive site surveys; additional reflection seismics to determine the location and geometry of the faults necessary for developing a drilling plan are needed. However, at present, we have no single onshore site that is preferred because there have not been any multidisciplinary studies conducted at any one site that can support drilling at this time. If survey work is successful, we would prefer to target Lake Azuei and land near the southern shore of Lake Azuei as these sites would be more easily

linked due to their locations and because Lake Azuei offers a potential wealth of multidisciplinary data. However, near the southern shore of Lake Azuei, topography may present a problem for site surveys. We are currently in the process of planning a multidisciplinary onshore survey project for submission to the Agence Nationale de la Recherche (ANR) for funding. The project will target sites west of Lake Azuei and near the Momance River so that we can choose the best drilling location. Surveys will be conducted in collaboration with scientists from the Université d'Etat d'Haïti. The surveys will serve as fieldwork opportunities for Haitian students from the Université d'Etat d'Haïti. However, finding a sufficiently powerful seismic source to conduct a seismic reflection survey with a penetration depth > 1 km will likely be more challenging.

While more data need to be collected to justify drilling offshore, there are also many research opportunities for organic and/or inorganic geochemists, sedimentologists, paleoseismologists, paleoecologists, and biogeochemists to explore existing data and/or participate in the future drilling project. For example, 2 $\sim$ 80 cm long cores were collected in 2017 from Lake Azuei (http://projectlakeazuei.org, last access: 10 February 2020) with several intervals that have been dated with radioisotope methods (Cormier et al., 2018). Some cores offshore were taken during the Haiti-BGF and first Haiti-SIS cruise, but the data were insufficient to decide whether fluid is escaping or not. Cores from these campaigns were scarce and often short and did not provide any fluid geochemistry indicative of strong circulation. However, this of course does not prove that there are no fluids escaping along fault offshore. Other investigations, e.g., acoustic measurements in the water column, are needed to find places where seeps occur and other and longer cores, if possible – something we aim to address in the Haiti–TWiST marine campaign. Onshore, there is evidence of advected mantle-derived fluids, but more samples are needed to assess the temporal variability. We are also searching for additional researchers to assist with developing the paleorecord from the short cores (onshore and offshore). Moreover, this project is a unique opportunity for paleoclimate studies as Lake Azuei lies between two topographic highs and likely has erosional deposits. In particular, Lake Azuei appears to be anoxic at its depocenter, which makes for an ideal drilling target for paleoclimate studies. It may also be archiving key markers (such as maize pollens) that may have recorded when humans arrived in Hispaniola.

5 Concluding remarks

The western Hispaniola region presents a unique opportunity for an amphibious drilling project because it is bounded by two active strike-slip faults with the potential for vertical uplift onshore and offshore. In addition, the EPGFZ and OSFZ are both younger than previously drilled strike-slip faults, which makes drilling in the western Hispaniola region ideal for not only expanding our understanding of the physical and chemical properties of strike-slip faults at different stages of maturity but also for providing samples of a potentially propagating fault system.

During the 2019 Haiti-Drill workshop, we discussed themes such as the evolution of transpressional boundaries – how landscapes, hydrology, thermal regimes, and climate interact – and the nature of young fault zones. We identified key questions that link the onshore and offshore segments of the dual strike-slip system and made some preliminary drilling-scenario plans. Our research goals are largely related to seismotectonics – understanding how the OSFZ and EPGFZ strike-slip faults have evolved and their characteristics – how have they behaved in the past, how they behave today, and what controls that behavior. We have yet to decide how we will approach drilling – whether drilling through faults is possible or if we must drill next to the faults. Deciding this requires additional research, surveys, and expertise. In particular, high-resolution, wide-angle seismic reflection, geological mapping, heat flow measurements, and additional coring need to be done to enhance our understanding of the architecture, hydrothermal systems, and paleorecord of the region prior to deeper drilling. At least one deep marine survey has been planned, and funding for onshore surveys is currently being sought. At present, there are existing cores and seismic data that need additional analyses. We are specifically interested in enlarging the scientific team to help with additional analyses, future field work, and the long-term development of the full proposal. Anyone interested in access to data or participating in the long-term development of the amphibious drilling project is invited to contact Chastity Aiken, the corresponding author.

Data availability. All data are from third parties. Data for Fig. 1 are from DeMets et al. (2010). Data for Fig. 2 are from McCann (2006), ten Brink et al. (2011), and the International Seismological Centre (ISC). Earthquakes listed in the ISC catalog are openly available (http://www.isc.ac.uk, last access: 27 August 2020). Focal mechanisms shown in Figs. 2 and 3 are openly available from the Harvard Global Centroid Moment Tensor Catalog (GCMT; https://www.globalcmt.org/CMTsearch.html, last access: 27 August 2020). Ship track information shown in Fig. 4 is not openly accessible but is available upon request from the corresponding author.

Author contributions. NEZ conceived the idea for an amphibious drilling project onshore and offshore Haiti. CA improved upon the amphibious drilling project idea in this workshop report with contributions from all authors. CA, RW, and FK collected the data presented in Figs. 1–4. CA, RW, MHC, FK, AB, FR, WR, and NEZ contributed to the writing of the paper. DB, KG, and RM provided direction, advice, and feedback on this paper, which is necessary for this future drilling project to be successful.

Competing interests. The authors declare that they have no conflict of interest.

Acknowledgements. We extend our special thanks to Manuel Pubellier of École normale supérieure (ENS) – one of the initiators of this amphibious scientific drilling project aiming to better understand active faults in the Haiti region – and to Paul Mann, Jamie Austin, and one anonymous reviewer for their thoughtful reviews that enhanced the quality of this paper. The authors also express their sincere gratitude to the MagellanPlus SSC, Université de Bretagne occidentale, the Finistère prefecture, the Institute Français de Recherche pour l'Exploitation de la Mer (IFREMER), and the city of Brest, France, for financially supporting the 2019 Haiti-Drill workshop. In particular, this workshop was supported in part by ISblue, the "Interdisciplinary graduate school for the blue planet", a project cofinanced (grant no. ANR-17-EURE-0015) and administered by the French national research agency, ANR, within the French State program of Investments For The Future (PIA).

Review statement. This paper was edited by Will Sager and reviewed by Paul Mann, James A. Austin, and one anonymous referee.

References

Aiken, C., Chao, K., Gonzalez-Huizar, H., Douilly, R., Peng, Z., Deschamps, A., Calais, E., and Haase, J. S.: Exploration of remote triggering: A survey of multiple fault structures in Haiti, Earth Planet. Sc. Lett., 455, 14–24, https://doi.org/10.1016/j.epsl.2016.09.023, 2016.

Ali, S. T., Freed, A. M., Calais, E., Manaker, D. M., and McCann, W. R.: Coulomb stress evolution in Northeastern Caribbean over the past 250 years due to coseismic, postseismic and interseismic deformation, Geophys. J. Int., 174, 904–918, https://doi.org/10.1111/j.1365-246X.2008.03634.x, 2008.

Ando, M.: Geological and geophysical studies of the Nojima Fault from drilling: An outline of the Nojima Fault Zone Probe, Isl. Arc, 10, 206–214, https://doi.org/10.1111/j.1440-1738.2001.00349.x, 2001.

Bakun, W. H., Flores, C. H., and ten Brink, U. S.: Significant earthquakes on the enriquillo fault system, Hispaniola, 1500–2010: implications for seismic hazard, B. Seismol. Soc. Am., 102, 18–30, https://doi.org/10.1785/0120110077, 2012.

Benford, B., DeMets, C., and Calais, E.: GPS estimates of microplate motions, northern Caribbean: evidence for a Hispaniola microplate and implications for earthquake hazard, Geophys. J. Int., 191, 481–490, https://doi.org/10.1111/j.1365-246X.2012.05662.x, 2012.

Bennett, R., Rodi, W., and Reilinger, R. E.: Global Positioning System constraints on fault slip rates in southern California and northern Baja, Mexico, J. Geophys. Res., 101, 21943–21960, https://doi.org/10.1029/96JB02488, 1996.

Boullier, A.-M., Fujimoto, K., Ito, H., Ohtani, T., Keulen, N., Fabbri, O., Amitrano, D., Dubois, M., and Pezard, P.: Structural evolution of the Nojima fault (Awaji Island, Japan) revisited from the GSJ drill hole at Hirabayashi, Earth Planets Space, 56, 1233–1240, https://doi.org/10.1186/BF03353345, 2004.

Burke, K., Fox, P. J., and Sengör, A. M. C.: Buoyant ocean floor and the evolution of the Caribbean, J. Geophys. Res., 83, 3949–3954, https://doi.org/10.1029/JB083iB08p03949, 1978.

Calais, E. and Mercier de Lépinay, B.: Strike-slip tectonic processes in the northern Caribbean between Cuba and Hispaniola (windward passage), Mar. Geophys. Res., 17, 63–95, https://doi.org/10.1007/BF01268051, 1995.

Calais, E., Perrot, J., and Mercier de Lépinay, B.: Strike-slip tectonics and seismicity along the northern Caribbean plate boundary from Cuba to Hispaniola, Geol. Soc. Am. Soc., 326, 125–169, https://doi.org/10.1130/0-8137-2326-4.125, 1998.

Calais, E., Freed, A., Mattioli, G., Amelung, F., Jónsson, S., Jansma, P., Hong, S.-H., Dixon, T., Prépetit, C., and Momplaisir, R.: Transpressional rupture of an unmapped fault during the 2010, Haiti earthquake, Nat. Geosci., 3, 794–799, https://doi.org/10.1038/ngeo992, 2010.

Calais, E., Symithe, S., Mercier de Lépinay, B., and Prépetit C.: Plate boundary segmentation in the northeastern Caribbean from geodetic measurements and Neogene geological observations, C. R. Geosci., 348, 42–51, https://doi.org/10.1016/j.crte.2015.10.007, 2016.

Charles, N., Cormier, M.-H., Sloan, H., Wattrus, N. J., Sorlien, C. C., Boisson, D., Guerrier, K., Hearn, C. K., King, J. W., Momplaisir, R., Symithe, S. J., and Ulysse, S. M. J.: Multichannel Seismic Survey of Lake Azuei (Haiti) Documents a Complex System of Active Transpressional Structures Across the North American-Caribbean Plate Boundary, Fall Meeting Am. Geophysical Union, 9–13 December 2019, San Francisco, USA, abstract no. 555543, https://doi.org/10.1002/essoar.10501580.1, 2019.

Corbeau, J., Rolandone, F., Leroy, S., Mercier de Lépinay, B., Meyer, B., Ellouz-Zimmermann, N., and Momplaisir, R.: The northern Caribbean plate boundary in the Jamaica Passage: Structure and seismic stratigraphy, Tectonophysics, 675, 209–226, https://doi.org/10.1016/j.tecto.2016.03.022, 2016a.

Corbeau, J., Rolandone, F., Leroy, S., Meyer, B., Mercier de Lépinay, B., Ellouz-Zimmermann, N., and Momplaisir, R.: How transpressive is the northern Caribbean plate boundary, Tectonics, 35, 1032–1046, https://doi.org/10.1002/2015TC003996, 2016b.

Corbeau, J., Rolandone, F., Leroy, S., Guerrier, K., Keir, D., Stuart, G., Clouard, V., Gallacher, R., Ulysse, S., Boisson, D., Momplaisir R. B.-A., Saint Preux, F., Prépetit, C., Saurel, J.-M., Mercier de Lépinay, B., and Meyer, B.: Crustal structure of western Hispaniola (Haiti) from a teleseismic receiver function study, Tectonophysics, 709, 9–19, https://doi.org/10.1016/j.tecto.2017.04.029, 2017.

Cormier, M.-H., Sloan, H., King, J. W., Boisson, D., Guerrier, K., Hearn, C. K., Heil, C. W., Kelly, R. P., Momplaisir, R., Murray, A. N., Sorlien, C. C., Symithe, S. J., Ulysse, S. M. J., and Wattrus, N. J.: Late Quaternary Fault-Related Folding, Uplifted Paleoshoreline, and Liquefaction Structures: Clues About Transpressional Activity Along the North America-Caribbean Plate Boundary From a Comprehensive Seismic Reflection Survey of Lake Azuei, Haiti, Fall Meeting Am. Geophys. Union, 10–14 December 2018, Washington, DC, USA, Poster EP51D-0692, https://doi.org/10.1002/essoar.10500232.1, 2018.

Darin, M. and Dorsey, R.: Reconciling disparate estimates of total offset on the southern San Andreas Fault, Geology, 41, 975–978, https://doi.org/10.1130/G34276.1, 2013.

DeMets, C. and Dixon, T.: New kinematic models for Pacific-North America motion from 3 Ma to present, I: Evidence for steady motion and biases in the NUVEL-1A model, Geophys. Res. Lett., 26, 1921–1924, https://doi.org/10.1029/1999GL900405, 1999.

DeMets, C., Gordon, R. G., and Argus, D. F.: Geologically current plate motions, Geophys. J. Int., 181, 1–80, https://doi.org/10.1111/j.1365-246X.2009.04491.x, 2010.

Eisen-Cuadra, A., Christian, A. D., Dorval, E., Broadaway, B., Herron, J., and Hannigan, R. E.: Metal Geochemistry of a Brackish Lake: Étang Saumâtre, Haiti, Medical Geochemistry, Springer Netherlands, 149–166, https://doi.org/10.1007/978-94-007-4372-4_9, 2013.

Ellouz, N., Leroy, S., Momplaisir, R., Mercier de Lépinay, B., and the Haiti-SIS group: From 2012 Haiti-SIS Survey: Thick-skin versus thin-skin tectonics partitioned along offshore strike-slip faults – Haiti, Fall Meeting Am. Geophys. Union, 9–13 December 2013, San Francisco, California, USA, Poster T23E-2648, 2013.

Ellouz-Zimmermann N., Hamon, Y., Deschamps, R., Battani, A., Darnault, R., and Pillot, D.: Rapport intermédiaire des observations terrain et analyses dans le système transpressif d'Haiti, Projet collaboratif Haiti-Faille, Rapport ref: 65948, 2016 (in French).

Famin, V., Raimbourg, H., Garcia, S., Bellahsen, N., Hamada, Y., Boullier, A.-M., Fabbri, O., Michon, L., Uchide, T., Ricci, T., Hirono, T., and Kawabata, K.: Stress rotations and the long-term weakness of the Median Tectonic Line and the Rokko- Awaji Segment, Tectonics, 33, 1900–1919, https://doi.org/10.1002/2014TC003600, 2014.

Gailler, A., Calais, E., Hébert, H., Roy, C., and Okal, E.: Tsunami scenarios and hazard assessment along the northern coast of Haiti, Geophys. J. Int., 203, 2287–2302, https://doi.org/10.1093/gji/ggv428, 2015.

Hashimoto, M., Fukushima, Y., and Fukahata, Y.: Fan-delta uplift and mountain subsidence during the 2010 Haiti earthquake, Nat. Geosci., 4, 255–259, https://doi.org/10.1038/ngeo1115, 2011.

Hayes, G., Briggs, R., Sladen, A., Fielding, E. J., Prentice, C., Hudnut, K., Mann, P., Taylor, F. W., Crone, A. J., Gold, R., Ito, T., and Simons, M.: Complex rupture during the 12 January 2010 Haiti earthquake, Nat. Geosci., 3, 800–805, https://doi.org/10.1038/ngeo977, 2010.

Hickman, S., Zoback, M., and Ellsworth, W.: Introduction to special section: Preparing for the San Andreas Fault Observatory at Depth, Geophys. Res. Lett., 31, L12S01, https://doi.org/10.1029/2004GL020688, 2004.

Hodell, D. A., Curtis, J. H., Jones, G. A., Higuera-Gundy, A., Brenner, M., Binford, M. W., and Dorsey, K. T.: Reconstruction of Caribbean climate change over the past 10 500 years, Nature, 352, 790–793, https://doi.org/10.1038/352790a0, 1991.

Hornbach, M., Braudy, N., Briggs, R. W., Cormier, M.-H., Davis, M. B., Diebold, J. B., Dieudonne, N., Douilly, R., Frohlich, C., Gulick, S. P. S., Johnson III, H. E., Mann, P., McHugh, C., Ryan-Mishkin, K., Prentice, C. S., Seeber, L., Sorlien, C. C., Steckler, M. S., Symithe, S. J., Taylor, F. W., and Templeton, J.: High tsunami frequency as a result of combined strike-slip faulting and coastal landslides, Nat. Geosci., 3, 783–788, https://doi.org/10.1038/ngeo975, 2010.

International Seismological Centre: On-line Bulletin, available at: http://www.isc.ac.uk (last access: 27 August 2020), 2014.

James, K., Cormier, M.-H., Sloan, H., Ramsamooj, T., Boisson, D., Guerrier, K., Hearn, C. K., King, J. W., Momplaisir, R., Symithe, S. J., Ulysse, S. M. J., and Wattrus, N. J.: Geomorphologic and Stratigraphic Evidence of Ongoing Transpressional Deformation Across Lake Azuei (Haiti), Fall Meeting Am. Geophysical Union, 9–13 December 2019, San Francisco, California, USA, abstract T31D-0268, https://doi.org/10.1002/essoar.10501568.1, 2019.

Kocel, E., Stewart, R. R., Mann, P., and Chang, L.: Near-surface geophysical investigation of the 2010 Haiti earthquake epicentral area: Léogâne, Haiti, Interpretation, 4, T49–T61, https://doi.org/10.1190/INT-2015-0038.1, 2016.

Lear, C. H., Rosenthal, Y., and Wright, J. D.: The closing of a seaway: ocean water masses and global climate change, Earth Planet. Sc. Lett., 210, 425–436, https://doi.org/10.1016/S0012-821X(03)00164-X, 2003.

Leroy, S.: Structure et origine de la Plaque Caraïbe: implications géodynamiques, Dissertation, Université Pierre et Marie Curie, Paris, 240 pp., available at: https://www.semanticscholar.org/paper/Structure-et-origine-de-la-plaque-caraibe.-Leroy/bc7ee1fdcd05c13ec40628041d70a511dff29cbe (last access: 27 August 2020), 1995.

Leroy, S., Ellouz-Zimmermann, N., Corbeau, J., Rolandone, F., Mercier de Lépinay, B., Meyer, B., Momplaisir, R., Granja Bruña, J.L., Battani, A., Baurion, C., Burov, E., Clouard, V., Deschamps, R., Gorini, C., Hamon, Y., Lafosse, M., Leonel, J., Le Pourheit, L., Llanes, P., Loget, N., Lucazeau, F., Pillot, D., Poort, J., Tankoo, K. R., Cuevas, J.-L., Alcaide, J.F., Jean, P., Munoz-Martin, A., Mitton, S., Rodridguez, Y., Schmitz, J., Seeber, L., Carbo-Gorosabel, A., and Munoz, S.: Segmentation and kinematics of the North American-Caribbean plate boundary offshore Hispaniola, Terra Nova, 27, 467–478, https://doi.org/10.1111/ter.12181, 2015.

Mann, P. and Burke, K.: Neotectonics of the Caribbean, Rev. Geophys., 22, 309–362, https://doi.org/10.1029/RG022i004p00309, 1984.

Mann, P., Taylor, F. W., Edwards, R. L., and Ku, T. L.: Actively evolving microplate formation by oblique collision and sideways motion along strike slip faults: An example from the northwestern Caribbean plate margin, Tectonophysics, 246, 1–69, https://doi.org/10.1016/0040-1951(94)00268-E, 1995.

Mann, P., Calais, E., Ruegg, J.-C., DeMets, C., Jansma, P.E., and Mattioli, G.S.: Oblique collision in the northeastern Caribbean from GPS measurements and geological observations, Tectonics, 21, 7-1–7-26, https://doi.org/10.1029/2001TC001304, 2002.

McCann, W. R.: Estimating the threat of tsunamigenic earthquakes and earthquake induced-landslide tsunami in the Caribbean, in: Caribbean Tsunami Hazard, edited by: Aurelio, M. and Philip, L., World Scientific Publishing, Singapore, 43–65, https://doi.org/10.1142/9789812774613_0002, 2006.

McHugh, C., Seeber, L., Cormier, M.-H., Dutton, J., Çagatay, N., Polonia, A., Ryan, W. B. F., and Gorur, N.: Submarine earthquake geology along the North Anatolia Fault in the Marmara Sea, Turkey: A model for transform

basin sedimentation, Earth Planet. Sc. Lett., 248, 661–684, https://doi.org/10.1016/j.epsl.2006.05.038, 2006.

McHugh, C., Seeber, L., Braudy, N., Cormier, M.-H., Davis, M. B., Diebold, J. B., Dieudonne, N., Douilly, R., Gulick, S. P. S., Hornbach, M. J., Johnson III, H. E., Mishkin, K. R., Sorlien, C. C., Steckler, M. S., Symithe, S. J., and Templeton, J.: Offshore sedimentary effects of the 12 January 2010 Haiti earthquake, Geology, 39, 723–726, https://doi.org/10.1130/G31815.1, 2011.

Moknatian, M., Piasecki, M., and Gonzales, J.: Development of Geospatial and Temporal Characteristics for Hispaniola's Lake Azuei and Enquillo Using Landsat Imagery, Remote Sensing, 9, 1–32, https://doi.org/10.3390/rs9060510, 2017.

Murakami M. and Tagami, T.: Dating pseudotachylyte of the Nojima fault using the zircon fission-track method, Geophys. Res. Lett., 31, L12504, https://doi.org/10.1029/2004GL020211, 2004.

Peng, Z., Gonzalez-Huizar, H., Chao, K., Aiken, C., Moreno, B., and Armstrong, G.: Tectonic tremor beneath Cuba triggered by the Mw8.8 Maule and Mw9.0 Tohoku-Oki earthquakes, B. Seismol. Soc. Am., 103, 595–600, https://doi.org/10.1785/0120120253, 2013.

Perrin, C., Manighetti, I., Ampuero, J.-P., Cappa, F., and Gaudemer, Y.: Location of largest earthquake slip and fast rupture controlled by along-strike change in fault structural maturity due to fault growth, J. Geophys. Res., 121, 3666–3685, https://doi.org/10.1002/2015JB012671, 2016.

Possee, D., Keir, D., Harmon, N., Rychert, C., Rolandone, F., Leroy, S., Corbeau, J., Stuart, G., Calais, E., Illsley-Kemp, F., Boisson, D., Momplaisir, R., and Prépetit, C.: The Tectonics and Active Faulting of Haiti from Seismicity and Tomography, Tectonics, 38, 1138–1155, https://doi.org/10.1029/2018TC005364, 2019.

Prentice, C., Mann, P., Peña, L. R., and Burr, G.: Slip rate and earthquake recurrence along the central Septentrional fault, North American – Caribbean plate boundary, Dominican Republic, J. Geophys. Res, 108, 2149, https://doi.org/10.1029/2001JB000442, 2003.

Prentice, C., Mann, P., Crone, A. J., Gold, R. D., Hudnut, K. W., Briggs, R. W., Koehler, R. D., and Jean, P.: Seismic hazard of the Enriquillo–Plantain Garden fault in Haiti inferred from palaeoseismology, Nat. Geosci., 3, 789–793, https://doi.org/10.1038/ngeo991, 2010.

Pubellier, M., Mauffret, A., Leroy, S., Vila, M., and Amilcar, H.: Plate boundary readjustment in oblique convergence: example of the Neogene of Hispaniola, Greater Antilles, Tectonics, 19, 630–648, https://doi.org/10.1029/2000TC900007, 2000.

Rolandone, F., Lucazeau, F., Poort, J., and Leroy, S.: Heat-flow estimates offshore Haiti in the Caribbean plate, Terra Nova, 32, 179–186, https://doi.org/10.1111/ter.12454, 2020.

Rosencrantz, E. and Mann, P.: SeaMARC II mapping of transform faults in the Cayman Trough, Caribbean Sea, Geology, 19, 690–693, https://doi.org/10.1130/0091-7613(1991)019<0690:SIMOTF>2.3.CO;2, 1991.

Saint Fleur, N., Feuillet, N., Grandin, R., Jacques, E., Well-Accardo, J., and Klinger, Y.: Seismotectonics of southern Haiti: A new faulting model for the 12 January 2010 M7.0 earthquake, Geophys. Res. Lett., 42, 10273–10281, https://doi.org/10.1002/2015GL065505, 2015.

Saint Fleur, N., Klinger, Y., and Feuillet, N.: Detailed map, displacement, paleoseismology, and segmentation of the Enriquillo-Plantain Garden Fault in Haiti, Tectonophysics, 778, 228368, https://doi.org/10.1016/j.tecto.2020.228368, 2020.

Scherer, J.: Catalogue chronologique des tremblements de Terre ressentis dans l'île d'Haïti de 1551 à 1900, in: Bulletin Semestriel de L'Observatoire Météorologique du Séminaire-Collège St-Martial, Port-au-Prince, Haiti, 147–151, 1913.

Symithe, S. and Calais, E.: Present-day shortening in Southern Haiti from GPS measurements and implications for seismic hazard, Tectonophysics, 679, 117–124, https://doi.org/10.1016/j.tecto.2016.04.034, 2016.

Symithe, S., Calais, E., Haase, J.S., Freed, A.M., and Douilly, R.: Coseismic Slip Distribution of the 2010 M7.0 Haiti Earthquake and Resulting Stress Changes on Regional Faults, B. Seismol. Soc. Am., 103, 2326–2343, https://doi.org/10.1785/0120120306, 2013.

Symithe, S., Calais, E., de Chabalier, J. B., Robertson, R., and Higgins, M.: Current block motions and strain accumulation on active faults in the Caribbean, J. Geophys. Res., 120, 3748–3774, https://doi.org/10.1002/2014JB011779, 2015.

Taylor, F. W., Mann, P., Valastro Jr., S., and Burke, K.: Stratigraphy and Radiocarbon Chronology of a Subaerially Exposed Holocene Coral Reef, Dominican Republic, J. Geol., 93, 311–332, https://doi.org/10.1086/628954, 1985.

ten Brink, U. S., Bakun, W. H., and Flores, C. H.: Historical perspective on seismic hazard to Hispaniola and the northeast Caribbean region, J. Geophys. Res., 116, B12318, https://doi.org/10.1029/2011JB008497, 2011.

ten Brink, U. S., Bakun, W. H., and Flores, C. H.: Seismic hazard from the Hispaniola subduction zone: Correction to "Historical perspective on seismic hazard to Hispaniola and the northeast Caribbean region," J. Geophys. Res., 116, 1–15, https://doi.org/10.1002/jgrb.50388, 2013.

Van Dusen, S. R. and Doser, D. I.: Faulting processes of historic (1917–1962) M >= 6.0 earthquakes along the north-central Caribbean margin, Pure Appl. Geophys., 157, 719–736, https://doi.org/10.1007/PL00001115, 2000.

Wang, J., Mann, P., and Stewart, R. R.: Late Holocene Structural Style and Seismicity of Highly Transpressional Faults in Southern Haiti, Tectonics, 37, 3834–3852, https://doi.org/10.1029/2017TC004920, 2018.

Wessels, R. J. F.: Tectonic evolution, fault architecture, and paleofluid circulation in transpressive systems – southern Haiti, Doctoral Thesis of the Sorbonne University, 382 pp., available at: https://tel.archives-ouvertes.fr/tel-02484820v2 (last access: 27 August 2020), 2018.

Wessels, R. J. F.: Chapter 15 – Strike-Slip Fault Systems Along the Northern Caribbean Plate Boundary, in: Transform Plate Boundaries and Fracture Zones, edited by: Duarte, J. C., 375–395, https://doi.org/10.1016/B978-0-12-812064-4.00015-3, 2019.

Wessels, R. J. F., Ellouz-Zimmermann, N., Bellahsen, N., Hamon, Y., Rosenberg, C., Deschamps, R., Momplaisir, R., Boisson, D., and Leroy, S.: Polyphase tectonic history of the Southern Peninsula, Haiti: from folding-and-thrusting to transpressive strike-slip, Tectonophysics, 751, 125–149, https://doi.org/10.1016/j.tecto.2018.12.011, 2019.

Whipple, K. and Meade, B. J.: Orogen response to changes in climatic and tectonic forcing, Earth Planet. Sc. Lett, 243, 218–228, https://doi.org/10.1016/j.epsl.2005.12.022, 2006.

Wiggins-Grandison, M. D. and Atakan, K.: Seismotectonics of Jamaica, Geophys. J. Int., 160, 573–580, https://doi.org/10.1111/j.1365-246X.2004.02471.x, 2005.

Zoback, M., Hickman, S., Ellsworth, W., and the SAFOD Science Team: Scientific Drilling Into the San Andreas Fault Zone – An Overview of SAFOD's First Five Years, Sci. Dril., 11, 14–28, https://doi.org/10.2204/iodp.sd.11.02.2011, 2011.

Sci. Dril., 28, 63–73, 2020
https://doi.org/10.5194/sd-28-63-2020

Scientific Drilling
Open Access

Scientific drilling workshop on the Weihe Basin Drilling Project (WBDP): Cenozoic tectonic–monsoon interactions

Zhisheng An[1,2], Peizhen Zhang[3], Hendrik Vogel[4], Yougui Song[1,2], John Dodson[1,5], Thomas Wiersberg[6], Xijie Feng[7], Huayu Lu[8], Li Ai[1], and Youbin Sun[1,2]

[1]State Key Laboratory of Loess and Quaternary Geology, Institute of Earth Environment, Chinese Academy of Sciences, Xi'an 710061, China
[2]CAS Center for Excellence in Quaternary Science and Global Change, Xi'an 710061, China
[3]School of Earth Sciences and Engineering, Sun Yat-Sen University, Guangzhou 510275, China
[4]Institute of Geological Sciences & Oeschger Centre for Climate Change Research, University of Bern, 3012 Bern, Switzerland
[5]School of Earth, Atmospheric and Environmental Sciences, University of Wollongong, Wollongong, NSW 2522, Australia
[6]GFZ German Research Centre for Geosciences, 14473 Potsdam, Germany
[7]Earthquake Administration of Shaanxi Province, Xi'an 710068, China
[8]School of Geography and Ocean Science, Nanjing University, Nanjing 210023, China

Correspondence: Zhisheng An (anzs@loess.llqg.ac.cn)

Received: 1 September 2020 – Revised: 27 October 2020 – Accepted: 2 November 2020 – Published: 1 December 2020

Abstract. The Weihe Basin, enclosed by the Chinese Loess Plateau to the north and the Qinling Mountains to the south, is an outstanding, world-class continental site for obtaining high-resolution multi-proxy records that reflect environmental changes spanning most of the Cenozoic. Previous geophysical and sedimentary studies indicate that the basin hosts 6000–8000 m thick fluvial–lacustrine sedimentary successions spanning the Eocene to Holocene. This sedimentary record provides an excellent and unique archive to decipher long-term tectonic–climate interactions related to the uplift of the Tibetan Plateau, the onset/evolution of the Asian monsoon, and the development of the biogeography of East Asia. Owing to its location at the interface of the opposing westerly and Asian monsoon circulation systems, the Weihe Basin also holds enormous promise for providing a record of changes in these circulation systems in response to very different boundary conditions since the Eocene. To develop an international scientific drilling programme in the Weihe Basin, the Institute of Earth Environment, Chinese Academy of Sciences, organized a dedicated workshop with 55 participants from eight countries. The workshop was held in Xi'an, China, from 15 to 18 October 2019. Workshop participants conceived the key scientific objectives of the envisaged Weihe Basin Drilling Project (WBDP) and discussed technical and logistical aspects as well as the scope of the scientific collaboration in preparation for a full drilling proposal for submission to the International Continental Scientific Drilling Program (ICDP). Workshop participants mutually agreed to design a two-phase scientific drilling programme that will in a first phase target the upper 3000 m and in a second phase the entire up to 7500 m thick sedimentary infill of the basin. For the purpose of the 7500 m deep borehole, the world's only drill rig for ultra-deep scientific drilling on land, Crust 1, which previously recovered the entire continental Cretaceous sediments in the Songliao Basin, will be deployed in the WBDP.

Published by Copernicus Publications on behalf of the IODP and the ICDP.

1 Introduction

The Earth has experienced remarkable climate and environmental changes during the last 65 million years. The most prominent characteristic of global Cenozoic climate evolution, primarily inferred by marine benthic oxygen isotope records, is a stepwise cooling since the Eocene from a hot "greenhouse" to a cold "icehouse" Earth, associated with the initiation and expansion of the bipolar ice sheets (Zachos et al., 2001; Westerhod et al., 2020). Against the backdrop of global cooling during the Cenozoic, the salient trend in Asia was the development of the coupled monsoon–arid environment system at tectonic timescales, which was largely driven by a reorganization of atmospheric circulation systems in response to the India–Asia collision and the subsequent uplift of the Tibetan Plateau, and the global cooling (Kutzbach et al., 1993; Ramstein et al., 1997, An et al., 2001; An, 2014; Lu et al., 2010). To date a continuous Cenozoic record capturing both the effects of global climate change and regional tectonics on Asian climate has yet to be recovered. Such a record is critical for enhancing our knowledge about when and how the Asian monsoon originated while at the same time enabling assessment of the mechanism of tectonic–climate interactions through the entire Cenozoic era. It will also provide information on how the Asian monsoon evolution influenced the development of Asian ecosystems up to the present day.

Being a critical and powerful approach in the geosciences, scientific drilling under the umbrella of the ICDP has been very successful over recent decades by providing critical materials from various key sites and pushing forward the frontiers of Earth sciences. Over the last 2 decades, ICDP has funded many drilling projects to address changes in the Earth's climate and ecosystem in the geological past. However, few of these have targeted continuous sedimentary strata dating beyond the Pleistocene. In East Asia, previous ICDP drilling projects have focused on the late Jurassic to Paleogene, mostly Cretaceous, Songliao Basin, as well as late Quaternary strata (Lake Qinghai, Fig. 1). To date, there has been a paucity of high-quality continental records for the intervening periods that have shaped the modern face of the Earth.

Due to the stepwise growth of the northern Tibetan Plateau during the late Cenozoic, a series of tectonic basins were developed in the surrounding areas, such as the Tarim Basin (Sun et al., 2009; Liu et al., 2014), Qaidam Basin (Yin et al., 2008; Zhang et al., 2012), Xining Basin (Fang et al., 2019), Linxia Basin (Fang et al., 2003), and Lanzhou Basin (Yue et al., 2001). Thick deposits of these basins provide direct evidence of a Cenozoic drying history of inland Asia (Dupont-Nivet et al., 2007; Wang et al., 2012; Liu et al., 2014; Li et al., 2014). Compared with sedimentary records of these inland basins, the Weihe Basin is tectonically related to the long-range effects of the uplift of the Tibetan Plateau, but the sedimentary records are more sensitive to monsoonal climate changes (Lu et al., 2018). Therefore, investigation into the sedimentary records in the Weihe Basin will deepen our understanding regarding when the coupled Asian monsoon–arid environmental system was formed and how the monsoon climate evolved in response to Tibetan Plateau growth and global cooling. The Weihe Basin, with its 6000–8000 m thick uninterrupted fluvial–lacustrine sedimentary succession spanning the Eocene to the present (Jia et al., 1966; Liu et al., 1960; Chen et al., 1977; RGS, 1989; Wang et al., 2013; Lu et al., 2018), is the most continuous continental archive of Cenozoic climate evolution in East Asia. Because of its unique geographical location, the region around the Weihe Basin is significantly affected by the Asian monsoon, which is a major component of global atmospheric circulation (An et al., 2015). Apart from its enormous promise for Cenozoic paleoclimate research, the Weihe Basin has also preserved evidence of the earliest appearance of hominins outside Africa (Maslin et al., 2015; Potts, 2013), known as the cradle of ancient Chinese civilization (An and Ho, 1989; Zhuo et al., 2016; Zhu et al., 2018).

Changes in the Earth's climate system on global and regional scales are attributed to both natural factors and human activities (IPCC, 2001). What we learn from the geological past about natural change is key to predicting Earth's future under the influence of ongoing anthropogenic effects. It is therefore important to understand the response of large-scale atmospheric circulations and ecosystems under analogous greenhouse climate conditions of the Cenozoic (Zachos et al., 2001; Haywood et al., 2016; Zhang et al., 2013). Owing to its continuity in sediment deposition, the Weihe Basin is ideally suited to producing a critically important record capable of elucidating the effect of global-scale climate and regional-scale tectonics on the evolution of the major atmospheric circulation systems in Asia and the response of eco-environmental systems to high atmospheric greenhouse gas concentrations during several critical warm periods (e.g. Kutzbach and Behling, 2004; Ji et al., 2018; Zhao et al., 2020).

Being located at the boundary between subtropical forest and the temperate vegetation zone (http://www.ecosystem.csdb.cn, last access: 18 November 2020), the Weihe Basin also offers the opportunity to depict changes in the time-transgressive evolution of Angiosperms and the expansion of grasses using the C_4 photosynthetic pathway and their links to Cenozoic tectonic–climate interactions (Wang et al., 2019). Similarly to the surface ecosystems, subsurface ecosystems also involve complex interactions between life and the environment. While the limits of life at depths in the marine sediment record are constantly being revised (Schippers et al., 2005; Flemming and Wuertz, 2019), similar studies from continental settings have been limited to date. Thick sedimentary strata of the Weihe Basin are an ideal complement that will help to characterize the limits of life as well as its metabolic pathways and products at depth in a continental setting, a goal that has so far not been targeted. Direct obser-

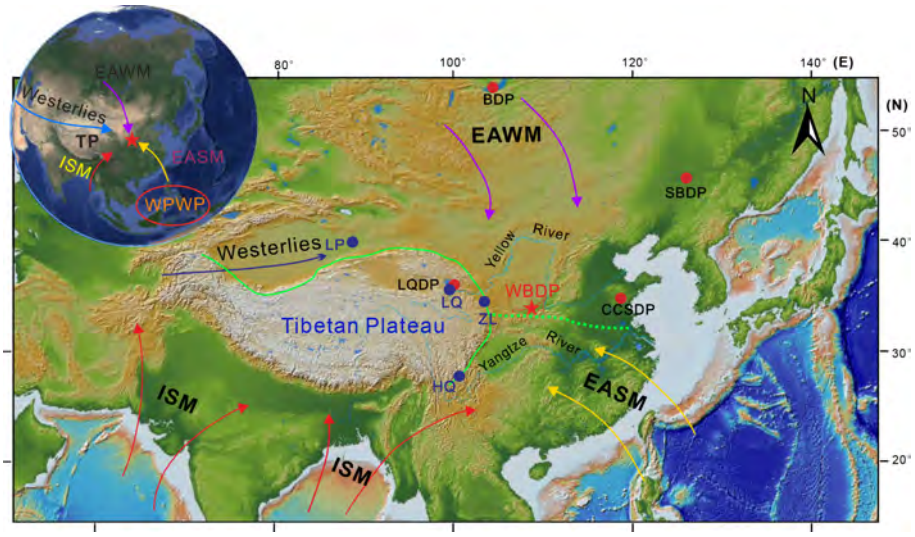

Figure 1. Atmospheric circulation systems in East Asia and locations of previous ICDP (red dots) and CESD (blue dots, Chinese Environmental Science Drilling) drilling sites and the proposed site of the Weihe Basin Drilling Project (WBDP; red star). BDP: Lake Baikal; SBDP: Songliao Basin; LQDP: Lake Qinghai; LP: Lop Nur; LQ: Lake Qinghai; ZL: Zhuanglang; and HQ: Heqing Paleolake. ISM: Indian Summer Monsoon; EASM: East Asian Summer Monsoon; EAWM: East Asian Winter Monsoon; and WPWP: West Pacific Warm Pool.

vations and measurements in a deep borehole will offer great promise for depicting how deep Earth ecosystems respond to an extreme environment.

The formation and evolution of the Weihe Basin are closely related to the long-range effects of the uplift of the Himalayan–Tibetan Plateau, growth of the Qinling Mountains, as well as the Ordos block deformation (Zhang et al., 1995, 2002; Shi et al., 2008; Liu et al., 2013; Shi et al., 2019). The thick sediment package retains a record of tens of millions of years of regional tectonic evolution with information continuously stored as denudation products in the Weihe Basin. The envisaged WBDP will provide a unique opportunity to closely capture mountain-building processes of the Qinling Mountains, the landform dividing northern and southern China geographically, biogeographically, and climatically, through proximal denudation products delivered by rivers draining the mountain range and deposited in the basin. Owing to its eastern location, the sedimentary record of the Weihe Basin also holds promise for identifying potential imprints of major uplift and exhumation events of the Tibetan Plateau, which played significant roles in the formation and evolution of the Asian monsoon–arid environmental systems (An et al., 2001, 2015).

2 Site description

The Weihe Basin is located in central China and extends 400 km from E to W (107–110°35′ E) and ∼30–80 km along its N–S axis (34–35°40′ N), covering an area of about 20 000 km^2 at an average elevation of 400 m above sea level (a.s.l.) (Fig. 2a). The Qinling Mountains to the south reach elevations of 2000–3700 m a.s.l., and the Weihe North Mountains to the north are at ∼900–1300 m a.s.l. The overall terrain of the Weihe Basin is inclined towards the east. The bedrock composition of the Weihe Basin is complex, with Paleozoic limestone in the northern basin and Archean–Proterozoic metamorphics and Mesozoic plutonics in the southern basin (Shi et al., 2008; Lin et al., 2015; Song et al., 2018). Climatologically, the area is located at the boundary between the subtropical monsoon and temperate monsoon areas, with rainfall being sourced primarily from the tropical Indo-Pacific oceans. Its annual average temperature is ∼12–14°, and the average annual precipitation is ∼500–700 mm, with 55 % of this precipitation falling during the summer monsoon-dominated season (June to September). The Weihe Basin is sensitive to changes in the Asian Monsoon (AM) circulation, characterized by seasonal shifts in wind direction between the cold and dry winter and the warm and humid summer. As an important component of the global climate system, the AM affects almost one-third of the world's population and is of major importance for regional socioeconomic and sustainable development.

Geophysical (reflection seismic and gravimetry) and borehole data suggest continuous subsidence for > 7000 m of sediment accommodation space in the two depocentres of the Weihe Basin (Chen et al., 1977; RGS, 1989; Xu et al., 2014; Liu et al., 2016; Li et al., 2016) (Fig. 2). Bio- and magneto-stratigraphy of outcrops and available drill cores indicates that sediments have accumulated continuously since the Eocene (e.g. Wang et al., 2013; Zhao et al., 2018; Lu et al., 2018). Lithologies consist mainly of fine-grained lacustrine sediments that are occasionally interspersed with somewhat coarser fluvial deposits (Chen et al., 1977; RGS,

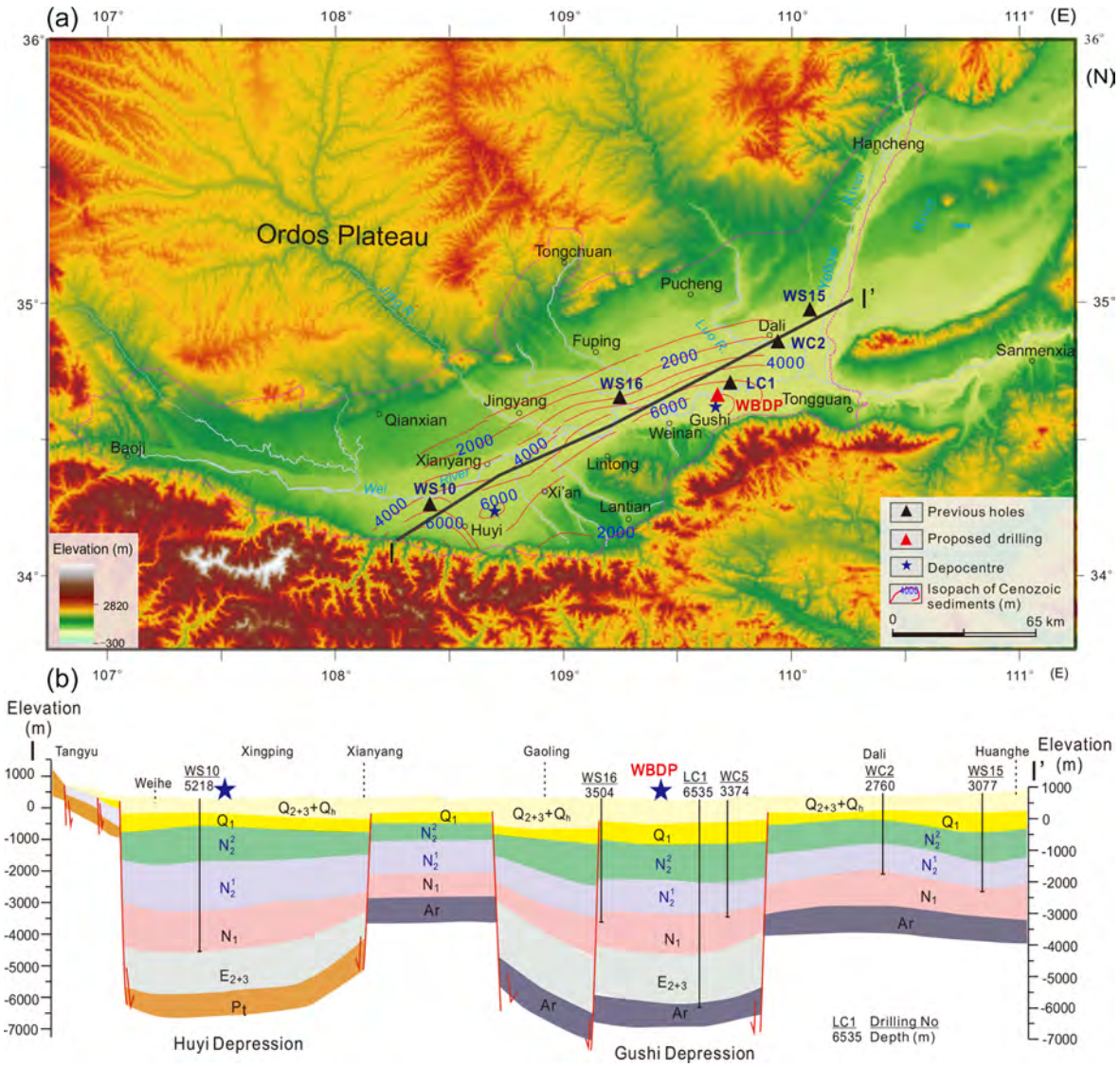

Figure 2. Isopach maps of Cenozoic sediments **(a)** and a stratigraphic cross section **(b)** through the Weihe Basin. Blue and red stars indicate the eastern and western depocentres.

1989; Lu et al., 2018; Liu et al., 2019). Recent investigations into outcrops in the forefront of the Li Shan and Qinling Mountains provide a preliminary framework of the Cenozoic basin stratigraphy and a glimpse into regional environmental changes (Wang et al., 2014; Lu et al., 2018). Unfortunately, these outcrops capture primarily proximal deposits composed of successions ranging from fluvial pebbles and sand layers to lacustrine silty clay deposits, providing only a general framework of Cenozoic depositional environments in the Weihe Basin (Wang et al., 2013). Due to the lack of temporal continuity, these deposits are not suitable for long-time high-resolution paleoclimatic reconstructions. Hence, the promising way to produce a continuous sedimentary record is through drilling in the depocentres of the Weihe Basin.

3 Previous investigations

Based on geophysical, tectonic, and geological evidence, there are three proposed formation mechanisms of the Weihe Basin, including the following: (1) the eastward extrusion of the Tibetan Plateau caused the extension of the Weihe Basin (Molnar and Tapponnier, 1975; Zhang et al., 1995), which is supported by mechanical simulation of indentation on plasticine models (Peltzer and Tapponnier, 1988); (2) continued Pacific–Eurasian collision in East Asia since the Mesozoic caused rifting in the Weihe Basin (Northrup et al., 1995; Ye et al., 1987); and (3) Cenozoic extension in the Weihe Basin resulted from the combined effects of the India–Asia Plate collision and subduction of the western Pacific Plate beneath the Asian Plate (Song et al., 2018). Provenance studies sug-

gest that deposition in the Weihe Basin is largely controlled by the uplift of the Qinling Mountains (Dong et al., 2011; Meng, 2017; Liu et al., 2019; Zhang et al., 2012), implying that a basin-range structure was formed and co-evolved since the early Cenozoic.

Previous geological surveys and pilot boreholes throughout the Weihe Basin have revealed that the basin contains a continuous, rapidly accumulating sedimentary succession, with accumulation rates averaging ~ 60–$100\,\mathrm{cm\,kyr^{-1}}$ in the depocentre for the last 50 Myr (Chen et al., 1977; RGS, 1989; Li, 2018). Numerous outcrops surrounding the Weihe Basin have been investigated in the past decades (e.g. Liu et al., 1960; Yue, 1989; Kaakinen et al., 2006; Wang et al., 2014; Lu et al., 2018; Wang et al., 2019; Zhao et al., 2020). Lithological and biostratigraphic investigations of exposed outcrops between Xi'an and Lantian suggest that the fluvial–lacustrine sequences during the Eocene to Miocene accumulated in the lower part, with the Red Clay and loess–paleosol sequences deposited in the upper part since the late Miocene (Lu et al., 2018, and references therein).

Since the 1990s, investigations into the depositional facies, stratigraphy, mammal fossil assemblages, carbonate isotopes, pollen, and phytolith assemblages of the sedimentary outcrops exposed in the southern margin of the Weihe Basin have revealed significant changes in the Cenozoic environmental characteristics of the region. For example, sedimentological and magnetostratigraphic results of the Duanjiapo Red Clay section, for the first time, revealed a major environmental shift around the latest Miocene (Zheng et al., 1992). This environmental change is also confirmed by a large-scale C_4/C_3 vegetation change inferred from the carbon isotope records of fossil teeth and soil carbonates in the loess–Red Clay sequence at Lantian (An et al., 2005; Passey et al., 2009) as well as in vertebrate fossils of the Bahe Formation (Kaakinen et al., 2006). Carbon isotope results from the Lantian and Weinan profiles show that C_4 grasses may have been a dominant grassland component already starting at ~ 11 Ma and experienced further stepwise expansions during the Pliocene, thereby suggesting early aridification in Asia (Sun et al., 2012; Wang et al., 2019). Quantitative phytolith- and pollen-based reconstructions of mean annual precipitation indicate a decrease from 800–1673 to 443–900 mm during the Pliocene, implying an important role of global cooling in driving Asian monsoon evolution (Wang et al., 2019; Zhao et al., 2020). Based on available data from the outcrops and borehole, a review work suggests that the Asian monsoon may have been initiated by the mid-Eocene (Lu et al., 2018).

Plio-Pleistocene glacial–interglacial to millennial monsoon variability has also been revealed by the loess sequences and borehole sediments in the Weihe Basin. The geochemical composition of the Weinan loess profile confirmed that high-frequency pulses of East Asian monsoon climate in the last two glaciations were linked to the climate of the North Atlantic region (Guo et al., 1996). In addition, glacial–interglacial changes in paleotemperature and precipitation have been quantitatively reconstructed using carbon isotopes and biomarkers from the Weinan loess profile (Sun et al., 2012; Thomas et al., 2017; Tang et al., 2017; Wang et al., 2018). To obtain high-resolution information on paleoenvironmental changes in the region, core LYH-1 (1097 m) was drilled in a residual lake (namely Luyanghu) in the northern Weihe Basin. Sedimentological and geochemical proxies from the upper 220 m of the core revealed that significant changes with a range of fluvial–lacustrine–eolian depositional environments were persistent over the last 1 Myr (Rits et al., 2016, 2017), likely reflecting monsoon-induced orbital- to millennial-scale hydroclimatic changes. Nine short cores (7–8 m) were recently retrieved from the proposed drilling site in the Weihe Basin. These sedimentary records are mainly composed of fine-grained silts and comprise climatic signals with a high potential for resolving millennial monsoon variability since the last glaciation. Previous investigations clearly highlight the great potential of the sediments in the Weihe Basin for assessing the long-term trends and short-term variability of the Asian climate during the Cenozoic. Therefore, high-resolution and continuous reconstruction of the Cenozoic climate can be achieved by obtaining long and high-quality drill cores from the Weihe Basin's depocentre.

4 Geophysical survey results

High-resolution wide-angle and deep seismic refraction/reflection detection data suggest the presence of two depressions located in the western and eastern Weihe Basin (Liu et al., 2016; Cai, 2017; Li, 2018) (Fig. 3). The western depression (Huyi) is located between Zhouzhi and Huyi. Its southern boundary is the Qinling fault (F2), the northern boundary is the Weihe fault (F3), the eastern boundary is the Lintong–Chang'an fault (F4), and the western boundary is the Longxian–Qishan–Mazhao fault (F1). A 5218 m deep borehole (WS10) in the depocentre of the Huyi depression just penetrated into the late Eocene (Fig. 2b), suggesting the presence of a much thicker Cenozoic sediment package in the western depression. The thickness of unconsolidated sediments in the Huyi depression exceeds 6000 m based on time–depth conversion of two-way travel time at the base of the central depression of about ~ 4–4.5 s. The deep seismic reflection profile shows that there are six major stratigraphic interfaces. Note that the integrity of the Huyi depression is lost due to the cutting of an east–west fault at depth.

The eastern depression (Gushi) is located between Weinan and Dali (Fig. 4). Its southern boundary is the Weinan–Jingyang fault (F5), the Weinan pediment fault (F6), and the Huashan pediment fault (F7), and its northern boundary is the Kouzhen–Guanshan fault (F8) and the Shuangquan–Linyi fault (F9). This depression is oriented E–W in general, with a maximum N–S width of 38 km. The Gushi depression is only

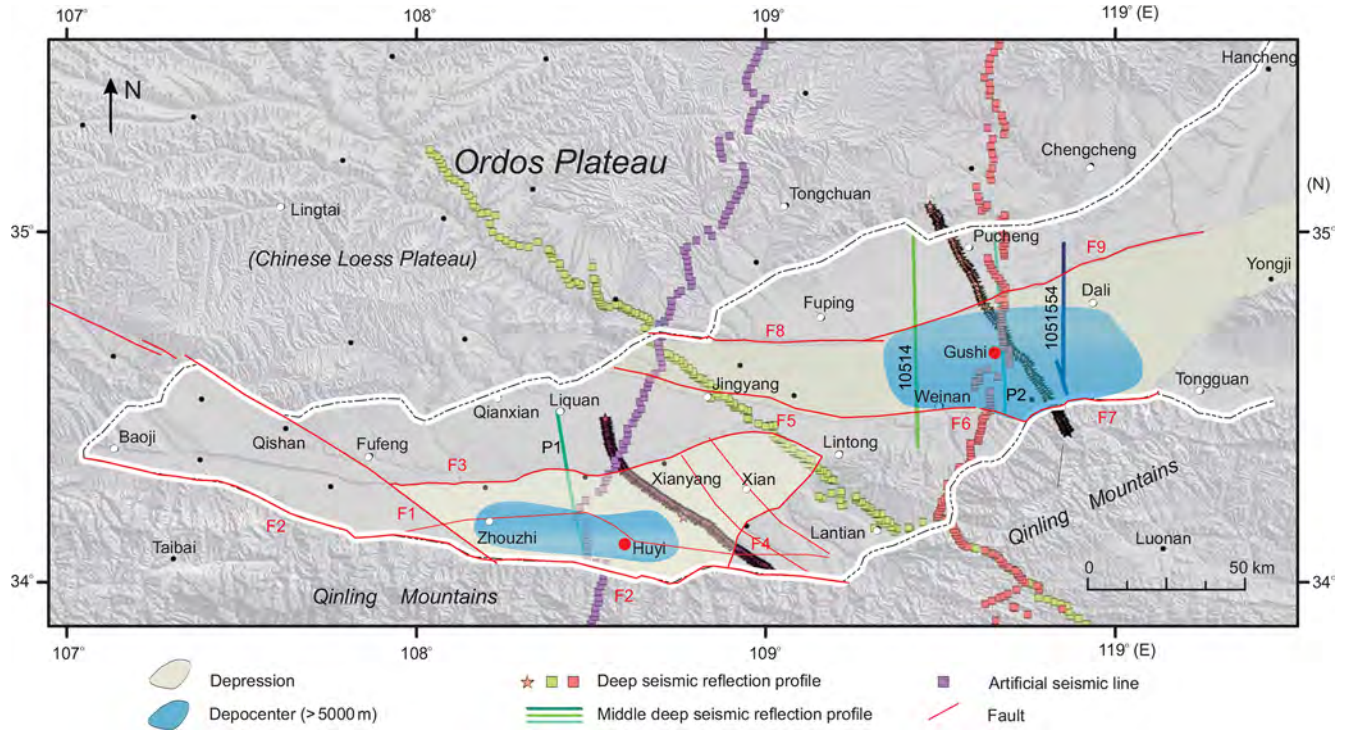

Figure 3. Geophysical surveys in the Weihe Basin.

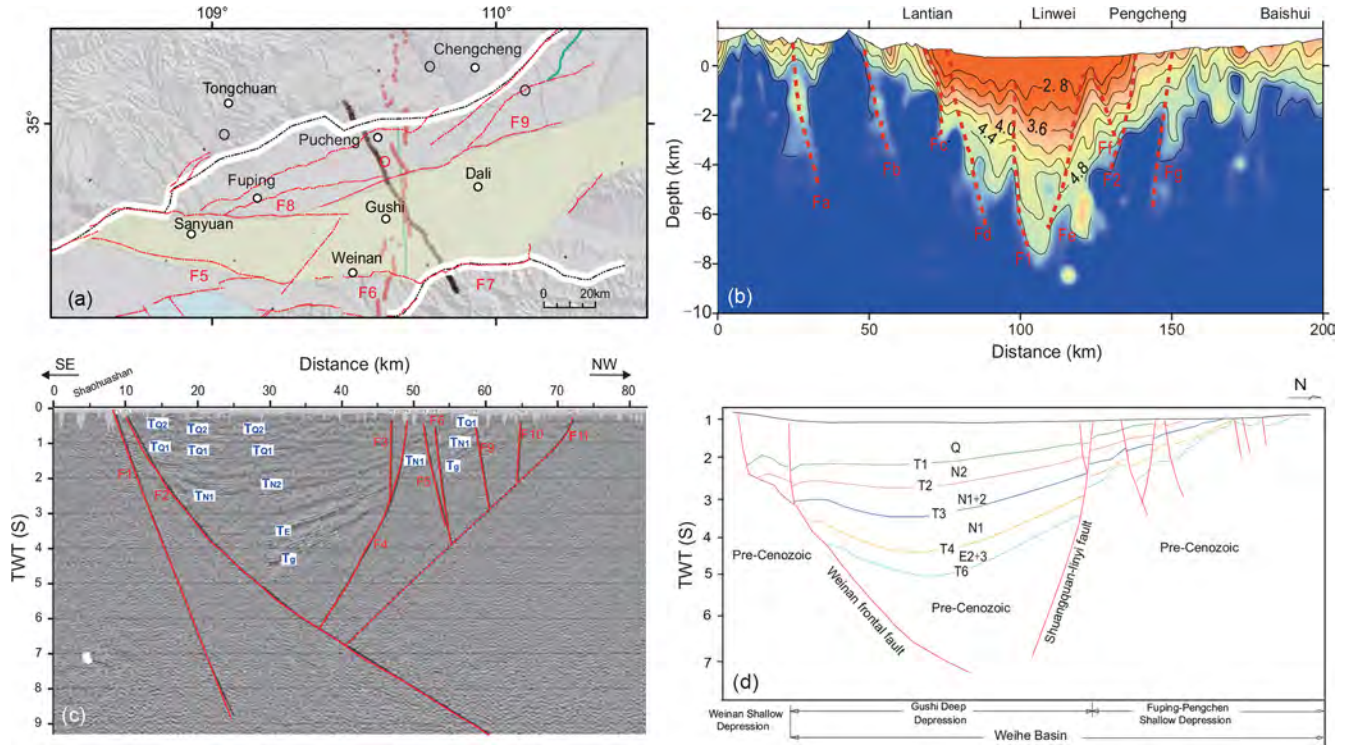

Figure 4. Geophysical survey interpretation of the eastern depression (Gushi) in the Weihe Basin. **(a)** Seismic survey lines in the eastern (Gushi) depression. **(b)** Wide-angle reflection results show that the depth of the Gushi depression can reach ~7500 m. **(c)** Deep seismic reflection profile. **(d)** Stratigraphical interpretation based on mid–deep seismic reflection data.

surrounded by minor faults near its edges and lacks major faults crossing the depocentre (Fig. 4a). Wide-angle reflection shows that the thickness of acoustically well-stratified sediments deposited in the Gushi depression reaches up to 7500 m (Fig. 4b) based on a two-way travel time of ∼ 4.7 s, and deep seismic reflection indicates the Cenozoic sediment may be deeper (Fig. 4c). The superimposed deep seismic reflection profile shows that there are six major stratigraphic interfaces, designated as T1–6, respectively (Fig. 4d). T1 indicates the basal boundary of the Quaternary, T4 denotes the basal boundary of the Neogene, and T6 may reflect the bedrock surface. The major geothermal and soluble helium gas resources were found within the Mio-Pliocene sediments (N_{1-2}) between T3 and T2, deposited under fluvial to shallow lacustrine conditions (Li, 2018). Recently, the PetroChina Changqing Company drilled a 6535 m long borehole 16 km east to the depocentre of the Gushi depression down to the bedrock (for the location, see LC1 in Fig. 2), which revealed that the thickness of the Cenozoic strata is ∼ 6490 m and that the bedrock underlying the Cenozoic is Ordovician limestone.

5 Workshop

Based on promising survey information, scientists from the Institute of Earth Environment, Chinese Academy of Sciences, organized an international workshop on 15–18 October 2019 in Xi'an, which assembled 55 scientists from eight countries, representing various scientific domains, to specify the key objectives of the WBDP and the global significance of reconstructing Cenozoic climate evolution and tectonic–climate interaction. The morning session on the first day focused on the formation and evolution of the Weihe Basin from tectonic and sedimentary evidence, the Cenozoic depositional environments and paleoenvironmental evolution from the geophysical, outcrop, and drill core data, and the potential of the thick and continuous Cenozoic deposits in the Weihe Basin for paleoclimate research. The afternoon session focused on basin evolution, paleoclimatology, basin–mountain coupling, sedimentary stratigraphic cycle correlation, and paleo-CO_2 concentration reconstructions.

A field excursion was conducted on the second day. In the morning the team visited outcrops showcasing the Cenozoic lacustrine and eolian Red Clay–loess deposits exposed in the southern margin of the Weihe Basin (the northern slope of the Qinling Mountains). In the afternoon the team evaluated the proposed drill site in the Gushi depression in light of logistical and technical aspects. Group discussion resumed on the third day, during which participants thoroughly evaluated the drilling plan, scientific goals, and the technical feasibility of the envisioned WBDP. A detailed analytical programme was discussed in the workshop, including on-site downhole logging of physical parameters and monitoring of fluids and gases as well as off-site analyses including chronological (magnetostratigraphy, ^{14}C and burial $^{26}Al/^{10}Be$ dating), sedimentological (lithostratigraphy, structures, grain size), mineralogical/sediment provenancing (clay mineralogy, zircon ages), geochemical (major, minor, trace element geochemistry, stable H–C–N–O, and selected metal isotopic compositions), and biological (biomarkers along with compound specific H and C isotope compositions, pollen, plant silica, microchar) proxies.

The workshop concluded with clear research goals for tectonic, paleoclimatic, environmental, and geobiologic studies in the Weihe Basin and also formulated a management plan with timelines for the application of drilling and research proposals to the ICDP and other funding agencies. Three leading PIs (Zhisheng An, Peter Molnar, and Peizhen Zhang) will take overall responsibility for assembling and coordinating the WBDP. Five Co-PIs (John Dodson, Carmala Garzione, Hendrik Vogel, Mark Lever, and Youhong Sun) will lead and coordinate the multi-disciplinary and multi-national science team organized into five Working Groups. These five Working Groups were designed to optimize the workflow of on-site drilling and logging and off-site research of paleoclimate, tectonics, geomicrobiology, and data–model synthesis. The Synthesis Working Group will compare sedimentary records of different inland basins to decipher the long-term changes in the monsoon–arid environmental system and their dynamical links to regional tectonics and global climate change (e.g. Sun et al., 2009; Zhang et al., 2012; Liu et al., 2014). Moreover, integration of the WBDP with recently accomplished IODP projects (e.g. in the South China Sea, Bay of Bengal, Arabian Sea, and Japan Sea) surrounding the Asian continent will provide valuable insights into how these processes (tectonics, climate, the deep biosphere) were coupled during the Cenozoic.

As the main outcome of the workshop, participants proposed an integrated two-phase scientific drilling project to obtain as complete as possible sedimentary drill cores from the lacustrine and fluvial–lacustrine succession in the eastern Gushi depression of the Weihe Basin. WBDP Phase I will target the upper ∼ 3000 m thick sediment package to reconstruct orbital-to-millennial climate variability and to address the microbial community–environment relationship since the late Miocene (∼ 10 Ma). WBDP-Phase II aims to produce a ∼ 7500 m long continuous sedimentary record that spans the entire Cenozoic and with the Earth's most recent transition from hot greenhouse to cold icehouse climate conditions. Owing to the long time spans covered by both project phases, the WBDP will also allow us to provide answers to long-standing tectonic–climate interaction questions and help unravel the interplay of climate and tectonics in the evolution of angiosperms and the C_4 photosynthetic pathway. In summary, the two-phase WBDP aims to decipher (1) onset and evolution of the Asian Paleomonsoon since the Eocene, (2) variability of atmospheric circulation and continental climate under warm periods with high atmospheric CO_2 concentrations, (3) mountain–basin coupling processes,

(4) Cenozoic tectonic–climate interactions, and (5) limits of life at depth in continental sediments.

6 Participants of the workshop (alphabetical order)

Zhisheng An (Institute of Earth Environment, Chinese Academy of Sciences, IEECAS), Paul Baker (Duke University, USA), Daniel Breecker (University of Texas at Austin, USA), Hong Chang (IEECAS), Feng Cheng (Rochester University, USA), Leon Clarke (Manchester Metropolitan University, UK), Steven Clemens (Brown University, USA), Jun Deng (China University of Geoscience, Beijing), John Dodson (University of Wollongong, Australia), Shuwen Dong (Nanjing University), Yunpeng Dong (Northwest University), Ying Dong (Xi'an Center of Geological Survey, CGS), Xiaonan Duan (Chinese Academy of Sciences), Robert Duce (Texas A & M University, USA), Xijie Feng (Earthquake Administration of Shaanxi Province, China), Sherilyn Fritz (University of Nebraska, Lincoln, USA), Anlin Guo (Northwest University), Matthias Halisch (Leibniz Institute for Applied Geophysics, Germany), Huayu Lu (Nanjing University), Yuanbiao Hu (China University of Geoscience, Beijing), Zihan Huang (Nanjing University), Shugang Kang (IEECAS), Wenyuan Li (Xi'an Center of Geological Survey, CGS), Yu Liu (IEECAS), Jian Liu (Xi'an Center of Geological Survey, CGS), Xingxing Liu (IEECAS), Qingtian Lyu (Chinese Academy of Geological Sciences), Michael Meadows (University of Cape Town, South Africa), Xiaoke Qiang (IEECAS), Jianguo Ren (National Natural Science Foundation of China), Tada Ryuji (University of Tokyo, Japan), Pingping Sun (Xi'an Center of Geological Survey, CGS), Yougui Song (IEECAS), Youbin Sun (IEECAS), Youhong Sun (China University of Geoscience, Beijing), Hendrik Vogel (University Of Bern, Switzerland), Kexin Wang (Nanjing University), Pujun Wang (Jilin University), Sumin Wang (Nanjing Institute of Geography and limnology, CAS), Xulong Wang (IEECAS), Yichao Wang (Nanjing University), Thomas Wiersberg (GFZ German Research Centre for Geosciences, Germany), Jingsui Yang (Nanjing University), Yongkang Yin (Jilin University), Xuefeng Yu (IEECAS), Leping Yue (Northwest University), Christian Zeeden (Leibniz Institute for Applied Geophysics, Germany), Guowei Zhang (Northwest University), Hang Zhang (IEECAS), Hanzhi Zhang (Nanjing University), Maosheng Zhang (Xi'an Center of Geological Survey, CGS), Peizhen Zhang (Sun Yat-Sen University), Weijian Zhou (IEECAS), Xiulan Zong (IEECAS), and Li Ai (IEECAS).

Data availability. No data sets were used in this article.

Author contributions. ZA, PZ, YSu, and TW conceived and designed the workshop. YSu, LA, YSo, and HL organized the workshop. ZA, YSo, HV, YSu, and LA prepared the paper, XF contributed to the geophysical figures and interpretation, HL contributed to the field trip of the workshop and previous investigation sections of the paper. PZ, JD, TW, HL, and XF discussed and revised the manuscript. The WBDP consortium provided intellectual input to the paper and workshop.

Competing interests. Author Thomas Wiersberg is a member of the editorial board of *Scientific Drilling*.

Acknowledgements. We would like to thank the Institute of Earth Environment, Chinese Academy of Sciences; State Key Laboratory of Loess and Quaternary Geology; Xi'an Center of Geological Survey; and Nanjing University for supporting the workshop. We thank Chengshan Wang, Shuwen Dong, and Rixiang Zhu for suggesting this workshop; Xiaoke Qiang and Hong Chang for organizing the field trip; and Youhong Sun and Yuanbiao Hu for the design of drilling engineering. Special thanks to ICDP for help in organizing this workshop.

Financial support. This workshop was funded by the External Cooperation Program (132B61KYSB20170005) and the Strategic Priority Research Program (XDB40000000) from the Chinese Academy of Sciences (CAS), State Key Laboratory of Loess and Quaternary Geology, and China Geological Survey (DD20190294).

Review statement. This paper was edited by Ulrich Harms and reviewed by Jef Vandenberghe and Steven Clemens.

References

An, Z.: Late Cenozoic Climate Change in Asia: Loess, Monsoon and Monsoon-arid Environment Evolution, Developments in Paleoenvironmental Research, Springer, Dordrecht, the Netherlands, 587 pp., 2014..

An, Z. and Ho, C.: New Magnetostratigraphic Dates of Lantian Homo erectus, Quaternary Res., 32, 213–221, https://doi.org/10.1016/0033-5894(89)90077-X, 1989.

An, Z., Kutzbach, J. E., Prell, W. L., and Porter, S. C.: Evolution of Asian monsoons and phased uplift of the Himaya-Tibtan plateau since Late Miocene times, Nature, 411, 62–66, https://doi.org/10.1038/35075035, 2001.

An, Z., Huang, Y., Liu, W., Guo, Z., Steven, C., Li, L., Warren, P., Ning, Y., Cai, Y., and Zhou, W.: Multiple expansions of C_4 plant biomass in East Asia since 7 Ma coupled with strengthened monsoon circulation, Geology, 33, 705–708, https://doi.org/10.1130/G21423.1, 2005.

An, Z., Wu, G., Li, J., Sun, Y., Liu, Y., Zhou, W., Cai, Y., Duan, A., Li, L., Mao, J., Cheng, H., Shi, Z., Tan, L., Yan, H., Ao, H., Chang, H., and Feng, J.: Global Monsoon Dynamics and Climate Change, Annu. Rev. Earth. Pl. Sc., 43, 29–77, https://doi.org/10.1146/annurev-earth-060313-054623, 2015.

Cai, X.: Exploration and development of geothermal and two kinds of gas (water soluble gas and Helium) resources in Weihe Basin, Science Press, Beijing, China, 1–217, 2017.

Chen, W., Chen, J. X., and Yun, Q.: Report on the Geological Results of the Oil Survey in the Fenwei Basin. Third Survey Team 301 Unit, State geology administration of China, Xianyang, China, 1–112, 1977.

Dong, Y., Zhang, G., Neubauer, F., Liu, X., Genser, J., and Hauzenberger, C.: Tectonic evolution of the Qinling orogen, China: Review and synthesis, J. Asian Earth Sci., 41, 213–237, https://doi.org/10.1016/j.jseaes.2011.03.002, 2011.

Dupont-Nivet, G., Krijgsman, W., Langereis, C. G., Abels, H. A., Dai, S., and Fang, X.: Tibetan plateau aridification linked to global cooling at the Eocene–Oligocene transition, Nature, 445, 635–638, https://doi.org/10.1038/nature05516, 2007.

Fang, X., Garzione, C., Van der Voo, R., Li, J., and Fan, M.: Flexural subsidence by 29 Ma on the NE edge of Tibet from the magnetostratigraphy of Linxia Basin, China, Earth Planet. Sc. Lett., 210, 545–560, https://doi.org/10.1016/S0012-821X(03)00142-0, 2003.

Fang, X., Fang, Y., Zan, J., Zhang, W., Song, C., Appel, E., Meng, Q., Miao, Y., Dai, S., Lu, Y., and Zhang, T.: Cenozoic magnetostratigraphy of the Xining Basin, NE Tibetan Plateau, and its constraints on paleontological, sedimentological and tectonomorphological evolution, Earth-Sci. Rev., 190, 460–485, https://doi.org/10.1016/j.earscirev.2019.01.021, 2019.

Flemming, H.-C. and Wuertz, S.: Bacteria and archaea on Earth and their abundance in biofilms, Nat. Rev. Microbiol. 17, 247–260, https://doi.org/10.1038/s41579-019-0158-9, 2019.

Guo, Z., Liu, T., Guiot, J., Wu, N., Lü, H., Han, J., Liu, J., and Gu, Z.: High frequency pulses of East Asian monsoon climate in the last two glaciations: link with the North Atlantic, Clim. Dynam., 12, 701–709, https://doi.org/10.1007/s003820050137, 1996.

Haywood, A. M., Dowsett, H. J., and Dolan, A. M.: Integrating geological archives and climate models for the mid-Pliocene warm period, Nat. Commun., 7, 10646, https://doi.org/10.1038/ncomms10646, 2016.

IPCC.: Climate change 2001: The scientific basis, in: Contribution of Working Group I to the Third Assessment Report of the Intergovernmental Panel on Climate Change, edited by: Houghton, J. T., Ding, Y., Griggs, D. J., Noguer, M., van der Linden, P. J., Dai, X., Maskell, K. and Johnson, C. A., Cambridge University Press, Cambridge, UK, 2001.

Ji, S., Nie, J., Lechler, A., Huntington, K. W., Heitmann, E. O., and Breecker, D. O.: A symmetrical CO_2 peak and asymmetrical climate change during the middle Miocene, Earth Planet. Sc. Lett., 499, 134–144, https://doi.org/10.1016/j.epsl.2018.07.011, 2018.

Jia, L., Zhang, Y., and Huang, W.: The Cenozoic Group of Lantian, in: Institute of Vertebrate Paleontology and Paleoanthropology IVPP, edited by: Institute of Vertebrate Paleontology and Paleoanthropology (IVPP) of the Chinese Academy of Sciences, Proceedings of the field conference on the Cenozoic Group of Lantian, Shaanxi Province, 3–8 November 1964, Xian, China, Science Press, Beijing, China, 1–31, 1966.

Kaakinen, A., Sonninen, E., and Lunkka, J. P.: Stable isotope record in paleosol carbonates from the Chinese Loess Plateau: Implications for late Neogene paleoclimate and paleovegetation, Palaeogeogr. Palaeocl., 237, 359–369, https://doi.org/10.1016/j.palaeo.2005.12.011, 2006.

Kutzbach, J. E. and Behling, P.: Comparison of simulated changes of climate in Asia for two scenarios: Early Miocene to present, and present to future enhanced greenhouse, Global Planet. Change, 41, 157–165, https://doi.org/10.1016/j.gloplacha.2004.01.015, 2004.

Kutzbach, J. E., Prell, W., and Ruddiman, W. F.: Sensitivity of Eurasian climate to surface uplift of the Tibetan Plateau, J. Geol., 101, 177–190, available at: https://www.jstor.org/stable/30081146 (last access: 18 November 2020), 1993.

Li, J., Fang, X., Song, C., Pan, B., Ma, Y., and Yan, M.: Late Miocene–Quaternary rapid stepwise uplift of the NE Tibetan Plateau and its effects on climatic and environmental changes, Quaternary Res., 81, 400–423, https://doi.org/10.1016/j.yqres.2014.01.002, 2014.

Li, Y.: Helium accumulation conditions and resource prospects in Weihe Basin, China, Geological Publishing House, Beijing, China, 1–286, 2018.

Li, Z. C., Li, W. H., Li, Y. X., Li, Y. H., and Han, W.: Cenozoic stratigraphy and paleoenviroments in the Weihe area, Shaanxi Province, J. Stratigraphy, 40, 168–179, 2016.

Lin, A., Rao, G., and Yan, B.: Flexural fold structures and active faults in the northern–western Weihe Graben, central China, J. Asian Earth Sci., 114, 226–241, https://doi.org/10.1016/j.jseaes.2015.04.012, 2015.

Liu, J., Zhang, P., Lease, R. O., Zheng, D., Wan, J., Wang, W., and Zhang, H.: Eocene onset and late Miocene acceleration of Cenozoic intracontinental extension in the North Qinling range–Weihe graben: Insights from apatite fission track thermochronology, Tectonophysics, 584, 281–296, https://doi.org/10.1016/j.tecto.2012.01.025, 2013.

Liu, J., Chen, X., Shi, W., Chen, P., Zhang, Y., Hu, J., Dong, S., and Li, T.: Tectonically controlled evolution of the Yellow River drainage system in the Weihe region, North China: Constraints from sedimentation, mineralogy and geochemistry, J. Asian Earth Sci., 179, 350–364, https://doi.org/10.1016/j.jseaes.2019.05.008, 2019.

Liu, T., Ding, M., and Gao, F.: Cenozoic stratigraphic sections between Xi'an and Lantian, Chin. J. Geol., 4, 199–208, 1960.

Liu, W., Liu, Z., An, Z., Sun, J., Chang, H., Wang, N., Dong, J., and Wang, H.: Late Miocene episodic lakes in the arid Tarim Basin, western China, P. Nat. Acad. Sci. USA, 111, 16292, https://doi.org/10.1073/pnas.1410890111, 2014.

Liu, Z., Bai, Y., and Zhou, L.: Basin structure and hydrocarbon accumulation conditions of the Weihe Basin, Petro. Geol. Experi., 38, 584–591, 2016.

Lu, H., Zhang, H., Wang, Y., Zhao, L., Wang, H., Sun, W., and Zhang, H.: Cenozoic depositional sequence in the Weihe Basin (central China): a long-term record of Asian monsoon precipitation from the greenhouse to icehouse earth, Quaternary Sci., 38, 1057–1067, 2018.

Lu, H. Y., Wang, X. Y., and Li, L. P.: Aeolian sediment evidence that global cooling has driven late Cenozoic stepwise aridification in central Asia, Geol. Soci., Lon. Spec. Pub., 342, 29-44, https://doi.org/10.1144/SP342.4, 2010.

Maslin, M. A., Shultz, S., and Trauth, M. H.: A synthesis of the theories and concepts of early human evolution, Philos. T. Roy. Soc. B, 370, 20140064, https://doi.org/10.1098/rstb.2014.0064, 2015.

Meng, Q. R.: Origin of the Qinling Mountains, Sci. Sin. Terrae, 47, 412–420, https://doi.org/10.1360/N072016-00422, 2017 (in Chinese).

Molnar, P. and Tapponnier, P.: Cenozoic tectonics of Asia – effects of a continental collision, Science, 189, 419–426, https://doi.org/10.1126/science.189.4201.419, 1975.

Northrup, C. J., Royden, L. H., and Burchfiel, B. C.: Motion of the Pacific plate relative to Eurasia and its potential relation to Cenozoic extension along the eastern margin of Eurasia, Geology, 23, 719–722, https://doi.org/10.1130/0091-7613(1995)023<0719:Motppr>2.3.Co;2, 1995.

Passey, B. H., Ayliffe, L. K., Kaakinen, A., Zhang, Z., Eronen, J. T., Zhu, Y., Zhou, L., Cerling, T. E., and Fortelius, M.: Strengthened East Asian summer monsoons during a period of high-latitude warmth? Isotopic evidence from Mio-Pliocene fossil mammals and soil carbonates from northern China, Earth Planet. Sc. Lett., 277, 443–452, https://doi.org/10.1016/j.epsl.2008.11.008, 2009.

Peltzer, G. and Tapponnier, P.: Formation and evolution of strike-slip faults, rifts, and basins during the India-Asia collision-an experimental approach, J. Geophy. Res.-Sol. Ea., 93, 15085–15117, https://doi.org/10.1029/JB093iB12p15085, 1988.

Potts, R.: Hominin evolution in settings of strong environmental variability, Quaternary Sci. Rev., 73, 1–13, https://doi.org/10.1016/j.quascirev.2013.04.003, 2013.

Ramstein, G., Fluteau, F., Besse, J., and Joussaume, S.: Effect of orogeny, plate motion and land–sea distribution on Eurasian climate change over the past 30 million years, Nature, 386, 788–793, https://doi.org/10.1038/386788a0, 1997.

RGS (Reginal Geological Survey): Regional Geology of Shaanxi Province, Shaanxi Province, Shanxi, Geological Publishing House, Beijing, China, 1–698, 1989.

Rits, D. S., Prins, M. A., Troelstra, S. R., van Balen, R. T., Zheng, Y., Beets, C. J., Wang, B., Li, X., Zhou, J., and Zheng, H.: Facies analysis of the Middle and Late Quaternary sediment infill of the northern Weihe Basin, Central China, J. Quaternary Sci., 31, 152–165, https://doi.org/10.1002/jqs.2853, 2016.

Rits, D. S., Beets, C. J., Prins, M. A., van Balen, R. T., Troelstra, S. R., Luo, C., Wang, B., Li, X., Zhou, J., and Zheng, H.: Geochemical characterization of the middle and late Pleistocene alluvial fan-dominated infill of the northern part of the Weihe Basin, Central China, Palaeogeogr. Palaeocl., 482, 57–69, https://doi.org/10.1016/j.palaeo.2017.05.030, 2017.

Schippers, A., Neretin, L. N., Kallmeyer, J., Ferdelman, T. G., Cragg, B. A., John Parkes, R., and Jørgensen, B. B.: Prokaryotic cells of the deep sub-seafloor biosphere identified as living bacteria, Nature, 433, 861–864, https://doi.org/10.1038/nature03302, 2005.

Shi, W., Chen, L., Chen, X., Cen, M., and Zhang, Y.: The Cenozoic tectonic evolution of the faulted basins in the northern margin of the Eastern Qinling Mountains, Central China: Constraints from fault kinematic analysis, J. Asian Earth Sci., 173, 204–224, https://doi.org/10.1016/j.jseaes.2019.01.018, 2019.

Shi, Y., Feng, X., Dai, W., Ren, J., Li, X., and Han, H.: Distribution and structural characteristics of the Xi'an Section of the Weihe Fault, Acta Seism. Sini., 21, 636–651, 2008.

Song, P., Teng, J., Zhang, X., Liu, Y., Si, X., Ma, X., Qiao, Y., and Dong, X.: Flyover Crustal Structures Beneath the Qinling Orogenic Belt and Its Tectonic Implications, J. Geophys. Res.-Sol. Ea., 123, 6703–6718, https://doi.org/10.1029/2017jb015401, 2018.

Sun, J., Zhang, Z., and Zhang, L.: New evidence on the age of the Taklimakan Desert, Geology, 37, 159–162, https://doi.org/10.1130/G25338A.1, 2009.

Sun, J., Lü, T., Zhang, Z., Wang, X., and Liu, W.: Stepwise expansions of C_4 biomass and enhanced seasonal precipitation and regional aridity during the Quaternary on the southern Chinese Loess Plateau, Quaternary Sci. Rev., 34, 57–65, https://doi.org/10.1016/j.quascirev.2011.12.007, 2012.

Tang, C., Yang, H., Dang, X., and Xie, S.: Comparison of paleotemperature reconstructions using microbial tetraether thermometers of the Chinese loess-paleosol sequence for the past 350000 years, Sci. China Earth Sci., 60, 1159–1170, https://doi.org/10.1007/s11430-016-9035-y, 2017.

Thomas, E. K., Clemens, S. C., Sun, Y. B., Huang, Y. S., Prell, W., Chen, G. S., Liu, Z. Y., and Loomis, S.: Midlatitude land surface temperature impacts the timing and structure of glacial maxima, Geophys. Res. Lett., 44, 984–992, https://doi.org/10.1002/2016gl071882, 2017.

Wang, B., Zheng, H., Wang, P., and He, Z.: The Cenozoic strata and depositional evolution of Weihe Basin: Progresses and problems, Adv. Earth Sci., 28, 1126–1135, 2013.

Wang, B., Zheng, H., He, Z., Wang, P., Kaakinen, A., and Zhou, X.: Middle Miocene eolian sediments on the southern Chinese Loess Plateau dated by magnetostratigraphy, Palaeogeogr. Palaeocl., 411, 257–266, https://doi.org/10.1016/j.palaeo.2014.07.007, 2014.

Wang, H., Lu, H., Zhao, L., Zhang, H., Lei, F., and Wang, Y.: Asian monsoon rainfall variation during the Pliocene forced by global temperature change, Nat. Commun., 10, 5272, https://doi.org/10.1038/s41467-019-13338-4, 2019.

Wang, Z., An, Z., Liu, Z., Qiang, X., Zhang, F., and Liu, W.: Hydroclimatic variability in loess δD wax records from the central Chinese Loess Plateau over the past 250 ka, J. Asian Earth Sci., 155, 49–57, https://doi.org/10.1016/j.jseaes.2017.11.008, 2018.

Westerhold, T., Marwan, N., Drury, A. J., Liebrand, D., Agnini, C., Anagnostou, E., Barnet, J. S. K., Bohaty, S. M., De Vleeschouwer, D., Florindo, F., Frederichs, T., Hodell, D. A., Holbourn, A. E., Kroon, D., Lauretano, V., Littler, K., Lourens, L. J., Lyle, M., Pälike, H., Röhl, U., Tian, J., Wilkens, R. H., Wilson, P. A., and Zachos, J. C.: An astronomically dated record of Earth's climate and its predictability over the last 66 million years, Science, 369, 1383, https://doi.org/10.1126/science.aba6853, 2020.

Xu, S., Mi, N., Xu, M., Wang, L., Li, H., and Yu, D.: Crustal structures of the Weihe graben and its surroundings from receiver functions, Sci. China Earth Sci., 57, 372–378, https://doi.org/10.1007/s11430-013-4719-x, 2014.

Ye, H., Zhang, B. T., and Mao, F. Y.: The Cenozoic tectonic evolution of the great north china – 2 types of rifting and crustal necking in the great north china and their tectonic implications, Tectonophysics, 133, 217–227, https://doi.org/10.1016/0040-1951(87)90265-4, 1987.

Yin, A., Dang, Y.-Q., Zhang, M., Chen, X.-H., and McRivette, M. W.: Cenozoic tectonic evolution of the Qaidam basin and its surrounding regions (Part 3): Structural geology, sedimentation, and regional tectonic reconstruction, GSA Bull., 120, 847–876, https://doi.org/10.1130/B26232.1, 2008.

Yue, L.: Magnetostratigraphical study of the loess section at Duanjiapo, Lantian, Shaanxi, Geol. Rev., 35, 479–488, 1989.

Yue, L., Heller, F., Qiu, Z., Zhang, L., Xie, G., Qiu, Z., and Zhang, Y.: Magnetostratigraphy and pavleo-environmental record of Tertiary deposits of Lanzhou Basin, Chin. Sci. Bull., 46, 770–773, https://doi.org/10.1007/BF03187220, 2001.

Zachos, J., Pagani, M., Sloan, L., Thomas, E., and Billups, K.: Trends, rhythms, and aberrations in global climate 65 Ma to present, Science, 292, 686–693, https://doi.org/10.1126/science.1059412, 2001.

Zhang, P., Wang, Q., and Ma, Z.: GPS velocity field and active crustal blocks of contemporary tectonic deformation in continental China, Earth Sci. Front., 9, 430–441, 2002.

Zhang, W., Appel, E., Fang, X., Song, C., and Cirpka, O.: Magnetostratigraphy of deep drilling core SG-1 in the western Qaidam Basin (NE Tibetan Plateau) and its tectonic implications, Quaternary Res., 78, 139–148, https://doi.org/10.1016/j.yqres.2012.03.011, 2012.

Zhang, Y. Q., Vergely, P., and Mercier, J.: Active faulting in and along the Qinling Range (China) inferred from spot imagery analysis and extrusion tectonics of south China, Tectonophysics, 243, 69–95, https://doi.org/10.1016/0040-1951(94)00192-C, 1995.

Zhang, Y. G., Pagani, M., Liu, Z., Bohaty, S. M., and Deconto, R. M.: A 40-million-year history of atmospheric CO_2, Philos. T. Roc. Soc. A, 371, 20130096, https://doi.org/10.1098/rsta.2013.0096, 2013.

Zhao, L., Lu, H., and Tang, L.: Cenozoic palynological records and vegetation evolution in the Weihe Basin, Central China, Quaternary Sci., 38, 1083–1093, https://doi.org/10.11928/j.issn.1001-7410.2018.05.03, 2018.

Zhao, L., Lu, H., Wang, H., Meadows, M., Ma, C., Tang, L., Lei, F., and Zhang, H.: Vegetation dynamics in response to evolution of the Asian Monsoon in a warm world: Pollen evidence from the Weihe Basin, central China, Global Planet. Change, 193, 103269, https://doi.org/10.1016/j.gloplacha.2020.103269, 2020.

Zheng, H., An, Z., and Shaw, J.: New contributions to Chinese Plio-Pleistocene magnetostratigraphy, Phys. Earth Planet. Int., 70, 146–153, https://doi.org/10.1016/0031-9201(92)90177-W, 1992.

Zhu, Z., Dennell, R., Huang, W., Wu, Y., Qiu, S., Yang, S., Rao, Z., Hou, Y., Xie, J., Han, J., and Ouyang, T.: Hominin occupation of the Chinese Loess Plateau since about 2.1 million years ago, Nature, 559, 608–612, https://doi.org/10.1038/s41586-018-0299-4, 2018.

Zhuo, H., Lu, H., Wang, S., Ahmad, K., Sun, W., Zhang, H., Yi, S., Li, Y., and Wang, X.: Chronology of newly-discovered Paleolithic artifact assemblages in Lantian (Shaanxi province), central China, Quaternary Res., 86, 316–325, https://doi.org/10.1016/j.yqres.2016.08.008, 2016.

Sci. Dril., 28, 75–91, 2020
https://doi.org/10.5194/sd-28-75-2020

Scientific Drilling
Open Access

Borehole research in New York State can advance utilization of low-enthalpy geothermal energy, management of potential risks, and understanding of deep sedimentary and crystalline geologic systems

Teresa Jordan[1], Patrick Fulton[1], Jefferson Tester[2], David Bruhn[3], Hiroshi Asanuma[4], Ulrich Harms[5], Chaoyi Wang[6], Doug Schmitt[7], Philip J. Vardon[8], Hannes Hofmann[9], Tom Pasquini[10], Jared Smith[11], and the workshop participants✚

[1]Earth and Atmospheric Sciences, Cornell University, Ithaca, NY 14853, USA
[2]Chemical and Biomolecular Engineering, Cornell University, Ithaca, NY 14853, USA
[3]Civil Engineering and Geosciences, Delft University of Technology, Delft, 2600, the Netherlands
[4]National Institute of Advanced Industrial Science and Engineering, Fukushina Renewable Energy Research Institute, Koriyama, Fukushima Prefecture, 963-0298, Japan
[5]ICDP/Geomechanics and Scientific Drilling, GFZ German Research Centre for Geosciences, Potsdam, 14473 Germany
[6]Physics and Astronomy, Purdue University, West Lafayette, IN 47907 USA
[7]Earth, Atmospheric and Planetary Sciences, Purdue University, West Lafayette, IN 47907 USA
[8]Geoscience and Engineering, Delft University of Technology, Delft, 2628 CN, the Netherlands
[9]Helmholtz Centre Potsdam GFZ German Research Centre for Geosciences, Potsdam, 14473, Germany
[10]Gulf Plains Prospecting Company, Kingwood, TX 77345 USA
[11]Engineering Systems and Environment, University of Virginia, Charlottesville, VA 22904 USA
✚A full list of authors appears at the end of the paper.

Correspondence: Teresa Jordan (tej1@cornell.edu)

Received: 8 July 2020 – Revised: 22 October 2020 – Accepted: 5 November 2020 – Published: 1 December 2020

Abstract. In January 2020, a scientific borehole planning workshop sponsored by the International Continental Scientific Drilling Program was convened at Cornell University in the northeastern United States. Cornell is planning to drill test wells to evaluate the potential to use geothermal heat from depths in the range of 2700–4500 m and rock temperatures of about 60 to 120 °C to heat its campus buildings. Cornell encourages the Earth sciences community to envision how these boreholes can also be used to advance high-priority subsurface research questions. Because nearly all scientific boreholes on the continents are targeted to examine iconic situations, there are large gaps in understanding of the "average" intraplate continental crust. Hence, there is uncommon and widely applicable value to boring and investigating a "boring" location. The workshop focused on designing projects to investigate the coupled thermal–chemical–hydrological–mechanical workings of continental crust. Connecting the practical and scientific goals of the boreholes are a set of currently unanswered questions that have a common root: the complex relationships among pore pressure, stress, and strain in a heterogeneous and discontinuous rock mass across conditions spanning from natural to human perturbations and short to long timescales. The need for data and subsurface characterization vital for decision-making around the prospective Cornell geothermal system provides opportunities for experimentation, measurement, and sampling that might lead to major advances in the understanding of hydrogeology, intraplate seismicity, and fluid/chemical cycling. Subsurface samples could also enable regional geological studies and geobiology research. Following the workshop, the U.S. Department of Energy awarded funds for a first exploratory borehole, whose proposed design and research plan rely extensively on the ICDP workshop recommendations.

Published by Copernicus Publications on behalf of the IODP and the ICDP.

1 Introduction: a convergence of society's need for low-carbon heat and Earth scientists' need to understand continental crust

Global warming and climate change have become the ultimate challenge for a sustainable environment from now into the foreseeable future. The key to minimizing their impacts is to utilize renewable energy sources to significantly reduce or neutralize the carbon footprint of human activities. Geothermal energy is one widely available resource within the set of available and promising resources which, if intensively deployed, would deliver this environmental value. However, the lack of fundamental scientific and engineering understanding of the subsurface conditions that control the transfer of deeply sourced heat in rock to circulating fluids, along with a need to better understand and manage induced seismicity, has impeded the widespread commercialization of geothermal resources. The pragmatic barrier is that a high investment cost must be paid in advance, while we remain unable to reliably predict that heat can be produced. The potential scientific breakthroughs which can improve predictability of success, costs, and risks would also advance fundamental understanding of continental crust.

More than one-quarter of the world's population lives in the temperate to polar climates north of 35° N and south of 35° S latitude where, for most of them, the mean annual temperature is less than 11 °C (52 °F) (Kummu and Varis, 2011). Under those conditions, hot water and space heating are needed for residences and for most indoor working environments. For the 85 % of that high-latitude population who reside in the European Union, United States, and Russia, the consumption of low-temperature heat in homes and commercial buildings is a large fraction (about 21 %) of total energy used (see Sect. 2). A future carbon-neutral world necessitates shifting the source of this heat from combustion of fossil fuels to a renewable, widely available, low-carbon energy source.

A thermal resource available almost everywhere is geothermal energy. However, at present only high-enthalpy volcanic systems and young rift zones are utilized commercially for electric power generation, and low-temperature geothermal resources are underexploited and underexplored. The utilization of 55–85 °C water from the Dogger sedimentary rock aquifer near Paris, France, to heat over 200 000 housing units exemplifies the potential (https://www.brgm.eu/project/geothermal-database-on-dogger-aquifer-paris-basin, last access: 20 November 2020). Likewise, geothermal heat from the Delft Sandstone has grown to support 3 % of the heat used for greenhouse horticulture in the Netherlands (https://www.ebn.nl/wp-content/uploads/2018/04/EBN-poster-numbers2016.pdf, last access: 20 November 2020). Yet both those cases also exemplify the limitations: our current ability to extract water that carries the geothermal heat is limited to places with high fluid transmissivity, and those optimum rock conditions are not widespread at the subsurface depths with suitable temperatures. From the perspective of routine drilling technology, depth itself is not a problem, although it is an expense, as subsurface temperatures in the range of 50–100 °C are obtained at most locations at moderate depths (< 3 km). Rather, the main physical limitations are low porosity and low permeability. Vast areas of the continents lack the natural hydrological capacity traditionally sought in the high-enthalpy systems, as a consequence of the fact that crystalline basement rocks occur either at the surface or within a few kilometers' depth below the surface. The transmissivity of those rocks is likely low and, in general, poorly documented. If this natural geothermal heat resource is to significantly help move human communities off of fossil fuels, what is currently a highly uncertain geothermal technology must advance to become a low-risk, routine option among sources of heat.

One of the typical geological environments with untapped potential at a few kilometers' depth is the lower strata of sedimentary basins and the underlying crystalline basement (Camp et al., 2018; Limberger et al., 2018). The possibility that Cornell University may drill an exploratory borehole to a depth in the range of 4–5 km, which will penetrate nearly 3 km of Paleozoic sedimentary rocks and ≥ 1 km of granulite-grade Grenville metamorphic rocks, sets up an opportunity for novel scientific experimentation to examine the stress state, hydrogeological and geomechanical conditions, and the rock and fluid responses to perturbations, both natural and anthropogenic. Using such a borehole laboratory, there will be broad applicability for the understanding to be gained of the state of stress within crystalline basement in an area of very low natural seismicity and of how low-permeability sedimentary rocks as well as heterogeneous mid- to high-grade metamorphic rocks near the sedimentary–basement contact respond to the complex relationships between pore pressure, stress and strain.

In an idealized geothermal energy extraction project, heated fluids are extracted, the energy is harvested, the cooled fluids are recycled by injection into a target formation to absorb again the geothermal heat, and the fluid and heat cycling continues. Yet near Cornell University and many other places globally, natural in situ conditions are not likely to provide sufficient contact of circulating fluids with rock surfaces to achieve acceptable rates of geothermal energy extraction. In such cases, enhanced geothermal system (EGS) technologies are needed to promote fluid circulation and fluid–rock contact area. However, drilling, artificial permeability improvement, and fluid cycling all cause perturbations in the subsurface that may have hazardous consequences, ranging from induced seismicity to contamination of groundwater with geothermal fluids. The EGS activities

may also fail to achieve the energy extraction targets, which creates very high financial risks for an EGS.

Interestingly, the uncertainties of induced seismic risk and of financial risk are rooted in the same scientific unknowns: the complex relationships among pore pressure, stress, and strain in rock with pre-existing heterogeneity, across conditions spanning from natural to short-duration human perturbation (e.g., stimulation of fractures) and to long-term human forcings (e.g., sustained injection and production of water supplies, hydrocarbons, or geothermal brines).

Knowledge of geological features, temperature profile, stress variations, and permeability with increasing depth and with changing rock type is essential to ensure the proper deployment of EGS applications while minimizing the environmental impact. However, in continental crust, a surprising lack of understanding of stress and permeability hinders practical developments of EGS at the scale necessary for real applications in which benefits balance costs. Our primary scientific goal is to gain an understanding of the spatial distribution and temporal evolution of stress and permeability with depth and the intertwined relationships with temperature, lithology, faults, natural fracture groups, rock fabric, and mineral dissolution and precipitation. This knowledge will elevate the understanding of (1) how the near-field crust immediately reacts to changes in pore pressure, geochemistry, and resultant thermo-chemo-poroelastic effects; (2) the influences on far-field crust accounting for a stress halo and fluid migration; and (3) the risks of induced seismicity and contamination.

Consequently, a borehole needed to provide data vital for making decisions about the prospective Cornell geothermal system can also be an opportunity for experimentation, measurement, and sampling that might lead to major scientific advances in the understanding of crustal hydrology, earthquakes in plate interiors, and fluid-chemical cycling. To explore the merits of turning a Cornell test borehole into a broader borehole of scientific opportunity, the ICDP sponsored a borehole science planning workshop at Cornell University on 8–10 January 2020.

2 Why central New York State and why now?

Central New York State in northeastern North America is just one location, yet its need for the conversion to a low-carbon energy source by which to warm residences and commercial buildings and to heat water is an extremely common situation for much of Earth's population. Cornell University seeks to lead the way in demonstrating one path forward that could be widely deployed.

2.1 Carbon neutrality in temperate climate, cloudy, heavily populated areas is not easy

Cornell University selected 2035 as the date by which to become carbon-neutral on its Ithaca, New York, campus. The goal was adopted without an operational plan that was feasible using available technologies of the adoption year, 2013. A similar pledge was made in 2019 by the State of New York in the cold-climate northeastern USA on stable North American continental crust. The state pledged to eliminate net greenhouse gas emissions by 2050, also without an existing plan encompassing the removal of carbon from the energy used to heat residential and commercial buildings. In New York State, the contribution of heating to carbon emissions is large: about 35 % of New York's annual primary energy is consumed for heating, using energy sources dominated by the combustion of natural gas, fuel oil and propane. In New York State, on-site fossil fuel combustion in the residential, commercial and industrial sectors – all of which predominantly supply low-temperature space and water heating – contributes 30 % of greenhouse gas emissions, compared to electricity production contributing 13 % and transportation 36 % (EIA, 2018a, b, 2019; McCabe et al., 2016; NYSERDA, 2019). The comparatively low carbon footprint of New York's electricity generation is due to major hydropower and nuclear contributions. It is evident that the eventual successful decarbonization of the heating of homes and commercial buildings in heavily populated regions demands an overhaul of the energy supply for heating, such as by use of geothermal energy.

The concept under evaluation by Cornell University, to utilize geothermal heat by tapping fluids in rock at temperatures in the range of 60–120 °C, could also serve widely in New York State to heat residences and commercial buildings, for certain industrial activities, and to assist controlled agriculture operations for food production. Although New York State has banned high-volume hydraulic fracturing in horizontal wells, as practiced for production of gas or oil from organic-rich shale, the long-established use of hydraulic pressure to stimulate existing fractures remains legal. Hence both the options of natural transmissivity and fluid flow through stimulated fractures are plausible fluid-flow pathways. Nevertheless, the technical uncertainty and investment risks for direct-use geothermal energy projects are dominated by the uncertainty about establishment of fluid flow through a well field that is sufficiently dispersed to sweep heat from rock surfaces in a large volume of rock, rather than to short-circuit through a small set of flow paths. The university's view of the next step to test the opportunity is that there are three intertwined objectives: to develop a demonstration reservoir using a well pair that will deliver 20 % of Cornell's heating demand, to de-risk the deployment of geothermal direct-use heating throughout New York and other states with similar geology and climate, and to engender activities that are in keeping with the core university mission: research advances, education, and outreach with novel solutions for broader societal issues.

2.2 Accessing geothermal resources where continental geology is "normal": a world class problem at a geologically representative site

The ICDP-supported workshop focused on land owned by Cornell University in Ithaca, NY, USA, where the surface geology consists of Devonian sedimentary rock and the subsurface geology includes 2.80 km ± 0.2 km of Paleozoic sedimentary rocks overlying complex Precambrian-age metamorphic rocks (Fig. 1). Nearby, the sedimentary rocks are documented (Camp et al., 2018; Al Aswad, 2019) and the metamorphic rocks inferred to be of very low permeability. According to Limberger et al. (2018), across 16 % of Earth's land surface there exist generally comparable geothermal reservoir systems: a thick sedimentary column over continental basement. That statistic demonstrates the commonality of Ithaca, NY, with a large fraction of the globe. Nevertheless, for central New York, the paucity of sufficient porosity in all but a tiny fraction of the strata sets the possible geothermal reservoirs apart from the desirable "Hot Sedimentary Aquifers" reservoir category considered to be especially good targets for geothermal heat extraction (Wright and Culver, 1991), like the highly permeable Dogger Limestone of the Paris Basin (Le Brun et al., 2011). Instead, the central New York State data lead to anticipation that the conditions will be more like those documented by Dillinger et al. (2016) in the Cooper Basin of Australia, where complex diagenesis resulted in low permeability and lack of sufficient fluid production at a geothermal test well. For Cornell, it is likely that access to the geothermal heat will require fracture flow, which puts in the spotlight the natural characteristics of fractures in both sedimentary and metamorphic rocks and raises key questions about the behavior of those fractures in the ambient stress field under the perturbed conditions that might be imposed in an effort to hydraulically stimulate flow along fractures or that might develop during long-term geothermal field production.

Large areas of all continents are underlain at several kilometers' depth by mid-grade to high-grade metamorphic complexes that formed in ancient orogenic belts. Like many locations, the basement rocks anticipated in the proposed Cornell borehole will be composed of complex, heterogeneous lithologies, with anisotropic mineralogical, petrological and fabric characteristics, in which occur numerous generations of fractures that formed since peak metamorphism and are filled with multiple generations of minerals. The region is an archetypical domain of a very low level of natural seismic activity (Fig. 1) – in a circular area exceeding 13 000 km^2 centered on Cornell University, there have been no earthquakes of magnitude > 2.5 in at least a century. A set of scientific experiments designed for and conducted in a deep borehole in central New York State can address questions that are generic and not specific to the eastern United States.

Integration of findings for the continental crust of New York with those expected from a similar set of experiments designed for a geothermal borehole at TU Delft in the Netherlands (Vardon et al., 2020) could, together, illuminate answers to a series of basic questions, in the interest of accelerating the safe use of subsurface thermal energy. Is the continental crust everywhere at a condition of critical stress (Zoback and Gorelick, 2012)? How heterogeneous is the stress field with depth and across lithologic boundaries? How does the subsurface, especially at the sedimentary rock–basement interface, respond to perturbations? And how will potential chemical and mineralogical reactions during operations couple to permeability, pressure transmission, and strain? Answers to these questions can provide broad insight into seismic risks and potentially how to mitigate them. Technical risks can also be addressed by determining whether the sedimentary rock–basement interface is a relevant geothermal development target and under what rock conditions artificial stimulation could improve permeability to achieve adequate fluid flow and prolonged heat transfer to permit direct use of geothermal energy where continental crust is naturally of low permeability.

3 Workshop structure

The workshop was designed to maximize cross-disciplinary sharing and debate, to minimize passively listening to prepared presentations, and to lead to one or more innovative scientific projects worthy of funding. The organizers could anticipate what might be some of the big scientific themes that would become transformed into tractable borehole science projects as a result of the workshop, yet we did not wish to squelch thoughts outside of the bounds of our preconceived notions. The invitation and application process had assembled a large group with little shared background knowledge of the major questions in one another's area of interest. The focus would be a specific location with unchangeable (albeit partially unknowable) subsurface materials, and the participants would need a simple but comprehensive introduction to the materials. We did not want the group to disperse without written outcomes that would lead to submitted proposals for funds needed to conduct the science research program.

The first two days of the 3-day workshop involved 35 visitors and 26 Cornell faculty, technical staff, and students. The third day of the workshop was limited to a proposal writing team of six visitors and one of the Cornell hosts and a report writing team of two visitors and one of the Cornell hosts. The first two days were dedicated to a series of breakout sessions and plenary sessions. The single hour of background presentations conveyed a quick picture – 5 min limits – of the state of the art in themes we expected to be major science challenges and major approaches to illuminating key processes as well as the nature of the materials and structures expected in the Ithaca subsurface. A poster session was available during all breaks, and several meters of core through rocks similar

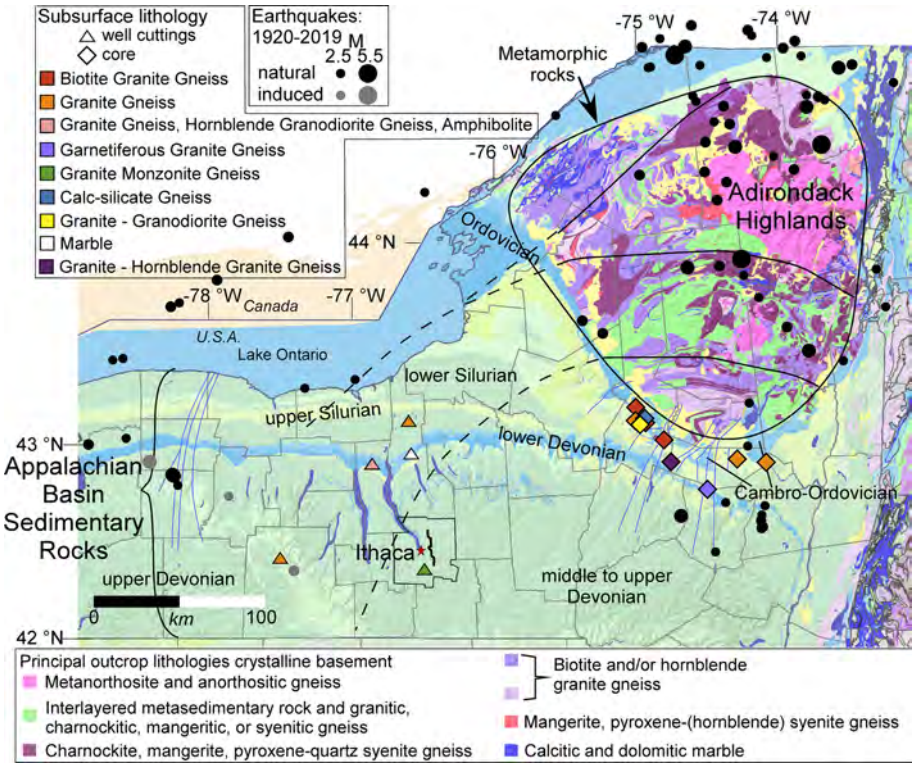

Figure 1. Map of geology and historical earthquakes in New York State. Geological map shows bedrock composition immediately subjacent to soil and Holocene sediments (USGS map source, https://mrdata.usgs.gov/geology/state/map.html?x=-75.6897884252848&y=42.9882351360762&z=7#, last access: 20 November 2020). The Adirondack Mountains in northern New York are enclosed in a subcircular black polygon. For sedimentary rocks of the Appalachian Basin, the geological periods corresponding to some of the mapped colors are labeled on the map. Subsurface basement lithologies are known from petrographic analysis of samples of cores and cuttings that are archived by the New York State Museum (Benjamin R. Valentino, unpublished data, 2016). Positions of major shear zones of the Adirondack crystalline rocks (solid black lines) are from Valentino et al. (2008) and Valentino and Chiarenzelli (2018). Projections of those shear zones beneath the Appalachian strata (dashed black lines) are based on Chiarenzelli and Valentino (2020). The set of blue lines in western New York is the Clarenden–Lynden fault zone, and the set of blue lines adjacent to the southern Adirondacks are faults that cut lower Ordovician, Cambrian and basement units (from Jacobi, 2002). Earthquakes are from USGS compilation span January 1920–20 January 2020 (USGS Earthquake Catalog, https://earthquake.usgs.gov/earthquakes/map/, last access: 20 November 2020; details of search listed among references cited). Induced earthquakes in western New York are attributable to brine mining-related work and to brine injection tests in an attempt to develop new caverns for gas storage (Smith et al., 2005; Horowitz et al., 2017). Polygon surrounding Ithaca delineates Tompkins County. A black line near Ithaca shows the location of a seismic reflection profile leased by Cornell to establish the distribution of faults and folds (Fig. 3).

to what are expected below Ithaca were on display. Even after opportunely adding three extra talks while the workshop progressed, the total structured workshop time dedicated to slide presentations was about 8 %. There were three length exceptions, yet only 15 min each: Cornell's lead engineer in the Earth Source Heat project team, the Dean of Engineering, and representatives of the U.S. Continental Scientific Drilling Program and the New York State Museum. The latter short presentation introduced the materials, services, and protocols for data and samples that are hosted by their organizations and available for integration into a proposed Cornell-based test borehole scientific program.

In the remaining > 90 % of the time, the dominant activities were breakout discussions interspersed with plenary discussions. The first breakout groups were seeded with five topics, populated by self-selected participants, and dedicated to brainstorming. The second breakout activity moved the regional geological experts into the other groups, as a knowledge resource. In the third breakout session, the geologically oriented group reconvened while the drilling group disbanded, and those experts placed their drilling and borehole management experience in the science-focused breakouts. Through that series of slightly shifting breakout themes and participants and intervening plenary discussions, the interest groups evolved from laudatory-but-impractical dreams to a more realistic borehole project design. On the second day, new breakout groups were constituted based on expertise rather than interest, and these groups critiqued and refined

the research approaches suggested by the first-day groups. A session was dedicated to considering the operational coexistence that would be needed between the scientific projects and the Cornell ESH borehole team, whose focus would be on managing risk, minimizing costs, and achieving the practical goals of the borehole. In anticipation that funds needed for some of the scientific experiments would need to be raised from multiple funding sources and that principal investigators behind these complementary projects would not necessarily be Cornell University personnel, a hypothetical organizational structure to coordinate and evaluate proposed borehole sampling and experiments was unveiled and critiqued, benefitting from feedback from participants with experience in other collaborative natural laboratories.

Undoubtedly this workshop structure would have appeared to be quite messy if one were watching the events. Yet the outcome was that the full group of participants was energetically involved and learning from one another at a high rate. The theme area interest groups as well as the workshop group as a whole moved forward to create an integrated science plan and experimental framework that became physically realistic, albeit complex and challenging.

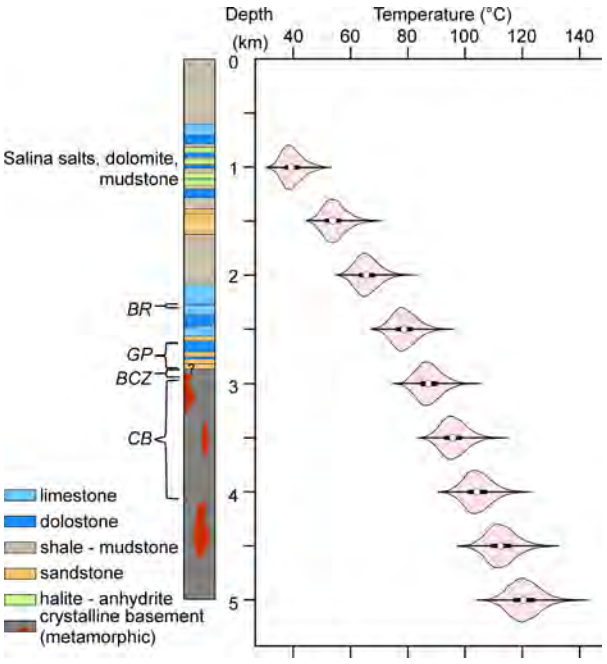

Figure 2. Left: approximate geological column near Ithaca, NY. Paleozoic sedimentary rocks extend to about 2850 m depth ±200 m, underlain by metamorphic basement. Targeted intervals to probe for their geothermal reservoir conditions are indicated by brackets, corresponding to the BR (Black River), GP (Galway and Potsdam), BCZ (basement contact zone), and CB (crystalline basement). Cuttings from 46 m (150 ft) penetration into the basement by a borehole 10 km south of Cornell indicate a hydrothermally altered granitic to monzonitic gneiss (Benjamin R. Valentino, unpublished data, 2016). Near Cornell's campus, xenocrysts in kimberlites are very rich in Mg, suggestive of granulite-grade marble in the upper basement (Kay et al., 1983). Right: predicted temperature–depth profile below Cornell University in Ithaca, NY, based on geostatistical interpolation of the surface heat flow as estimated from corrected borehole temperatures in the Appalachian Basin near Ithaca, utilizing 10 000 Monte Carlo replications to incorporate the uncertainty in geologic properties and heat flow estimates (Smith, 2019). The uncertainty distribution of predicted temperatures for each 0.5 km depth interval is shown as a pale red violin plot (kernel density plot). White circles are placed at the median predicted temperature at each depth, and a narrow black box in the center spans the 25th to 75th percentile estimates.

4 Geological features of the Cornell borehole project site

Existing borehole and geophysical data for New York State indicate that the Ithaca area basement rocks are likely similar to those which crop out in the Adirondack Mountains (Fig. 1), which is a Grenville age mid- to high-grade metamorphic dome. We expect the basement to be a mixture of metasedimentary and meta-igneous rocks, repeatedly folded while ductile (McLelland et al., 2010; Chiarenzelli et al., 2011; Valentino et al., 2019). If represented by the Adirondack Mountains, the petrological heterogeneity likely spans marbles to anorthosite, with compositionally variable gneisses and schists. Cuttings and kimberlite xenocrysts (Kay et al., 1983) in the region near Cornell University confirm this degree of variability.

The length scale of compositional heterogeneity in the basement likely spans centimeters to tens of kilometers, and there would likely be strong anisotropy of metamorphic fabrics at scales of millimeters to kilometers. Superimposed brittle fractures in the Adirondacks are abundant, with dominant orientations trending NE and NW, and most are filled with mineral veins (Wiener and Isachsen, 1987; Valentino et al., 2016). Whether any of the outcrop fracture properties are applicable to the deep subsurface of the Appalachian Basin is unknown.

The dominant sedimentary rocks near Cornell are an upward progression from basal sandstones, to carbonates, and to siliciclastic mudstone and sandstone, interrupted by hundreds of meters of Silurian evaporite deposits, dolomite, and mudstones (Salina Group) and by two intervals of organic-rich shales (Fig. 2). The best-documented structures near Ithaca are of two types. First, there are small-magnitude extensional or transtensional fault sets localized in narrow, shallow grabens (Fig. 3), known well for hosting major gas fields (Smith, 2006). The second type of structures are small magnitude folds and thrusts of the distal Alleghanian Orogeny, localized within and above the weak shales and evaporites of the Silurian section (Fig. 3).

Thermochronological data imply that Cornell's near-surface strata were originally covered by 3 ± 1 km thickness of Carboniferous and Permian strata, all of which

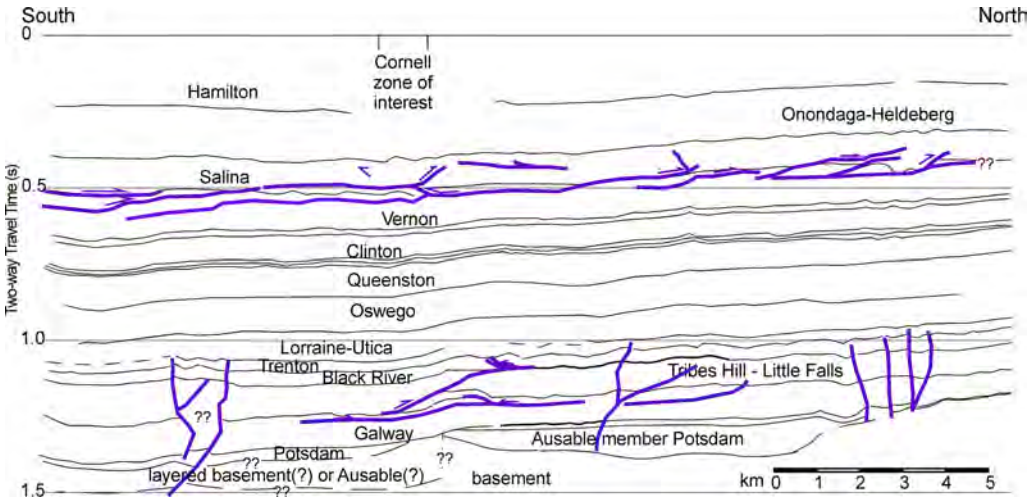

Figure 3. Line drawing of an interpreted seismic reflection profile (location in Fig. 1) which traverses a short distance east of Cornell's targeted geothermal well field area of interest. Black thin lines are stratigraphic contacts within the sedimentary rock column. Purple thick lines are faults. Near 0.5 s TWTT, the set of faults are thrusts within the weak series of Silurian mudstones and evaporites. Between 1.0 and 1.5 s TWTT the faults are of two classes. The small-offset sub-vertical sets are typical of the Trenton–Black River grabens, related to wrench faults. The sub-horizontal faults are small displacement thrusts. Both the shallow and deep thrusts likely were active during the Alleghanian Orogeny. Interpretation by Jordan (2019).

were erosionally removed (Miller and Duddy, 1989; Roden and Miller, 1989; Heizler and Harrison, 1998; Shorten and Fitzgerald, 2019). During Paleozoic deposition and the subsequent long hiatus, today's preserved strata experienced extensive compaction and cementation, which rendered them strong. With few exceptions, the sedimentary rocks of the deepest 1 km of the Appalachian Basin in New York State have porosity $< 10\,\%$, and the dominant porosity is $< 5\,\%$ (Martin, 2011; Al Aswad, 2019). Localized higher fracture porosity is inferred but not measured (Martin, 2011). In general, there is a lack of permeability data. We deduce that permeability for this rock interval must be less than in productive gas fields north and west of Cornell, where the *best* values range from 0.1 to 4 millidarcy (10^{-16}–10^{-15} m^2) (Lugert et al., 2006), and therefore permeability of most of the deep strata is likely on the order of microdarcy (10^{-18} m^2). Near Cornell, the known exceptions occur in narrow, localized pods of hydrothermal dolomite associated with grabens, where much higher porosity and good permeability occur within a single 30 m thick interval about 500 m above the basement (Smith 2006; Camp and Jordan, 2016).

Available data suggest that the porewater throughout the column of sedimentary rocks possesses a summed Na and Cl concentration between 200 000 and 300 000 mg L^{-1} (Waller et al., 1978; Lynch and Castor, 1983; Blondes et al., 2017). Although very saline, the brine composition is within the range of basinal brines known globally (Houston et al., 2011). The pore fluids in the crystalline basement rocks are not documented; they might be similarly concentrated brines with somewhat distinctive compositions (e.g., Frape et al., 1984) or they might be much less saline.

Ithaca has at least one highly unusual geological feature, which likely will not generalize to most other continental crust: very narrow (centimeter to meter) late Mesozoic kimberlite dikes are abundant in north-trending fractures in the Ithaca region (Fig. 3) (Kay et al., 1983; Bailey et al., 2017). Limited geochronological data indicate that dike intrusion occurred around 146–148 Ma (U–Pb ages; Heaman and Kjarsgaard, 2000) or in two clusters between 113 and 146 Ma (K–Ar ages) (Basu et al., 1984; Bailey and Lupulescu, 2015). The heat pulse associated with the kimberlites decayed long ago.

The deep geology below Ithaca also has numerous uncertainties. One category of uncertainty is natural fractures at depths below the weak mudrocks and evaporites of the Silurian (Fig. 3). Another uncertainty is the nature of features that control gentle folds deep in the sedimentary column (Fig. 3). Whether these are related to inherited topography at the top of the crystalline basement or represent reactivation of basement faults during the Alleghanian Orogeny cannot be resolved with the available subsurface data. These uncertainties likely contribute to the commonality with other potential geothermal energy sites in continental interiors – there are always unknowns regarding the mechanical conditions and heterogeneities within the subsurface.

5 Findings

5.1 Multiple, complementary boreholes improve the scientific value of a project

A strategy for a scientific borehole mission at Cornell University must be placed in the context of coexistence with a pair of boreholes planned to demonstrate the viability of producing geothermal fluid at a sufficient flow to meet 20 % of Cornell's building heat needs. Those demonstration boreholes must be wide enough in diameter to sustain production at a flow rate on the order of 30–70 kg s^{-1}; typically, due to this flow rate, geothermal production wells are wider in diameter than used for the oil and gas industry, groundwater production, or mineral exploration. Hence careful consideration is needed of what types of in-borehole activities and monitors are compatible with the needs of a well that eventually may function as either an injection or withdrawal well. Given that the geothermal demonstration wells would be wide in diameter, cased through intervals that present environmental or borehole management risks, maintained in a disturbed condition if production is initiated, and necessarily that their operations would prioritize the success of the geothermal project, there would be both short-term design and long-term management challenges related to co-located scientific program activities. The design and management challenges for scientific activities include the following general possibilities: interruptions to the higher-priority geothermal-focused activities; costly delays in higher-priority activities; technical incompatibility between methods of anchoring permanent monitoring equipment and casing programs; and the potential for stuck tools or borehole wall damage or collapse, which place future access and use of the borehole at risk of failure.

The scientific and geothermal demonstration boreholes are unambiguously complementary to one another in their missions, data streams, and outcomes. Nevertheless, discussions at the ICDP Workshop of efforts to complete in the same borehole both programs, science and geothermal operations, repeatedly arrived at concerns that workarounds to do both would create a higher-priced, technically more challenging borehole program with higher overall likelihood of technical failure.

An alternative is to design the initial geothermal borehole demonstration project as a three-hole system (Fig. 4). A first stage would include two boreholes. Hole 1A would be a slimmer diameter hole to the top of the basement and a short distance into the basement, preferably 100–200 m, from which an extensive rock core would be extracted. Hole 1B would follow soon thereafter and be a borehole of wide enough diameter to potentially be used for well field extraction or injection and drilled to the intended project total depth, preferably 1–2 km into the crystalline basement. Hole 1A would serve as a dedicated exploratory/observation hole in which investigations would be undertaken to address uncertainties regarding hydrologic properties and conditions, thermal resource potential, coupled thermo–hydro–chemical–mechanical behavior, and chemical reactivity. These studies, complemented by geophysical and geologic investigations and modeling analysis, would provide important insights for designing subsequent production wells and help reduce risk for the project overall.

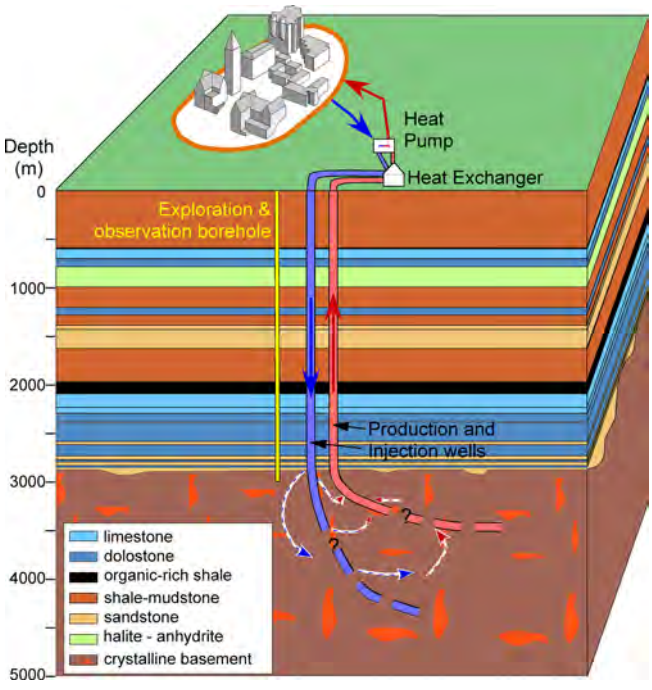

Figure 4. Schematic of the geology beneath Cornell and of the three boreholes recommended by the workshop exercise. An initial borehole is recommended as stage 1A (yellow well), which would be dedicated to collection of samples and data and later be transformed into a long-term observatory. Holes 1B and 2 are the other two wells illustrated. Those pilot demonstration wells would be of wider diameter, adequate for producing or injecting the large-volume flux needed for a successful geothermal heat project. Perturbations of the near-field subsurface by drilling, testing, stimulating, and producing the wide-diameter wells would be monitored by equipment installed in the smaller diameter borehole as well as by seismometers at the surface and in shallow boreholes.

In the short term, Hole 1A would be characterized with a battery of geophysical wireline logs to directly measure physical properties, characterize fractures, orient core, and indicate stress, and a vertical seismic profile to tie core and reflection seismic depths (Table 1). Prior to completion, quantitative measures of in situ liquid transmissivity and stress at successive depths are necessary to characterize the reservoir and assist in the assessment of seismic risk. During completion, Hole 1A would be equipped with fiber optic cables to allow for short- and long-term monitoring of the vertical profile of temperature and strain, with seismometers and with pressure sensors. Hole 1A would be available for subsequent geophysical investigations intended to assist

Table 1. Initial borehole logs, tests and samples recommended for Hole 1A and their purposes.

Borehole logs, tests, and samples	Categories and purposes (categories: 1 – hydrological assessment; 2 – thermal resource assessment; 3 – fracture stimulation/mechanical response and seismic risk; 4 – chemical/mineralogical reactivity; 5 – thermal/mineralogical history; 6 – microbiology)
Online gas monitoring	(1, 3) Indicate in near-real time the passage of drill bit into rock with different pore fluids or changed efficacy of fracture permeability
Wireline logs: caliper; natural gamma; neutron; density; electrical resistivity; sonic; borehole televiewer	(1, 3, 4) Document rock lithology, porosity and fluid distribution in rock, and differentiate fresh versus saline water, gas, and oil (3) Determine seismic wave velocity (1, 3) Locate and characterize fractures (3, 4) Document orientation of lithologic fabric (3) Document borehole breakouts to characterize stress orientation and maximum horizontal stress magnitude
Fracture tests at numerous depths	(1) Establish vertical profile of minimum compressive stress magnitudes. (3) Establish vertical profile of formation pore-pressure magnitudes.
Packer (flow) tests at target horizons	(1) Hydraulic transmissivity
Cuttings and coring (full diameter preferred at all depths)	(2, 3) Rock lithology, stratigraphic identification, unit thicknesses (3) Properties of mineralized fractures (1, 2, 3, 4) Laboratory measurements of physical properties for constraining stress determinations and models.
Fiber optic based Distributed Temperature, Strain rate, and Acoustic Sensing	(1, 2, 3) Identify fluid inflow/outflow zones, thermal recovery, and strain responses to drilling perturbation along full length borehole. (3) monitor hydrologic and strain response to subsequent operations
Wireline in situ fluid sampling	(4) In thick zones of enhanced permeability, obtain formation fluid sample
Fiber optic DTS	(1) Identify fluid inflow/outflow zones along full length borehole, characterize background temperature along borehole.
Fiber optic (DSS/DAS)	(3) Document strain responses to perturbations along full length borehole and monitor seismic wave field along full length borehole.
Core analyses refined	(1,2,4) Mineralogy; geochemistry; geomechanical and thermo-poroelastic properties; thermal conductivity, diffusivity, and heat capacity; access porewater samples; natural gamma; density; porosity; P-wave velocity; electrical resistivity (3) Fracture properties; structural fabric; mineral-filled fracture properties (5) Thermochronological analyses of progressive depths (5) Petrology and geochemistry (6) Characteristics of microbes in varying host rocks across range of temperatures
Analyze fluid samples	(4) Determine fluid chemistry, integrate viscosity and density into production models, begin to evaluate scaling (6) Characteristics of microbes in varying host rocks/fluids across range of temperatures and salinities
Install and monitor borehole seismometer	(3) Document background seismicity. Refine velocity models (for site seismic response model).
Hydraulic well tests	(1) Hydraulic properties of screened/open interval (e.g., transmissivity, permeability, specific storage) and thermal cycling (pump) tests

in planning for the production drilling and for longer-term monitoring of the disturbed rock mass.

By having a dedicated observation hole, borehole investigations (including and beyond those in Table 1) are possible which could provide broadly applicable scientific insights. For example, an understanding of the thermal and mineralogic history of deep geology within the region can be assessed, the deep microbiology can be sampled and evaluated, and the coupled thermo–hydro–chemical–mechanical processes associated with subsurface perturbations can be

monitored, analyzed, and compared with other geologic settings around the world.

A key part of the completion of Hole 1A will be maintaining, ideally for many years, some direct access to the reservoir to allow for direct sampling of fluids and the monitoring of pressures and productivity during the later production. The preliminary results from Hole 1A would be used to finalize the drilling plan for the first production-diameter Hole 1B.

The exploratory borehole would be designed to be vertical to facilitate testing and stratigraphic mapping. In contrast, the production demonstration borehole might intentionally deviate from vertical in order to optimally access the reservoir, or it might involve laterals.

Once both Holes 1A and 1B exist, inter-borehole communication of fluids, pressure, and temperature can be investigated. After formation tests and fracture tests are performed using one or both of these boreholes, the need for a stimulation plan to develop sufficient fracture permeability to maintain viable heat production would be re-evaluated and the detailed plan finalized and conducted. Then the second stage would begin, the drilling of another production Hole 2, planned to land within the zone of fractures stimulated from the 1B borehole.

Whichever borehole plan advances, it will be accompanied by monitoring of seismic activity using a local seismic array that has been operational since 2019 and that might be densified during drilling and testing. Furthermore, group discussions revealed that there is considerable value to complementing the borehole observations with advanced seismic probing of the area near the proposed geothermal well field. Seismic fracture mapping (Sicking and Malin, 2019) offers the possibility of independent documentation of the spatial variability of permeability in the rock volume, and a three-dimensional seismic reflection profile would enhance understanding and modeling of the shape of the sedimentary rock–basement interface, with its key mechanical role. Although these advanced seismic experiments might be conducted prior to drilling the first well, alternatively they could be conducted in the months between boring Holes 1A and 1B and therefore take advantage of newly available sonic velocity data from the borehole and of the potential to combine surface seismic nodes with instruments in Hole 1A.

The workshop led to an appreciation that the scientific value of subsurface studies would be greatly enhanced by including both the small diameter Hole 1A and demonstration project Hole 1B. The core scientific problems involve the behavior of a *volume* of rock: the coupled responses among stress, strain, mineralogy and chemistry of the rock-fluid system in the volume when perturbed. Given a single borehole as the initial experiment, the information derived from tests would inform us of a single vertical column of rock, whose horizontal dimension is limited to a few square meters. If instead there are two initial boreholes (1A, 1B), the logging data set and active tests will document the properties, conditions, and heterogeneity of a more representative rock volume.

Even more importantly, Hole 1A would be a relatively inexpensive investment to reduce subsequent risks during drilling of the more costly production holes. First, documentation of the temperature profile below Cornell would remove the uncertainty on existing temperature estimates (Fig. 2) which have been used as the basis for assessing the economic viability of a geothermal well field. Second, conducting much of the logging and coring in the comparatively slim hole would greatly reduce the risk of damage or borehole loss to the first demonstration well. Third, data and insight from an integrated package of samples and rock property logs and tests in Hole 1A would allow refinement of the drilling and casing plan for the primary, wide borehole (Hole 1B). Fourth, while formation tests and fracture tests are conducted in the broad diameter well, simultaneous observations in the observation Hole 1A would underpin better interpretations on which further major decisions (preparations for stage 2) will rely. In combination with geophysical data collected in paired borehole–surface experiments, the heterogeneity, vertically and horizontally, of the first two wells would lay the foundation for characterizing the anisotropy of rock, fractures and fluids prior to drilling the third well. This 3-D information would improve models of what will occur during stimulation and inform the design of a third borehole. Having a firm basis in advance for those models would improve the value of the exercise of model validation through comparison of fractures and fluids in the third borehole to the models and comparison of modeled stimulation to true stimulation data.

5.2 Unique properties of the proposed borehole(s) location

Counterintuitively, the lack of anything "special" about a central New York State borehole site is one of the most compelling attributes of this project. To date, scientific boreholes in continental crust have been selected to investigate active tectonic (e.g., Wenchuan Fault, Alpine Fault, San Andreas Fault, East African rift zone; Mori and Ellsworth, 2014) or volcanic systems (e.g., Iceland's Krafla volcano, Japan's Unzen volcano, the US's Yellowstone plume; Kukkonen and Fridleifsson, 2014), or very rare but large ancient cataclysmic events like meteorite impacts (e.g., Chicxulub, Chesapeake Bay; Koeberl and Claeys, 2014). Only the hydrocarbon industry, waste disposal industry, and mining industry drill several-kilometer boreholes into "normal" crust, and those wells focus on a commercial purpose with few or no opportunities for experiments to probe basic scientific questions. This leaves the Earth sciences community with large gaps in understanding of the "average" intraplate continental crust. Boring (drilling) and investigating a "boring" location is in fact novel.

The number of boreholes drilled for scientific purposes or used as holes of opportunity in "boring" older cratons re-

mains very small. That said, such boreholes, which include the Kola "superdeep" borehole in the former Soviet Union, the German KTB project, the Finnish Outokumpu drilling, and most recently the Swedish Scientific Drilling Program, have overturned many of the long-standing presumptions of the characteristics of the crust. Specific examples of breakthroughs include the topics of the existence of fluids (e.g., Lodemann et al., 1997; Smithson et al., 2000), fluid chemistry (e.g., Kietäväinen et al., 2013), gas compositions (e.g., Wiersberg et al., 2020) and seismic characterization (e.g., Simon et al., 2017; Schijns et al., 2012). The Swedish program completed two boreholes, COSC-1 to nearly 2500 m depth in late 2014 and COSC-2 to 2276 m in 2020. Although the scientific goals of the Swedish boreholes differ, their experiences will be invaluable in planning and deploying Hole 1A.

A 2014 summary of completed ICDP projects (de Wit, 2014) illuminated that the proposed Cornell borehole, planned to traverse Devonian through Cambrian strata and continue well into rocks that achieved their mid- to high-grade metamorphic status 1000–1350 Ma, also targets an interval of Earth history that has been ignored in all but two ICDP boreholes.

Cornell University is committed to broad and rapid public dissemination of all data extracted from the borehole. Rather than the development of tools or methods hoped to provide industrial and business advantages, as might be common in some boreholes with experimental activities, the university's intent is that the borehole activities and data be widely disseminated. The workshop served as the initial opportunity to consider some models for archiving and distributing samples and data, such as the usual procedures recommended by ICDP and IODP.

Furthermore, the willingness of Cornell to host a scientific borehole at the initiation of the large-scale geothermal energy experiment provides the opportunity for characterization and monitoring of the natural, unperturbed subsurface state over a large depth range and then to continuously measure natural and human-perturbed changes over time. If appropriately designed and installed, the proposed Cornell borehole set would measure field-scale characteristics, and its findings can be integrated with what is learned in mesoscale underground laboratories that enable and host long-term monitoring, such as the Sanford Underground Research Facility (South Dakota, USA) and Bedretto Underground Laboratory (southern Switzerland).

5.3 The natural organization of scientific themes into an integrated borehole program

The workshop participants focused largely on research themes that related to Earth's internal dynamic activities, a major emphasis for the ICDP program. Three major themes are tightly connected: fluids and elemental cycling, seismicity across a range of length scales, and controlling subsurface fractures and fluid flow. These themes would likely be at the heart of a project that is well positioned to garner sufficient funds to carry out a deep borehole program. Two other major themes, of deep life and of the thermal–chemical–mineralogical evolution from Proterozoic through Phanerozoic times, excited many participants. While it is perceived that these two themes are unlikely to independently attract sufficient funds to drill a borehole, the workshop group welcomed the beneficial knowledge of deep life and deep history that can be extracted from samples and conditions at a borehole.

5.3.1 Fluid cycling, fractures, seismicity, and working constructively with the subsurface to harness geothermal energy

In low-porosity sedimentary rocks and in mid- to high-grade metamorphic rocks, what is the natural state of fluid cycling and of fractures, and how would the extent and variability of fractures determine the fluid flow through fracture permeability if the system is intentionally perturbed? How do perturbations transmitted across long distances act to either restrain or cause induced earthquakes? How close to critical failure are various parts of the deep strata and the crystalline basement?

A Cornell scientific borehole project has the potential to address all of these fundamental questions regarding the stress response of low-porosity sedimentary rocks, metamorphic rocks, and their fracture systems to pressure perturbations near the interface of strata with the basement. To test the hypothesis that continental crust is everywhere critically stressed (Zoback and Gorelick, 2012), a borehole experiment should document stress, fracture, and hydrological conditions through a vertically extensive volume that transects varying rock types, and the experiment should monitor strain and flow responses to imposed perturbations (Table 1, categories 1–4). That information can be a foundation for better understanding natural intraplate earthquakes across a range of scales and induced seismicity. A Cornell scientific borehole project also has the potential to greatly reduce uncertainty on coupled thermal–hydraulic models, to guide reservoir stimulation, and to underpin a risk mitigation strategy. For heat extraction and reservoir stimulation, are there characteristic sets of fracture properties and variable responses of fractures in varying lithologies, which should influence a design to establish efficient distributed fluid flow through fracture permeability? For risk-management design, is the hypothesis that the risk of inducing felt earthquakes would decrease if a slightly under-pressured reservoir condition is created by pumping consistent with the rock-fluid-stress system? The workshop focused on how to achieve both scientific and pragmatic goals which share a mechanical–thermal–hydrological–chemical system.

Analyses of induced earthquakes over the last decade have illuminated major uncertainties about rock response to stress and fluid flow near the interface between sedimentary rocks

and their crystalline basement. Fluid pressure changes can influence the stress state and failure of rocks through the direct influence of pore pressure and through poroelastic strain effects. Using a global data set of seismic events around single injection wells and their spatial and temporal patterns, Goebel and Brodsky (2018) deduced that these seismic events reflect both induced pore-pressure changes and poroelastic coupling of the rock framework and that the contributions of those two phenomena differ between the cases of injection into "soft" sedimentary rocks compared to crystalline basement rocks. For injection into crystalline basement rocks, the detected fracture slip fits the prediction that the slip results from stress perturbation across faults close to failure that are in direct communication with fluid migration. On the other hand, injection into sedimentary rocks generated not only seismic events due to that direct pore-pressure effect, but also a much wider and longer-lasting field of slipping fractures that reflected the poroelastic response of the stress field within both the sedimentary units and underlying basement. Furthermore, Goebel and Brodsky (2018) attribute the distinction between sedimentary and basement rock behavior to the bulk elasticity, and they relate the different elasticity to porosity, which is generally higher for sedimentary than crystalline basement rocks. It is an open question whether all sedimentary rocks are essentially equal in this behavior or whether low-permeability rocks like those of an old, deeply buried sedimentary basin would transmit stress and fluids differently than more porous strata. Goebel and Brodsky (2018) consider the permeability differences to be of second-order importance, although indeed permeability influences the spatial extent reached by injected fluid. Studies such as those conducted by the National Research Council (2013) emphasize the role of faults and fractures as avenues for fluid flow, and even mineral-filled fractures of certain compositions (e.g., clays) are credited with efficient transmission of pore fluid pressure (Gray, 2017).

The potential that the sedimentary rock–crystalline basement interface region plays a non-linear role in the coupling of stress, fluids, strain and earthquakes led the ICDP-sponsored workshop participants to prioritize extensive sampling and testing in the deeper sector of the strata and the upper hundred meters of the basement.

5.3.2 The ubiquitous hidden biosphere

The deep biosphere remains little known, though it is anticipated that it participates in the natural cycles of elements (Pedersen, 2000). Limits to life may be dictated by high temperature, nutrient scarcity, high pressure, and/or extreme salinity, all of which are probable in a Cornell-located borehole. Even if the absolute limit of life has not been crossed in the rocks near the bottom of the proposed borehole, the energy available to maintain life will likely be extraordinarily limited and of uncertain origin, with possibilities inclusive of the solid organic matter in rock, chemical reactions, seismic processes and radioactive decay (Lever et al., 2015). To date, the deepest documented microbes have been found deeper than 3 km and at temperatures up to about 100 °C (Magnabosco et al., 2018). Whereas the known temperature range of life spans −40 to 122 °C (Takai et al., 2008), microbiologists anticipate that basic constituents of life, like RNA and amino acids, fail at high temperatures (Lever et al., 2015) and hence expect that temperature will determine one of the limits of life. The proposed borehole will intercept rocks below 2 km depth and will access rock temperatures around 100 °C and possibly higher, with extremely saline brines in the pores of the sedimentary rocks and unknown pore fluid compositions in the basement rocks. These gradients and properties create the opportunity to investigate the nature of microbes across a temperature gradient for which microbial activities and characteristics are hypothesized to decline and change (Table 1, category 6). If there is a pore fluid change near the sedimentary rock to basement contact, there may be major consequences for the microbial population.

Furthermore, studies to date indicate that deep microbial life could prove to be sensitive to the mineral substrate in the compositionally variable subsurface of the proposed borehole region. A review of the literature reveals functional roles for Fe- and S-bearing minerals and some clays yet also suggests that other clays and the abundant mineral-forming element aluminum inhibit some microbial species (Röling et al., 2015). The petrologically diverse sedimentary rocks to be traversed by the proposed borehole could enable examination of the microbial populations as functions of mineralogy, including strong contrasts of the limestone and dolomite intervals to the host minerals in other borehole sites whose microbiology has been examined, such as oceanic basalts (Salas et al., 2015) and granite (Swanner and Templeton, 2011). A central New York borehole also has a good likelihood of intersecting marble in the basement. Those marbles, whose pressure and temperature history and perhaps pore fluids differ markedly from the diagenetic conditions of the carbonates in the deep sedimentary units, may provide a useful opportunity to investigate contrasts between the microbial communities of sedimentary and metamorphic carbonate rocks. Despite the lack of participation in the workshop by any experts in deep microbial life, samples from this borehole could be the foundation for research to develop and test widely applicable hypotheses.

5.3.3 Tectonics and thermal history near a boundary between major Precambrian tectonic domains

Ithaca, New York, lies near the projected position of a Proterozoic tectonic domain boundary and in the heart of a region of prolific Mesozoic kimberlite dikes. Either attribute alone is a worthy point of departure for hypotheses concerning how today's heat flow evolved from the starting point of Proterozoic or Juro-Cretaceous tectonic activity.

A Mesoproterozoic crustal-scale shear zone separates much different metamorphic domains and passes from exposed (in the Adirondack Mountains) to buried (beneath the Appalachian Basin) and has been proposed to pass a short distance west of Ithaca (Fig. 1) or under Ithaca. In the Adirondacks, the boundary is wider than 20 km, characterized by high finite strain in ductile shear under granulite conditions (Valentino et al., 2019). The shear zone separates rocks of distinctive lithologies and ages, with the core of the Grenville orogenic belt to the north and west, and granitic composition rocks in the shear zone are geochemically of a magmatic arc origin. Valentino et al. (2019) interpret the shear zone to have formed by the collision of plates around the margins of the Laurentian continental block. If the shear zone extrapolation through the region near Ithaca were correct, then granulite metamorphic-grade meta-igneous rocks (anorthosite–mangerite–charnockite–granite) with scraps of dismembered metasedimentary rocks may be likely northwest or west of Ithaca, whereas granulite-grade tonalitic gneisses and complex metasedimentary rocks may be expected in Ithaca as well as in the south and east. Borehole samples would enable investigation of compositions, geochemistry, and geochronology with which to test the hypothesis that a terrane boundary separates Ithaca from the main Grenville orogenic core.

Kimberlite dikes are so abundant (Kay et al., 1983; Bailey et al., 2017) in north-trending fractures in the Ithaca region that there is a high probability of encountering one or more dikes in a 4 km long borehole, especially if it is deviated from vertical. If so, xenoliths and xenocrysts will provide evidence of the composition of the crustal rock through which the kimberlite arose, and populations of kimberlite xenoliths and xenocrysts collected deep in a borehole will be less diluted by the column of sedimentary rocks than are kimberlite samples studied to date. Crustal materials in the kimberlites may enable a better interpretation of the local gravity and magnetic anomalies and in turn may provide insight into the spatial heterogeneity of crustal composition. Many questions remain about the cause of the abundant kimberlites. Geochemical and thermobarometric studies of kimberlite samples should provide evidence about the magma source(s), some 150 km deep in the mantle (Kay et al., 1983). These early Cretaceous high-velocity intrusions reflect a history of paleo-strain. Can the variability of locations of kimberlites and their xenolith compositions illuminate the variability of strain responses among the various types of basement lithologies?

Shorten and Fitzgerald (2019) demonstrated that a transition occurred approximately 145 Ma from a long interval of rapid exhumation and cooling to conditions of slow exhumation and cooling. This inflection is approximately coeval with kimberlite intrusions in the earliest Cretaceous. An integrated thermochronological study of a vertical profile of borehole materials (Table 1, category 5), including kimberlites at one or more depth, offers the possibility of exploring the modern retention of low-temperature features across the modern-geothermal gradient and the opportunity to examine the post-emplacement thermal history of kimberlites where they have not been exposed to near-surface weathering.

5.3.4 Summary of scientific themes

All of these research themes are interconnected. For example, fractures and fluid migration are related to the mechanical and lithological heterogeneity that was instituted by both Precambrian orogenic activity and Phanerozoic structural adjustments to near-field and far-field phenomena. Integrated borehole measurements and experiments will reveal how the preexisting mechanical and lithological heterogeneity controls and interacts with stress and about the nature of active processes that link thermal, hydrological, and chemical processes to mechanics and to one another. Even the amount and nature of life in the deep strata and crystalline basement are likely to be linked to Precambrian–Paleozoic conditions which produced the substrate in which today's life exists and to the thermo–hydro–chemical–mechanical system which is their modern environment.

6 Conclusions

The ICDP-supported borehole planning workshop held during January 2020 in Ithaca, New York, USA, was an efficient and effective forum through which to advance the strategy for and design of a scientific borehole in continental crust. The workshop participants transformed a skeletal idea – an opportunity to utilize a proposed geothermal demonstration borehole for scientific research – into a much better developed scientific vision and the beginning of a pragmatic scientific and engineering plan. The diverse experiences and deep expertise of the workshop participants included specializations ranging from regional geology to experimental rock mechanics to geothermal borehole engineering to fracture stimulation to hydrogeology to earthquake seismology, and beyond. Collectively, this group honed a plan suitable to the northern Appalachian Basin which will illuminate how the pre-existing mechanical and lithological heterogeneity controls and interacts with stress. The discussions led to a conviction that the planned geothermal demonstration project can better encourage wide deployment of low-temperature geothermal energy technology, one of Cornell's goals, by utilizing scientific borehole studies to deepen understanding of rock behavior in the deep subsurface before and during well-field operations.

The borehole science plan that evolved (Table 1) will be costly. Ultimately, as the Cornell University drilling plan unfolds in the next few years, its features will be constrained by the details of costs, by the funds available from sources such as scientific consortia, government agencies and donors, and by initial results. A proposal to the U.S. Department of Energy that was submitted after the workshop was selected

to be funded, hence Hole 1A is now in the planning phase with a drilling target of 2021. Beyond Cornell's research and geothermal demonstration plans, there will be lasting value if the essence of the integrated plan to advance understanding of thermal–hydrological–mechanical–chemical behavior of old continental crust is used by other groups at different locations.

Data availability. No data sets were used in this article.

Team list. Teresa Jordan (Cornell University, USA), Patrick Fulton (Cornell University, USA), Jefferson Tester (Cornell University, USA), David Bruhn (Technical University Delft, the Netherlands/GFZ, Germany), Hiroshi Asanuma (National Institute of Advanced Industrial Sciences and Technology, Japan), Noriyoshi Tsuchiya (Tohoku University, Japan), Shigemi Naganawa (Akita University, Japan), Frederic Guinot (From Bottom to Top SàRL, Geneva, Switzerland), Hannes Hofman (GFZ Potsdam, Germany), Thomas Neumann (Technical University Berlin, Germany), Phil Vardon (TU Delft, the Netherlands), Ulrich Harms (ICDP/GFZ, Potsdam, German), Xiaodong Ma (ETH Zurich, Switzerland), Kazuya Ishitsuka (Kyoto University, Japan), Fuqiong Huang (China Earthquake Networks Center, China), Anders Noren (Continental Scientific Drilling Coordination Office, University of Minnesota, USA), Tom Pasquini (Kingwood, Texas, USA), Dorivaldo Santos (Pennsylvania State University, USA), Jared Smith (University of Virginia, USA), Trenton Cladouhos (Cyrq Energy Inc., USA), Joseph Moore (University of Utah, USA), Andy Barbour (U.S. Geological Survey, USA), Thomas Goebel (University of Memphis, USA), Nicholas Davatzes (Temple University, USA), Stephen E. Laubach (University of Texas at Austin, USA), Douglas Schmitt (Purdue University, USA), Chaoyi Wang (Purdue University, USA), David W. Valentino (State University of New York at Oswego, USA), Jeffrey R. Chiarenzelli (St. Lawrence University, USA), Brian Slater (New York State Museum, USA), Derek Elsworth (Pennsylvania State University, USA), Srisharan Shreedharan (Pennsylvania State University, USA), Suzanne Baldwin (Syracuse University, USA), Paul Fitzgerald (Syracuse University, USA), David M. Jenkins (Binghamton University USA), Natalia Zakharova (Central Michigan University, USA), Tieyuan Zhu (Pennsylvania State University, USA), Robert R. Bland (Cornell University, USA), Rick Burgess (Cornell University, USA), Larry Brown (Cornell University, USA), Matthew Pritchard (Cornell University, USA), Richard Allmendinger (Cornell University, USA), J. Olaf Gustafson (Cornell University, USA), Steve Beyers (Cornell University, USA), Sriramya Nair (Cornell University, USA), Greg McLaskey (Cornell University, USA), Greeshma Gadikota (Cornell University, USA), Suzanne M. Kay (Cornell University, USA), Frank Horowitz (Cornell University, USA), Anthony R. Ingraffea (Cornell University, USA), Nicolas Rangel Jurado (Cornell University, USA), Muawia Barazangi (Cornell University, USA), Jacob Simon (Cornell University, USA), Ivanakbar Purwamaska (Cornell University, USA), Jacob Paul (Cornell University, USA), Karin Olson Hoal (Cornell University, USA), David Hysell (Cornell University, USA), Lynden A. Archer (Cornell University, USA), and Larry Cathles (Cornell University, USA).

Author contributions. TJ, UH and CW framed the paper and wrote initial text at the conclusion of the workshop. TJ, PF and JT completed the initial draft. DB, HA, DS, PJV, HH, TP, and JS made substantial suggestions and additions that led to the finalized manuscript. TJ prepared the illustrations.

Competing interests. All but one author declares they have no conflict of interest. Ulrich Harms is the Executive Secretary and Head of Operational Support Group for the ICDP, one of the parent organizations of *Scientific Drilling*.

Acknowledgements. The workshop organizers and participants greatly appreciated the ICDP's support and guidance. We appreciate greatly the support of the Cornell University Departments of Chemical and Biomolecular Engineering and of Earth and Atmospheric Sciences in the form of extensive organizational efforts by staff professionals Polly Marion and Carolyn Headlam and the participation of Lance Collins, Dean of Engineering. We thank the New York State Museum, Cyrq Energy, Inc., U.S. Geological Survey and U.S. Department of Energy, which each supported the participation by an individual, and New York State Museum for the loan of core. Koenraad Beckers is thanked for correspondence and data regarding Europe and Russia's energy utilization. John Shervais and John Eichelberger are thanked for their comments on an earlier draft of this paper.

Financial support. This research has been supported by the International Continental Scientific Drilling Program (grant no. 11-2019).

Review statement. This paper was edited by Tomoaki Morishita and reviewed by John Eichelberger and John Shervais.

References

Al Aswad, J. A.: A Stratigraphic and Petrophysical Study of In-situ Geothermal Reservoir Quality of the Cambro-Ordovician Strata in the Subsurface at Cornell University, Ithaca, New York, MS Thesis, Ithaca, New York, USA, 1–172, 2019.

Bailey, D. G. and Lupulescu, M. V.: Spatial, temporal, mineralogical, and compositional variations in Mesozoic kimberlitic magmatism in New York State, Lithos, 212, 298–310, 2015.

Bailey, D. G., Lupulescu, M. V., and Chiarenzelli, J. R.: Kimberlites in the Cayuga Lake region of central New York: The Six Mile Creek, Williams Brook, and Taughannock Creek dikes, in: New York Geological Association 89th Annual Meeting Field Trip Guidebook, edited by: Muller, O. H., Alfred University, Alfred, New York, USA, 160–190, 2017.

Basu, A. R., Rubury, E., Mehnert, H., and Tatsumoto, M.: Sm-Nd, K-Ar and petrologic study of some kimberlites from eastern United States and their implication for mantle evolution, Contrib. Mineral. Petr., 86, 35–44, 1984.

Blondes, M. S., Gans, K. D., Engle, M. A., Kharaka, Y. K., Reidy, M. E., Saraswathula, V., Thordsen, J. J., Rowan, E. L., and Mor-

rissey, E. A.: US Geological Survey National Produced Waters Geochemical Database v2. 3 (PROVISIONAL), US Geological Survey: US Geological Survey, Eastern Energy Resources Science Center, Reston, VA, USA, available at: https://eerscmap.usgs.gov/pwapp/ (last access: 23 October 2019), 2017.

Camp, E. and Jordan, T.: Feasibility study of repurposing Trenton–Black River gas fields for geothermal heat extraction, southern New York, Geosphere, 13, GES01230-1-14, https://doi.org/10.1130/GES01230.1, 2016.

Camp, E. R., Jordan, T. E., Hornbach, M. J., and Whealton, C. A.: A probabilistic application of oil and gas data for exploration stage geothermal reservoir assessment in the Appalachian Basin, Geothermics, 71, 187–199, https://doi.org/10.1016/j.geothermics.2017.09.001, 2018.

Chiarenzelli, J. R. and Valentino, D. W.: Exposed basement rock and geophysical trends in New York State: poster presentation at ICDP Workshop at Cornell University, 8–9 January 2020, Ithaca, New York, USA, 2020.

Chiarenzelli, J., Valentino, D., Lupulescu, M., Thern, E., and Johnston, S.: Differentiating Shawinigan and Ottawan orogenesis in the central Adirondacks, Geosphere, 7, 2–22, 2011.

de Wit, M.: The science plan – preamble, in: Unravelling the Workings of Planet Earth, Science Plan for 2014–2019, edited by: Horsfield, B., Knebel, C., Ludden, J., and Hyndman, R., International Continental Scientific Drilling Program, Potsdam, Germany, 18–22, 2014.

Dillinger, A., Ricard, L. P., Huddlestone-Holmes, C., and Esteban, L.: Impact of diagenesis on reservoir quality in a sedimentary geothermal play: a case study in the Cooper Basin, South Australia, Basin Res., 26, 252–272, 2016.

EIA: State energy data systems (SEDS): 1960–2016 (complete), U.S. Energy Information Administration, available at: https://www.eia.gov/state/seds/ (last access: 20 November 2020), 2018a.

EIA: 2015 Residential energy consumption survey (RECS), U.S. Energy Information Administration, available at: https://www.eia.gov/consumption/residential/data/2015 (last access: 20 November 2020), 2018b.

EIA: 2012, Commercial buildings energy consumption survey (CBECS), U.S. Energy Information Administration, available at: https://www.eia.gov/consumption/commercial/data/2012 (last access: 20 November 2020), 2019.

Frape, S. K., Fritz, P., and McNutt, R. H. T.: Water-rock interaction and chemistry of groundwaters from the Canadian Shield, Geochim. Cosmochim. Ac., 48, 1617–1627, 1984.

Goebel, T. H. W. and Brodsky, E. E.: The spatial footprint of injection wells in a global compilation of induced earthquake sequences, Science, 361, 899–904, 2018.

Gray, I.: Effective stress in rock, Proceedings of the Eighth International Conference on Deep and High Stress Mining, 28–30 March 2017, Perth, Australia, edited by: Wesseloo, J., 199–207, 2017.

Heaman, L. M. and Kjarsgaard, B. A.: Timing of eastern North American kimberlite magmatism: continental extension of the Great Meteor hotspot track, Earth Planet. Sci. Lett., 178, 253–268, 2000.

Heizler, M. T. and Harrison, T. M.: The thermal history of the New York basement determined from $^{40}Ar/^{39}Ar$ K-feldspar studies, J. Geophys. Res.-Sol. Ea., 103, 29795–29814, 1998.

Horowitz, F. G., Ebinger, C., and Jordan, T. E.: Identifying faults Associated with the 2001 Avoca induced (?) seismicity sequence of western New York State using potential field wavelets, AGU Fall Meeting Abstracts, 11–15 December 2017, New Orleans, Louisiana, USA, S23C-0835, 2017.

Houston, S., Smalley, C., Laycock, A., and Yardley, B. W. D.: The relative importance of buffering and brine inputs in controlling the abundance of Na and Ca in sedimentary formation waters, Mar. Petrol. Geol., 28, 1242–1251, 2011.

Jacobi, R. D.: Basement faults and seismicity in the Appalachian Basin of New York State, Tectonophysics, 353, 75–113, 2002.

Jordan, T.: Geological evaluation of subsurface features near Ithaca, NY: interpretations of seismic reflection profiles collected by the petroleum industry, eCommons, 1–44, available at: https://ecommons.cornell.edu/handle/1813/69546 (last access: 20 November 2020), 2019.

Kay, S. M., Snedden, W. T., Foster, B. P., and Kay, R. W.: Upper mantle and crustal fragments in the Ithaca kimberlites, J. Geol., 91, 277–290, 1983.

Kietäväinen, R., Ahonen, L., Kukkonen, I. T., Hendriksson, N., Nyyssönen, M., and Itävaara, M.: Characterisation and isotopic evolution of saline waters of the Outokumpu Deep Drill Hole, Finland–Implications for water origin and deep terrestrial biosphere, Appl. Geochem., 32, 37–51, 2013.

Koeberl, C. and Claeys, P.: Cataclysmic events – Impact craters and processes, in: Unravelling the Workings of Planet Earth, Science Plan for 2014–2019, edited by: Horsfield, B., Knebel, C., Ludden, J., and Hyndman, R., International Continental Scientific Drilling Program, Potsdam, Germany, 66–73, 2014.

Kukkonen, I. T. and Fridleifsson, G. O.: Heat and Mass Transfer, in: Unravelling the Workings of Planet Earth, Science Plan for 2014–2019, edited by: Horsfield, B., Knebel, C., Ludden, J., and Hyndman, R., International Continental Scientific Drilling Program, Potsdam, Germany, 42–55, 2014.

Kummu, M. and Varis, O.: The world by latitudes: A global analysis of human population, development level and environment across the north–south axis over the past half century, Appl. Geogr., 31, 495–507, 2011.

Le Brun, M., Hamm, V., Lopez, S., Ungemach, P., Antics, M., Aussear, J. Y., Cordier, E. Giuglaris, E., Goblet, P., and Lalos, P.: Hydraulic and thermal impact modeling at the scale of the geothermal heating doublet in the Paris Basin, France, Geothermal Reservoir Engineering, Thirty-Sixth Workshop, 31 January–2 February 2011, Stanford, CA, USA, SGP-TR-191, 1–14, 2011.

Lever, M. A., Rogers, K. L., Lloyd, K. G., Overmann, J., Schink, B., Thauer, R. K., Hoehler, T. M., and Jørgensen, B. B.: Life under extreme energy limitation: a synthesis of laboratory-and field-based investigations, FEMS Microbiol. Rev., 39, 688–728, 2015.

Limberger, J., Boxem, T., Pluymaekers, M., Bruhn, D., Manzella, A., Calcagno, P., Beekman, F., Cloetingh, S., and van Wees, J.-D.: Geothermal energy in deep aquifers: A global assessment of the resource base for direct heat utilization, Renew. Sust. Energ. Rev., 82, 961–975, 2018.

Lodemann, M., Fritz, P., Wolf, M., Ivanovich, M., Hansen, B. T., and Nolte, E.: On the origin of saline fluids in the KTB (continental deep drilling project of Germany), Appl. Geochem., 12, 831–849, 1997.

Lugert, C., Smith, L., Nyahay, R., Bauer, S., and Ehgartner, B.: Systematic technical innovations initiative for brine disposal in the northeast, New York State Energy Research and Development Authority Contract Number 6940, Albany, NY, USA, 1–269, 2006.

Lynch, R. S. and Castor, T. P.: Auburn Low-Temperature Geothermal Well, Final Report: NYSERDA Report 84-18, Albany, NY, USA, 1–277, 1983.

Magnabosco, C., Lin, L.-H., Dong, H., Bomberg, M., Ghiorse, W., Stan-Lotter, H., Pedersen, K., Kieft, T. L., van Heerden, E., and Onstott, T. C.: The biomass and biodiversity of the continental subsurface, Nat. Geosci., 11, 707–717, 2018.

Martin, J.: Carbon sequestration feasibility study in the Chautauqua County, New York area, New York State Energy Research and Development Authority 10498, Albany, NY, USA, 1–424, 2011.

McCabe, K., Gleason, M., Reber, T., and Young, K. R.: Characterizing U.S. heat demand for potential application of geothermal direct use, Proceedings 40th GRC Annual Meeting, 23–26 October 2016, Sacramento, CA, USA, 1–22, available at: https://www.nrel.gov/docs/fy17osti/66460.pdf (last access: 20 November 2020), 2016.

McLelland, J. M., Selleck, B. W., and Bickford, M. E.: Review of the Proterozoic evolution of the Grenville Province, its Adirondack outlier, and the Mesoproterozoic inliers of the Appalachians, in: From Rodinia to Pangea: The Lithotectonic Record of the Appalachian Region, edited by: Karabinos, P. M., Hibbard, J. P., Bartholomew, M. J., and Tollo, R. P., Geological Society of America Memoir 206, Boulder, Colorado USA, 1–29, 2010.

Miller, D. S. and Duddy, I. R.: Early Cretaceous uplift and erosion of the northern Appalachian Basin, New York, based on apatite fission track analysis, Earth Planet. Sc. Lett., 93, 35–49, 1989.

Mori, J. and Ellsworth, W.: Active Faults and Earthquakes, in: Unravelling the Workings of Planet Earth, Science Plan for 2014–2019, edited by: Horsfield, B., Knebel, C., Ludden, J., and Hyndman, R., International Continental Scientific Drilling Program, Potsdam, Germany, 24–31, 2014.

National Research Council: Induced seismicity potential in energy technologies, U.S. National Academies Press, Washington, DC, USA, https://doi.org/10.17226/13355, 2013.

NYSERDA: New York State Greenhouse Gas Inventory: 1990–2016, Final Report, New York State Energy Research and Development Authority, Albany, NY, USA, available at: https://www.nyserda.ny.gov/About/Publications/EA-Reports-and-Studies/Energy-Statistics (last access: 20 November 2020), 2019.

Pedersen, K.: Exploration of deep intraterrestrial microbial life: current perspectives, FEMS Microbiol. Lett., 185, 9–16, 2000.

Roden, M. K. and Miller, D. S.: Apatite fission-track thermochronology of the Pennsylvania Appalachian Basin, Geomorphology, 2, 39–51, 1989.

Röling, W. F. M., Aerts, J. W., Patty, C. H. L., Ten Kate, I. L., Ehrenfreund, P., and Direito, S. O. L.: The significance of microbe-mineral-biomarker interactions in the detection of life on Mars and beyond, Astrobiology, 15, 492–507, 2015.

Salas, E. C., Bhartia, R., Anderson, L., Hug, W. F., Reid, R. D., Iturrino, G., and Edwards, K. J.: In situ detection of microbial life in the deep biosphere in igneous ocean crust, Front. Microbiol., 6, 1260, https://doi.org/10.3389/fmicb.2015.01260, 2015.

Schijns, H., Schmitt, D. R., Keikkinen, P. J., and Kukkonen, I. T.: Seismic anisotropy in the crystalline upper crust: observations and modelling from the Outokumpu scientific borehole, Finland, Geophys. J. Int., 189, 541–553, 2012.

Shorten, C. M. and Fitzgerald, P. G.: Post-orogenic thermal history and exhumation of the northern Appalachian Basin: Low-temperature thermochronologic constraints, Basin Res., 31, 1017–1039, 2019.

Sicking, C. and Malin, P.: Fracture Seismic: mapping subsurface connectivity, Geosciences, 9, 1–35, 2019.

Simon, H., Buske, S., Krauss, F., Giese, R., Hedin, P., and Juhlin, C.: The derivation of an anisotropic velocity model from a combined surface and borehole seismic survey in crystalline environment at the COSC-1 borehole, central Sweden, Geophys. J. Int., 210, 1332–1346, 2017.

Smith, J. D.: Exploratory spatial data analysis and uncertainty propagation for geothermal resource assessment and reservoir models, PhD Thesis, Cornell University, Ithaca, NY, USA, 1–255, 2019.

Smith, L. B.: Origin and reservoir characteristics of Upper Ordovician Trenton-Black River hydrothermal dolomite reservoirs in New York, AAPG Bull., 90, 1691–1718, https://doi.org/10.1306/04260605078, 2006.

Smith, L., Lugert, C., Bauer, S., Ehgartner, B., and Nyahay, R.: Final Report: Systematic Technical Innovations Initiative Brine Disposal in the Northeast, National Energy Technology Lab (DOE) DE-FC26-01NT41298, Albany, New York, USA, 2005.

Smithson, S. B., Wenzel, F., Ganchin, Y. V., and Morozov, I. B.: Seismic results at Kola and KTB deep scientific boreholes: velocities, reflections, fluids, and crustal composition, Tectonophysics, 329, 301–317, 2000.

Swanner, E. and Templeton, A.: Potential for nitrogen fixation and nitrification in the granite-hosted subsurface at Henderson Mine, CO, Front. Microbiol., 2, 254, https://doi.org/10.3389/fmicb.2011.00254, 2011.

Takai, K., Nakamura, K., Toki, T., Tsunogai, U., Miyazaki, M., Miyazaki, J., Hirayama, H., Nakagawa, S., Nunoura, T., and Horikoshi, K.: Cell proliferation at 122C and isotopically heavy CH_4 production by a hyperthermophilic methanogen under high-pressure cultivation, P. Natl. Acad. Sci. USA, 105, 10949–10954, 2008.

USGS Earthquake Catalog: https://tinyurl.com/yyewvgax, last access: 20 November 2020.

Valentino, D. W. and Chiarenzelli, J. R.: The Piseco Lake Shear Zone: a Shawinigan cryptic suture in the southern Adirondack Mountains, New York, New York State Geological Association, Castleton, Vermont, USA, 90, 139–156, 2018.

Valentino, D. W., Chiarenzelli, J. R., Piaschyk, D., Williams, L., and Peterson, R.: The southern Adirondack sinistral transpressive shear system, Friends of the Grenville Field Trip, Indian Lake, New York, USA, 1–56, 2008.

Valentino, D. W., Valentino, J. D., Chiarenzelli, J. R., and Inclima, R. W.: Faults and Fracture Systems in the Basement Rocks of the Adirondack Mountains, New York, Adirondack Journal of Environmental Studies, 20, 101–117, 2016.

Valentino, D. W., Chiarenzelli, J. R., and Regan, S. P.: Spatial and temporal links between Shawinigan accretionary orogenesis and massif anorthosite intrusion, southern Grenville province, New York, USA, J. Geodynam., 129, 80–97, 2019.

Vardon, P., Bruhn, D., Steiginga, A., Cox, B., Abels, H., Barnhoorn, A., Drijkoningen, G., Slob, E., and Wapenaar, K.: A Geothermal Well Doublet for Research and Heat Supply of the TU Delft Campus, arXiv [preprint], arXiv:2003.11826, 26 March 2020.

Waller, R. M., Turk, J. T., and Dingman, R. J.: Potential effects of deep-well waste disposal in Western New York, US Geol. Surv. Professional Paper 1053, Washington, DC, USA, 1–39, 1978.

Wiener, R. W. and Isachsen, Y. W.: Detailed studies of selected, well-exposed fracture zones in the Adirondack Mountains dome, New York, New York State Geological Survey, Albany, NY, USA, 1–92, 1987.

Wiersberg, T., Pierdominici, S., Lorenz, H., Almqvist, B., Klonowska, I., and C.O.S.C.S. Team: Identification of gas inflow zones in the COSC-1 borehole (Jamtland, central Sweden) by drilling mud gas monitoring, downhole geophysical logging and drill core analysis, Appl. Geochem., 114, 104513, https://doi.org/10.1016/j.apgeochem.2019.104513, 2020.

Wright, P. M. and Culver, G.: Nature of Geothermal Resources, in: Geothermal Direct Use Engineering and Design Guidebook, edited by: Lienau, P. J. and Lunis, B. C., U. S. Department of Energy Idaho Operations Office, Idaho Falls, Idaho, USA, 23–50, available at: https://inis.iaea.org/collection/NCLCollectionStore/_Public/23/044/23044859.pdf (last access: 20 November 2020), 1991.

Zoback, M. D. and Gorelick, S. M.: Earthquake triggering and large-scale geologic storage of carbon dioxide, P. Natl. Acad. Sci. USA, 109, 10164–10168, 2012.

Sci. Dril., 28, 93–112, 2020
https://doi.org/10.5194/sd-28-93-2020

Scientific Drilling
Open Access

Report on ICDP Deep Dust workshops: probing continental climate of the late Paleozoic icehouse–greenhouse transition and beyond

Gerilyn S. Soreghan[1], Laurent Beccaletto[2], Kathleen C. Benison[3], Sylvie Bourquin[4], Georg Feulner[5], Natsuko Hamamura[6], Michael Hamilton[7], Nicholas G. Heavens[8], Linda Hinnov[9], Adam Huttenlocker[10], Cindy Looy[11], Lily S. Pfeifer[1], Stephane Pochat[12], Mehrdad Sardar Abadi[1], James Zambito[13], and the Deep Dust workshop participants✚

[1]School of Geosciences, University of Oklahoma, Norman, Oklahoma, 73019, USA
[2]BRGM, 45060 Orléans, France
[3]Geology and Geography, West Virginia University, Morgantown, 26506, USA
[4]Université de Rennes, CNRS, Géosciences Rennes – UMR 6118, 35000 Rennes, France
[5]Earth System Analysis, Potsdam Institute for Climate Impact Research, Potsdam, Germany
[6]Department of Biology, Kyushu University, Fukuoka, 819-0395, Japan
[7]Jack Satterly Geochronology Laboratory, University of Toronto, Toronto, M5S3B1, Canada
[8]Space Sciences Institute, Boulder, Colorado, 80301, USA
[9]Atmospheric, Oceanic, and Earth Sciences, George Mason University, Fairfax, 22030, USA
[10]Keck School of Medicine, University of Southern California, Los Angeles, 90033, USA
[11]Department of Integrative Biology, University of California-Berkeley, Berkeley, 94720, USA
[12]Laboratoire de Planétologie et Géodynamique Université de Nantes, Nantes Cedex, 44322, France
[13]Geology Department, Beloit College, Beloit, 53511, USA
✚A full list of authors appears at the end of the paper.

Correspondence: Gerilyn S. Soreghan (lsoreg@ou.edu)

Received: 24 February 2020 – Revised: 26 May 2020 – Accepted: 12 August 2020 – Published: 1 December 2020

Abstract. Chamberlin and Salisbury's assessment of the Permian a century ago captured the essence of the period: it is an interval of extremes yet one sufficiently recent to have affected a biosphere with near-modern complexity. The events of the Permian – the orogenic episodes, massive biospheric turnovers, both icehouse and greenhouse antitheses, and Mars-analog lithofacies – boggle the imagination and present us with great opportunities to explore Earth system behavior. The ICDP-funded workshops dubbed "Deep Dust," held in Oklahoma (USA) in March 2019 (67 participants from nine countries) and Paris (France) in January 2020 (33 participants from eight countries), focused on clarifying the scientific drivers and key sites for coring continuous sections of Permian continental (loess, lacustrine, and associated) strata that preserve high-resolution records. Combined, the two workshops hosted a total of 91 participants representing 14 countries, with broad expertise. Discussions at Deep Dust 1.0 (USA) focused on the primary research questions of paleoclimate, paleoenvironments, and paleoecology of icehouse collapse and the run-up to the Great Dying and both the modern and Permian deep microbial biosphere. Auxiliary science topics included tectonics, induced seismicity, geothermal energy, and planetary science. Deep Dust 1.0 also addressed site selection as well as scientific approaches, logistical challenges, and broader impacts and included a mid-workshop field trip to view the Permian of Oklahoma. Deep Dust 2.0 focused specifically on honing the European target. The Anadarko Basin (Oklahoma) and Paris Basin (France) represent the most promising initial targets to capture complete or near-complete stratigraphic coverage through continental successions that serve as reference points for western and eastern equatorial Pangaea.

Published by Copernicus Publications on behalf of the IODP and the ICDP.

> Between a marvelous deployment of glaciation, a strangely dispersed deposition of salt and gypsum, an extraordinary development of red beds, a decided change in terrestrial vegetation, a great depletion of marine life, a remarkable shifting of geographic outlines, and a pronounced stage of crustal folding, the events of the Permian period constitute a climacteric combination. Each of these phenomena brings its own unsolved questions, while their combination presents a plexus of problems of unparalleled difficulty. More than any other period since the Proterozoic, the Permian is the period of problems.
>
> Chamberlin and Salisbury, Geology v. II, Earth History, 1905

1 Introduction

The Permian (299–252 Ma) records a fundamental reorganization in tectonic, climatic, and biologic components of the Earth system. Plate collisions leading to the assembly of the supercontinent Pangaea culminated by middle Permian time, expressed at low latitudes by the formation of the Central Pangaean Mountains and associated orogenic belts (e.g., Domeier and Torsvik, 2014; Fig. 1). The Permian records multiple large mafic magmatic events, including those affecting the Central Pangaean Mountains (Ernst and Buchan, 2001). Additionally, the Variscan system of western and central Europe was a global focus of expansive and explosive silicic-intermediate volcanism (Soreghan et al., 2019) associated with both construction and collapse of the Central Pangaean Mountains (e.g., Menard and Molnar, 1988; Burg et al., 1994). Extensive plutonism and orogenic collapse also took place in the Moroccan and Appalachian parts of this system (e.g., Valentino and Gates, 2001; EL Hadi et al., 2006). The magnitude of the Permian climate transition is unique for the Phanerozoic: Earth's penultimate global icehouse peaked during the early Permian, yielding to full greenhouse conditions by the late Permian – our only example of icehouse collapse during a time with known complex terrestrial ecosystems (Gastaldo et al., 1996). The late Paleozoic icehouse was the longest and most intense glaciation of the Phanerozoic (Feulner, 2017), and reconstructed atmospheric composition includes both the lowest CO_2 and (inferred) highest O_2 levels of the Phanerozoic (Berner, 2006; Foster et al., 2017) – the latter presumably spurred by the massive proliferation of vascular land plants (Berner, 2003), possibly exacerbated by weathering of the tropical mountains (Goddéris, 2017) as well as enhanced marine productivity (Sur et al., 2015; Chen et al., 2018; Sardar Abadi et al., 2020). High-resolution CO_2 reconstructions include values comparable to those anticipated for Earth's immediate future (Montañez et al., 2016). Fundamental shifts occurred in atmospheric circulation, notably development of a global megamonsoon (Parrish, 1993), and the tropics are inferred to have been anomalously arid (e.g., Tabor and Poulsen, 2008), although the latter could alternatively reflect paleogeographic details that remain poorly resolved (Fig. 1; Domeier and Torsvik, 2014; Tomezzoli et al., 2018; Muttoni and Kent, 2019). Evolution of the terrestrial biosphere during the Carboniferous produced the first tropical rainforests (Cleal and Thomas, 2005) and terrestrial ecosystems of "modern" complexity and structure, with food webs centered on carnivores consuming novel vertebrate herbivores (Sues and Reisz, 1998). By Permian time, extreme environments are well documented in the form of, e.g., voluminous dust deposits (Soreghan et al., 2008b, 2015a), acid saline lakes and groundwaters (Benison et al., 1998), extreme continental temperatures (Zambito and Benison, 2013), and biotic crises and extirpations of spore plants from equatorial Euramerica (DiMichele et al., 2006; Sahney et al., 2010), ultimately culminating at the end of the Permian with the largest extinction event in the Phanerozoic (e.g., Twichett et al., 2001; Erwin, 2006). Figure 2 illustrates major trends in varied aspects of the Permian Earth system.

The dynamic Earth system of the Permian and the sensitivity of the tropics to climate forcings in particular motivate an international drilling program to focus on recovery of high-resolution continental records from both western and eastern low-latitude Pangaea in addition to auxiliary science objectives. To address this, 67 scientists and students from nine countries gathered in Norman, Oklahoma (USA), on 7–10 March 2019 to discuss plans for an international drilling project to target objectives in both the US and western Europe. The project was dubbed "Deep Dust" for the intended focus on eolian-transported fines, which are interpreted to compose much of the sediment ultimately captured in eolian, lacustrine, and associated depositional environments of the Anadarko Basin of Oklahoma and selected Permian basins of western Europe. The workshop began with overviews of the key science objectives, which included themes on paleoclimate, paleobiology, the microbial biosphere (both modern deep and fossil Earth surface), and auxiliary science, as well as presentations on the regional geology of the Anadarko and western European basins (Table 1). The rest of the workshop focused on breakout groups and summary plenary sessions on topics of scientific methodologies, drilling logistics (site selection, hazards, logging, operations), education and outreach, and funding. Following discussions of science objectives and geology of potential sites, participants took a field excursion to view target Permian strata of the Anadarko Basin, which consist predominantly of very fine-grained red beds and evaporites, with discussions focused on interpretations of the predominance of eolian and lacustrine environments (Giles et al., 2013; Sweet et al., 2013; Foster et al., 2014; M. Soreghan et al., 2018). The field excursion con-

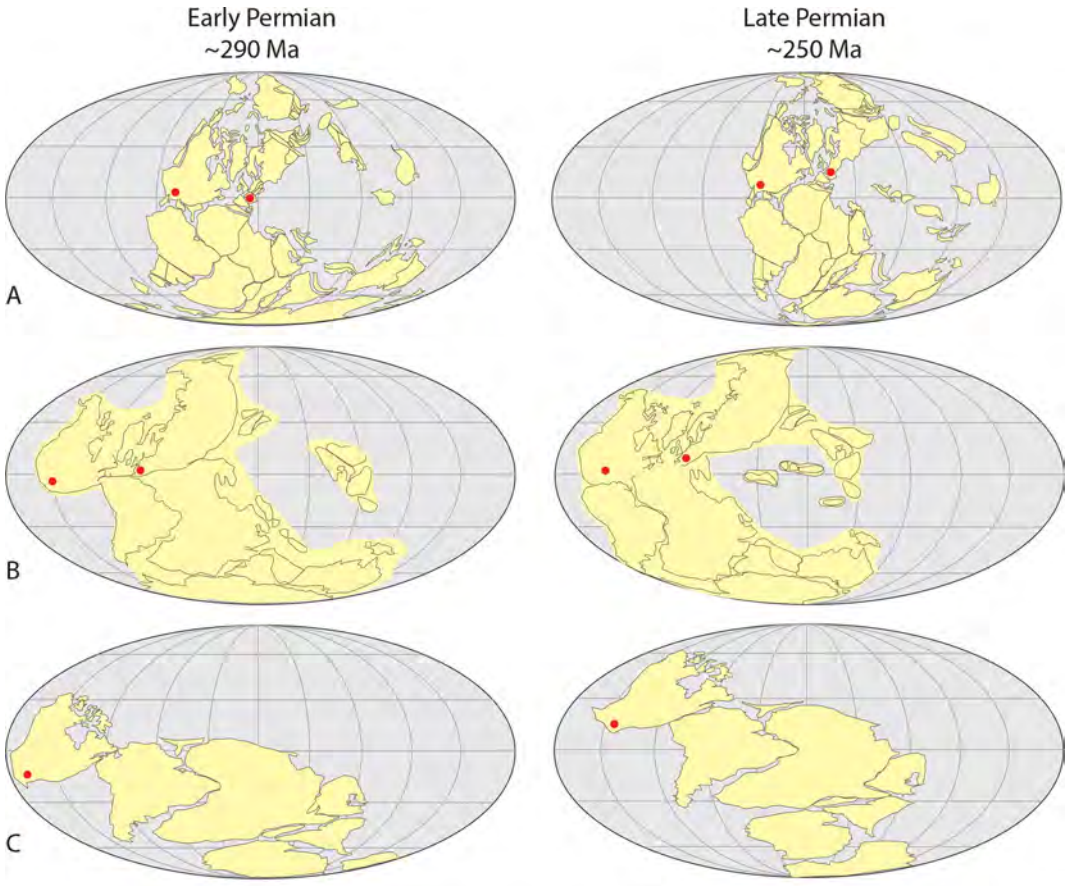

	Anadarko Basin		Paris Basin	
	Early	*Late*	*Early*	*Late*
A	5°N	5-10°N	0-3°N	15°N
B	5-10°S	0-5°N	3°N	10°N
C	15°S	10°N	N/A	N/A

Figure 1. Paleogeography during the early to late Permian redrafted from the reconstructions of **(a)** Domeier and Torsvik (2014), **(b)** Muttoni and Kent (2019), and **(c)** Tomezzoli et al. (2018). Red dots show drill target paleo-positions within the equatorial Central Pangaean Mountains (western US – western equatorial Pangaea and western Europe – eastern equatorial Pangaea). A significant difference between **(a)** and **(b)** relates to the contrasting reconstructions of Pangaea A and Pangaea B. Pangaea A prevails for the later Permian, whereas some prefer Pangaea B for the early Permian. The reconstruction of Tomezzoli et al. (2018) focuses on Laurentia and Gondwana. In all cases, the target sites are generally equatorial but vary by up to ∼ 18° (coordinates for each configuration summarized in the table below).

cluded with an unscheduled but quintessentially Oklahoman bovine rescue. A follow-on workshop (dubbed "Deep Dust 2.0") held in Paris (27–28 January 2020) involved 33 scientists from eight countries in western–central Europe and focused on honing the European coring site(s). After an overview of the regional geology, paleoenvironments, and expected facies in basins of western and central Europe (Polish Basin, Italian basins, German basins, Swiss Plateau, UK and Irish basins, and the French Lodève and Paris basins), presentations (Table 1) focused on topics such as the utility of plant fossils, Permian geothermal resources, and the positions and perspectives of the BRGM (Bureau de Recherches Géologiques et Miniéres) and CNRS (Centre National de la Recherche Scientifique) regarding a proposed research coring project.

2 Compelling science enabled by coring the Permian

The Deep Dust 1.0 workshop (in Oklahoma) included plenary presentations (Table 1) that provided overviews of geologic evidence and modeling results on Permian paleoenvironment and paleoclimates, extreme environments of the Permian, the Permian carbon cycle, terrestrial biosphere and

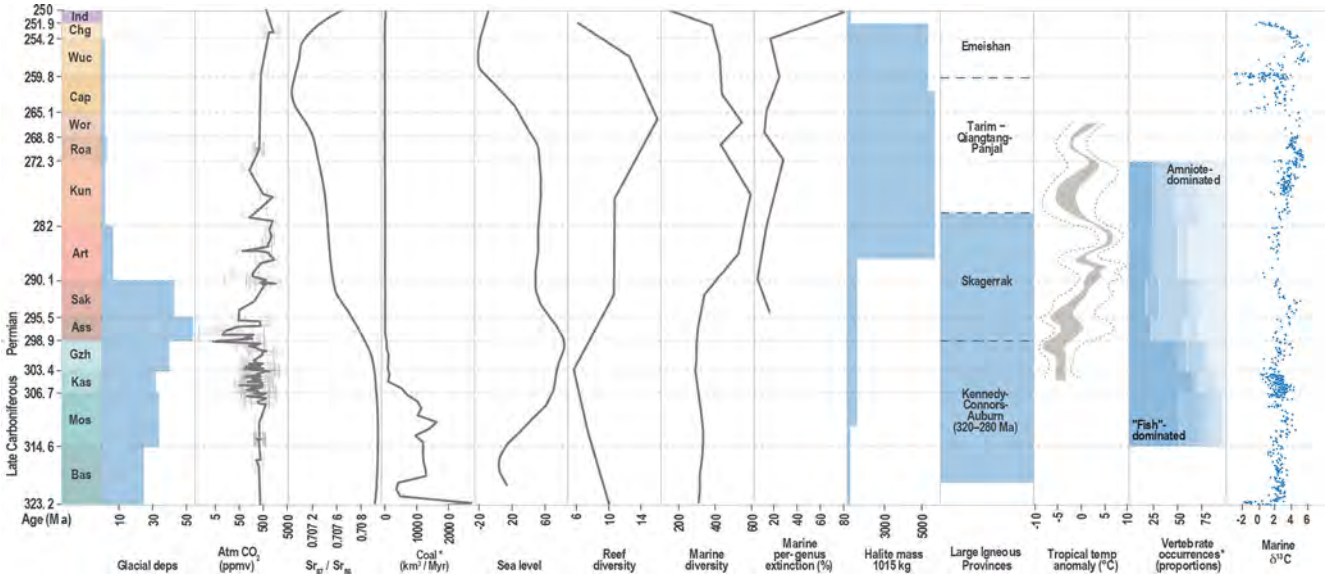

Figure 2. Illustration of documented glacial deposits (Soreghan et al., 2019), atmospheric pCO_2 (Montañez et al., 2016; Foster et al., 2017), strontium isotope signature (McArthur et al., 2001), terrestrial and North American terrestrial organic sediment (coal, lignite, anthracite, and tar) accumulation* (Nelsen et al., 2016), sea-level changes (Haq and Schutter, 2008), mean species richness of reef builders in 10 Myr bins (Kiessling, 2005; Alroy et al., 2008; Payne and Clapham, 2012), halite mass (Hay et al., 2006; Warren, 2016), and large igneous provinces (LIP Commission) during the late Carboniferous (Pennsylvanian) and Permian (323–251 Ma), proportion of vertebrate (fish versus amniote-dominant) species in the North American continental realm (Pardo et al., 2019), a tropical temperature curve adapted from Montañez et al. (2007), and marine C^{13} adapted from Saltzmann and Thomas (2012). * indicates North America only, otherwise global signatures.

Table 1. European target decision matrix.

	Paris Basin	Switzerland	Poland	Germany	UK/Ireland Plymouth Bay (offshore)
Seismic 2D/3D	Y (2D)	Y (2D-3D)	Y (2D)	Y	Y (2D)
Borehole data on seismic[1]	Y	Y	Y	Y	Y (2)
Overburden	1.1 km	1 km			~ 100 m
Target thickness	3.5 km	4 km	1 km	> 10 km	4 km
Facies fine?[2]	Y	N (?)	N	N	Mixed
Ashes?	Y?	Y	Y?	Y	N
Biostratigraphy?	Y	Y	Y	Y	N
C–P boundary?	Y	Y	Y	Y locally	Y
P–T boundary?	N	Y	N	Y locally	Y

[1] Borehole data – within 5 km of proposed location
[2] Predominantly (> 80 %) fine facies

run-up to the Great Dying, and aspects of the deep microbial biosphere. In discussions, participants identified the following major science objectives and rationales for coring these rocks, which are neither well preserved nor very accessible in outcrops, and for which minimal core exists. A list of questions associated with the major and supplementary science topics appears in a data supplement table; overviews appear below. Coring is essential to (1) access buried upland records, (2) achieve continuous records in basinal regions, and (3) recover a pristine section suitable for application of various sedimentologic, geochemical, fluid-inclusion, rock-magnetic, magnetostratigraphic, paleontologic, and geochronologic approaches (i.e., Soreghan et al., 2015b; Benison et al., 2015). Additionally, during the course of both workshops, participants suggested considering expansion to a staged project that could incorporate coring in (1) multiple basins of western Europe and (2) in mid-paleolatitude sites (e.g., China). Such an expanded approach would better inform paleoclimate modeling.

2.1 Equatorial paleoclimate of peak icehouse and icehouse collapse

The basal Permian records the most extreme phase of the late Paleozoic ice age (LPIA), which was the longest-lived and most intense icehouse of the Phanerozoic. Continental glaciation extended to latitudes as low as 32° S (Evans, 2003), and the Carboniferous–Permian boundary interval archives the most widespread evidence for glacial deposits of the LPIA (Fielding et al., 2008; Soreghan et al., 2019; Fig. 2). The acme conditions of the Asselian yielded to a massive reduction in ice (as recorded by number of ice-contact deposits) in the Sakmarian, followed by ultimate disappearance of the vestigial Gondwanan glacial deposits (Australia) in the Wuchiapingian age (Fig. 2). The role of pCO_2, which reached remarkably low values during the LPIA, is an established factor in the severity of the icehouse, but contributory factors might include negative radiative forcing from volcanic aerosols (Soreghan et al., 2019). Fine-grained loessitic and lacustrine strata of the target regions preserve high-resolution records of paleoclimate in these "far-field" equatorial regions, including lower Permian cyclothemic strata that record unequivocal glacial–interglacial swings, yielding upward to entirely continental successions, such as those seen in the upper Pennsylvanian through lower Permian of mid-continental North America (e.g., Heckel, 1990; Giles et al., 2013). The cause(s) of the LPIA deglaciation remain(s) in debate, in addition to the rate of deglaciation; carbon cycling played a key role, but the mechanisms for changing pCO_2 as well as the role(s) of other factors remain(s) debated. Addressing these and related issues will require data types such as additional constraints on high-resolution pCO_2, atmospheric dust loading, and records of source-region denudation (from thermochronology). Combining this with a high-resolution Sr isotope curve can help address the relative roles of weathering and other forcing in driving deglaciation and, in the longer term, the apparent aridification of equatorial Pangaea. Our understanding of the aridification hinges on accuracy of paleogeographic reconstructions; although reconstructions vary (Fig. 1), the variation falls largely within $\sim 15°$ of the Equator, suggesting that aridification relates primarily to changing equatorial hydroclimate rather than latitudinal drivers. However, the Pangaea A versus Pangaea B configurations (Domeier and Torsvik, 2014; Tomezzoli et al., 2018; Muttoni and Kent, 2019) for early Permian time have profoundly different implications for the continentality of western Europe, in particular. In principle, such pronounced differences between continental reconstructions could be tested by running climate-model simulations for different reconstructions and comparing simulated precipitation and evaporation patterns with the distribution of lithological indicators such as coal or evaporite (Cao et al., 2019).

The possibility that glaciation affected low–moderate-elevation uplands of both the western (US) and eastern (Europe) equatorial regions (Becq-Giraudon et al., 1996; Soreghan et al., 2008a, 2014; Pfeifer et al., 2020a) in the early Permian remains highly controversial but is potentially testable by coring regions proximal to buried paleo-uplands to seek evidence for ice-contact and/or pro- and peri-glacial deposition. Furthermore, the unique geological setting of the Anadarko Basin records epeirogenic subsidence that preserved buried paleo-highs (Soreghan et al., 2012), thus enabling (via coring) access to upland environments. Low-latitude upland glaciation – if substantiated – could reflect increased glacial-phase albedo from high loading of bright aerosols, greater exposure of bare ground due to vegetation changes during glacials (Falcon-Lang and DiMichele, 2010), or other as-yet undiscovered climate forcings. Evidence for low-latitude glaciation across equatorial Pangaea during the late Paleozoic would radically change our understanding of this period in Earth's history – a critical interval for the evolution of land animals and plants. It would spur research on influences of alternative boundary conditions and climate forcings. Furthermore, changes in erosional conditions imposed by climate can affect surface expression of tectonic processes (e.g., Molnar and England, 1990; Sternai et al., 2012). These inter-relations are even more intriguing given glaciation, as ice growth and associated erosion affect uplift and subsidence (e.g., Molnar and England, 1990; Champagnac et al., 2009).

2.2 Atmospheric dust and the Pangaean megamonsoon

Also intensifying through later Permian time was the Pangaean megamonsoon, repeatedly inferred from both modeling and data (e.g., Kutzbach and Gallimore, 1989; Parrish, 1993; M. Soreghan et al., 2002, 2018; Tabor and Montanez, 2002) but poorly constrained in terms of its evolution and drivers. Dust (loess) deposits capture an excellent archive of the monsoon, as well documented by work on the Quaternary monsoonal record archived in the Chinese Loess Plateau (e.g., Sun et al., 2006), and the Permian preserves the most voluminous dust deposits known in Earth's history (Soreghan et al., 2008b, 2015a). But the drivers behind this remarkable production and accumulation of dust and the effects of such an extreme (mineral-aerosol-rich) atmospheric composition remain unknown. The forcing(s) associated with atmospheric aerosols constitute one of the largest uncertainties in climate modeling from near to deep time (Schwartz and Andreae, 1996; NRC, 2011; Heavens et al., 2012; Lee et al., 2016). Continuous coring will enable us to tap the full extent of this dust record recovered in unambiguous stratigraphic superposition, assess extent of atmospheric dust loading, and use dust provenance (with, e.g., geochemistry and detrital zircon geochronology) to build a high-resolution archive of atmospheric circulation of unprecedented (tens of millions of years) duration. Because targeted dust deposits lie in both western and eastern Pangaea, we can assess spatiotemporal patterns of continental climate change, e.g., the nature and pace of proposed east-

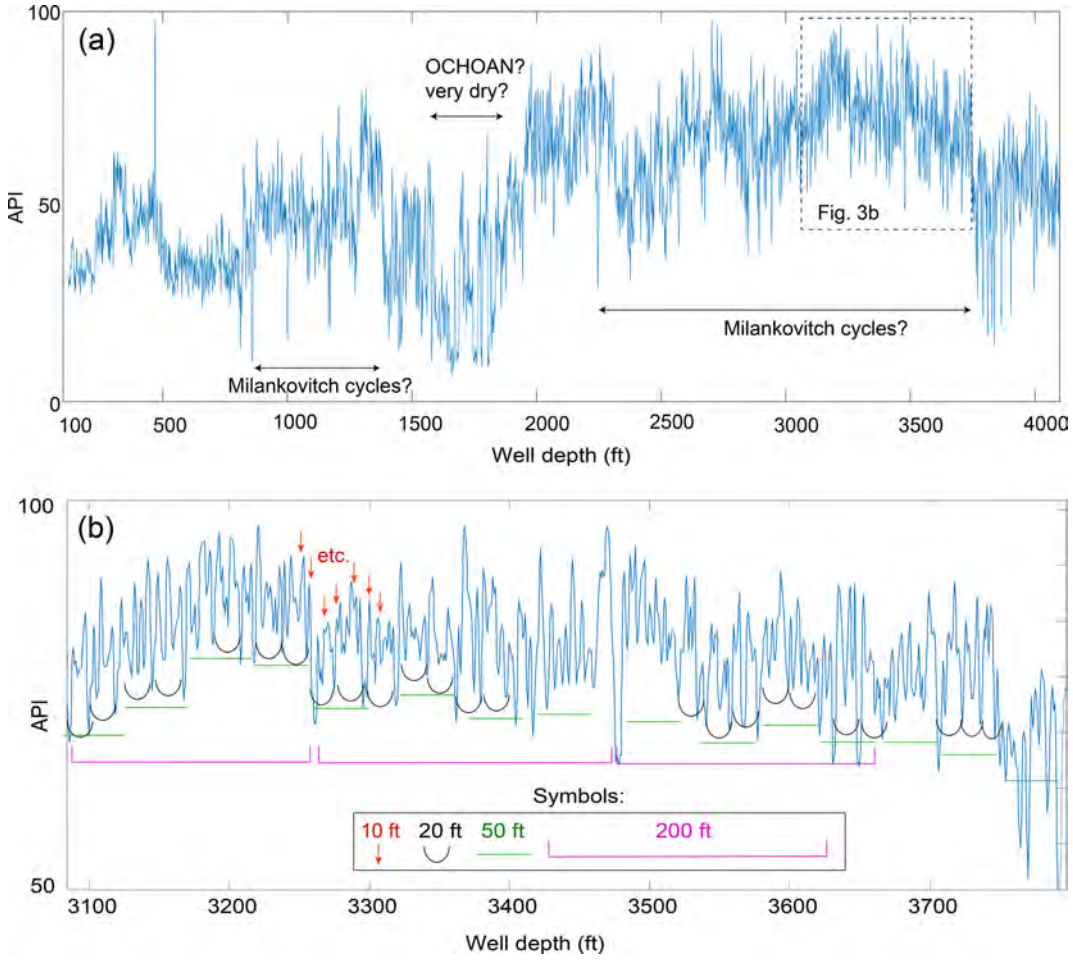

Figure 3. Gamma ray (GR) log from the Schneberger 1-19 Well, Atoka Burns Flat, Washita County, Oklahoma, USA (S19; T10N, R19W; elevation 593 m). **(a)** Log from 100 to 4100 ft (well log depth scale) with preliminary interpretations of intervals with possible Milankovitch cyclicity and possible position of the North American Ochoan Stage (earliest Lopingian). The dashed box indicates a detailed portion of the log examined further in **(b)**. **(b)** Detail from 3090 to 3790 ft displaying pervasive superimposed GR cycles with thicknesses of 10, 20, 50, and 200 ft (see "Symbols"), possibly indicating, respectively, precession index, obliquity, short orbital eccentricity, and long orbital eccentricity cycles.

wardly progressing aridification (Tabor and Poulsen, 2008). Quantitative cyclostratigraphic analysis of high-quality well-log records as shown in Fig. 3 will enable assessment of astronomical forcing of tropical climate/hydroclimate through the Permian icehouse–greenhouse transition up to the end-Permian mass extinctions. The discovery of astronomical forcing signatures in continental western Pangaea will provide "floating" astrochronologies and opportunities to correlate the signatures with biostratigraphically constrained marine Paleotethyan counterparts described by Wu et al. (2013) and Fang et al. (2015, 2017) and with continental eastern Pangaea (Huang et al., 2020; Pfeifer et al., 2020b). These correlations will be enhanced greatly by adding paleomagnetic and (post-Kiaman) polarity data, achievable by virtue of obtaining continuous records in both western and eastern equatorial Pangaea.

2.3 The later Permian: extreme environmental and biotic records leading up to the Great Dying

The later Permian accommodates the final icehouse collapse and the transition to one of the most extreme greenhouse times known in Earth's history (Triassic), with the intercalated largest extinction known – the Permian–Triassic (P–T) extinction event. The P–T event has been linked in part to massive large igneous province (LIP) volcanism in Siberia (Siberian Traps), a region containing enormous volumes of carbon- and evaporite-rich strata, exacerbating the release of large amounts of greenhouse gases and halocarbons into the atmosphere (e.g., Svensen et al., 2009). Middle Permian–early Triassic red-bed-hosted halite records extreme continental conditions, such as hyperaridity, local air temperatures as high as 73 °C, and a diurnal temperature range up to 28 °C (Zambito and Benison, 2013), as well as extremely

acid saline lakes and groundwaters with pH as low as 0 (Benison et al., 1998; Andeskie et al., 2018). New fluid inclusion methods have documented atmospheric O_2 from Proterozoic halite (Blamey et al., 2016), suggesting that atmospheric O_2 may also be analyzed from fluid inclusions in Permian halite; these types of analyses are uniquely enabled by coring the types of deposits preserved in the target regions. Much of the research on the run-up to the P–T crisis focuses on the marine record (e.g., Erwin, 1994; Wignall and Twitchett, 1996). In contrast, this proposed ICDP project will target high-resolution, continental successions sensitive to climatic and environmental conditions, including lacustrine, paleosol, and fine-grained eolian (e.g., loess) deposits, that we anticipate have the potential to preserve palynological as well as other records of paleoecological conditions and transitions. Physiological performance in modern tropical ectotherms is impacted by even small-magnitude climate warming, underscoring the vulnerability of low-latitude regions to climate change. Spanning the equatorial region west to east enables differentiation of local from regional-to-global changes in the continental record of the conditions leading to extinction and test hypotheses of a west–east lag in the loss of peri-Tethyan aquatic diversity and increased terrestrial diversity (Pardo et al., 2019). We anticipate the possibility that the targeted coring regions will enable elucidation of climatic and biotic changes through the middle and late Permian in particular, which are poorly documented.

2.4 Nature of the modern and fossil deep microbial biosphere

Discussion of questions on the deep microbial biosphere focused on both the microbes living today and those potentially preserved from Permian time – the latter representing a truly unique opportunity. The Anadarko Basin, for example, is the deepest sedimentary basin on the North American craton, with significant basinal fluid migration, documented by modern sulfide- and sulfur-rich springs such as Zodletone Spring (https://www.mindat.org/loc-305255.html, last access: 20 September 2020), which boosts a highly diverse and complex microbial ecosystem (Luo et al., 2005). Coring is essential to test the limits and nature of the deep biosphere here. Microbial life – potentially present in fluids or rock surfaces – might be driven by the redox transformation of abundant (trace) elements in the basin such as arsenic and iron (Amstaetter et al., 2010) or might utilize metabolic pathways associated with hydrocarbons (Hamamura et al., 2005; Foght et al., 2017).

As noted above, coring strata from the target basins hold the potential to enable unprecedented analyses of the *fossil* microbial biosphere, locked within fluid inclusions of Permian evaporites preserved exclusively at depth (e.g., Satterfield et al., 2005; Benison, 2019). These previous studies demonstrated that microbial life existed in the Permian at $pH < 1$, $pH < 0$, and $pH < -1$ – among the environments with the lowest pH and water activity known to host life (Benison, 2013). Several questions arise from these observations, such as whether the Permian microbes remain viable and whether relationships exist between the modern and Permian microbial biospheres, for which the host lithology has remained constant for nearly 300 Myr. Finally, such extreme, iron-rich, acidic conditions as those of these Permian red beds provide sedimentary analogs to past Martian surface conditions, including potential biosignatures. The Permian evaporites of Kansas preserved only in cores contain fossil microbes and organic compounds both as solid inclusions and within fluid inclusions (e.g., Benison, 2019). Iron oxide concretions in recent siliciclastic sediments associated with acid saline lakes in Western Australia contain microfossils (Farmer et al., 2009). Our proposed coring would provide reference comparison samples for sediments and rocks returned from Mars, with significant implications for astrobiology.

2.5 Auxiliary science

Finally, breakout groups discussed auxiliary science objectives that could be pursued in addition to the primary paleoclimatic/paleoenvironmental/microbial objectives. These objectives included red-bed sedimentology, induced seismicity, tectonics, geothermal energy, hydrology, and drilling engineering. Additionally, a fundamental advance will be the ability to build paleomagnetic and magnetostratigraphic reference sections for the Permian to help resolve long-standing paleogeographic enigmas with implications for paleoclimate. If we wish to advance paleoclimatic understanding and disentangle local from global effects, we must accurately locate the study areas in paleogeographic space. A viable approach to resolving the ongoing controversy of Pangaea A versus Pangaea B configurations (Fig. 1), for example, is by magnetic studies of long continuous cores at the target sites.

The prevalence of Permian red beds is renowned but puzzling; ideas for this geochemical anomaly have centered predominantly on a climatic control (Barrell, 1908; Walker, 1967, 1974; Dubiel and Smoot, 1994; Parrish, 1998), although Sheldon (2005) called into question whether red indicates any specific paleoclimatic parameters. The remarkable atmospheric oxygen levels perhaps played a role (e.g., Glasspool and Scott, 2010). More recent data on iron geochemistry of Permian loess from scattered sites throughout the western US reveal mysteriously high iron bioavailability (i.e., high values of highly reactive iron to total iron), with major implications for fertilization of primary productivity and thus carbon cycling (Sur et al., 2015; Sardar Abadi et al., 2020) during this interval, yet the origin of this reactivity remains enigmatic. Coring would enable assessment of iron reactivity in dust across vast stretches temporally and spatially: through the entire Permian, and across the tropical landmass, which would help address drivers for the reactivity and help address the origin of red beds.

Figure 4. Examples of the lower Permian paleo-loess of (left) the mid-continent US and (right) France. Left: the middle Permian Flowerpot Shale of the Anadarko Basin, western Oklahoma (Sweet et al., 2013). Right: the middle Permian Salagou Formation of the Lodève Basin, southern France (Pfeifer et al., 2016, 2020a, b).

The proposed sites capture rather unique tectonic settings, as both the Anadarko Basin and Permian basins of western–central Europe occupy regions either proximal to or atop (respectively) collapsed paleo-highlands of the greater Central Pangaean Mountains. Both received sediment from major orogenic belts of these systems: the Appalachian orogen in the case of the Anadarko Basin (e.g., Soreghan et al., 2019) and the Variscan core in the case of Permian basins of France (e.g., Pfeifer et al., 2016). Given the expected continuity of the target sections, it might be possible to constrain unroofing of the Appalachian and Variscan orogens using detrital zircon and apatite thermochronology. Preliminary work on a partial Permian section from the Lodève Basin (southern France) revealed remarkably high rates (1–17 mm yr^{-1}) of exhumation in the Variscan orogen, comparable to present rates of Himalayan uplift (Pfeifer et al., 2016). Together with recent work that reveals mean Variscan paleoelevations of 3300 ± 1000 m at ca. 300 Ma (Dusséaux, 2019), this has significant implications for understanding climatic–tectonic interactions.

The incidence of induced seismicity in Oklahoma (and many other regions, especially in regions exploited for hydrocarbon or geothermal energy) has increased significantly in the last decade and holds significant societal implications. In Oklahoma, most of the induced seismicity is linked to fluid injection associated with wastewater disposal or hydraulic fracturing (Chen et al., 2017; Ellsworth, 2013; Keranen and Weingarten, 2018; Langenbruch et al., 2018), where most of the wastewater is produced from unconventional shales that commonly include significant ratios of formation saltwater along with the hydrocarbons (Ellsworth, 2013). Globally, incidences of induced seismicity have been associated with fluid injection, hydrocarbon extraction, and geothermal energy, among many other causes (Foulger et al., 2018). Instrumentation of a borehole with fiber-optic cabling could enable distributed acoustic sensing of seismicity, strain, and auxiliary assessments of geothermal gradient, and shallow hydrogeology helpful for studying seismicity as well as a number of other studies. Observations of these parameters are relatively rare in the target region of Oklahoma. Finally, a fully cored borehole could be a compelling test facility for new drilling technology – specifically as a geothermal test well. Most oil and gas wells do not have the required size or depth required for clean energy development such as enhanced geothermal systems. In western Europe, Permian strata are a growing target for potential geothermal energy production; specific in situ measurements (e.g., hydraulic production test) and high-resolution lab investigations (petrophysics properties, small-scale fracturing, temperatures) would serve as a reference for future investigations in both the US and European sites.

3 Suitability of archives and indicators

Targeted sections preserve primarily continental records because the main science drivers center on paleoclimate and paleoenvironments. Between the western and eastern equatorial sites, lithologic compositions expected potentially include (predominantly) paleo-loess deposits and subordinate evaporites in lowland basinal sections (Fig. 4) but also mixed-lithology (carbonate–clastic) cyclothems of epeiric deposition (basal Permian) in basinal sites and possible ice-contact or pro-/peri-glacial deposits in upland-proximal sites. For the lowland sites, we are specifically targeting sections ex-

pected to consist predominantly (>80 %) of fine-grained sediments thought to comprise loess and dust trapped ultimately in lacustrine settings. Like lacustrine sediment, loess is considered the most comparable to marine sediment in recording continuous- or near-continuous deposition (Begét and Hawkins, 1989); accordingly, loess and lakes archive the highest-resolution continental archives for paleoclimatic and auxiliary reconstructions. Loess deposits in particular, which include intercalated paleosols, preserve up to millennial-scale records of continental climate, including atmospheric circulation (dust loading, wind direction, and strength from provenance and grain size) and precipitation (from magnetic susceptibility, e.g., M. Soreghan et al., 2014; Yang and Ding, 2013; Soreghan et al., 2015a; Maher, 2016) as well as – potentially – paleotemperature and atmospheric pCO_2 in hosted paleosols (e.g., Tabor and Myers, 2015). Anisotropy of magnetic susceptibility in loess is well studied as an excellent potential for reconstructing wind directions and also intensity variations (e.g., Liu et al., 1999; Zhu et al., 2004; Nawrocki et al., 2006; Zhang et al., 2010). Eolian dust trapped by lacustrine or shallow marine environments holds the potential for organic preservation and thus associated organic geochemical and biomarker analyses. Evaporites preserve continental temperatures and brine compositions at temporal resolutions as fine as diurnal (e.g., Benison and Goldstein, 1999; Zambito and Benison, 2013). Cyclothems preserve an archive of glacial–interglacial variations from which we can potentially extract paleotemperature, ice-volume variations, and continental weathering flux (e.g., Elrick and Scott, 2010; Theiling et al., 2012; Elrick et al., 2013). Proglacial and associated deposits establish the former extent and nature of glaciation.

Thermochronology through clastic successions can reveal long-term denudation in these uplift-proximal regions, potentially shedding light on both tectonic and tectonic–climatic interactions (e.g., Reiners and Brandon, 2006). Many of the sedimentologic, geochemical, and fluid inclusion tools require pristine samples recoverable only by coring, and achievement of high-resolution temporal trends, especially those employing, e.g., quantitative cyclostratigraphy and magnetostratigraphy, demand continuous and stratigraphically complete sampling through sections with unambiguous stratigraphic superposition. Currently, we lack such data for the Permian; rather, climate-sensitive records are limited to spatially and temporally discrete sampling of mostly outcrops, with very few North American data in the later Permian (e.g., Tabor and Poulsen, 2008; atmospheric pCO_2 data of Montañez et al., 2007, 2016). These studies suggest an increasing trend in pCO_2 and equatorial aridity from the late Carboniferous to the middle Permian as well as substantial glacial–interglacial variability in both parameters from the middle Carboniferous to the early Permian.

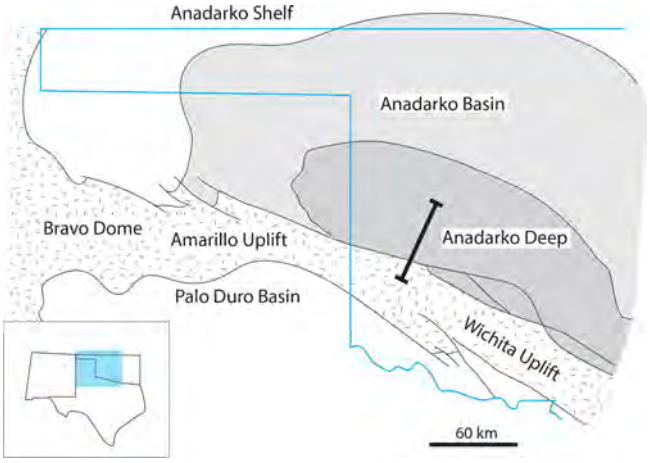

Figure 5. Plan view image of the Anadarko Basin (modified from Hentz, 1994). The bold line denotes the approximate location of the 3D seismic line in Fig. 7. Note that both the Amarillo Uplift and Bravo dome (and much of the Wichita Uplift) are in the subsurface.

4 Site selection

The Anadarko Basin (Oklahoma, USA) and Paris Basin (France, western Europe) preserve what are likely the most complete records of the continental Permian on Earth and sample the antipodes of equatorial Pangaea. Furthermore, the partial preservation of paleo-upland regions in both the Wichita Uplift (Anadarko Basin system; Soreghan et al., 2012) and Variscan system (below the Brécy Basin; Beccaletto et al., 2015) presents the rare opportunity to access archives of moderate-paleoelevation sites; together with ongoing research positing high elevations (>3000 m; Dusséaux, 2019) and possible upland glaciation for the Variscan system, these localities are globally unique.

4.1 Western Pangaean site: Anadarko Basin (Oklahoma)

The Anadarko Basin (Fig. 5) of the southern mid-continental US is the deepest sedimentary basin on the North American craton, owing to a dual history of Neoproterozoic-Cambrian (failed) rifting followed 300 Myr later by late Paleozoic compressional deformation associated with western Pangaean assembly (Johnson, 1988). This basin represents the southern limit of a widespread subsiding region during Permian time that extended across mid-continental North America – a largely endorheic basin akin in scale and character to the greater Lake Chad region of modern Africa. The sedimentary record in the Anadarko Basin is especially complete for the late Carboniferous–Permian, with preservation of ∼ 2000 m of Permian strata alone (Soreghan et al., 2012; Fig. 6) comprising predominantly continental (paleo-loess/dust, lacustrine, and evaporite) deposits, with (basal) epeiric cyclothems of a mixed carbonate–clastic character (Johnson, 1988). Re-

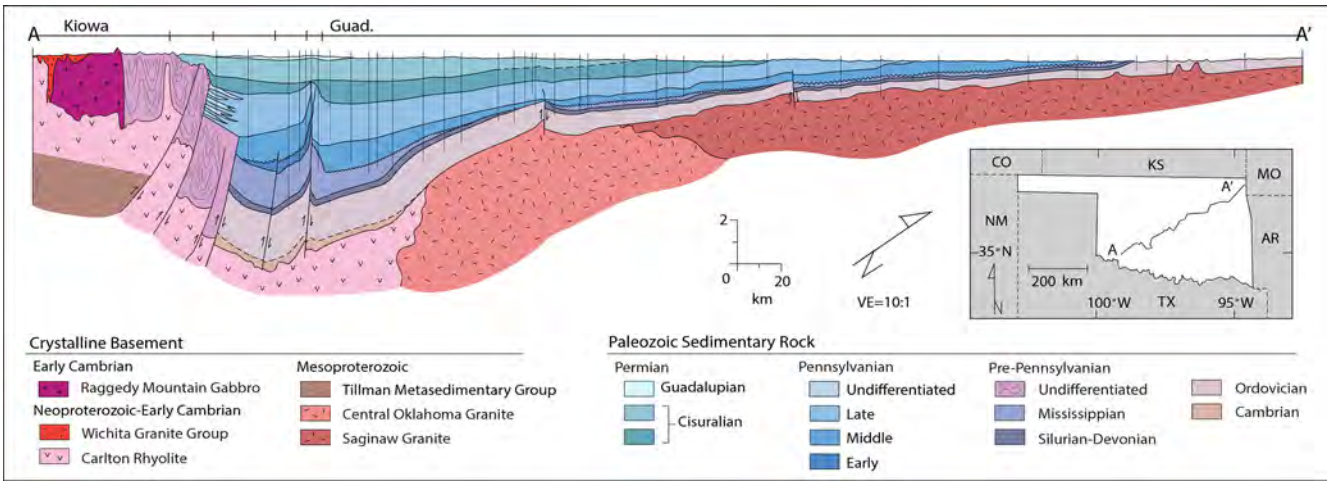

Figure 6. Cross section of the Anadarko Basin, from the basin deep (SW) to the shelf (NE). Thin vertical lines are locations of the boreholes (logs) used for the interpretation. The seismic line (shown as "S" on the inset map) in Fig. 7 depicts (approximately) the boxed region. Cross section modified from Witt et al. (1971).

markably, the Permian subsidence event affected both the basin and the adjacent uplift (Wichita Uplift), resulting in preservation of a Permian landscape (Soreghan et al., 2012) and burial of upland strata in the subsurface along the southern basin margin. Industry seismic data are accessible to guide drill site locations (cf. Fig. 7).

4.2 Eastern Pangaean site(s): European target(s)

The Deep Dust 2.0 workshop focused specifically on a comprehensive assessment of Permian basins in western and central Europe. Participants converged on prioritizing a reference section that could reasonably be expected to house a continuous section of predominantly fine-grained continental facies that includes the C–P boundary and approaches as closely as possible the P–T boundary. The only area in western Europe containing the P–T boundary occurs in the central part of the Germanic Basin (Bourquin et al., 2011), and the correlation with the Paris Basin is well established (e.g., Bourquin et al., 2006, 2009). Moreover, the C–P boundary is well defined and dated in nearby outcrops and subsurface data (Ducassou et al., 2019; Pellenard et al., 2017; Mercuzot et al., 2020; Mercuzot, 2020). A number of basins in Germany contain parts of the Permian, with extensively cored sections, but the common occurrence of coarse-grained, high-energy facies (e.g., inferred alluvial-fan, fluvial, volcaniclastic) and lack of a single site traversing the entire (or nearly entire) section are problematic from the perspective of the primary science drivers for the Deep Dust project. Other criteria considered in narrowing the selection included availability of seismic data (constrained by boreholes), thicknesses of target and overburden, and expected dating potential (e.g., by ashes and/or biostratigraphy). Ultimately, the southwestern Paris Basin emerged as the best location for a reference section. However, participants were keen to consider a drilling program that could include additional localities in a staged approach. The Permian of eastern equatorial Pangaea (France) is partially exposed in dismembered rift basins of the Variscan–Hercynian orogenic belt of central and southern France, such as the Lodève Basin (Fig. 8) that formed as a result of orogenic collapse (Burg et al., 1994; Praeg, 2004). These basins preserve a sedimentary succession analogous to that of the Anadarko Basin, with drab-hued carbonaceous upper Carboniferous strata yielding upsection to fine-grained red-bed lacustrine, eolian, and rare evaporitic sediments through the Permian (e.g., Pochat and Van Den Driessche, 2011), including extensive loess deposits (Pfeifer et al., 2016, 2020a). In the Paris Basin, numerous late Paleozoic "sub-basins" have been recognized since the 1960s but lie beneath the Ceno-Mesozoic cover. The southwestern Paris Basin in particular remains virtually unexplored with no core except for a 110 m core of Permian red beds (Juncal et al., 2018) and three wells reaching a maximum of 1600 m in the upper Carboniferous to upper Permian section (Bertray, Brécy, and Saint-Georges-sur-Moulon) with available well-log data (gamma ray, sonic) and cutting descriptions. Recent pre-stack migration processing reprocessing of vintage seismic data reveals a significant Permian section here (Fig. 10). The Permian section extends over an area of several thousand km^2, with thicknesses reaching 3000 m (Beccaletto et al., 2015; Figs. 9, 10).

Permian strata of the southwestern Paris Basin accumulated "above" the internal zone and suture of the Variscan belt, south of the Variscan front during the late-to-post orogenic extensional processes (Faure, 1995; Baptiste et al., 2016). These basins formed after the main Variscan deformation and thus the Permian strata remain virtually undisturbed by Variscan orogenesis. The post-orogenic subsidence (from

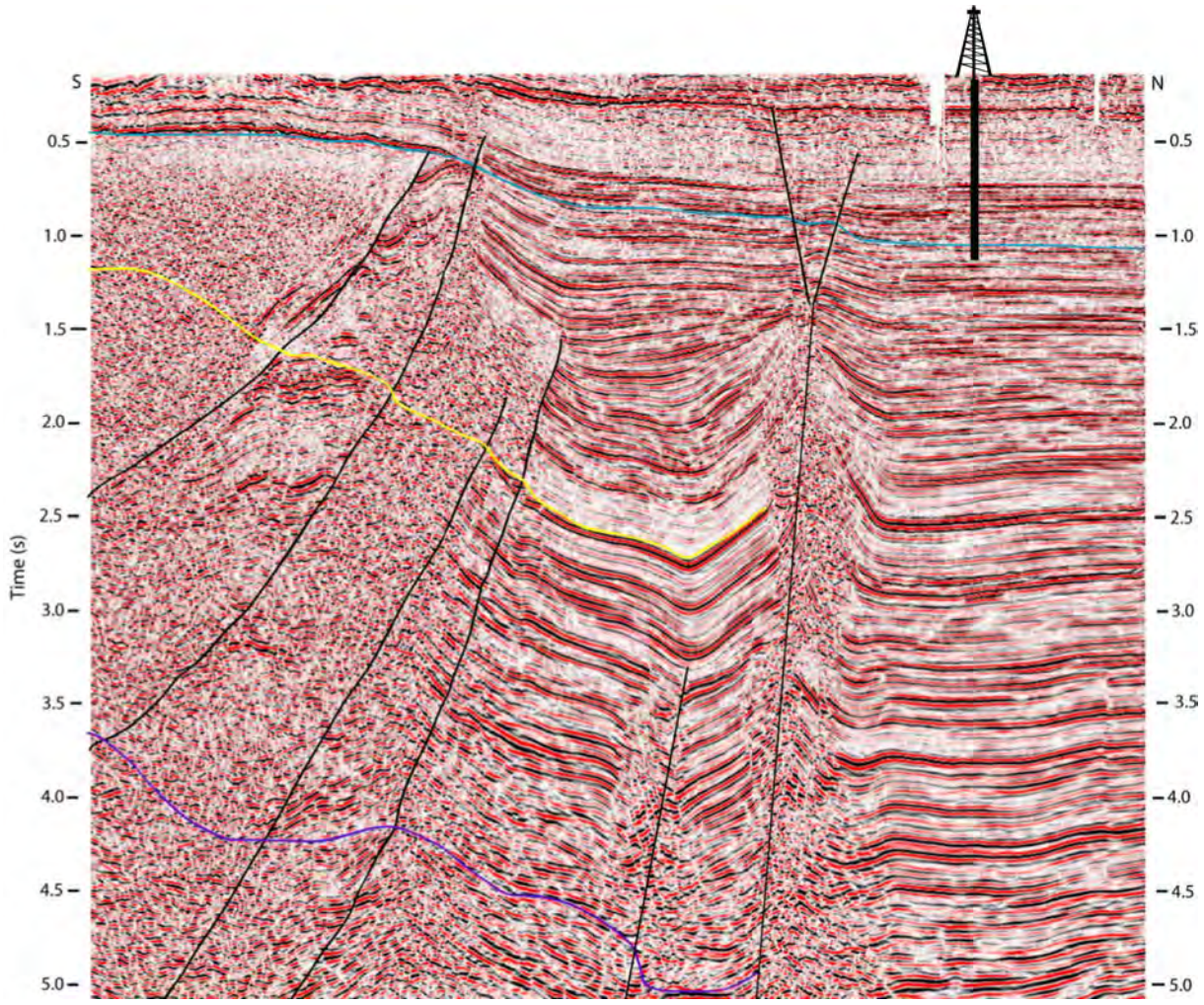

Figure 7. Vertical time slice from a 3D seismic volume acquired across the Frontal Fault zone of the Wichita–Anadarko system, extending from the (subsurface) Wichita Uplift (left) into the deep Anadarko Basin (right). See Fig. 6 for the approximate location of the line (line length ∼ 60 km). Vertical scale shows two-way travel time (seconds). Stratal markers as follows: base Pennsylvanian – yellow, base Permian – blue. From Rondot (2009). A potential (basinal) drill site is indicated with the derrick symbol.

tectonic to thermal) during the late Paleozoic enabled preservation of a nearly complete stratigraphic succession from late Carboniferous to late Permian time, with an unconformity at the Permian–Triassic boundary (as is the case across western–central Europe; e.g., Bourquin et al., 2011). Strata of the southwestern Paris Basin accumulated during two successive tectonic phases (Beccaletto et al., 2015).

- An initial period of opening of the (Arpheuilles, Contres, and Brécy) basins, during which Stephanian conglomeratic/coal facies accumulated under a strong structural control (normal- and strike-slip faulting, with development of a clastic wedge); this represents about 20 % of the (Stephanian)–Permian section.
- Subsequent Permian and pre-Triassic tectonic activity (northwest–southeast-oriented strike–slip faulting in the Arpheuilles Basin, uplift of the margins of the three basins), resulting in tectonic subsidence and associated sedimentation in these basins. The Permian strata here consist mainly of mudstone or silty mudstone, with rare thin interbeds of sandy, carbonate, intra-clastic conglomeratic, or evaporitic facies. Occurrences of fine to coarse sandstone occur in the top interval. These lithologies are analogous to those in neighboring basins, where they are interpreted as restricted lacustrine to localized fluvial facies and are analogous to those inferred for the Anadarko Basin of Oklahoma.

Thus, although the uppermost Carboniferous–lower Permian strata exist in isolated basins, the rest of the Permian sedimentary section accumulated across a broad region as demonstrated by the reinterpretation of newly reprocessed seismic lines (Fig. 10). As these basins were later covered by Triassic strata (Fig. 9), the Permo-Carboniferous section

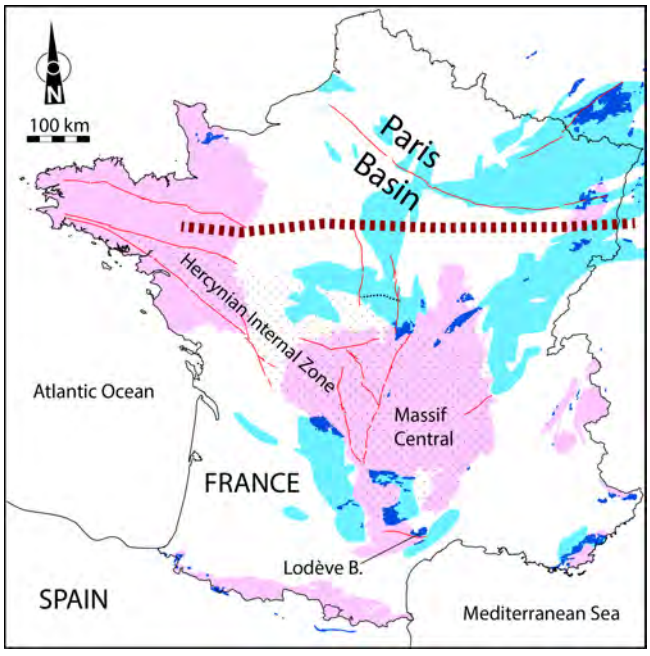

Figure 8. Top – simplified geology of France. Dark blue regions are basins with Permian strata exposed (e.g., Lodève), whereas light blue regions denote Permian strata buried by Mesozoic overburden. The bold dotted line crossing the E–W span of the Paris Basin is the location of the cross-section line in Fig. 9. The fine dotted line in the southern–central part of the basin is the location of the seismic line in Fig. 10 (modified from Beccaletto et al., 2015).

was essentially protected from Meso-Cenozoic tectonic uplift and subsequent erosion. Importantly, this same situation does not hold for the strata now exposed in regions such as the Lodève Basin. The Permian of subsurface basins such as those beneath the southwestern Paris Basin have been affected by a slight pre-Triassic tilting and by Oligocene brittle normal faulting (represented by nearly vertical faults in Fig. 10), without major tectonic perturbation. Other northern European basins offer less complete and partly marine stratigraphic sections for this interval, owing to slower rates of subsidence and the influence of the Zechstein Sea (e.g., Doornenbal and Stevenson, 2010).

We provisionally propose the southwestern Paris Basin as our coring target to capture a continuous lowland record in eastern equatorial Pangaea. We recommend a coring target in what is projected to be the most stratigraphically complete section: in the Brécy (sub)basin, where the Permian reaches a thickness of $\sim$ 3000 m, beneath a Mesozoic cover of $\sim$ 1000 m (Figs. 9, 10).

5 The need for coring

Intact and complete continental stratal records from the mid-Permian through Triassic of Pangaea are rare (in both outcrop and standard cores). Within the Anadarko Basin, outcrops are stratigraphically and lithologically incomplete due to intercalated halite in parts of the section, which dissolves at and near the surface (Benison et al., 2015). Furthermore, the gentle dip across a region with minimal relief creates limited outcrop opportunities. Although the Anadarko Basin hosts hundreds of thousands of boreholes owing to nearly a century of hydrocarbon extraction, minimal core exists of the Permian owing to its status as overburden. However, the rare cores that have been recovered yield a wealth of high-resolution paleoenvironmental, paleoclimatological, and microbiological data about Pangaea (e.g., Benison et al., 1998; Zambito and Benison, 2013; Foster et al., 2014; M. Soreghan et al., 2018; Benison, 2019; Andeskie and Benison, 2020). Similarly, although the Paris Basin has been a target for resources preserved in especially the Mesozoic section, no extensive Permian core exists. Here, the Permian is reachable exclusively through subsurface coring.

Coring will enable acquisition of long, continuous records through even friable lithologies, with the unambiguous stratigraphic superposition needed to construct permanent reference sections for the Permian. It will also enable exploration of sediment preserved atop buried paleouplands. The importance of this time period, encompassing biotic crises such as the end-Guadalupian biotic event and major climate change, combined with the exceptional preservation of rocks by purposeful and well-planned coring, makes a compelling case for scientific drilling (Soreghan et al., 2014). Finally, continuous coring of stratigraphically unambiguous sections will enable application of comprehensive paleomagnetic and magnetostratigraphic studies critical to resolving arguably the most fundamental aspect of the Permian world: which geographic reconstruction (Fig. 1) is accurate?

6 Dating potential

Permian strata of the Anadarko Basin have been dated with invertebrate as well as vertebrate fauna, palynology, chemostratigraphy, magnetostratigraphy, and geochronology (tephras), with much work occurring relatively recently (e.g., Denison et al., 1998; Steiner, 2006; Tabor et al., 2011; Geissman et al., 2012; Foster, 2013; Tian et al., 2020). The strata in Permian basins of France accumulated in close proximity to major volcanic centers and thus contain abundant, dateable ash beds (e.g., Bruguier et al., 2003; Michel et al., 2015). We envision greatly refining age models through the Permian in both regions using a combination of the following approaches.

- Geochronology: ash beds are well known throughout the Carboniferous–Permian section of, e.g., the Lodève Basin (Michel et al., 2015), southern Paris Basin (Ducassou et al., 2019), Autun Basin (Pellenard et al., 2017), and associated Carboniferous–Permian basins of France and adjoining regions, and these should be especially visible in the core. Permian volcanism was

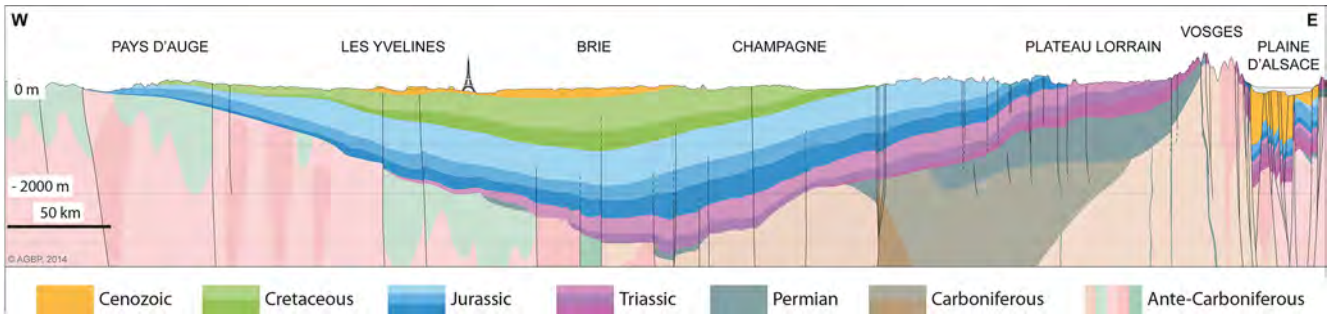

Figure 9. East–west transect through the Paris Basin.

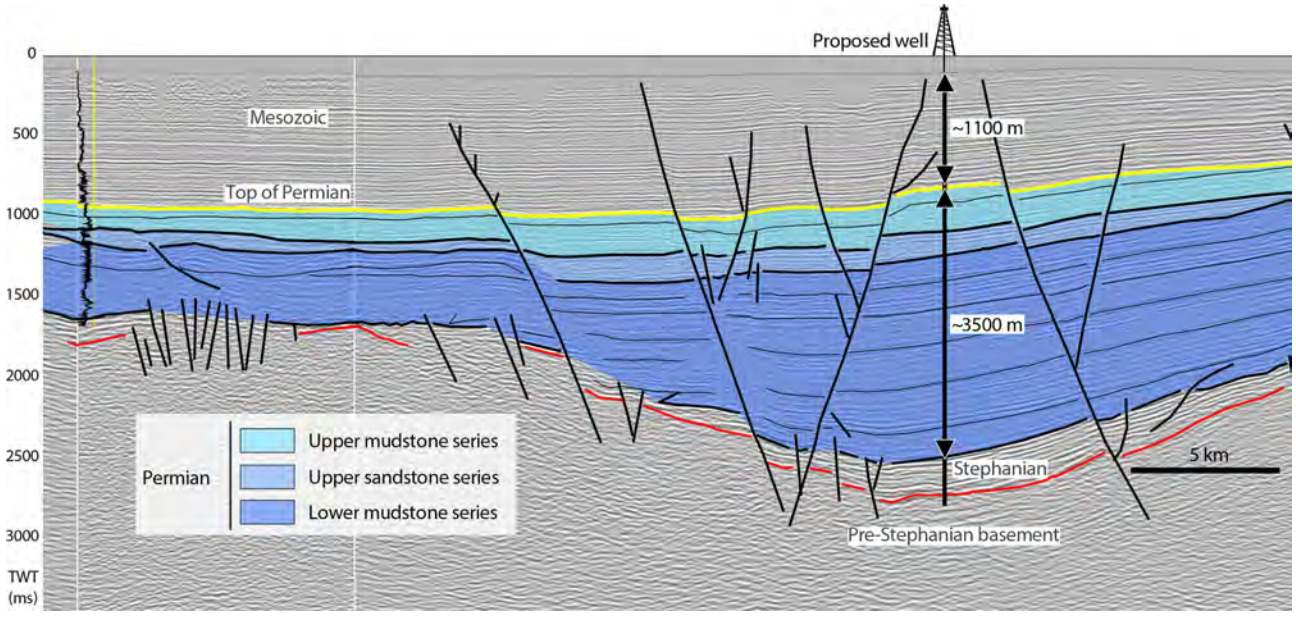

Figure 10. Southwestern Paris Basin (Brécy Basin) seismic line (line of section indicated by fine dotted line in the southern Paris Basin in Fig. 8). Seismic interpretation of lithologies and estimation of thicknesses from the main depocenter in the Brécy area, with a potential drill site indicated by the derrick symbol.

farther removed from the Anadarko Basin, but tephras (likely from Permian arc(s) of northwestern Mexico) are well recognized in the youngest Permian strata here (Tabor et al., 2011; Geissman et al., 2012) and have been long recognized by industry geologists in the Upper Pennsylvanian and Permian sections of the nearby Permian Basin in western Texas (personal communication, E. Kvale, 2015; S. Ruppel, 2016; Tian et al., 2020). High-resolution chemical abrasion ID-TIMS zircon geochronology can be employed to provide essential absolute ages, aid in correlations, and constrain sedimentation rates. Additionally, in regions distal to (but downwind of) volcanic eruption centers, detrital zircon geochronology can augment dating by recovering a cluster of the youngest zircons to provide a maximum age of deposition (e.g., Fan et al., 2015); detrital zircons are abundant in fine-grained Permian strata of both the Anadarko and French basins (Sweet et al., 2013; Foster et al., 2014; Pfeifer et al., 2016).

– Magnetostratigraphy: although the Permian encompasses the Kiaman Superchron, spanning from ~ 320 Ma (mid-Bashkirian) to ~ 265 Ma (late Wordian), the Permian of both the Anadarko and French Permian basins captures the termination of the superchron and the subsequent record of reversal stratigraphy (Steiner, 2006; Foster et al., 2014; Evans et al., 2014), recognizable even at these relatively low paleolatitudes. Recovery of continuous core with unambiguous stratigraphic superposition is critical for magnetostratigraphic efforts.

– Chemostratigraphy: Sr isotopes have been applied to carbonate and sulfate-rich strata in the Permian of the Anadarko Basin (Denison et al., 1998), but the po-

tential exists to build on this, particularly because of the dramatic decline in the $^{87}Sr/^{86}Sr$ through the proposed study interval. In addition, carbon isotope stratigraphy of early diagenetic dolomitic cements in the upper Permian and Permo-Triassic boundary strata from the nearby Palo Duro Basin suggest that carbon isotope stratigraphy may be a viable means of stratigraphic correlation for later Permian strata (Tabor et al., 2011).

– Paleontology: for the continental sections, paleobotanical specimen data can be quite useful and can be preserved in red beds. For example, for the Anadarko Basin, regional trends in the appearance and relative abundance of marker taxa from both wetland and seasonally dry assemblages can be tied to well-characterized sections in northern–central Texas and central New Mexico, thereby facilitating an understanding of regional vegetational patterns (e.g., DiMichele et al., 2006). The same is true for the pollen assemblages these plants produced. Pollen and spores (palynomorphs) are generally poorly preserved in red beds but common in non-oxidized sediments, including the Permian of the Anadarko Basin (e.g., Wilson, 1962), and can occur in evaporites intercalated within the red beds. The valves of Conchostracans (clam shrimps) are also well known and zoned from Permian red beds (Scholze and Schneider, 2015). For the limestone-bearing epeiric strata of the lowermost section in the Anadarko and French Permian basins, conodonts and fusulinids are abundant and well zoned at cyclothem-scale (substage) resolution. Sedimentological information, such as grain size (silts and clays) and sediment color (darker gray), can be used to identify the most promising facies for palynological analysis.

– Cyclostratigraphy: the emerging chronostratigraphic power of cyclostratigraphy will likely play an important role in dating the cores. Astronomical forcing is global, and so astronomically forced cyclostratigraphic patterns should be correlatable from marine to continental facies, in the same way that, for example, the Quaternary Chinese Loess Plateau magnetic susceptibility record (Fig. 12 in Ding et al., 2002) and the Lake Baikal biosilica record (Fig. 3 in Williams et al., 1997) correlate with the marine $\delta^{18}O$ record. For much (if not all) of the time coverage anticipated for these cores, there is either existing marine cyclostratigraphy tied to conodont zones and/or radioisotope dating (Wu et al., 2013, 2019; Fang et al., 2015, 2017), which makes this dating approach possible.

To tackle the problem of constructing a complete geochronology, proxy stratigraphic series constructed from the cores will be analyzed for plausible sediment accumulation rates that convert the proxy sequences into a time series with significant astronomical frequencies. This is the goal of the objective methods "average spectral misfit" (Meyers and Sageman, 2007) and "time optimization" (TimeOpt; Meyers, 2015, 2019). Successful ASM or TimeOpt applications can be used to extract the orbital eccentricity signal from the proxy sequences, which then can be matched to similarly processed marine cyclostratigraphy using statistical correlation methods such as Match (Lisiecki and Lisiecki, 2002) or HMM-Match (Lin et al., 2014). The results of these statistical correlations can be used to project marine biostratigraphic (conodont, fusulinid) zones, as well as other age data, into the core sections.

7 Concluding recommendations

The events of the Permian capture profoundly extreme swings in Earth system behavior, justifying a focus on paleoenvironmental conditions for this project, but with strong auxiliary science objectives. Two sites are admittedly inadequate to capture global conditions, but the proposed initial sites in the Anadarko and Paris basins offer unrivaled opportunities to establish stratigraphically complete global reference sections spanning equatorial Pangaea, to which various outcrop sections could be tied for building an integrated record. Abundant opportunities exist for science outreach and education associated with the remarkable events of the Permian – the icehouse-to-greenhouse transition, Great Dying, mega dust bowl and megamonsoon, Mars analog conditions, and the Permian megafauna of the equatorial region, in addition to the auxiliary science topics.

Data availability. No data sets were used in this article.

Supplement. The supplement related to this article is available online at: https://doi.org/10.5194/sd-28-93-2020-supplement.

Team list. Steve Adams (USA), Jennifer Auchter (USA), Cédric Bailly (France), Lucas Pinto Heckert Bastos (Brazil), Sietske Batenburg (France), Laurent Beccaletto (France), Heather Bedle (USA), Kathy Benison (USA), Alicia Bonar (USA), Didier Bonijoly (France), Sylvie Bourquin (France), Brett Carpenter (USA), Teodoriu Catalin (USA), Ying Cui (USA), Anne-Christine Da Silva (Belgium), Anne-Laure Decombeix (France), Jose. B. Diez (Spain), David Duarte (USA), Shannon Dulin (USA), Steve Dworkin (USA), Majie Fan (USA), Chris Fielding (USA), Tracy Frank (USA), Georg Feulner (Germany), Frédéric Fluteau (France), Sylvain Garrel (USA), Aude Gebelin (GB), Ute Gebhardt (Germany), Svetoslav Georgiev (USA), Charles Gilbert (USA), Martha-Elisabeth Gibson (GB), Annette E. Götz (Germany), Stéphane Guillot (France), Natsuko Hamamura (Japan), Mike Hamilton (Canada), Uli Harms (Germany), Nick Heavens (USA), Christoph Heubeck (Germany), Linda Hinnov (USA), Adam K. Huttenlocker (USA), Libby R. W. Ives (USA), Ken Johnson (USA), Sue Kairo (USA), Lee Krumholz (USA), Alex Lay (USA), Richard Lupia (USA),

Andy Madden (USA), Joe Mason (USA), Austin McGlannan (USA), Eduardo Luiz Menozzo Da Rosa (USA), Mathilde Mercuzot (France), Yuki Morono (Japan), Andrea Moscariello (Switzerland), Amy Myrbo (USA), Pierre Nehlig (France), Anders Noren (USA), Hendrik Nowak (Italy), Francisca Oboh-Ikuenobe (USA), Silvia Omodeo-Sale (Switzerland), Jeremy Owens (USA), Damien Pas (Belgium), Kathryn N. Pauls (USA), Lily Pfeifer (USA), Pierre Pellenard (France), Isabella Ploch (Poland), Stéphane Pochat (France), Marc Poujol (France), Nathan M. Rabideaux (USA), Jahandar Ramezani (USA), Troy Rasbury (USA), Zeev Reches (USA), Jean-Baptiste Regnet (France), Dean Richmond (USA), Philippe Robion (France), Lara Rodriguez-Delgado (USA), Alastair Ruffell (GB), Mehrdad Sardar Abadi (USA), Johann Schnyder (France), Lynn Soreghan (USA), Amalia Spina (Italy), Holly Stein (USA), Alisan Sweet (USA), Ryan Totten (USA), Arne Ulfers (Germany), Huaichun Wu (China), Chenliang Wu (China), Wan Yang (USA), Molly Yunker (USA), Richard Yuretich (USA), Jay Zambito (USA), Christian Zeeden (Germany).

Author contributions. GSS convened the workshop in Oklahoma, drafted the manuscript, and conducted revisions. LB and SB convened the workshop in Paris and contributed text and figures relevant to the Paris Basin and European geology. KCB, GF, NM, MH, NGH, LH, AH, CL, LSP, SP, MSA, and JZ contributed text and/or figure content. Participants at both workshops contributed intellectual input.

Competing interests. The authors declare that they have no conflict of interest.

Acknowledgements. We thank ICDP for workshop funding of the Deep Dust project and all participants for constructive input and enthusiasm. We especially thank Uli Harms for continued encouragement and constructive suggestions and PhD student Lily Pfeifer for essential help in organizing the Norman workshop. Gerilyn S. (Lynn) Soreghan also thanks staff from the OU School of Geosciences (especially Ashley Tullius), faculty of the OU History of Science Department (Kerry Magruder) for additional logistical help, and Terry Nitzel for land access. We thank the reviewers for many constructive comments on an earlier version of this paper. Those interested in participating in Deep Dust are invited to contact the authors. We thank Enervest (S. Adams), SEI, and CGG for seismic images used during the workshop.

Financial support. This research has been supported by the ICDP (DeepDust2019 grant).

Review statement. This paper was edited by Jan Behrmann and reviewed by Flavio Anselmetti and Paul Olsen.

References

Alroy, A., Aberhan, M., Bottjer, D. J., Foote, M., Fürsich, F. T., Harries, P. J., Hendy, A. J. W., Holland, S. M., Ivany, L. C., Kiessling, W., Kosnik, M. A., Marshall, C. R., McGowan, A. J., Miller, A. I., Olszewski, T. D., Patzkowsky, M. E., Peters, S. E., Villier, L., Wagner, P. J., Bonuso, N., Borkow, P. S., Brenneis, B., Clapham, M. E., Fall, L. M., Ferguson, C. A., Hanson, V. L., Krug, A. Z., Layou, K. M., Leckey, E. H., Nürnberg, S., Powers, C. M., Sessa, J. A., Simpson, C., Tomašových, A., and Visaggi, C. C.: Phanerozoic trends in the global diversity of marine invertebrates, Science, 321, 97–100, https://doi.org/10.1126/science.1156963, 2008.

Amstaetter, K., Borch, T., Larese-Casanova, P., and Kappler, A.: Redox transformation of arsenic by Fe(II)-activated goethite (α-FeOOH), Environ. Sci. Technol., 44, 102–108, 2010.

Andeskie, A. S. and Benison, K. C.: Using sedimentology to address the marine or continental origin of the Permian Hutchinson Salt Member of Kansas, Sedimentology, 67, 882–896, 2020.

Andeskie, A. S., Benison, K. C., Eichenlaub, L. A., and Raine, R.: Acid-saline-lake systems of the Triassic Mercia Mudstone Group, County Antrim, Northern Ireland, J. Sediment. Res., 88, 385–398, 2018.

Baptiste, J., Martelet, G., Faure, M., Beccaletto, L., Reninger, P.-A., Perrin, J., and Chen, Y.: Mapping of a buried basement combining aeromagnetic, gravity and petrophysical data: The substratum of southwest Paris Basin, France, Tectonophysics, 683, 333–348, 2016.

Barrell, J.: Relations between climate and terrestrial deposits, continued, J. Geol., 16, 255–295, 1908.

Beccaletto, L., Capar, L., Serrano, O., and Marc, S.: Structural evolution and sedimentary record of the Stephano-Permian basins occurring beneath the Mesozoic sedimentary cover in the southwestern Paris basin (France), Bull. Soc. Géol. France, 186, 429–450, 2015.

Becq-Giraudon, J.-F., Montenat, C., and Van Den Driessche, J.: Hercynian high-altitude phenomena in the French Massif Central, tectonic implications: Palaeogeogr. Palaeocl., 122, 227–241, 1996.

Begét, J. E. and Hawkins, D. B.: Influence of orbital parameters on Pleistocene loess deposition in central Alaska, Nature, 337, 151–153, 1989.

Benison, K. C. and Goldstein, R. H.: Permian paleoclimate data from fluid inclusions in halite, Chem. Geol., 154, 113–132, 1999.

Benison, K. C.: Acid saline fluid inclusions: Examples from modern and Permian extreme lake systems, Geofluids, 13, 579–593, https://doi.org/10.1111/gfl.12053, 2013.

Benison, K. C.: How to search for life in Martian chemical sediments and their fluid and solid inclusions using petrographic and spectroscopic methods, Front. Environ. Sci., 7, 108, https://doi.org/10.3389/fenvs.2019.00108, 2019.

Benison, K. C., Goldstein, R. H., Wopenka, B., Burruss, R. C., and Pasteris, J. D.: Extremely acid Permian lakes and ground waters in North America, Nature, 392, 911–914, 1998.

Benison, K. C., Zambito, J. J., and Knapp, J. P.: Contrasting siliciclastic-evaporite strata in subsurface and outcrop: An example from the Permian Nippewalla Group of Kansas, USA, J. Sediment. Res., 85, 626–645, https://doi.org/10.2110/jsr.2015.43, 2015.

Berner, R. A.: GEOCARBSULF – A combined model for Phanerozoic atmospheric O_2 and CO_2, Geochim. Cosmochim. Ac., 70, 5653–5664, 2006.

Berner, R. A.: The long-term carbon cycle, fossil fuels and atmospheric composition, Nature, 426, 323–326, 2003.

Blamey, N. J. F., Brand, U., Parnell, J., Spear, N., Lecuyer, C., Benison, K. C., Meng, F., and Ni, P.: Paradigm shift in determining Neoproterozoic atmospheric oxygen, Geology, 44, 651–654, 2016.

Bourquin, S., Bercovici, A., López-Gómez, J., Diez, J. B., Broutin, J., Ronchi, A., Durand, M., Arche, A., Linol, B., and Amour, F.: The Permian-Triassic transition and the beginning of the Mesozoic sedimentation at the Western peri-Tethyan domain scale: palaeogeographic maps and geodynamic implications, Palaeogeogr. Palaeocl., 299, 265–280, 2011.

Bourquin, S., Guillocheau, F., and Péron, S.: Braided river within an arid alluvial plain (example from the early Triassic, western German Basin): criteria of recognition and expression of stratigraphic cycles, Sedimentology, 56, 2235–2264, 2009.

Bourquin, S., Peron, S., and Durand, M.: Lower Triassic sequence stratigraphy of the western part of the Germanic Basin (west of Black Forest): fluvial system evolution through time and space, Sediment. Geol., 186, 187–211, 2006.

Bruguier, O., Becq-Giraudon, J. F., Champenois, M., Deloule, E., Ludden, J., and Mangin, D.: Application of in situ zircon geochronology and accessory phase chemistry to constraining basin development during post-collisional extension: a case study from the French Massif Central, Chem. Geol., 201, 319–336, https://doi.org/10.1016/j.chemgeo.2003.08.005, 2003.

Burg, J.-P., Van Den Driessche, J., and Brun, J.-P.: Syn- to post thickening extension in the Variscan belt of western Europe: modes and structural consequences, Géologie de la France, 3, 33–51, 1994.

Cao, W., Williams, S., Flament, N., Zahirovic, S., Scotese, C., and Müller, R.: Palaeolatitudinal distribution of lithologic indicators of climate in a palaeogeographic framework, Geol. Mag., 156, 331–354, https://doi.org/10.1017/S0016756818000110, 2019.

Chen, X., Nakata, N., Pennington, C., Haffener, J., Chang, J. C., and He, X.: The Pawnee earthquake as a result of the interplay among injection, faults and foreshocks, Sci. Rep., 7, 1–18, https://doi.org/10.1038/s41598-017-04992-z, 2017.

Chamberlin, T. C. and Salisbury, R. D.: Geology – Vol II Earth History, Henry Holt and Company, New York, 1905.

Champagnac, J.-D., Schluneggar, F., Norton, K., von Blanckenburg, F., Abbuhl, L. M., and Schwab, M.: Erosion-driven uplift of the modern Central Alps, Tectonophysics, 474, 236–249, https://doi.org/10.1016/j.tecto.2009.02.024, 2009.

Chen, J., Montañez, I. P., Qi, Y., Shen, S., and Wang, X.: Strontium and carbon isotopic evidence for decoupling of pCO2 from continental weathering at the apex of the late Paleozoic glaciation, Geology, 46, 395–398, 2018.

Cleal, C. J. and Thomas, B. A.: Palaeozoic tropical rainforests and their effect on global climates: is the past the key to the present?, Geobiology, 3, 13–31, 2005.

Denison, R. E., Kirkland, D. W., and Evans, R.: Using strontium isotopes to determine the age and origin of gypsum and anhydrite beds, J. Geol., 106, 1–17, 1998.

DiMichele, W. A., Tabor, N. J., Chaney, D. S., and Nelson, W. J.: From wetlands to wet spots: environmental tracking and the fate of Carboniferous elements in Early Permian tropical floras, in: Wetlands through time, edited by: Greb, S. F. and DiMichele, W. A., Geol. Soc. Am. Spec. Pap., 399, 223–248, 2006.

Ding, Z. L., Derbyshire, E., Yang, S. L., Yu, Z. W., Xiong, S. F., and Liu, T. S.: Stacked 2.6-Ma grain size record from the Chinese loess based on five sections and correlation with the deep-sea $\partial^{18}O$ record, Paleoceanography, 17, 5-1–5-21, https://doi.org/10.1029/2001PA000725, 2002.

Domeier, M. and Torsvik, T. H.: Plate tectonics in the late Paleozoic: Geosci. Front., 5, 303–350, https://doi.org/10.1016/j.gsf.2014.01.002, 2014.

Doornenbal, J. C. and Stevenson, A. G. (Eds.): Petroleum Geological Atlas of the Southern Permian Basin Area. Houten, The Netherlands, EAGE, p. 342, 2010.

Dubiel, R. F. and Smoot, J. P.: Criteria for interpreting paleoclimate from red beds – a tool for Pangean reconstructions, in: Pangea: Global Environments and Resources, edited by: Embry, A. F., Beauchamp, B., and Glass, B. J., Canad. Soc. Petrol. Geol. Mem., 17, 295–310, 1994.

Ducassou, C., Mercuzot, M., Bourquin, S., Rossignol, C., Beccaletto, L., Pierson-Wickmann, A. C., Pellenard, P., Poujol, M., and Hue, C.: Sedimentology and U-Pb dating of Carboniferous to Permian continental series of the northern Massif Central (France): local palaeogeographic evolution and larger scale correlations, Palaeogeogr. Palaeocl., 533, 109228, https://doi.org/10.1016/j.palaeo.2019.06.001, 2019.

Dusséaux, C.: Topographic reconstructions of the Variscan belt of Western Europe through the study of fossil hydrothermal systems, PhD Thesis, University of Plymouth, 2019.

EL Hadi, H., Simancas, J. F., Tahiri, A., González-Lodeiro, F., Azor, A., and Martínez-Poyatos, D.: Comparative review of the Variscan granitoids of Morocco and Iberia: proposal of a broad zonation, Geodin. Acta, 19, 103–116, 2006.

Ellsworth, W. L.: Injection-induced earthquakes, Science, 341, https://doi.org/10.1126/science.1225942, 2013.

Elrick, M. and Scott, L. A.: Carbon and oxygen isotope evidence for high-frequency (10^4–10^5 yr) and My-scale glacio-eustasy in Middle Pennsylvanian cyclic carbonates (Gray Mesa Formation), central New Mexico, Palaeogeogr. Palaeocl., 285, 307–320, 2010.

Elrick, M., Reardon, D., Labor, W., Martin, J., Desrochers, A., and Pope, M.: Orbital-scale climate change and glacioeustasy during the Early Late Ordovician (Pre-Hirnantian) determined from $\partial^{18}O$ values in marine apatite, Geology, 41, 775–778, https://doi.org/10.1130/G34363.1, 2013.

Ernst, R. E. and Buchan, K. L.: Large mafic magmatic events through time and links to mantle-plume heads, in: Mantle Plumes: Their Identification Through Time, edited by: Ernst, R. E. and Buchan, K. L., Boulder, Colorado, Geol. Soc. Amer. Spec. Pap., 352, 483–575, 2001.

Erwin, D. H.: The Permo–Triassic extinction, Nature, 367, 231–236, 1994.

Erwin, D. H.: Extinction! How Life Nearly Ended 250 Million Years ago: Princeton University Press, 2006.

Evans, D. A. D.: A fundamental Precambrian-Phanerozoic shift in Earth's glacial style?, Tectonophysics, 375, 353–385, 2003.

Evans, M. E., Pavlov, V., Veselovsky, R., and Fetisova, A.: Late Permian paleomagnetic results from the Lodève, Le Luc, and Bas-Argens Basins (southern France): Magnetostratigraphy and geo-

magnetic field morphology, Phys. Earth Planet. Inter., 237, 18–24, https://doi.org/10.1016/j.pepi.2014.09.002, 2014.

Falcon-Lang, H. J. and DiMichele, W. A.: What happened to the coal forests during Pennsylvanian glacial phases?, Palaios, 25, 611–617, 2010.

Fang, Q., Wu, H. C., Hinnov, L. A., Jing, X. C., Wang, X. L., Yang, T. S., Li, H. Y., and Zhang, S. H.: Astronomical cycles of Middle Permian Maokou Formation in South China and their implications for sequence stratigraphy and paleoclimate, Palaeogeogr. Palaeocl., 474, 130–139, https://doi.org/10.1016/j.palaeo.2016.07.037, 2017.

Fang, Q., Wu, H., Hinnov, L. A., Jing, X., Wang, X., and Jiang, Q.: Geological evidence for the chaotic behavior of the planets and its constraints on the third order eustatic sequences at the end of the Late Paleozoic Ice Age, Palaeogeogr. Palaeocl., 440, 848–859, https://doi.org/10.1016/j.palaeo.2015.10.014, 2015.

Farmer, J. D., Bell III., J. F., Benison, K. C., Boynton, W. V., Cady, S. L., Ferris, F. G., MacPherson, D., Race, M. S., Thiemens, M. H., and Wadhwa, M.: Assessment of planetary protection requirements for Mars sample return missions, Space Studies Board, National Research Council, National Academy Press, Washington, D.C., 80 pp., 2009.

Faure, M.: Late orogenic Carboniferous extensions in the Variscan French Massif Central, Tectonics, 14, 132–153, 1995.

Feulner, G.: Formation of most of our coal brought Earth close to global glaciation, P. Natl. Acad. Sci. USA, 114, 11333–11337, https://doi.org/10.1073/pnas.1712062114, 2017.

Fielding, C. R., Frank, T. D., and Isbell, J. L.: The late Paleozoic ice age – a review of current understanding and synthesis of global climate patterns, 441, 343–354, 2008.

Foght, J. M., Gieg, L. M., and Siddique, T.: The microbiology of oil sands tailings: past, present, future, FEMS Microbiol. Ecol., 93, fix034, https://doi.org/10.1093/femsec/fix034, 2017.

Foster, G. L., Royer, D. L., and Lunt, D. J.: Future climate forcing potentially without precedent in the last 420 million years, Nat. Commun., 8, 14845, https://doi.org/10.1038/ncomms14845, 2017.

Foster, T. M., Soreghan, G. S., Soreghan, M. J., Benison, K. C., and Elmore, R. D.: Climatic and paleogeographic significance of eolian sediment in the Middle Permian Dog Creek Shale (Midcontinent U.S.). Palaeogeogr. Palaeocl., 402, 12–29, https://doi.org/10.1016/j.palaeo.2014.02.031, 2014.

Foulger, G. R., Wilson, M. P., Gluyas, J. G., Julian, B. R., and Davies, R. J.: Global review of human-induced earthquakes, Earth Sci. Rev., 178, 438–514. https://doi.org/10.1016/j.earscirev.2017.07.008, 2018.

Gastaldo, R., DiMichele, W., and Pfefferkorn, H.: Out of the icehouse into the greenhouse-A late Paleozoic analog for modern global vegetational change, GSA Today, 6, 1–7, 1996.

Geissman, J. W., Renne, P., Mitchell III., W. S., and Tabor, N. J.: Integrated magnetostratigraphy and geochronology of the "Ochoan" Quartermaster Formation of north Texas, Abstracts with Programs, Geol. Soc. Amer., 44, 29, 2012.

Giles, J. M., Soreghan, M. J., Benison, K. C., Soreghan, G. S., and Hasiotis, S. T.: Lakes, loess, and paleosols In the Permian Wellington Formation of Oklahoma, U.S.A.: Implications for paleoclimate and paleogeography of the Midcontinent, J. Sediment. Res., 83, 825–846, https://doi.org/10.2110/jsr.2013.59, 2013.

Glasspool, I. J. and Scott, A. C.: Phanerozoic concentrations of atmospheric oxygen reconstructed from sedimentary charcoal, Nat. Geosci., 3, 627–630, 2010.

Goddéris, Y.: Onset and ending of the late Palaeozoic ice age triggered by tectonically paced rock weathering, Nat. Geosci., 10, 382–388, 2017.

Hamamura, N., Olson, S. H., Ward, D. W., and Inskeep, W. P.: Diversity and functional analysis of bacterial communities associated with natural hydrocarbon seeps in acidic soils at Rainbow Springs, Yellowstone National Park, Appl. Environ. Microbiol., 71, 5943–5950, 2005.

Haq, B. U. and Schutter, S. R.: A chronology of Paleozoic sea-level changes, Science, 322, 64–68, 2008.

Hay, W. W., Migdisov, A., Balukhovsky, A. N., Wold, C. N., Flogel, S., and Soding, E.: Evaporites and the salinity of the ocean during the Phanerozoic: Implications for climate, ocean circulation and Life, Palaeogeogr. Palaeocl., 240, 3–46, https://doi.org/10.1016/j.palaeo.2006.03.044, 2006.

Heavens, N. G., Shields, C. A., and Mahowald, N. M.: Sensitivity of a deep time climate simulation to aerosol prescription, J. Adv. Model. Earth Syst., 4, M11002, https://doi.org/10.1029/2012MS000166, 2012.

Heckel, P. H.: Evidence for global (glacial-eustatic) control over upper Carboniferous (Pennsylvanian) cyclothems in midcontinent North America, Geol. Soc. London Spec. Publ., 55, 35–47, 1990.

Hentz, T. F.: Sequence stratigraphy of the Upper Pennsylvanian Cleveland Formation: A major tight-gas sandstone, western Anadarko Basin, Texas Panhandle, Am. Assoc. Pet. Geol. Bull., 78, 569–595, 1994.

Huang, H., Gao, Y., Jones, M. M., Tao, H., Alan, R., Ibarra, D. E., Huaichun, W., and Wang, C.: Astronomical forcing of Middle Permian terrestrial climate recorded in a large paleolake in northwestern China, Palaeogeogr. Palaeocl., 550, https://doi.org/10.1016/j.palaeo.2020.109735, 2020.

Johnson, K. S.: Anadarko Basin Symposium, Oklahoma Geological Survey, 90, 1–291, 1988.

Juncal, M., Bourquin, S., Beccaletto, L., and Diez, J.: New sedimentological and palynological data from the Permian and Triassic series of the Sancerre-Couy core, Paris Basin, France, Geobios, 51, 517–535, https://doi.org/10.1016/j.geobios.2018.06.007, 2018.

Keranen, K. M. and Weingarten, M.: Induced seismicity, Ann. Rev. Earth Planet. Sci., 46, 149–174, https://doi.org/10.1146/annurev-earth-082517-010054, 2018.

Kiessling, W.: Long-term relationships between ecological stability and biodiversity in Phanerozoic reefs, Nature, 433, 410–413, https://doi.org/10.1038/nature03152, 2005.

Kutzbach., J. E. and Gallimore, R. G.: Pangean climates: megamonsoons of the megacontinent, J. Geophys. Res., 94, 3341–3357, 1989.

Langenbruch, C., Weingarten, M., and Zoback, M. D.: Physics-based forecasting of man-made earthquake hazards in Oklahoma and Kansas, Nat. Commun., 9, 1–10, https://doi.org/10.1038/s41467-018-06167-4, 2018.

Lee, L. A., Reddington, C. L., and Carslaw, K. S.: On the relationship between aerosol model uncertainty and radiative forcing uncertainty, P. Natl. Acad. Sci. USA, 113, 5820–5827, https://doi.org/10.1073/pnas.1507050113, 2016.

Lin, L., Khider, D., Lisiecki, L. E., and Lawrence, C. E.: Probabilistic sequence alignment of stratigraphic records, Paleoceanography, 29, 976–989, https://doi.org/10.1002/2014PA002713, 2014.

Lisiecki, L. E. and Lisiecki, P. A.: Application of dynamic programming to the correlation of paleoclimate records, Paleoceanography, 17, 1049, https://doi.org/10.1029/2001PA000733, 2002.

LIP Commission, http://www.largeigneousprovinces.org/, last access: August 2020.

Liu, X., Xu, T., and Liu, T.: The Chinese loess in Xifeng, II. A study of anisotropy of magnetic susceptibility of loess from Xifeng, Geophys. J. Int., 92, 349–353, https://doi.org/10.1111/j.1365-246X.1988.tb01147.x, 1999.

Luo, Q., Krumholz, L. R., Najar, F. Z., Peacock, A. D., Roe, B. A., White, D. C., and Elshahed, M. S.: Diversity of the microeukaryotic community in sulfide-rich Zodletone Spring (Oklahoma), Appl. Environ. Microbiol., 71, 6175–6184, https://doi.org/10.1128/AEM.71.10.6175-6184.2005, 2005.

Maher, B. A.: Palaeoclimatic records of the loess/paleosol sequences of the Chinese Loess Plateau, Quaternary Sci. Rev., 154, 23–84, 2016.

McArthur, J. M., Howarth, R. J., and Bailey, T. R.: Strontium isotope stratigraphy: LOWESS version 3: best fit to the marine Sr-isotope curve for 0–509 Ma and accompanying look-up table for deriving numerical age, J. Geol., 109, 155–170, 2001.

Menard, G. and Molnar, P.: Collapse of a Hercynian Tibetan Plateau into a late Palaeozoic European Basin and Range province, Nature, 334, 235–237, 1988.

Mercuzot, M.: Reconstitutions paléoenvironnementales et paléoclimatiques en contexte tardi-orogénique des bassins Carbonifères-Permiens du nord du Massif Central, France, PhD thesis, University of Rennes, expected October 2020.

Mercuzot, M., Bourquin, S., Beccaletto, L., Ducassou, C., Rubi, R., and Pellenard, P.: Palaeoenvironmental reconstitutions at the Carboniferous-Permian transition south of the Paris Basin, France: implications on the stratigraphic evolution and basin geometry, Int. J. Earth Sci., accepted, 2020.

Meyers, S. R.: Cyclostratigraphy and the problem of astrochronologic testing, Earth Sci. Rev., 190, 190–223, https://doi.org/10.1016/j.earscirev.2018.11.015, 2019.

Meyers, S. R.: The evaluation of eccentricity-related amplitude modulation and bundling in paleoclimate data: an inverse approach for astrochronologic testing and time scale optimization, Paleoceanography, 30, 1625–1640, https://doi.org/10.1002/2015PA002850, 2015.

Meyers, S. R. and Sageman, B. B.: Quantification of deep-time orbital forcing by average spectral misfit, Am. J. Sci., 307, 773–792, https://doi.org/10.2475/05.2007.01, 2007.

Michel, L. A., Tabor, N. J., Montanez, I. P., Schmitz, M., and Davydov, V. I.: Chronostratigraphy and paleoclimatology of the Lodéve Basin, France: Evidence for a pan-tropical aridification event across the Carboniferous – Permian boundary, Palaeogeogr. Palaeocl., 430, 118–131, https://doi.org/10.1016/j.palaeo.2015.03.020, 2015.

Molnar, P. and England, P.: Late Cenozoic uplift of mountain ranges and global climate change: chicken or egg?, Nature, 346, 29–34, 1990.

Montañez, I. P., Tabor, N. J., Niemeier, D., DiMichele, W. A., Frank, T. D., Fielding, C. R., Isbell, J. L., Birgenheier, L. P., and Rygel, M.: CO_2-forced climate and vegetation instability during Late Paleozoic deglaciation, Science, 315, 87–91, 2007.

Montañez, I. P., McElwain, J. C., Poulsen, C. J., White, J. D., DiMichele, W. A., Wilson, J. P., Griggs, G., and Hren, M. T.: Climate, pCO2 and terrestrial carbon cycle linkages during late Palaeozoic glacial-interglacial cycles, Nat. Geosci., 9, 824–828, 2016.

Muttoni, G. and Kent, D. V.: Adrea as promontory of Africa and its conceptual role in the Tethys twist and Pangea B to Pangea A transformation in the Permian, Rivista Italiana di Paleontogia e Stratigrafia, 125, 249–269, 2019.

Nawrocki, J., Polechonska, O., Bogucki, A., and Łanczont, M.: Palaeowind directions recorded in the youngest loess in Poland and western Ukraine as derived from anisotropy of magnetic susceptibility measurements, Boreas, 35, 266–271, https://doi.org/10.1111/j.1502-3885.2006.tb01156.x, 2006.

Nelsen, M. P., DiMichele, W. A., Peters, S. E., and Boyce, C. K.: Delayed fungal evolution did not cause the Paleozoic peak in coal production, P. Natl. Acad. Sci. USA, 113, 2442–2447, 2016.

NRC (National Research Council), Understanding Earth's Deep Past – Lessons for Our Climate Future, National Academies Press, Washington, D.C., 194, 2011.

Pardo, J. D., Small, B. J., Milner, A. R., and Huttenlocker, A. K.: Carboniferous-Permian climate change constrained by early land vertebrate radiations, Nature Ecol. Evol., 3, 200–206, https://doi.org/10.1038/s41559-018-0776-z, 2019.

Parrish, J. T.: Paleoclimate of the supercontinent Pangea, J. Geology, 101, 215–233, 1993.

Parrish, J. T.: Interpreting Pre-Quaternary Climate from the Geologic Record, Columbia University Press, New York, 1998.

Payne, M. E. and Clapham, J. L.: End-Permian mass extinction in the oceans: an ancient analog for the twenty-first century?, Ann. Rev. Earth Planet. Sci., 40, 89–111, https://doi.org/10.1146/annurev-earth-042711-105329, 2012.

Pellenard, P., Gand, G., Schmitz, M, Galtier, J., Broutin, J., and Stéyer, J. S.: High-precision U-Pb zircon ages for explosive volcanism calibrating the NW European continental Autunian stratotype, Gondwana Res., 51, 118–136, 2017.

Pfeifer, L. S., Soreghan, G. S., Pochat, S., Van Den Driessche, J., and Thomson, S. N.: Permian exhumation of the Montagne Noire core complex recorded in the Graissessac-Lodève Basin, France, Basin Research, 30, 1–14, https://doi.org/10.1111/bre.12197, 2016.

Pfeifer, L. S., Soreghan, G. S., Pochat, S., and Van Den Driessche, J.: Paleoclimatic significance of Permian loess in eastern equatorial Pangea: The Lodève Basin (France), Geol. Soc. Am. Bull., https://doi.org/10.1130/B35590.1, 2020a.

Pfeifer, L. S., Hinnov, L. A., Zeeden, C., Rolf, C., Laag, C., and Soreghan, G. S.: Rock magnetic cyclostratigraphy of Permian loess in eastern equatorial Pangea (Salagou Formation, south-central France), Front. Earth Sci., 8, 241, https://doi.org/10.3389/feart.2020.00241, 2020b.

Pochat, S. and Van Den Driessche, J.: Filling sequence in Late Paleozoic continental basins: A chimera of climate change? A new light shed given by the Graissessac–Lodève basin (SE France), Palaeogeogr. Palaeocl., 302, 170–186, 2011.

Praeg, D.: Diachronous Variscan late-orogenic collapse as a response to multiple detachments; a view from the internides in

France to the foreland in the Irish Sea, Geol. Soc. Spec. Pub., 223, 89–138, 2004.

Reiners, P. W. and Brandon, M. T.: Using thermochronology to understand orogenic erosion, Ann. Rev. Earth Planet. Sci., 34, 419–466, 2006.

Rondot, A.: An Integrated Geophysical Analysis of Crustal Structure in the Wichita Uplift Region of Southern Oklahoma. M.S. Thesis, Norman, University of Oklahoma, 107 pp., 2009.

Saltzman, M. R. and Thomas, E.: Carbon isotope stratigraphy, in: The Geologic Time Scale 2012, edited by: Gradstein, F. M., Ogg, J. G., Schmitz, M., and Ogg, G., Elsevier, 207–232, 2012.

Sardar Abadi, M., Owens, J. D., Liu, X., Them II, T. R., Cui, X., Heavens, N. G., and Soreghan, G. S.: Atmospheric dust stimulated marine primary productivity during Earth's penultimate icehouse, Geology, 480, 247–251, https://doi.org/10.1130/G46977.1, 2020.

Satterfield, C. L., Lowenstein, T. K., Vreeland, R. H., Rosenzweig, W. D., and Powers, D. W.: New evidence for 250 Ma age of halotolerant bacterium from a Permian salt crystal, Geology, 33, 265–268, 2005.

Scholze, F. and Schneider, J. W.: Improved methodology of "conchostracan" (Crustacea: Branchiopoda) classification for biostratigraphy, Newsletters on Strat., 48, 287–298, 2015.

Schwartz, S. E. and Andreae, M. O.: Uncertainty in climate change caused by aerosols, Science, 272, 1121–1122, 1996.

Sheldon, N. D.: Do red beds indicate paleoclimatic conditions?: A Permian case study, Palaeogeogr. Palaeocl., 228, 305–319, 2005.

Soreghan, G. S., Soreghan, M. J., Poulsen, C. E., Young, R. A., Eble, C., Sweet, D. E., and Davogustto, O.: Anomalous cold in the Pangaean tropics, Geology, 36, 659–662, 2008a.

Soreghan, G. S., Soreghan, M. J., and Hamilton, M. A.: Origin and significance of loess in late Paleozoic western Pangaea: A record of tropical cold?, Palaeogeogr. Palaeocl., 268, 234–259, https://doi.org/10.1016/j.palaeo.2008.03.050, 2008b.

Soreghan, G. S., Keller, G. R., Gilbert, M. C., Chase, C. G., and Sweet, D.: Load-induced subsidence of the Ancestral Rocky Mountains recorded by preservation of Permian landscapes, Geosphere, 8, 654–668, https://doi.org/10.1130/GES00681.S1, 2012.

Soreghan, G. S., Sweet, D. E., and Heavens, N. G.: Upland glaciation in tropical Pangaea: Geologic evidence and implications for Late Paleozoic climate modeling, J. Geology, 122, 137–163, 2014.

Soreghan, G. S., Heavens, N. G., Hinnov, L. A., Aciego, S. M., and Simpson, C.: Reconstructing the dust cycle in deep time: The case of the Late Paleozoic icehouse, in: Earth-Life Transitions – Paleobiology in the Context of Earth System Evolution: The Paleontological Society Papers, edited by: Polly, P. D. and Fox, D. L., 21, 83–120, 2015a.

Soreghan, G. S., Benison, K. C., Foster, T. M., Zambito, J., and Soreghan, M. J.: The paleoclimatic and geochronologic utility of coring red beds and evaporites: a case study from the RKB core (Permian, Kansas, USA), Int. J. Earth Sci., 104, 1–17, https://doi.org/10.1007/s00531-014-1070-1, 2015b.

Soreghan, G. S, Soreghan, M. J., and Heavens, N. G.: Explosive volcanism as a key driver of the Late Paleozoic Ice Age, Geology, 47, 600–604, https://doi.org/10.1130/G46349.1, 2019.

Soreghan, M. J., Soreghan, G. S., and Hamilton, M. A.: Paleowinds inferred from detrital-zircon geochronology of upper Paleozoic loessite, western equatorial Pangea, Geology, 30, 695–698, 2002.

Soreghan, M. J., Heavens, N. G., Soreghan, G. S., Link, P. K., and Hamilton, M. A.: Abrupt and high-magnitude changes in atmospheric circulation recorded in the Permian Maroon Formation, tropical Pangaea, Geol. Soc. Am. Bull., 126, 569–584, https://doi.org/10.1130/B30840.1, 2014.

Soreghan, M. J., Swift, M. M., and Soreghan, G. S.: Provenance of Permian eolian and related strata in the North American Midcontinent: Tectonic and climatic controls on sediment dispersal in western tropical Pangea, in: Tectonics, Sedimentary Basins, and Provenance: A Celebration of the Career of William R. Dickinson, edited by: Ingersoll, R. V., Lawton, T. F., and Graham, S. A., Geol. Soc. Am. Spec. Pap., 540, 661–687, https://doi.org/10.1130/SPE540, 2018.

Steiner, M. B.: The magnetic polarity time scale across the Permian–Triassic boundary, in: Non-Marine Permian Biostratigraphy and Biochronology, edited by: Lucas, S. G., Cassinis, G., and Schneider, J. W., Geol. Soc. London, Spec. Pub., 265, 15–38, 2006.

Sternai, P., Herman, F., Champagnac, J. D., Fox, M., Salcher, B., and Willett, S. D.: Pre-glacial topography of the European Alps, Geology, 40, 1067–1070, https://doi.org/10.1130/G33540.1, 2012.

Sues, H.-D. and Reisz, R. R.: Origins and early evolution of herbivory in tetrapods, Trends Ecol. Evol., 13, 141–145, 1998.

Sun, Y., Lu, H., and An, Z.: Grain size of loess, palaeosol and Red Clay deposits on the Chinese Loess Plateau: Significance for understanding pedogenic alteration and palaeomonsoon evolution, Palaeogeogr. Palaeocl., 241, 129–138, 2006.

Sur, S., Owens, J. D., Soreghan, G. S., Lyons, T. W., Raiswell, R., Heavens, N. G., and Mahowald, N. M.: Extreme eolian delivery of reactive iron to late Paleozoic icehouse seas, Geology, 43, 1099–1102, https://doi.org/10.1130/G37226.1, 2015.

Svensen, H., Planke, S., Polozov, A. G., Schmidbauer, N., Corfu, F., Podladchikov, Y. Y., and Jamtveit, B.: Siberian gas venting and the end-Permian environmental crisis, Earth Planet. Sci. Lett., 277, 490–500, 2009.

Sweet, A. C., Soreghan, G. S., Sweet, D. E., Soreghan, M. J., and Madden, A. S.: Permian dust in Oklahoma: Source and origin for middle Permian (Flowerpot-Blaine) redbeds in western tropical Pangaea, Sediment. Geol., 284–285, 181–196, doi.org/10.1016/j.sedgeo.2012.12.006, 2013.

Tabor, N. J. and Montanez, I. P.: Shifts in late Paleozoic atmospheric circulation over western equatorial Pangea: insights from pedogenic mineral ∂^{18}O compositions, Geology, 30, 1127–1130, 2002.

Tabor, N. J. and Poulsen, C. J.: Palaeoclimate across the Late Pennsylvanian–Early Permian tropical palaeolatitudes: A review of climate indicators, their distribution, and relation to palaeophysiographic climate factors: Palaeogeogr. Palaeocl., 268, 293–310, 2008.

Tabor, N. J., Myers, T. S., Mack, G. H., Looy, C. V., and Renne, P. R.: Quatermaster Formation of north Texas, USA; Part I, Litho- and chemostratigraphy, Abstracts With Programs, Geol. Soc. Am., 43, 383, 2011.

Tabor, N. J. and Myers, T. S.: Paleosols as indicators of paleoenvironment and paleoclimate, Annual Rev. Earth Planet. Sci., 43, 333–361, 2015.

Theiling, B. P., Elrick, M., and Asmerom, Y.: Increased continental weathering flux during orbital-scale sea-level highstands: Evidence from Nd and O isotope trends in middle Pennsylvanian cyclic carbonates, Palaeogeogr. Palaeocl., 342–343, 17–26, https://doi.org/10.1016/j.palaeo.2012.04.017, 2012.

Tian, H., Fan, M., Chamberlain, K. R., Waite, L., and Stern, R. J.: Zircon LA-ICPMS and CA-TIMS U-PB dates of late Paleozoic volcanic tuffs in the Midland Basin, West Texas, Abstracts with Programs, Geol. Soc. Am., 52, 1, https://doi.org/10.1130/abs/2020SC-343618, 2020.

Tomezzoli, R. N., Tickj, H., Rapalini, A. E., Gallo, L. C., Cristallini, E. O., Arzadún, G., and Chemale Jr., F.: Gondwana's Apparent Polar Wander Path during the Permian – new insights from South America, Sci. Reports, 8, 8436, https://doi.org/10.1038/s41598-018-25873-z, 2018.

Twitchett, R. J., Looy, C. V., Morante, R., Visscher, H., and Wignall, P. B.: Rapid and synchronous collapse of marine and terrestrial ecosystems during the end-Permian biotic crisis, Geology, 29, 351–354, 2001.

Valentino, D. W. and Gates, A. E.: Asynchronous extensional collapse of a transpressional orogen: the Alleghanian central Appalachian Piedmont, USA, J. Geodyn., 31, 145–167, 2001.

Walker, T. R.: Formation of red beds in modern and ancient deserts, Geol. Soc. Am. Bull., 78, 353–68, 1967.

Walker, T. R.: Formation of red beds in moist tropical climates: A hypothesis, Geol. Soc. Am. Bull., 85, 633–638, 1974.

Warren, J. K.: Evaporites, A Geological Compendium, Second Edition, Springer International Publishing AG, Switzerland, p. 1813, 2016.

Wignall, P. B. and Twitchett, R. J.: Oceanic anoxia and the end Permian mass extinction, Science, 272, 1155–1158, https://doi.org/10.1126/science.272.5265.1155 1996.

Williams, D. F., Peck, J., Karabanov, E. B., Prokopenko, A. A., Kravchinsky, B., King, J., and Kuzmin, M. I.: Lake Baikal record of continental climate response to orbital insolation during the past 5 million years, Science, 278, 1114–1117, https://doi.org/10.1126/science.278.5340.1114, 1997.

Wilson, L. R.: A Permian fungus spore type from the Flowerpot Formation of Oklahoma, Oklahoma Geology Notes, 22, 91–96, 1962.

Witt, W. J.: Cross section of Oklahoma from SW to NE corners of state: Oklahoma City Geological Society, Oklahoma, 1971.

Wu, H., Fang, Q., Wang, X., Hinnov, L. A., Qi, Y., Shen, S., Yang, T., Li, H., Chen, J., and Zhang, S. A.: $\sim$ 34 M.y. astronomical time scale for the uppermost Mississippian through Pennsylvanian of the Carboniferous System of the Paleo-Tethyan Realm, Geology, 47, 83–86, https://doi.org/10.1130/G45461.1, 2019.

Wu, H., Zhang, S., Hinnov, L. A., Feng, Q., Jiang, G., Li, H., and Yang, T.: Time-calibration of Milankovitch cycles in the Late Permian, Nat. Commun., 4, 2452, https://doi.org/10.1038/ncomms3452, 2013.

Yang, S. and Ding, Z.: A 249 kyr stack of eight loess grain size records from northern China documenting millennial-scale climate variability, Geochem. Geophy., Geosy., 15, 798–814, https://doi.org/10.1002/2013GC005113, 2013.

Zambito, J. J. and Benison, K. C.: Extremely high temperatures and paleoclimate trends recorded in Permian ephemeral lake halite, Geology, 41, 587–590, https://doi.org/10.1130/G34078.1, 2013.

Zhang, R., Kravchinsky, V. A., Zhu, R., and Yue, L.: Paleomonsoon route reconstruction along a W-E transect in the Chinese Loess Plateau using the anisotropy of magnetic susceptibility: Summer monsoon model, Earth Planet. Sci. Lett., 299, 436–446, https://doi.org/10.1016/j.epsl.2010.09.026, 2010.

Zhu, R., Liu, Q., and Jackson, M. J.: Paleoenvironmental significance of the magnetic fabrics in Chinese loess-paleosol since the last interglacial (< 130 ka), Earth Planet. Sci. Lett., 221, 55–69, https://doi.org/10.1016/S0012-821X(04)00103-7, 2004.

Schedules

Due to the Corona pandemic situation, several expeditions and drilling projects are postponed until further notice.

IODP – Expedition schedule http://www.iodp.org/expeditions/

USIO operations	Platform	Dates	Port of origin
1 Exp 390C: South Atlantic Transect Reentry Installations	JOIDES Resolution	5 Oct–5 Dec 2020	Rio de Janeiro
2 Exp 395: Reykjanes Mantle Convection and Climate	JOIDES Resolution	6 Jun–6 Aug 2021	Reykjavik

ICDP – Project schedule http://www.icdp-online.org/projects/

ICDP project	Drilling dates	Location
1 JET	Oct–Dec 2020	Prees, UK
2 GRIND	Spring 2021	Namibia
3 STAR	Spring–Summer 2021	Central Apennines, Italy
4 Trans-Amazon	Spring–Summer 2021	Brazil (multiple locations)

Locations

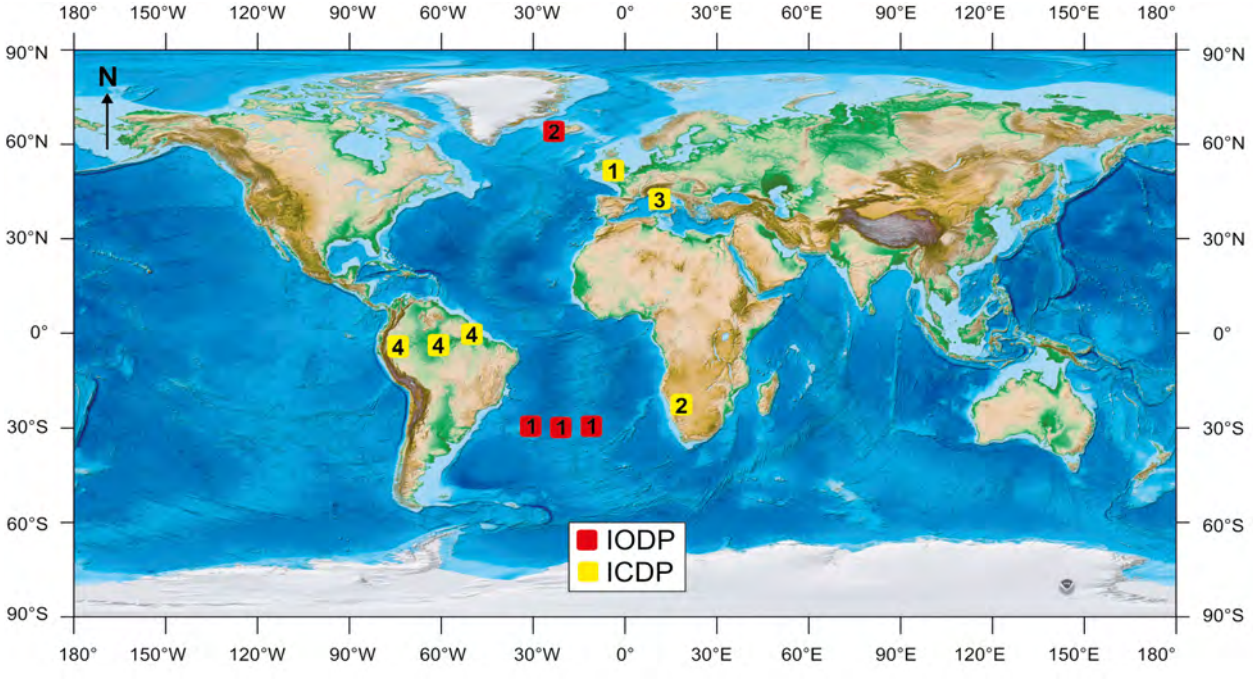

Topographic/Bathymetric world map with courtesy from NOAA (Amante, C. and B.W. Eakins, 2009. ETOPO1 1 Arc-Minute Global Relief Model: Procedures, Data Sources and Analysis. NOAA Technical Memorandum NESDIS NGDC-24. National Geophysical Data Center, NOAA. doi:10.7289/V5C8276M).

New ICDP Science Plan

The new Science Plan of the International Continental Scientific Drilling Program, ICDP was released on 1st October 2020. Its overarching motto is "Billions of Years of Earth Evolution", outlining the scientific objectives of continental scientific drilling for the coming decade. The four key scientific themes are: Geodynamic Processes, Geohazards, Georesources, and Environmental Change. In this framework future ICDP projects will focus on the evolution of planet Earth, past climates, the effects of large impacts and mass extinctions, the formation and wise utilization of our most significant resources, and in-situ monitoring of volcanoes and fault zones. The linkage to wider societal challenges will include climate action, mitigation of natural hazards, affordable clean energy, sustainable cities and communities and clean water and sanitation.

The Science Plan was developed in close cooperation with our offshore sibling, the International Ocean Discovery Program, IODP. Jointly with IODP we aim at fostering the successful cooperation by implementing new Land-to-Sea Drilling projects that require combined onshore and offshore –amphibious- scientific drilling to tackle the key scientific themes. We kindly invite you to discover our Science Plan and to start brainstorming about new drilling initiatives and to spread the word on ICDP in your science networks.

www.icdp-online.org/fileadmin/icdp/media/doc/ICDP_Science_Plan_2020-2030.pdf

www.icdp-online.org/fileadmin/icdp/media/doc/ICDP_Science_Plan_Video_small.mp4

New IODP Science Plan

October saw the release of a new scientific blueprint that will guide ocean drilling research into the middle of this century. Entitled "2050 Science Framework: Exploring Earth by Scientific Ocean Drilling," the 25-year plan is a product of a spirited and vigorous effort by the international community and brings a fresh approach to ocean drilling investigations, focusing on the interconnected processes that characterize the complex Earth system. Hundreds of marine scientists from around the world contributed to the production of the new framework, attending national workshops to share their views and providing input during several public review periods as the framework was under development. A 48-person, international writing and editing team, led by Anthony Koppers of Oregon State University (USA) and Rosalind Coggon of the University of Southampton (UK), produced the document, which can be accessed at http://www.iodp.org/2050-science-framework. The document's writing team also created a 12-page summary and a 2-page flyer for wider audiences; these can be found at the same web page.

The new framework comprises three major components: "Strategic Objectives" (general research areas that focus on Earth system interconnections), of which there are seven; five "Flagship Initiatives" (multi-disciplinary and multi-expedition projects that are expected to take years or even decades to fully explore); and four "Enabling Elements," which include topics such as broader impacts, technology development, and big data analytics.

Each of the three components is given equal weight in the framework's structure. The framework also emphasizes the societal relevance of scientific ocean drilling, such as its ability to provide context for future climate models, elucidate the processes that trigger life-threatening earthquakes and tsunamis, and investigate the limits and possible applications of life deep beneath the seafloor. Also stressed in the document are collaborations with other research programs and organizations, such as the International Continental Scientific Drilling Program and national space agencies.

The science plan for the current phase of scientific ocean drilling, the International Ocean Discovery Program, runs through 2023. While much remains to be determined with regard to implementation strategies for the next phase of scientific ocean drilling, the long timeline of the new framework will enable the evolution and refinement of its research goals as societal needs and technological capabilities evolve. Regular assessments will take place every five years in order to ensure that the framework maintains its cutting-edge aspirations.